Nanofibers and Nanocomposites Poly(3,4-ethylene dioxythiophene)/Poly(styrene sulfonate) by Electrospinning

A Thesis

Submitted to the Faculty

of

Drexel University

by

Afaf Khamis El-Aufy

in partial fulfillment of the

requirements for the degree

of

Doctor of Philosophy

March 2004

Dedications

This work cannot be dedicated to anyone but him.

For my first joy and my first creation; my beautiful daughter Sondus.

For the sweetest angle and the prettiest eyes; my baby Jannah,

For bringing me That man who is sharing with me the bad times before good ones, who teaches me the true meanings of love and fidelity; my wonderful devoted husband Mohamed.

For all the blessings I realize and the ones I do not.

For giving me the strength to finish this thesis, I dedicate my work (may he accepted it as my good deeds) to him only I dedicate it; to **Almighty ALLAH**.

Acknowledgments

It is both a privilege and a pleasure to thank all the people who have kept me productive, sane and happy at Drexel for the longest stretch of time I have continuously spent in one place.

First and foremost, my advisor Prof. Frank Ko deserves all the credit for introducing me to and making me feel at home in the nanoworld. His scientific intuition and camaraderie are perhaps only surpassed by his courage in allowing his students to wonder around the vast scientific landscape in order to train us to be free-thinking independent scientists at the end of the journey. I thank him for showing me how to be a competent researcher and infested me with the nanofibers fever.

I also have much appreciation for Prof. Allen MacDiarmid for his valuable advising and introducing me to intrinsically conductive polymer and methods for conductivity. His patient remarks and seminars clarify my understanding of conductive polymers.

My sincere thanks to Prof. Bahram Nabet, who was always there to answer my questions and teach me some of the difficult world of electrical engineering; he is a real friend and a good teacher to me.

I would be remiss if I did not acknowledge all the teachers; Prof. Kalidindi, Prof. Lawley, Prof. Gobran, Prof. Doherty, and Prof. M Barsoum, who taught me the courses and keeping my eyes, open to the (Materials) world beyond nanofibers.

I would like to thank all my committee members for sharing their invaluable time and knowledge to achieve my PhD degree; in alphabetical order, Prof. Y. Gogotsi, Prof. C. Li, Prof. M. Marcolongo, Prof. B. Nabet and Prof. G. Palmese.

I would like to thank the Ministry of Missions and Higher Education of Arab Republic of Egypt for financially supporting my study at Drexel University. I appreciate all the help of Prof. O. Zaky, Prof. A. El-khashab, Mr. M. Eid and Mr. A. Kenawy.

I would like to thank the ELECON, inc and TRITON system for supplying the PEDT polymer and Dr. P. Willis (Caltech) for supplying us with SWNTs.

The instruments used in this work are operated by A.J. Drexel Institute of Nanotechnology at Drexel University. The Raman spectrometer purchase was supported by NSF (DMR-0116645). The ESEM spectrometer purchase was supported by NSF (BES-0216343).

I deeply appreciate the help of Prof. C Li, his support and his group in particular Kishore for the DSC and TGA measurements.

I appreciate the help of Dr. Haihui Ye for his important contribution with TEM, Mr. T Kelly for helping with Raman spectroscopy and FT-IR, and Mr. D VonRohr for helping with SEM, OIM and answering many of my questions.

I would like to thank all my group members; Jason Lyons, Nick Titchenal, Johnason Ayutsede, Heejae, Millind Ghandi, Shiarali Rao, David Heldt and especially Hoa Lam for being a true friend and is always there when I need her help, our conversations, laughs and their help will always be fondly remembered. I express my sincere appreciation to all my Egyptian friends and their kind words over these years with my homesickness.

Finally I would like to thank my small family; my husband Mohamed Elgamssy, my daughters Sondus and Jannahtullah, for their support and the time I was supposed to spend with them and true appreciation for Jannah who doesn't realize the sacrifice she offered me. My deep appreciation to my extended family in Egypt; first and foremost, my parents Mr. Khamis El-Aufy and Ms Wahida for their support and taking care of little baby.

I would like to thank all my nephews and all my nieces for their true love and all my sisters especially Ms. Soad El-Aufy for being a candle in the dark night and for her encouraging me with her pure spirit, all my brother and my brothers in law in particular Mr. Essam El-Gharably for helping me since high school and till now, I really appreciate their support and thank them for believing in me that make this achievement a joint one.

Table of Contents

List of Tables

List of Figures

Abstract

Nanofibers and Nanocomposites of Poly(3,4-ethylene dioxythiophene)/Poly(styrene sulfonate) by Electrospinning

Afaf Khamis El-Aufy

Frank K. Ko, PhD Supervisor

Intrinsically conductive polymers such as PEDT are an important class of electroactive polymer being used in the form of films for electronic devices such as LED. In order to explore the feasibility of PEDT for wearable electronics, PEDT/PAN blend was converted to fibers and fibrous assemblies. Specifically PEDT polymer blends and their composites were converted to submicron and nanoscale fibers to explore the nanoscale effect on the conductivity of PEDT.

In order to organize the nanofibers to aligned and planar assemblies, various processing mechanisms were developed including “Dry Rotary Electrospinning” and “Self-assembled” yarn formation as well as non-woven random fiber mats. In order to optimize the electrospinning process, the fiber diameters of the PEDT fiber were correlated with polymer concentration.

The PEDT nanofibrous assemblies were characterized by Four-point probe electrical conductivity measurement and by microtensile testing. Confirming the significant effect of fiber diameter on electrical conductivity, a four-fold increase in electrical conductivity was observed as fiber diameter decrease from 260nm to 140nm.

To further explore advanced material concepts to introduce multiple functions to the electrospun yarn, single walled carbon nanotubes (SWNTs),

were successfully co-electrospun with PEDT/PAN blend. The inclusion of SWNTs shows further increase in electrical conductivity of nanofibrous yarn and the tensile strength increased by 50%.The Presence of SWNTs were confirmed by Raman spectroscopy and HREM which also show good alignments of CNTs within the nanofibers. The carbon nanotubes reinforced PEDT nanofibrous yarn was woven into a fabric to demonstrate the feasibility of the electrospun yarn as an attractive enabling material for wearable electronics.

Chapter 1: Introduction.

Electrostatic generation of ultra fine fibers ‘‘electrospinning’’ has been known since the 1930s [102]. This technique has been recently rediscovered for applications such as high performance filters [107, 111] and for scaffolds in tissue engineering [1] that utilize the unique characteristics of the high surface area; 10 m^2/g provided by the fibers. In this non-mechanical, electrostatic technique, a high electric field is generated between a polymer fluid contained in a glass syringe with a capillary tip and a metallic collection screen. When the voltage reaches a critical value, the charge overcomes the surface tension of the deformed drop of the suspended polymer solution formed on the tip of the syringe, and a jet is produced. The electrically charged jet undergoes a series of electrically induced bending instabilities during its passage to the collection screen that results in the hyper-stretching of the jet. This stretching process is accompanied by the rapid evaporation of the solvent molecules that reduces the diameter of the jet, in a cone-shaped volume called the ‘‘envelope cone’’. The dry fibers are accumulated on the surface of the collection screen resulting in a non-woven mesh of nano to micron diameter fibers. The process can be adjusted to control the fiber diameter by varying the charge density and polymer solution concentration, while the duration of electrospinning controls the thickness of fiber deposition [111].

In this thesis, a rotary dry electrospinning disc will be designed to align the electrospun fibers. The rotating speed of the disc will be studied to find the optimum condition for aligned uniform nanofibers. The effects of processing parameters on the

morphology of individual electro-spun PEO nanofibers will be explored. A Response Surface Methodology technique will be used to establish a 3^3 factorial experiments and to optimize the electrospinning processing parameters.

Since the initial discovery in 1977, that polyacetylene (CH)x, now commonly known as the prototype conducting polymer, the development of the field of conducting polymers, "synthetic metals", has continued to accelerate at an unexpectedly rapid rate and a variety of other conducting polymers and their derivatives have been discovered. Poly(3,4-ethylene dioxythiophene) doped with poly(styrene sulfonate), often abbreviated as PEDT or PEDT, was developed and used in many applications over the past decade. Numerous industrial and academic groups have limited their research in other conductive polymers due to they might yield toxic products upon degradation, while PEDT is one of the polymers that is possibly more environmentally "friendly" system.

The research and development efforts of the past ten years have quickly brought PEDT to the forefront of the field of conducting polymers. Its properties, being its high conductivity in combination with excellent stability, have allowed the material to now become industrially useful. As a result PEDT/PSS and its derivatives have found their way into several current applications, including as an antistatic material in photographic film, an electrode material in capacitors, LEDs and as a conducting layer in through-hole plating.

Potential new science/technology has been developed by combining the now well established field of electronic polymers with the emerging field of nanoscience. In our work, PEDT/PSS was selected to incorporate with poly(acrylonitrile) to form conducting nanofibers. The electrospinning of PEDT/PAN process is going to be investigated and

observe the effect of PEDT on electrospinning. The morphological properties of the electrospun fibers will be examines by scanning electron microscopy (SEM), while the chemical properties of the fibers versus the polymer will be analyzed by the help of Differential Scanning Calorimeter (DSC) and Fourier transform-infrared (FT-IR) spectroscopy. The stress-strain results will represents the mechanical properties of the electrospun fibers and the effect of PEDT content on the PEDT/PAN blend will be investigated.

Carbon nanotubes, long, thin cylinders of carbon, were discovered in 1991 by Iijima [151]. These are large macromolecules that are unique for their size, shape, and remarkable physical properties. They can be thought of as a sheet of graphite rolled into a cylinder. These intriguing structures have sparked much excitement in the recent years and a large amount of research has been dedicated to their understanding. These carbon nanotubes can be mixed with conductive and nonconductive polymers to form spinning dopes for co-electrospinning of conductive nanocomposite fibrils. By taking advantage of the high level of electrical conductivity and mechanical properties, the nanocomposite fibril concept will be demonstrated herein using single wall carbon nanotube as the filler.

SWNTs will be mixed with the PEDT/PAN polymer and co-electrospun into nanofibers. The characterizations of the electrospun SWNTs/PEDT fibers will be examined by SEM and high resolution transmission microscopy (HREM), Raman spectroscopy will be used to examine the presence of carbon nanotubes, while the inclusion of CNTs on the conductivity level and mechanical properties will be discussed.

The presence of conductive nanofibers will open the way to new applications and the possibility to form yarn, woven fabric and braiding of these fibers. One of the

interesting applications would be the wearable electronics which should possess flexible, lightweight and conductivity properties. These properties could be achieved by the conductive nanofibers. Conductive materials in fibrous form such as yarns and fabrics are preferred candidates for wearable electronics by serving as interconnects, functional devices and sensors.

In summary, the objectives of this thesis is to introduce the electrostatic spinning process for the formation of nanofibers of pure electronic polymers (in their semiconducting and metallic regimes) and/or their blends in conventional organic polymers for the purpose of ascertaining their applicability in the fabrication of nano-electronic devices for wearable electronics. However, the most satisfying part of our work is excitement that nanotechnology and nanoscience are creating here at Drexel and elsewhere. We have no doubts that the excitement will continue to grow, as we enter the second decade of nanotechnology science.

Chapter 2: Background and Significance.

2.1 Intrinsically Conductive Polymers (ICP) and their applications.

Since MacDiarmid et al, [2] discovered that polyacetylene $(CH)_x$ (now commonly known as the prototype conducting polymer) can reach extremely high electrical conductivities, the field of conducting polymers, which are often referred to as synthetic metals, has attracted the interest of many scientists[3]. Much of the combined research efforts of industrial, academic, and government researchers have been directed toward developing materials that are application stable in the conducting state, easily processable, and relatively simple to produce at low cost. With the many difficulties encountered in accomplishing these goals, only recently have companies [4, 5] been able to bring products to the market.

Over the past 30 years, conducting polymers (e.g. poly-(*p*-phenylene), poly(phenylenevinylene), polypyrrole, polythiophene, poly(heteroaromatic vinylenes), and polyaniline) have attracted the most attention of researchers[101,6]. Of these polymers, the polyaniline family stands out for its ability to form processable conductive forms at relatively low cost and in bulk amounts [7]. Also, polyaniline holds a special position amongst conducting polymers in that its most highly conducting doped form can be reached by two completely different processes- protonic acid doping and oxidative doping [8]. Despite mentioned advantages, numerous industrial and academic groups have limited their research in polyaniline chemistry due to the possible presence

of benzidine moieties in the polymer backbone, which might yield toxic (carcinogenic) products upon degradation [9].

While the (hetero) aromatic polypyrrole and polythiophene, as well as poly(p-phenylene vinylene), are possibly more environmentally "friendly" systems, they have the disadvantage of being insoluble and infusible[10]. In order to overcome these problems, numerous substituted derivatives of these polymers have been developed that carry alkyl, alkoxy, and other substituents along their backbones [104,11].

At this stage, it is preferable to give the definitions [106], of some terms so the reader can understand them in the following sections.

Synthetic metal

Intrinsically conducting polymer (ICP) more commonly known, as synthetic metal is an organic polymer that possesses the electrical, electronic, magnetic, and optical properties of a metal while retaining the mechanical properties, processibility, etc. commonly associated with a conventional polymer.

Conducting polymers

A physical mixture of a non-conductive polymer with a conducting material such as a metal of carbon powder distributed throughout the material.

Electronic polymers

Conjugated organic polymers that are either electrical insulators or semiconductors. that can have their conductivity increased by several orders of magnitude from the semiconductor regime

The concept of doping

Is the unique, central, underlying, and unifying theme, which distinguishes conductive polymers, from all other types of polymers. During the doping process, an organic polymer either an insulator or semiconductor having a small conductivity, typically in the range from 10^{-10} to 10^{-5} S/cm, is converted to a polymer which is in the 'metallic' conducting regime (~1-10^{4} S/cm).

The various possible electron band structures found in solids at 0K are shown in Figure 2.1 . The band structures [12] are classified; based on electrical properties of materials, into in a metal, a semimetal, an insulator, and a semiconductor. The gray areas indicate regions filled with electrons. Blue areas are regions that could accept electrons promoted from the filled levels.

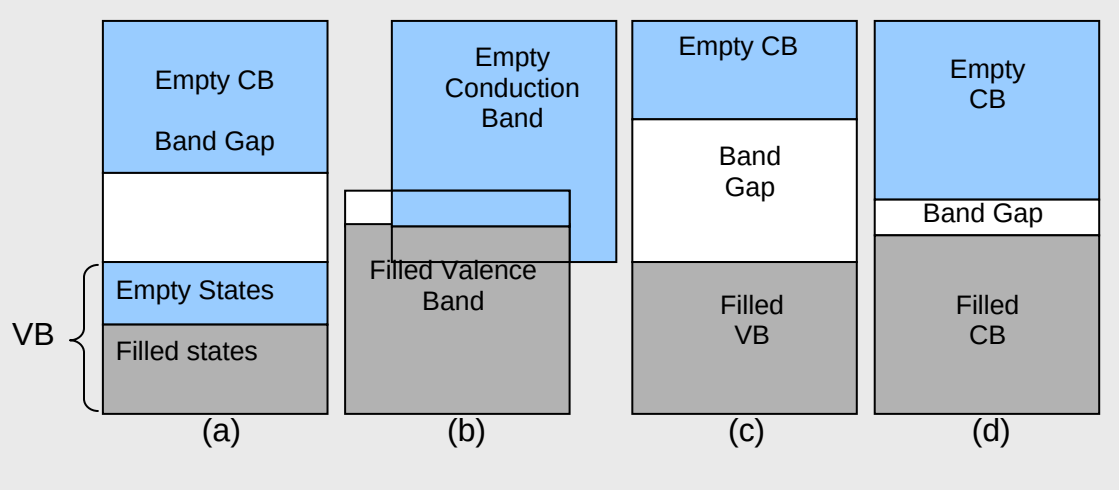

Figure 2. 1 The band structures of solids, (a) Metal, (b) Semimetal, (c) Semiconductor, and (d) Insulator.

Different types of doping synthesis [7]

1. *Redox doping*: All the conducting polymers (and most of their derivatives), e.g. polypyrrole, polythiophene, polyfuran and polyaniline undergo either p- (paritial oxidation) and or/n- (partial reduction) redox doping by chemical and/or electrochemical processes during which the number of electrons associated with the polymer backbone changes [54].
2. *Doping involving no dopant ions*
    a. Photo-Doping: When trans-$(CH)_x$ for example, is exposed to radiation of energy greater than its band-gap, electrons are promoted across the gap and the polymer undergoes 'photo-doping [13].
    b. Charge-injection doping: Is most conveniently carried out using a metal/insulator/semiconductor (MIS) configuration involving a metal and a conducting polymer separated by a thin layer of a high dielectric strength insulator [14, 15].

Non-Redox Doping or Protonic-acid doping: this type of doping differs from redox doping in that the number of electrons associated with the polymer backbone does not change during the doping process. The energy levels are rearranged during doping. The emeraldine base form of polyaniline was the first example of this process [16].

Figure 2. 2 shows an example of doping process. Conductive polyaniline can be obtained by chemical oxidation (p-doping) of leucoemeraldine base. It's the reaction of a solution of chlorine in carbon tetrachloride proceeds to give emeraldine hydrochloride.

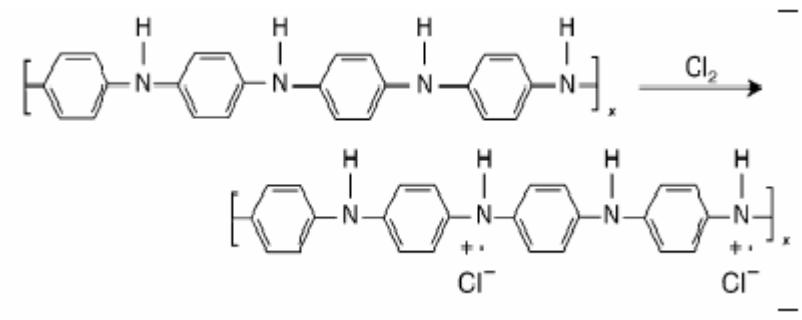

Figure 2. 2 The doping process of Polyaniline.

ICP applications

Intrinsically conductive polymers can be used for several applications such as; Low cost semiconductor chips, integrated circuits to electrodes, light weight battery, sensors, electrochromic displays, static-free packaging

2.2 PEDT Polymer.

During the second half of the 1980s, scientists at the Bayer AG research laboratories in Germany developed a new polythiophene derivative, poly(3,4-ethylenedioxythiophene), having the backbone shown structure in Figure 2.3 [17].This polymer often abbreviated as PEDT or PEDOT was initially developed to give a soluble conducting polymer that lacked the presence of undesired α, β- and β,β-couplings within the polymer backbone [18]. PEDT was initially found to be an insoluble polymer, yet exhibited some very interesting properties. In addition to a very high conductivity (300 S/cm), PEDT was found to be almost transparent in thin, oxidized state [11, 19].

The solubility problem was subsequently circumvented by using a water-soluble polyelectrolyte, poly(styrene sulfonic acid) (PSS), as the charge-balancing dopant during polymerization to yield PEDT/PSS. This combination resulted in a water-soluble polyelectrolyte system with good film-forming properties, high conductivity (10 S/cm), high visible light transmissivity, and excellent stability [20].

Driven by the properties and utility of PEDT/PSS, a number of research groups have entered the area of PEDT chemistry over the past decade. Figure 2.4 shows the great increase in the number of publications over the past decade. This indicates the great interest of new materials, processes, and industrial applications.

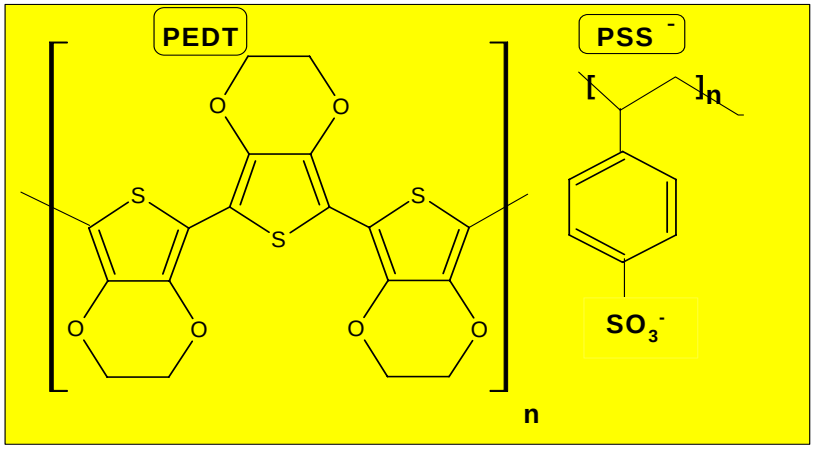

Figure 2. 3 Chemical Structure of PEDT/PSS conductive polymer.

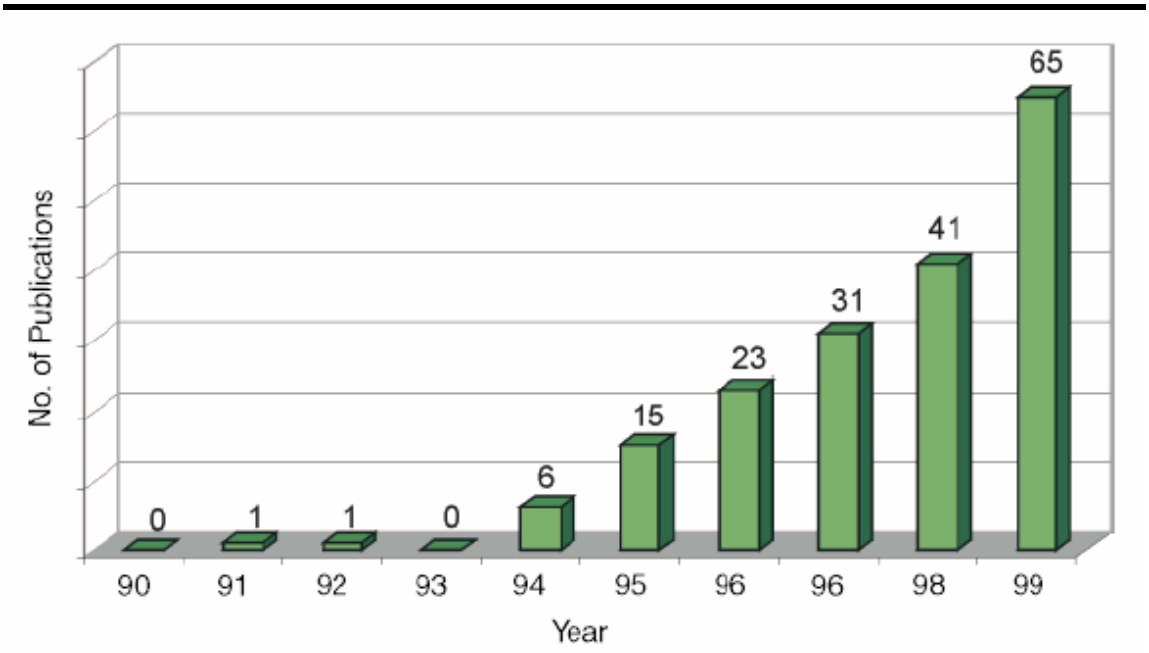

Figure 2. 4 Development of the number of journal publications on PEDT over the past decade (1990-1999).

2.3 Synthesis and Characterization of PEDT, PEDT/PSS.

F. Jonas et al [21], divided the synthesis of PEDT derivatives into three different types of polymerization reactions:

- Oxidative chemical polymerization of the EDOT-based monomers.
- Electrochemical polymerization of the EDOT-based monomers.
- Transition metal-mediated coupling of dihalo derivatives of EDOT.

2.3.1 Oxidative chemical polymerization of EDOT-based monomers.

A new polythiophene derivative has been synthesized [11] by chemical oxidative polymerization of the monomer 3,4-ethylenedithiathiophene (EDTT). Chemical polymerization of EDT derivatives can be carried out using several methods and oxidants. [22] The classical method employs oxidizing agents such as $FeCl_3$ or $Fe(OTs)_3$.

Chemical polymerization of alkylated [23] or alkoxylated [24] EDT derivatives results in regio-random PEDT derivatives that are soluble in common organic solvents such as chloroform and tetrahydrofuran (THF). As a result these polymers can be characterized using standard structural methods; for example, gel permeation chromatography (GPC) determined M_w values for a PEDT range from 10,000-25,000 g/mol.

De Leeuw et al [25] have reported a second polymerization method of EDT. Utilizing $Fe^{III}(Ots)_3$, at elevated temperature, in combination with imidazole as a base, resulted in a black insoluble and infusible PEDT film that after rinsing with water and n-butanol, exhibited conductivities of up to 550 S/cm [26].

The third, and most practically useful, polymerization method for EDT is the so-called BAYTRON P synthesis that was developed at Bayer AG. [20] and modified by ELECON, inc [27]. This method utilizes the polymerization of EDT in an aqueous polyelectrolyte (most common PSS) solution using $Na_2S_2O_8$ as the oxidizing agent. Carrying this reaction out at room temperature results in a dark blue, aqueous PEDT/PSS dispersion, which is commercially available from Bayer AG under the trade name BAYTRON P (see Figure 2. 5) and from ELECON, under the trade name ELEFLEX-

2000. An interesting aspect of BAYTRON P and ELEFLEX-2000 is that, after drying, the remaining PEDT/PSS film is highly conducting, transparent, mechanically durable, and insoluble in any common solvent.

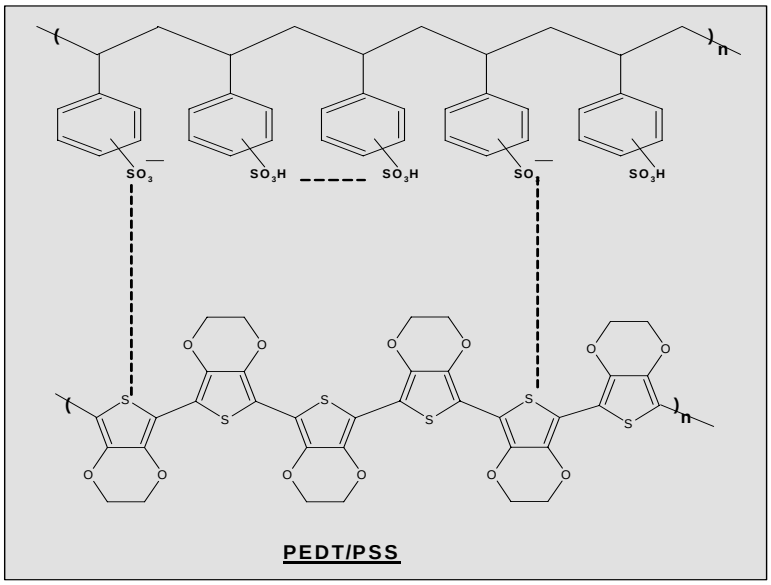

Figure 2. 5 PEDT/PSS conductive polymer produced by Bayer & Elecon Co.

Inganäs [28] and co-workers, who were the first to propose a structural model for tosylate-doped PEDT, presented an important contribution to the structural characterization of PEDT. Using de Leeuw's chemical method extended to a surface-confined polymerization, they [23] prepared thin PEDT films that were subsequently studied with grazing incidence X-ray diffraction using synchrotron radiation. From these studies they concluded that the material is very anisotropic and that there is a limited crystalline order in these thin films. Furthermore, they have evidence for a Para-

crystalline state with small Para-crystalline regions. The same group also studied PEDT's electronic structure by X-ray and ultraviolet photoelectron spectroscopy, [26] as well as by spectroscopic ellipsometry.[24] These results suggest that PEDT prepared in this manner can be seen as an anisotropic metal. C. Wang et al [29] reported that, the FT-IR spectra of the neutral polymer PEDT indicate a regular structure formed via α,α coupling of thiophene rings. The PEDT polymer shows two absorption bands at 341 nm and 413-419 nm in NMP solution in the UV-vis luminescence with peak at ca. 552 nm.

2.3.2 Electrochemical Polymerization of EDT Derivatives.

Another especially useful polymerization method utilizes electrochemical oxidation of the electron-rich EDT-based monomers. This method stands out, as it requires only small amounts of monomer, short polymerization times, and can yield both electrode-supported and freestanding films. In the case of EDT itself, electrochemical polymerization results in the formation of a highly transmissive sky blue, doped PEDT film at the anode [30,31]. A variety of electrolytes are compatible with EDT-derivative polymerization, including polyelectrolytes, as was nicely demonstrated by Wernet and co-workers, [32] or using an aqueous micellar medium [33].

A slightly modified electrochemical polymerization method, electrochemical desilylation, uses α,ω-disilylated EDT-based monomers [34]. This method, which is based on the loss of a trimethylsilyl (TMS) group, leads to polymers having the same nominal repeat unit as that obtained from polymerization of the parent monomers. Two benefits stand out in using bis-TMS-derivatized monomers. First, the films formed adhere more strongly to oxide-based electrode surfaces (indium tin oxide (ITO), Au, et.)

giving them enhanced switching properties. In addition, as more complex and larger multi-ring monomers are prepared, TMS derivatization increases their solubility greatly, therefore improving their polymerization characteristics.

2.3.3 Transition Metal-Mediated Coupling of Dihalo Derivatives of EDT.

Many thiophene-based polymers have been prepared over the years using transition metal-catalyzed coupling of activated organometallic derivatives [35]. Yamamoto et al. recently applied this methodology to the direct formation of neutral PEDT [36]. Though this method yields materials with low molecular weight, it may prove especially interesting when it is applied to monomers with solublizing side groups.

I. Winter et al [37] studied the thermal ageing of PEDT. The oxidatively prepared poly(3,4-ethylenedioxythiophene tetrachloroferrate) (PEDT) has been characterized by X-ray absorption spectroscopy and XPS to study the thermal degradation of the polymer. XANWS spectra were measured at the Electron Stretcher Accelerator ELSA in Bonn and compared with measurements made with a conventional XPS technique. These investigations show that after 48h at 150^{o}C, due to baking and moisture, irreversible structural changes in the polymer main chain occur. They were identified as a partial oxidation of the sulfur of the polymer backbone to the sulfate anion and the decomposition of the counter ion resulting in loss of conductivity.

Sankaran and Reynolds [38] reported the syntheses of two new derivatives of 3,4-ethylenedioxythiophene (EDOT) specifically 5-octyldioxeno[2,3-$_c$]thiophene (EDOT-C_8) and 5-tetradecyldioxeno[2,3-c]thiophene (EDOT-C_{14}), and their polymers. The PEDT-C_8 and PEDT-C_{14} formed oxidize with relatively low peak potentials at –0.22

and –0.19V, respectively, indicating the doped form of the polymer to be quite stable. Both PEDT-C_8 and PEDT-C_{14} show two reduction processes with peaks at –0.18 and –0.16 V ($E_{c2,p}$) and –0.55 and –0.36 V ($E_{c1,p}$) respectively. Optoelectrochemical studies reveal an E_g of 1.75 eV for both polymers. They mentioned that the polymers are electrochromic, relatively transmissive and light gray in the oxidized form, while being opaque and deep purple in the reduced form exhibiting high electrochromic contrasts. They applied long term switching studies in 0.1 M $LiClO_4$/PC with Li/Li^+ as a reversible counter electrode showing that PEDT, PEDT-C_8 and PEDT-C_{14} retained 65%, 50%, and 62% of their electroactivity after 6000, 9000, and 16,000 double switches, respectively.

Yamato et al [39] carried out the electrochemical polymerization of 3,4-ethylenedioxythiophene (EDT) in the presence of monomeric anions or polyanions in electrolyte solutions. While no free-standing films of poly (3,4-ethylenedioxythiophene), (PEDT) were obtained using novel polyanions as Dopants, they obtained a flexible conducting polymer using novel polyanions, e.g. sulfated poly(β-hydroxyethers) (S-PHE), sulfated poly(β-hydroxyethers) having trifluoromethyl groups (S-PHEF), and sulfated polybutadiene (S-PBD). They reported that the conductivity of these PEDT polyanion composites exceeded 150S/cm, and reached as high as 400 S/cm when S-PHEF was used as dopant.

Y. Kudoh et al [40] found that a good yield of poly (3,4-ethylenedioxythiophene), (PEDT) was obtained by emulsion polymerization in which an anionic surfactant and $Fe_2(SO_4)_3$ were used as an emulsifier and an oxidant, respectively. The major feature of this polymerization was that highly conductive PEDT was formed

in an aqueous medium containing such a low concentration of 3,4-ethylenedioxythiophene), (EDOT) and $Fe_2(SO_4)_3$ as 0.05M.

A. Lima et al [41] carried out the electropolymerization of 3,4-ethylenedioxythiophene (EDT) and its hydroxymethyl derivative (EDTM) in sodium dodecylbenzenesulfonate aqueous solution by cyclic voltammeter and chronoamperometry on a platinum electrode. They reported that PEDTM seemed to be irreversibly damaged at lower potentials than PEDT (+ 1.2 V/SCE versus + 1.4 V/SCE, respectively).

S. Armes and R. Corradi [29,42] have synthesized poly(3,4-ethylenedioxythiophene), (PEDT), using $FeCl_3$, $Ce(SO_4)_2$ and $(NH_4)_2Ce(NO_3)_6$ oxidants. Greater than stoichiometric amounts of $FeCl_3$ were required for reseonable yields. They produced PEDT using the ceric-based oxidants that contained significant quantities of unidentified cerium compounds and conductivities as high as 20 S/cm were obtained.

K. Xing et al [43], investigated the electronic structure of poly(3,4-ethylenedioxythiophene), (PEDT) by X-ray and ultraviolet photoelectron spectroscopies as well as quantum chemical calculations. They observed significant differences in the photoelectron spectra between as prepared chemically neutralized and anion-doped PEDT thin films. The electronic structures of as-prepared neutral and doped PEDT obtained from the photoelectron spectra were in good agreement with the results of new quantum chemical electronic structure calculations. They mentioned that the surface concentration effect is probably the reason to make the large-anion-doped polymer a more suitable candidate as an electrode in polymer light-emitting diodes (LEDs) than the small-anion-doped polymer.

R. Reynolds et al [44] reported that Alkyl derivatized poly(3,4-ethylenedioxythiophenes), (PEDT's) exhibit a high degree of visible light transparency in the oxidized state, which being an opaque blue in the reduced state. They mentioned that, these polymers could be switched rapidly (sub-second) between states with high optical contrasts of up to 60% ΔT.

Xiwen and Iguanas [45] found that poly(3,4-ethylenedioxythiophene), (PEDT) has the different oxidation levels; (polaron, bipolaron, and metallic states), using *in situ* UV-VIS-NIR spectroscopy. They mentioned that, the transitions between the different oxidation levels were never clearly observed in cyclic voltammetry (CV). Instead a broad oxidation peak and two reduction peaks were shown. The CV of PEDT at macroelectrodes showed a pair of redox peaks separated by 0.9 V at low scan rates, indicating two irreversible electron transfer steps. Using an ultramicroelectrode, they found those two pairs of redox peaks in PEDT.

Levin et al [46] measured the temperature dependence of the electrical conductivity σ(*(T)*) and the magnetoconductivity σ(*B,T*) of poly (3,4-ethylenedioxythiophene) (PEDT) films heavily doped with CF3SO3 down to *T*= 150 mK in magnetic fields up to *B* = 9T. It was shown that, below 1 K, σ*(T)* α 1n *T* and σ(*B,T*) depends significantly on the orientation of *B* parallel or perpendicular to the film surface.

G. Greczynski and Salaneck [47] studied thin films of an electrically conducting polymer blend, poly(3,4-ethylenedioxythiophene) oxidized with poly(4-styrenesulfonate), PEDT-PSS, using X-ray and ultraviolet photoelectron spectroscopy. They studied the thermal effects and the influence of hydrochloric acid on the chemical and electronic structures of the films. They identified three chemically different species

in pristine PEDT-PSS, namely poly(4-styrenesulfonic acid), poly(sodium 4-styrenesulfonate) and poly(3,4-ethylenedioxythiophene).

A. Heeger et al [48] reported the reflectance spectrum of poly(3,4-ethylenedioxythiophene) (PEDT) doped with PF_6 with DC conductivity of 230 S/cm at room temperature, measured over a wide frequency range from 50 to $5X10^4$ cm^{-1} (0.006-6 eV). They mentioned that, the reflectance, *R(ω)*, of PEDT-PF6 is characterized by metal-like signatures in the infrared (IR), including high *R(ω)* in the far-IR and a plasma frequency of approximately 1.2 eV, characteristic of a disordered metal near the metal-insulator (M-I) transition. The reflectance spectrum was in good quantitative agreement with the "localization-modified Drude (LMD) model". They stated that since the onset of the interband absorption (below 1.5 eV) was at a lower energy than in other conducting polymers, PEDT-PF_6 showed low absorption in the visible range between 2 and 3eV. Their spectroscopic results demonstrated that that doped PEDT system could be utilized as a transparent electrode for optoelectronic devices.

Randriamahazaka et al [49] studied the electrodeposition mechanisms of 3,4-ethylenedioxythiophene (EDOT) according to electrocrystallization theory. The analysis of the chronoamperograms indicated that the initial stage of the electrodeposition was a combination of instantaneous 2-D and instantaneous 3-D mechanisms since the electrodeposition was carried out under charge transfer control rather than diffusion. In the later stages, layer-by-layer growth mode in accordance with the Stranski-Krastanov model was observed. They studied the stability of PEDT during successive polarization between –0.6 and 0.5 V at a scan rate of 0.2 V s^{-1} in acentonitrile and in aqueous

solutions containing tetrabutylammonium perchlorate and lithium perchlorate as the electrolyte.

A. Heeger et al [50] investigated the temperature dependences of the conductivity σ(T) and magnetoconductivity (MC) of poly(3,4-ethylenedioxythiophene), PEDT, doped with PF_6, BF_4 and CF_3SO_3 , down to 1.2 K. They found the transition in σ(T) from a negative to positive temperature coefficient of resistivity, TCR below 10K for samples with $\rho_T = \rho(1.4K)/\rho$ (291 K) ≈ 1.5-2.8. For negative and positive TCR the σ(T) was isotropic and ~ $T^{1/2}$. The MC is negative, isotropic and ~ H^2 and $H^{1/2}$ at low and high magnetic field respectively. They explained the results as a result of the dominant influence of electron-electron interactions on the σ(T).

Reynolds and Morvant reported [51] the first in situ conductivity measurements of PEDT, which was grown laterally on large gap lateral growth electrodes (gap distance 200μm) to give relatively thick films (93.3-22.5 μm) with maximum in situ conductivities of 0.2-13.0 S/cm depending on growth conditions. It was demonstrated that PEDT can be fully switched from its nonconductive state at –0.6 V to its fully conductive state at +0.1V versus Ag/Ag^+. A negligible effect of solvent (PC, THF, and H_2O) and electrolyte ($Li(CF_3SO_2)_2N$, $LiClO_4$, $LiBF_4$, and TBAP) used during both electropolymerization and redox switching on the in situ conductivity of PEDT demonstrated the versatility of using PEDT as a conducting material under a wide variety of conditions.

Niu et al [52] stated that, the Crystalline characteristics and surface morphology of PEDT films on a platinum surface can easily be controlled in electrochemical synthesis by tuning the polymerization potential. At lower switching potentials, a dense

amorphous PEDT film on the platinum surface was obtained, and at higher potential, a porous crystalline film was formed. Froyer et al [53] carried out the study of EDT and its electrochemically synthesized polymer by means of Raman and UV-vis-NIR absorption spectroscopies. They also studied the doping –dedoping process of PEDT with these methods. An assignment of the Raman lines was attempted for both monomer and polymer, and dynamical calculations were performed to obtain characteristic valence-force-field of these compounds. Their work provided a good basis for calculations of force constants and coordinates of the perturbed structure created by doping. This work resulted in a better understanding of the spectra, structure and optical effects in PEDT and similar compounds.

2.4 Properties of PEDT.

Examining the range of polymers that have been accessed using the PEDT building block, one is struck by its synthetic flexibility and utility. Its highly electron-rich nature plays a profound role in the optical, electrochemical, and electrical properties of the resultant polymers. The conducting form of PEDT stands out for its high degree of visible light transmissivity and concurrent environmental stability, which is important for industrial applications. EDT polymerizes rapidly and efficiently, leading to highly electroactive PEDT films that adhere well to typical electrode materials and have a low oxidation potential, which provides for facile, long-term electrochemical switching. As illustrated by the many derivatives shown above, PEDT provides materials with a range of bandgaps, yielding films having colors over the entire spectral range. Here, the properties of the neutral state followed by the oxidatively doped and conducting forms,

and finally addresses the redox switching properties of PEDT and its derivatives are addressed.

Bradley et al [54] stated that the electrical properties of conducting polymers are strongly dependent on their film morphology and the chemical and physical structure, which in turn can be strongly modified via a variety of post-deposition treatments. They used the aqueous dispersion of PEDT with polyelectrolyte, PSS as the conducting polymer PEDT/PSS in their study. They reported the conductivity and morphology of spin-coated films and their dependence on heat treatment procedures in both air and N_2 atmosphere.

2.4.1 Neutral PEDT and Derivatives.

PEDT exhibits an electronic bandgap, defined as the onset of the π-π* absorption, of 1.6±1.7 eV and a πmax of 610 nm, making it deep blue in color [13]. Due to its low oxidation potential, thin films of neutral PEDT must be handled carefully as they oxidize rapidly in air. Solutions of the alkyl derivatives, prepared via oxidative polymerization, are sufficiently stable to allow molecular and macromolecular characterization [47,48] .These solutions show an absorption onset at 1.8 eV and a λ_{max} at 575 nm (2.15 eV) since the polymer is more conformationally disordered than in the film form. The soluble PEDT derivatives can be solution processed by casting and spraying methods.

Inganas et al [55] stated that, PEDT is a conjugated polymer with high electrical conductivity in the doped state, good thermal and chemical stability and fast electrochemical switching. The material can be used as an antistatic layer, and would

have potential for use as a (transparent) electrode material and for electrochromic applications. They studied thin films (<1μm) of doped PEDT with variable angle spectroscopic ellipsemetry. Reflectance and transmission measurements were also performed.

2.4.2 Band-gap Control in PEDT and Derivatives.

The synthetic flexibility of EDT, coupled with its recent commercial availability as BAYTRON M, has made it an excellent component for variable-bandgap conjugated polymers. In general, the electronic band-gap of a conjugated chain is controlled by varying the degree of π-overlap along the backbone via steric interactions, and by controlling the electronic character of the π-system with electron donating or accepting substituents [56]. The latter is accomplished by using substituents and co-repeat units that adjust the highest occupied molecular orbital (HOMO) and lowest unoccupied molecular 2orbital (LUMO) energy levels of the π-system. A broad family of EDT-based polymers has been prepared with higher energy gaps than the parent PEDT. By using a series of oxidatively polymerizable bis-EDT±arylenes, polymers with band gaps ranging from 1.4-2.5 eV has been prepared. As such, neutral polymers with colors ranging from blue through purple, red, orange, green, and yellow have been made available. This is illustrated in Figure 2.6, which shows the rainbow of colors possible in PEDT derivatives. Low band-gap polymers have been prepared by combining the electron-rich EDT unit with a thienopyrazine unit, which also has the possibility of being n-type doped [57].

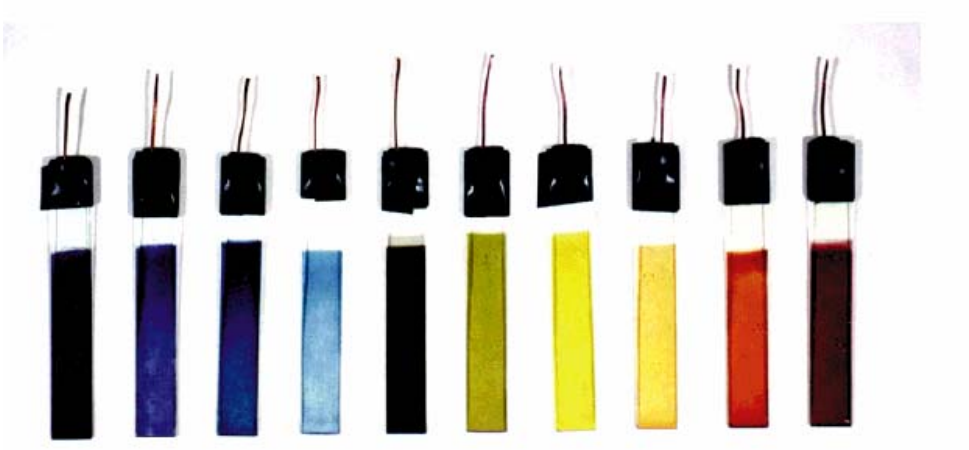

Figure 2. 6 Photograph of variable band gap EDT-based copolymers, demonstrating the range of accessible colors.

2.4.3 Conducting Properties of PEDT and Derivatives.

Using the Bayer oxidative polymerization process in solution, a surface-confined chemical polymerization method, and concurrent electropolymerization/deposition methods, PEDT is prepared in its more stable doped and conducting form. Films cast from the aqueous PEDT/PSS solution (BAYTRON P) have a high degree of mechanical integrity with conductivities ranging between 1 and 10 S/cm. These films are highly stable and can be treated for up to 1000 hrs at 100 °C with no change in conductivity [11]. These properties, coupled with PEDT/PSS's high level of transmissivity of visible light has led to its use as an antistatic material in photographic film applications

One method of enhancing the properties of electroactive polymers, while simultaneously preparing useful materials, is through polymer blending. For example,

poly(aniline camphor sulfonic acid) (PANI-CSA) blends with poly (methylmethacrylate) (PMMA) and nylon exhibit quite high conductivities (1-10 S/cm) at relatively low (1 %) loading levels of the conducting polymer in the host [58]. This high conductivity is attributed to the formation of a continuous network of the conducting polymer, which is phase separated from the host. These concepts have been extended to PEDT/PSS blended with polar host polymers (e.g., poly(vinylpyrrolidone) (PVP)) [59]. In this instance, as illustrated in Figure 2.7, treatment of the blend with a bivalent metal (e.g., Mg^{2+}) leads to ionic cross-linking and enhanced electrical properties at quite low (< 10 %) loading levels. In addition, the use of crystallization-induced phase separation between PEDT/PSS with poly(ethylene oxide) has been shown to form blends with continuous domains of PEDT/PSS, which exhibit higher conductivities when compared to blends prepared with amorphous host polymers. Conducting polymer blends may prove useful, especially in applications where concurrent control of optical and electronic properties is required. An example of this is cladding layers in electro-optic device structures. Blends of PEDT/PSS with poly(vinyl alcohol) have been used to provide a large effective poling field across a nonlinear optical (NLO) active layer, which is required for dipole orientation [60].

Using electrochemical polymerization methods, careful control of polymerization conditions (concentration, temperature, electrode materials, etc.) allows the preparation of free-standing PEDT films using a variety of dopant anions [61]. The conductivities of these films are found to be a function of the nature of the dopant anion with room-temperature conductivities typically ranging from 10^0 -10^2S/cm. Use of PF_6^- as the dopant counterion has provided especially interesting materials with high room-

temperature conductivities (300 S/cm) and a temperature dependence of conductivity, which suggests the material is on the metallic side of the metal-to-insulator transition.

Use of polymeric electrolytes can also lead to PEDT films via electropolymerization and chemical polymerization [30, 54]. In fact, films up to 20 meters in length were prepared using a rotating stainless-steel anode. PEDT films doped with sulfated poly(β-hydroxyether) (PEDT/S±PSE) exhibit excellent mechanical properties imparted by the polyelectrolyte dopant with concurrent high conductivities in the range of 150-180 S/cm. Conductivities as high as 400 S/cm were reported when using a bis-trifluoromethyl-functionalized sulfated poly(β-hydroxyether), while the use of more flexible polymeric dopants led to films that could be elongated between 80 and 110 % when heated. In the future, promise for PEDT films with enhanced properties is held as a deeper understanding is gained of polymer/ion interactions (e.g., the use of surfactant dopant ions [62] and the effect of synthetic conditions on polymer structure, including molecular weight.

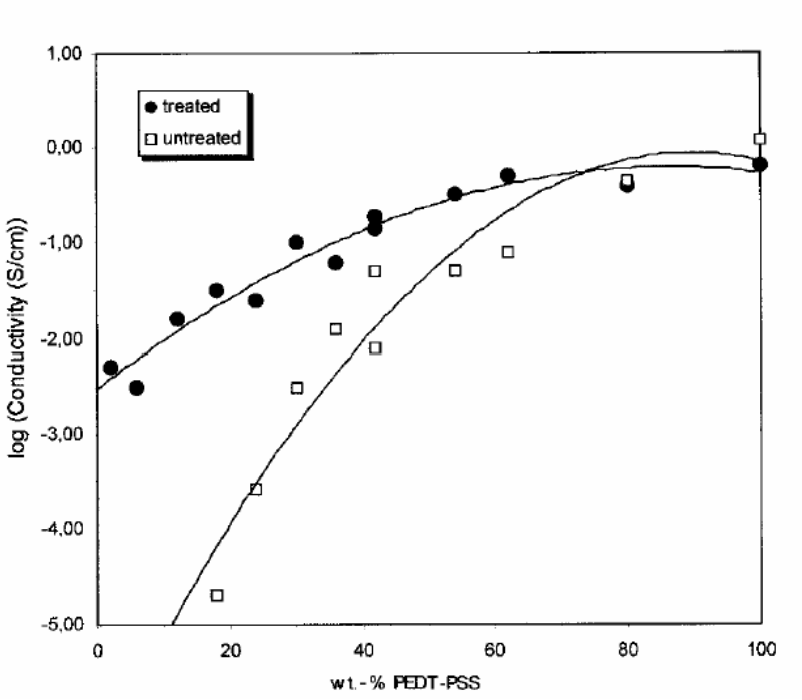

Figure 2. 7 Conductivity of PEDT/PSS/PVP blends at different compositions, untreated (□) and treated (●) with 0.25 M aq. $MgSO_4$ solution [63].

The conductivity and magnetoresistance of poly(3,4-ethylenedioxythiophene)/poly(styrenesulfonate) (PEDT/PSS)had been studied as a function of temperature by A. Heeger et al [64]. They stated that, the room temperature conductivities are dependent on the pH of the solutions from which the films were cast; values as high as 20 S/cm could be obtained in films cast from solutions with pH values in the range 0-3. The temperature dependence of the electrical conductivity is characteristic of granular metals (strongly disordered inhomogeneous systems),

$\sigma(T) = \sigma_0 \exp\left[-\left(T_0/T\right)^{1/2}\right]$. It is mentioned that the low-temperature magnetoresistance of PEDT/PSS is positive and follows an H^2 dependence at low magnetic fields

2.4.4 Electrochemistry of PEDT and Derivatives.

The combination of an especially low oxidation potential and a relatively low band gap gives PEDT some unique electrochemical and spectroscopic properties not accessible in other polymers. As the band gap is located at the transition between the visible and near-IR regions of the spectrum, PEDT is strongly cathodically coloring and much more transmissive to visible light (sky-blue transparent) in the doped and conducting state than it is in the reduced state (deep blue) [65]. The polymer exhibits a relatively broad cyclic voltammetric response with an $E_{1/2}$ of about 0.0 V vs. Ag/Ag + when being cycled between doped and undoped states, which could also be characterized by Raman spectroscopy [66]. One interesting observation is that PEDT can be electrochemically switched without the use of a conducting electrode support. Chemically deposited films were found to switch efficiently between doped and undoped states when the films were prepared on insulating polyester sheets [67]. Examination of the spectroelectrochemical series for PEDT shows the evolution of a very strong near-IR and mid-IR [68] absorption as the polymer becomes conducting that tails strongly into the visible region. This tailing was found to be repressed in alkyl-substituted PEDT and PProDT derivatives, which greatly enhances the transmissivity of the conducting form of these polymers and increases the electrochromic contrast accessible with the films, as illustrated by Figure 2. 8 for PproDT-Me_2 [29, 69, 70]. At the same time, these

derivatized PEDTs exhibit especially fast (sub-second) switching times for the large optical changes being attained.

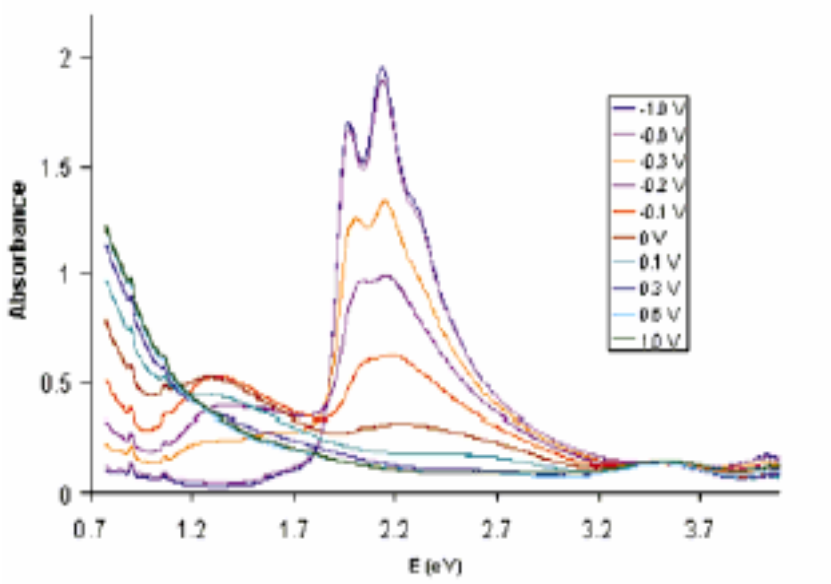

Figure 2. 8 Spectroelectrochemistry of PProDT-Me_2.

By incorporating PEDT and other EDT-based polymers into solid-state electrochemical cells, it was shown that electrochromic devices were possible with relatively small switching voltages (1.5 V), thus enabling possible applications in smart windows [71]. By using a dual polymer device construction, it was then shown that a range of colors could be accessed and devices with substantial electrochromic contrasts could also display sub-second switching times [72]. These latter devices are self-sealing

to prevent ambient exposure and, as the EDT polymers have such excellent redox properties, tens of thousands of deep double switches could easily be attained.

At the present time, the PEDT family of polymers is receiving a significant amount of attention as an electrode material for a variety of applications. One of the most prevalent of these has been as a conducting buffer between the optically transparent ITO and the light-emitting or hole transporting materials in organic and polymer LEDs [73]. PEDT has been used to improve the charge transfer rates between an electrode and a redox couple in photoelectro-chemical cells [74]. Studies of PEDT electrochemistry in phosphate buffers show an especially high level of stability when compared to polypyrrole, suggesting that this family of polymers may also prove useful in biosensors and other applications using biological media [75].

S. Ghosh & Inganas [76] presented a novel and simple method of preparation of a conducting network, by physical crosslinking of microgel particles of PEDT. PEDT doped with excess PSS had excess negative charge, which was used to form ionic bonds with multivalent cations for the physical crosslinking.

2.5 Applications for PEDT Derivatives.

As made obvious by the many interesting properties accessible by PEDT and its derivatives, the applications for these polymeric organic conductors will be wide-ranging [11].

2.5.1 Antistatic Treatment of Plastics Using PEDT/PSS.

Plastics tend to undergo static charging in dry air as a result of friction. Walking over synthetic carpeting can create a charge of up to several thousand volts, which is discharged when, for instance, a door handle is touched. The same effect is observed in the production and processing of photographic films during fast winding if these have not received antistatic treatment. The discharges occur with a flash of light, pre-exposing the film and making it unusable. Another field in which static charging must be avoided is the packaging of electronic components since present-day transistors and voltages in excess of 100 V irreversibly damage integrated circuits.

In order to prevent these effects from occurring in practice, photographic films and packaging films for electronic components are given an antistatic treatment by increasing the conductivity of the plastic so that charge can be eliminated more readily or does not build up in the first place. In most cases, a surface resistance of $<10^{9}$ Ω/□ will ensure that a plastic is antistatic.

It should be noted that, apart from the antistatic treatment of photographic films, PEDT/PSS coatings could also be used for the antistatic treatment of other plastics, [77] as well as glass. Through the addition of appropriate binders, suitably coordinated with the particular substrate used, it is possible to achieve transparent to slightly gray coatings with a surface resistance ranging between 200 and 10^{7} Ω/□, suggesting that this material may prove useful in many other applications.

2.5.2 PEDT as an Electrode Material for Solid Electrolyte.

Capacitors

A second application for PEDT derivatives is their use as electrodes in solid electrolyte capacitors, as illustrated schematically in Figure 2.9 [78]. To prepare these capacitors, the surface of an aluminum or tantalum electrode was roughened by etching or metal powder was sintered, in order to attain a high surface area electrode with a high capacitance. A thin film of metal oxide, which would serve as a dielectric, was subsequently applied to the electrode by anodization. A counter-electrode was finally applied to complete the capacitor. In the preparation of conventional capacitors, this last step was performed by multiple impregnations with manganese nitrate solution and subsequent pyrolysis to form electrically conductive manganese dioxide [79].

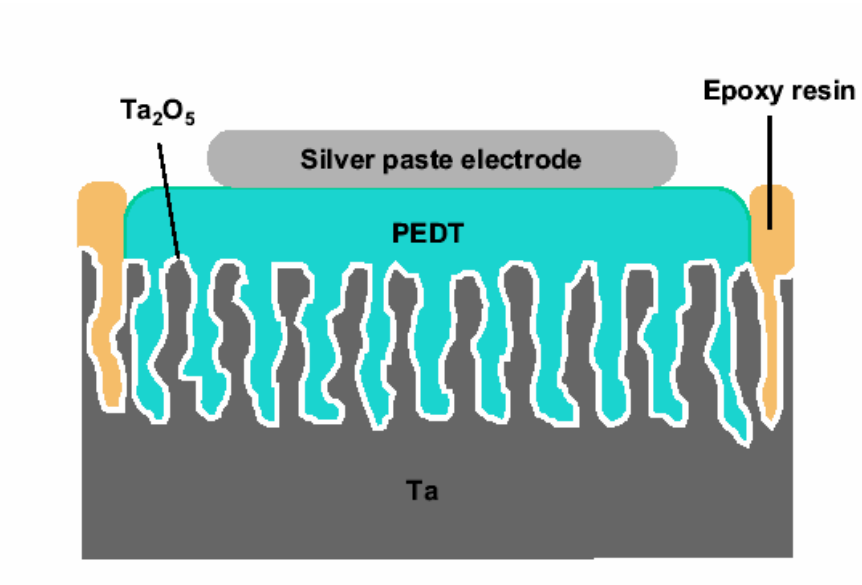

Figure 2. 9 Set-up of a PEDT-coated Ta/Ta2O5 Capacitor.

Bayer AG developed a process using PEDT and a simple impregnation step as opposed to pyrolysis or electrochemistry [80].In this new process, a solution of EDT and an oxidizing agent were coated onto a tantalum oxide-coated tantalum foil. Once the solvent was evaporated the EDT polymerizes, directly forming a counter-electrode of conductive PEDT. The capacitance of such capacitors is comparable to that of similar liquid electrolyte capacitors, but the high-frequency properties [81] were considerably better.

Sapp et al [82] constructed a series of dual polymer electrochromic devices (ECDs) based on 12 complementary pairs of conducting polymer films using PEDT-containing conducting polymers. Poly[3,6-bis(2-3,4-ethylenedioxythiophene))-N-methylcarbozole] (PEDT-NCH_3Cz), poly[3,6-bis(2-(3,,4-ethylenedioxythiophene))-N-eicosylcarbazole] (PBEDOT-$NC_{20}H_{41}Cz$), and poly[4,4'-bis(2-(3,4-ethylenedioxthiophene))biphenyl] (PBEDOT-BP)were utilized as anodically coloring polymers that electrochemically switch between an oxidized deep blue absorptive state and a transmissive (orange or yellow) reduced state. Poly(3,4-ethylenedioxythiophene) (PEDT) and its alkyl derivatives (PEDT-$C_{14}H_{29}$ and PEDT-$C_{16}H_{33}$) had been used as high-contrast cathodically coloring polymers that switch between a deep blue absorptive state in the reduced form and a sky blue, highly transmissive state in the oxidized form.

Inganas et al [83] made micron- and submicron-sized light-emitting diodes (LEDs) using conjugated polymers as electroluminescent layers and contact materials. Two different routes to make arrays of such small light sources had been developed. They discussed the benefits and drawbacks of the use of the conjugated polymer poly(2,3-ethylene-dioxythiophene) as hole injector in polymer LEDs .

2.5.3 Other Applications for PEDT Derivatives.

A new conductive adhesive epoxy system based on PEDT had been formulated and characterized by Chevrot et al [84]. They claimed that the bulk resistivity of that system (1ohms.cm) exceeds antistatic range (10^3 to 10^8 ohm.cm) obtained with a polyaniline-filled epoxed system. The threshold percolation was obtained with a PEDT concentration of 55%w/w. Thermal ageing studies showed that the conductive adhesive exhibits a good electrical stability up to 120^0C under a dry atmosphere and up to 60^oC under humid atmosphere (40% moisture content)[85].

Wehrmann et al [86] prepared light-emitting diodes LEDs by depositing three organic layers successively by spin-coating and evaporation techniques. The first layer of PEDT/PSS smoothed the indium-tin oxide (ITO) surface, reduced the probability of electrical shorts and was beneficial for a high overall yield of the operating devices. Above all, that layer promoted hole-injection as an important parameter for higher efficiencies and prolonged operation life. The results depicted in Figure 2.10 show that depositing PEDT/PSS onto ITO was beneficial not only for polymeric but also for molecular LEDs.

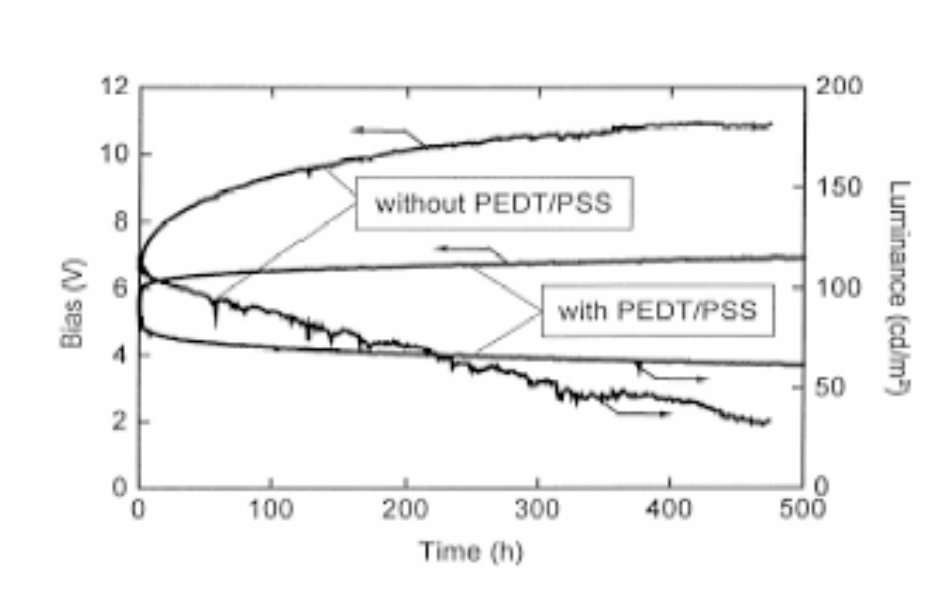

Figure 2. 10 Lifetime data of the three-layer and the two –layer device driven at constant current (I = 8 mA/cm^2). The bias and the luminance are monitored simultaneously. In the three-layer device, with the PEDT/PSS layer the lifetime is prolonged and the electrical noise due to micro-shorts is reduced.

They stated that the second layer of spin-coated dendritic phenylamines (TDAPB), with high glass transition temperature, modulates the injection of holes into the emitting layer formed by evaporated Alq. They compared the characteristics and operation lifetime data of devices with and without PEDT/PSS and it was shown that the combination of polymeric and monomeric organic layers leads to highly efficient devices, opening new ways to modify device architectures.

Besides the above-mentioned applications, PEDT-based polymers are currently, and will in the future be, applied in many other applications. Examples are through-hole plating of printed circuit boards, [87]antistatic coatings for cathode ray tubes to prevent dust attraction, [88] primers for electrostatic spray coating of plastics, [89] hole-injecting

layers on ITO substrates for organic electroluminescent devices,[90] transparent electrodes for inorganic electroluminescent devices (ITO replacement), [91] sensors, [92] re- chargeable batteries, cathode radiation tubes (CRTs), [93] photodiodes, [94] electrochromic windows, corrosion protection, [95] membranes for the preparation of 4Π beta radioactive sources, and photovoltaic devices. [96] Of utmost importance, these examples show that PEDT is one of the few organic conducting polymers that have successfully found its way from a laboratory curiosity into multiple technical applications.

2.6 Why Nanofibers?

Conductive polymers open the way for enormous applications due to its flexibility, lightweight besides the metallic electrical properties. Using these conductive polymers in the form of nanofiberous assemblies give us two directions of advantages. The first advantage, by using the fibrous form will give the opportunity of having electronic textiles and obtaining the tactile properties for different applications.
The second direction is using those fibers in nanoscale, which will provide the fundamental building blocks for the construction of devices and structures.

Unusual current conduction properties arise when the size of (nano) wires are reduced below certain critical thickness. Nabet [97] proposed that below certain critical thickness in (nano) wires current conduction will increase. Further, the rectifying contact to a wire will work better if the wire size is reduced below such a critical thickness. Hence, it's expected that the new wires and contacts, the diodes that form the building

blocks of electronics will behave more favorably when forced to operate in reduced dimensional regimes.

He classified the types of contact; to a nano wire exist, to three different types: Ohmic, Rectifying, and Tunneling. Ohmic contact is an ideal contact in which electron wave is not reflected from the wire. Current conduction is then the property of the wire, not the contact and is by definition the product of cross sectional area A, carrier concentration n, and carrier velocity v, ($I = A\ q\ n\ v$). However, below a critical thickness of A, carrier concentration changes due to change in density of states, and more importantly, the velocity of carriers is altered due to change in scattering. This is because the electrons in a 1D system can only scatter by completely reversing their direction; while in 2D and 3D they can scatter by change of angle of motion [98]. Hence, it is concluded that current conduction should increase below a critical diameter. This is schematically shown in Figure 2.11, where it's proposed that

$I(A_1) + I(A_2) > I(A_3)$ even though $A_3 = A_1 + A_2$

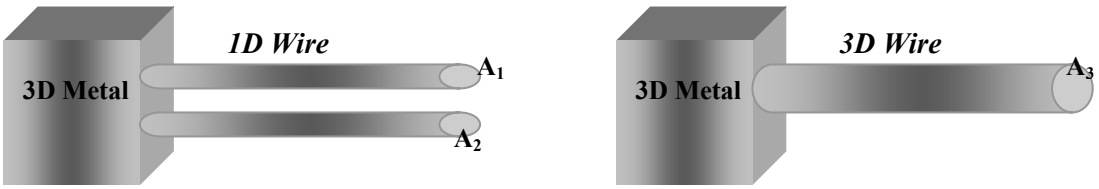

Figure 2. 11 Below a critical thickness the system in the left conducts more current than the one on the right even though they both have the same cross-sectional area. Metals from Ohmic contacts.

Rectifying (or schottky) contacts are produced in systems of different electron affinities. Current transports in these systems are based on kinetic energy requirements for motion form one system to another. Thermionic emission of carriers is the typical source of conduction in these systems. In a 3D-1D contact, calculation of themionic current consists of the carriers that have enough kinetic energy to overcome the barrier between the two systems. However, both carrier concentration and velocity change due to carrier confinement in a wire since: a) density of electronic states change, and b) electron energy is quantized. As a result the electrons that are emitted from metal to a nano wire have to occupy higher states causing a barrier height increase. Derivation [99] is reported showing a much higher barrier height and a different thermal signature compared to metal to bulk material. Hence, below critical thickness the system rectifies better. This is schematically shown in Figure 2.12, where it is proposed that $I(A_1) + I(A_2) > I(A_3)$ even though $A_3 = A_1 + A_2$

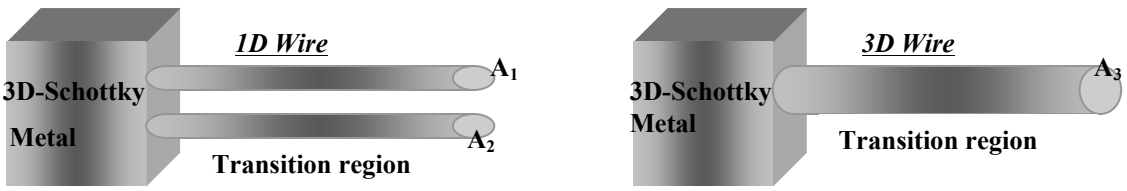

Figure 2. 12 Below a critical thickness the system in the left conducts less current (rectifies better) than the one on the right even though they both have the same cross-sectional area. Metals form rectifying Schottky contacts.

He mentioned [197] that tunneling contacts; since half a century ago it has been proposed that a 1D electron system should behave very differently for 2D and 3D systems due to interaction among its electrons. In a 1D system the electrons are collectively excited producing what is known as the Luttinger [100] (as opposed to Fermi) liquid. This property then alters the tunneling probabilities compared to 3D systems.

As illustrated in Figure 2. 13, by applying the conductivity equation $\sigma = L/(A*\Omega)$ to different cross-section size, it is concluded that; the lower the cross-section area, the higher the electrical conductivity. The circular cross-section possesses higher electrical conductivity values than the square cross- section. In order to transfer the conductive polymer into nanofibers, electrospinning process is used as it is the popular and simple method for that purpose.

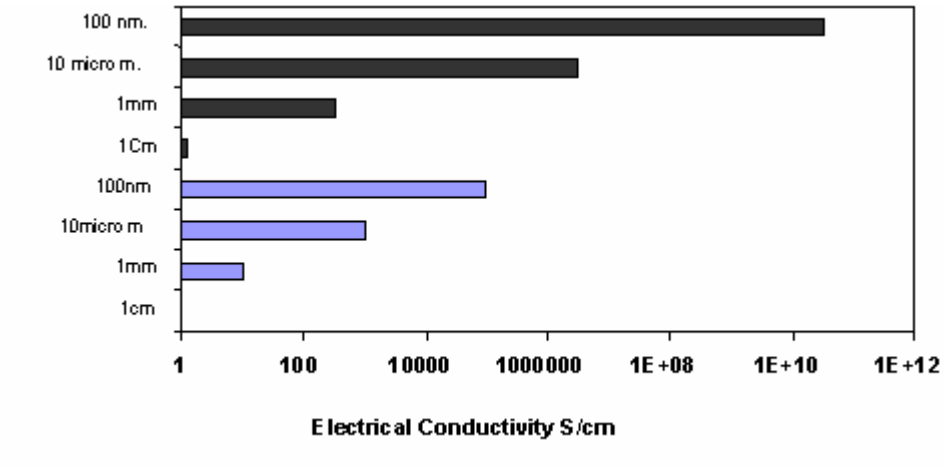

Figure 2. 13 Effect of fiber diameter on electrical conductivity.

Chapter 3: The Electrospinning Process.

3.1 Electospinning and Nanofibers Technology.

Electrospinning is a unique process in that it is able to produce ultra-thin fibers ranging from a few nanometers to several micrometers. Electrospinning is a simple process; it occurs when the electrical forces at the surface of a polymer solution or melt overcome the surface tension and force an electrically charged jet of polymer hit the surface of a grounded target.

As shown in Figure 3.1, a high electric field at the surface of a polymer liquid produces forces that are opposed to surface tension. For most polymer solutions, at electric fields smaller than the electrical breakdown strength of air, the electrical forces are greater than the surface tension. The charged liquid surface of the polymer is unstable, and charged jets of liquid are ejected. In a low molecular weight liquid, such a jet will quickly collapse into droplets. In a polymer solution, the jets often splay into many smaller fibers because of the radial forces produced by the charge on the fiber surface. The smaller fibers dry, leaving many continuous nanofibers. The nanofibers are collected on a flat metal screen, a rotating drum, in liquids, or in other ways. Non-woven sheets, typically about 100 microns thick, are produced. Nanofibers were electrospun form many kinds of synthetic polymers, DNA and other naturally occurring biopolymers, and polymer precursors of carbon and ceramic fibers.

A number of amazing characteristics arise when polymer fiber materials shrink in diameter from micrometers to sub-microns or nanometers. Among their important

properties, two that stand out are a very large ratio of surface area to volume, and superior mechanical performance (stiffness and tensile strength) compared to any other known fiber-material form. For example, textile fibers; with a diameter of 10 microns, have specific surface areas of around 700 square meters per kilogram, as calculated. Nanofibers with a diameter of 100 nm have specific surface areas 100 times greater.

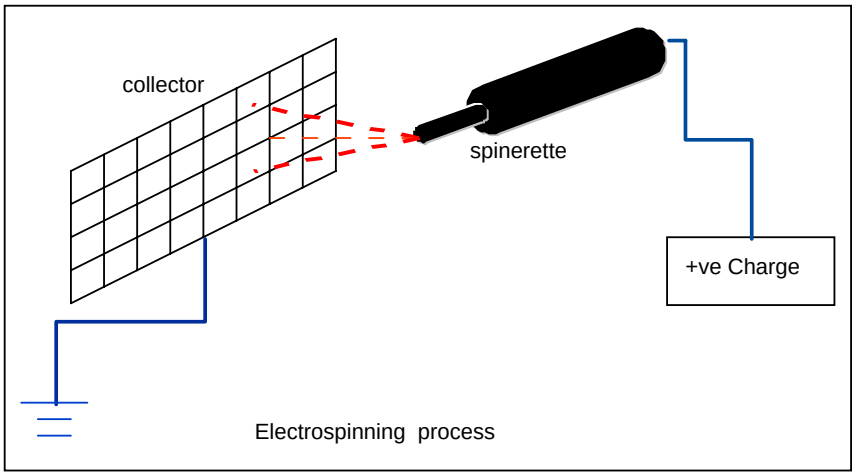

Figure 3. 1The Electrospinning Process.

These outstanding properties make polymer nanofibers optimal candidates for important applications such as filtration, biomedicine, protective clothing, electrical and optical use, nanosensors, and nanocomposites. In the following sections we will discuss electrospinning & nanofibers production, modeling, and applications.

3.1.1 Electrospinning and Nanofibers: Processing & Characterizations.

The electrospinning process has been documented for a long time. Threads of molten sealing wax were formed by using a high electric field in the early 20th century [101]. The electrospinning process was first patented by Formhals [102] in 1934 and he succeeded to make fine polymer fibers. An electrostatic fountain was invented by Vonnegut and Neubauer [103] and they mentioned that when the spray of droplets was illuminated with a beam of parallel white light, colors were seen.

In 1971, Baumgarten [104] produced acrylic micro-fibers by using electrical forces. The fibers diameters were in range from 0.05 to 1.1 microns. He populated that there is a relation ship between fiber diameters, jet length, solution viscosity; solution feed rate & surrounding gas. He indicated that spinning velocity probably reached and perhaps exceeded the velocity of sound in air. Electric field maps and other theoretical considerations showed that electric conductivity plays an important role in the spinning mechanism. Larrondo & Manely[105] moved a forward step by making continuous fibers of polyethylene & polypropylene using electric fields as the driving force.

Doshi & Renker[106,107] used electro-spinning to make fibers of water soluble poly(ethylene oxide) with diameters of 0.05 to 5 microns. They described the electrospinning process, the processing conditions, fiber morphology, and some possible uses of electrospun fibers. Reneker and Chun [108] stated that electrospinning provided a straightforward and practical way to produce polymer fibers with diameters ranging form 40-2000 nm.

Jaeger et al [109] observed chain packing in electrospun PEO via the atomic force microscope AFM. They concluded that at the molecular level the electrospun PEO

fibers posses a highly ordered surface layer. That ordered surface layer could be the result of the electrospinning process, or it could be a residue of the droplet formation.

Vancso et al [110] used the electrospinning technique to spin ultra-thin fibers from several polymer/solvent systems. The diameter of the electrospun fibers ranged from 16 nm to 2000 nm. They stated that the "beads on a string" morphology could be avoided if PEO was spun from solution in chloroform; the resulting fibers showed a lamellar morphology.

Gibson & Rivin [111] studied the transport properties of electrospun nanofibers mats& they mentioned that the electrospun layers present minimal impedance to moisture vapor diffusion required for evaporative cooling. While the beads phenomenon was studied by Reneker et al [112], they found that the formation of the beaded nanofibers could be considered as the capillary breakup of the electrospinning jets by surface tension, altered by the presence of electrical forces. The surface tension and viscoelestic properties of polymer solution are the key parameters in the process. Increasing net charge density favors formation of small diameter fibers. Decreasing the surface tension coefficient of the solvent favors the formation of larger diameter fibers.

Nanofibers of aromatic heterocyclic polybenzimidazole PBI were electrospun by Kim [113]. The diameter of these fibers was around 300 nm. The mechanical strength of the non-woven sheets of nanofibers was increased by treatment in sulfuric acid and heat.

Deitzel et al [114] evaluated systematically the effects of two of the most important processing parameters: Spinning voltage and solution concentration, on the morphology of the fibers formed. They found that spinning voltage was strongly correlated with the formation of bead defects in the fibers, and that current measurement

might be used to signal the onset of the processing voltage at which the bead defect density increased substantially. Solution concentration had been found to most strongly affect fiber size, with fiber diameter increasing with increasing solution concentration according to a power law relationship. In addition, electrospinning from solutions of high concentration had been found to produce a bimodal distribution of fiber sizes, reminiscent of distributions observed in the similar droplet generation process of electrospray.

Demir et al [115] had successfully produced ultra fine elastic fibers with submicron diameters by electrospinning of polyurethane urea solutions. Fiber diameters in the range 7 nm to 1500 nm were obtained by varying the solution concentration. He stated that fiber diameters increase as the third power of solution concentration. Viscosity, i.e. the concentration of the solution and temperature, was the dominant factor among the other solution properties. They found that it was possible to improve the fiber morphology by increasing the solution temperature. Fibers spun at high temperature were uniform unlike those obtained at room temperature. Moreover, high temperature made the electrospinning process quick, so it is an important advantage from the aspect of industrial applications.

The intrinsic structure [116] of PLA and PA6 fibers with diameters down to 50 nm do not differ to an appreciable extent from those found for much thicker fibers obtained by melt extrusion. Thin PVA/copper acetated composite fibers were prepared [117] by using sol-gel processing and the electrospinning technique. After calcinations of the above precursor fibers, CuO superfine fibers with a diameter of 100-200 nm could be successfully obtained.

Solutions of poly(ethylene-co-vinyl alcohol) or EVOH, ranging in composition from 56 to 71 wt% vinyl alcohol, could be [118] readily electrospun at room temperature from solutions in 70% 2-propanol/water (rubbing alcohol). Fiber diameters of ca. 0.2-8.0 μm were obtained depending upon the solution concentration, an attractive range for tissue engineering, wound healing, and related applications. Viswanathamurthi et al [119] prepared Niobium oxide/poly(vinylacetate) composite nanofibers by electrospinning. Pure ceramic niobium oxide fibers were obtained by high temperature calcinations of the organic-inorganic composite nanofibers. It was observed that both the morphology and the crystallinity of the fibers depend on the calcinations temperature.

The stress-strain behavior of an electrospun thermoplastic polyurethane was observed [120] and compared to the bulk material form which it was spun. The apparent molecular orientation in the electrospun fibers leaded to the pronounced reduction in elongation to failure of the electrospun mat, relative to the bulk.

Zong et al investigated [121] the microstructure, morphology and texture of electrospun poly(glycolide-co-lactide) non-woven membranes after post-draw and thermal treatments to tailor the degradation and mechanical properties. The crystal orientation improved significantly when the membrane was drawn and annealed. As the elongation ratio increased, the degree of orientation and the tensile strength were increased. The corresponding tensile retention time was also increased from 2 to 12 days during in vitro degradation.

3.1.2 Electrospinning and Nanofibers : Modeling & simulation.

The electrospinning process is a fluid dynamics related problem. In order to control the property, geometry, and mass production of the nanofibers, it is necessary to understand quantitatively how the electrospinning process transforms the fluid solution through a millimeter diameter capillary tube into solid fibers which are four to five orders smaller in diameter.

The first try to study the electrospinning process was introduced by Sir Taylor [122]. He introduced for the first time the "Taylor's cone" which by definition is the semi-vertical sphere of the polymer droplet when it suspended out from its vertices at the tip of the capillary. Taylor also showed that the critical voltage Vc (expressed in kilovolts) at which the maximum jet fluid instability develops is given by:

$$V_c^2 = 4\frac{H^2}{L^2}\left(\ln\frac{2L}{R} - 1.5\right)(0.117\pi.R.\gamma) \qquad \textbf{Equation 2. 1}$$

where H is the distance between the electrodes (the capillary tip and the collecting screen), L is the length of the capillary tube, R is the radius of the tube, and γ is surface tension of the fluid (units: H, L, and R in cm, γ in dyne per cm). In spinning, the flow beyond the spinneret is mainly elongational.

Hendricks et al [123] also calculated the minimum spraying potential of a suspended, hemispherical, conducting drop in air as

$$V = 300\sqrt{20\pi.r.\gamma} \qquad \textbf{Equation 2. 2}$$

where r is the jet radius. If the surrounding medium is not air but a nonconductive liquid immiscible with the spinning fluid, drop distortion will be greater at any given electric field and , therefore, the minimum spinning voltage will be reduced [124]. This means

that if the electrospinning process is encapsulated in vacuum, the required voltage will lower.

An estimate of the spinning rate was made [125] by measuring the length of PE fiber obtained in a known interval of time. The rate was of the order of 1 m min^{-1} and , it increased with the applied field strength. For the particular temperature (200^{o}C) at which the measurements wee made, the relation between the spinning rate and electric field strength E is of the form

$$rate = Ae^{bE} \qquad \textbf{Equation 2. 3}$$

Where A and b are constants with values 38.7 and 0.16, respectively, if the rate is expressed in cm min^{-1} and E in kV cm^{-1}.

Smith [126] studied the electrospinning phenomenon and introduced a relationship between the capillary radius plane distance and the applied voltage as:

$$V_o = A_1\left[\frac{2Tr\cos\theta_{oc}}{\varepsilon_o}\right]^{0.5}\ln\left(\frac{4h}{r_c}\right) \qquad \textbf{Equation 2. 4}$$

Where T, θ_o, and ε_o are surface tension, cone half angle, and permittivity of free space, respectively. He concluded that the capillary radius would be increased as the onset potential increased, the plane distance would increase with increasing the onset potential, and the surface tension would be in direct proportional with the onset potential.

The velocity profile inside the liquid cone at the base of an electrically driven jet was examined [127] by inserting tracer particles into the liquid. Observations of these particles at high magnification demonstrated the presence of an axisymmetric circulation

inside the cone due to interfacial electrical shear stress. That observation had led to a better understanding of the mechanism of electrostatic jet formation. An analytical solution was presented which predicts the velocity profile inside the cone. The surface velocity were expressed as

$$v_r = \frac{1}{r}\left(-B + 2C\cos\theta_o\right) + \frac{\dot{v}}{2\pi(1-\cos\theta_o)r^2} \qquad \textbf{Equation 2. 5}$$

where Band C are arbitrary constants, θ is the semi-cone angle, r is the spherical radius of the cone, $\dot{v}$ is the volumetric flow rate and $2\pi(1\text{-}\cos\theta_o)r^2$ is the steradian area of the cone.

Fang et al [128] introduced a relationship between the applied voltage, surface tension, air permittivity and capillary radius. Difference between the calculated jet diameter from the equation and the experimentally measured value had been recorded.

$$E = \sqrt{\frac{4\gamma}{\varepsilon_0 R}} \qquad \textbf{Equation 2. 6}$$

where E is the electrospinning voltage, R is the capillary radius, and γ is the surface tension.

Reneker et al [129] analyzed and explained the reasons for the instability, using a mathematical model. The rheological complexity of the polymer solution was included, which allowed consideration of viscoelastic jets. It was shown that the longitudinal stress caused by the external electric field acting on the charge carried by the jet stabilized the straight jet for some distance. Then a lateral perturbation grew in response to the repulsive forces between adjacent elements of charge carried by the jet. The motion of segments of the jet grew rapidly into an electrically driven bending instability. The

three-dimensional paths of continuous jets were calculated, both in the nearly straight region where the instability grew slowly and in the region where the bending dominated the path of the jet.

Shin et al[130,131,132] investigated the stability of electrospinning PEO jet using a technique of asymptotic expansion for the equations of electro-hydrodynamics in powers of the aspect ratio of the perturbation quantity, which was the radius of the jet and was assumed to be small. After solving the governing equations thus obtained, they found that the possibility for three types of instabilities exists. The first is the classical Rayleigh instability, which is axisymmertic with respect to the jet centerline. The second is again an axisymmetric instability, which may be referred to as the second axisymmetric instability. The third is a nonaxisymmetric instability, called "whipping" instability, mainly by the bending force. Keeping all the other parameters unchanged, the electric field strength will be proportional to the instability level. Namely, when the field is the lowest, the Rayleigh instability occurs, whereas the bending (or whipping) instability corresponds to the highest field. Shin et al have also experimentally observed that the phenomenon of so-called "inverse-cone" in which the primary jet was thought to be split into multiple jets is actually caused by the bending instability.

Regarding the fluid jet diameter, Baumgarten [4] noticed that as viscosity of the polymer solvent increased, the spinning drop changed from approximately hemispherical to conical. By using equi-potential line approximation calculation, he obtained an expression to calculate the radius r_o of a spherical drop (jet) as follow

$$r_o^3 = \frac{4\varepsilon \dot{m}_o}{k\pi\sigma\rho} \qquad \textbf{Equation 2. 7}$$

where ε is the permittivity of the fluid (in coulombs/volt-cm), $\dot{m}_0$ is the mass flow rate (gram/sec) at the moment were r_o is to be calculated, k is a dimensionless parameter related with the electric currents, σ is the electric conductivity (amp/volt cm), and ρ is density (g/cm^3).

Spivak et al [133] formulated a general electro-hydrodynamic model of a weakly conductive viscous jet accelerated by an external electric field, taking into account inertial, hydrostatic, viscous, electric, and surface tension forces. Nonlinear rheologic constitutive equation for jet radius was derived and analyzed which is

$$R^* = 2\left[\varepsilon_o \sigma_s\right]^{1/3}\left(\frac{Q}{J}\right)^{2/3} \qquad \textbf{Equation 2. 8}$$

where σ_s is the coefficient of surface tension, ε_o is the permittivity of vacuum, Q is the volumetric flow rate, and J is the electric current. The model predictions were in agreement with experimental observations. They stated that the mathematical model could be used for better control and optimization of the electrospinning process.

The Berry number has been re-introduced by Ko et al [134]. They studied the influence of polymer molecular conformation in solution, described by Berry number *Be*, on a electrospun poly(L-lactic acid)/chloroform system giving the following equation:

$$Be = [\eta]c \qquad \textbf{Equation 2. 9}$$

where[η] is the intrinsic viscosity of the polymer ([η]=the ratio of specific viscosity to concentration at infinite dilution) and c is the concentration of the solution. It had been

found that the degree of entanglement of polymer chains in solution could be described by *Be* [135]. When the polymer is in a very dilute solution, polymer molecules are so far apart in the solution that individual molecules rarely touch each other and *Be* is less than unity. When the polymer concentration is increased, at some overlap concentration the individual molecules interact and therefore become entangled; *Be* is then greater than unity.

A characteristic feature of the electrospinning process is the onset of a chaotic oscillation of the electrospinning jet. Deitzel et al [136] demonstrated the feasibility of dampening that instability and controlling the deposition of sub-micron polymer fibers on a substrate through use of an electrostatic lens element and collection target of opposite polarity.

3.1.3 Electrospinning and Nanofibers : Applications.

One of the most important applications of traditional (micro-size) fibers, especially engineering fibers such as carbon, glass, and Kevlar fibers, is to be used as reinforcements in composite developments. With these reinforcements, the composite materials can provide superior structural properties. Needless to say, nanofibers will also eventually find important applications in making nanocomposites. This is because nanofibers can have even better mechanical properties than micro fibers of the same materials, and hence the superior structural properties of nanocomposites can be anticipated.

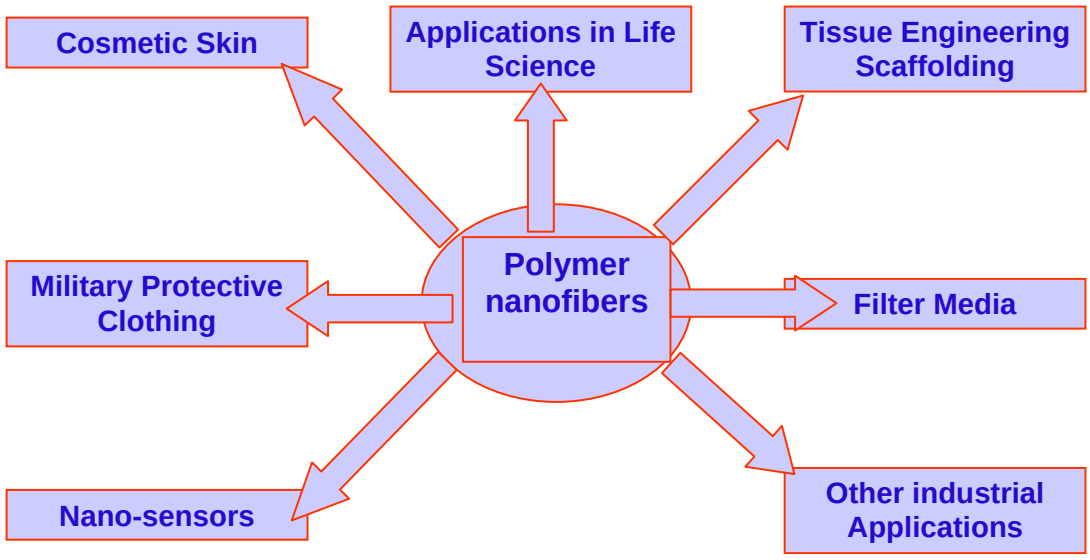

Figure 3. 2 Potential applications of electrospun polymer nanofibers.

In addition to composite reinforcement, other application fields based on electrospun polymer nanofibers have been steadily extended especially in recent years. More extended or perspective application areas are summarized in Figure 3.2.

Thin fibers of calf thymus Na-DNA were electrospun [29] from aqueous solutions with concentrations from 0.3 to 1.5%. The electrospun DNA fibers had diameters around 50 to 80 nanometers. During electrospinning a process called splaying caused the jet to split longitudinally into two smaller jets, which split again, repeatedly, until the very small diameter fibers were formed. The small diameter fibers were transparent in ordinary 100 kV electron microscopes. Fibers could be spun from samples of DNA as small as one milligram.

Chun et al produced [137] carbon nanofibers using electrospinning techniques. Electrospun carbon precursor fibers, based on polyacrylonitrile and mesophase pitch, having diameters in the range from 100 nm to a few microns, were stabilized and carbonized. These carbon nanofibers had a very high aspect ratio. Nanopores were produced in carbon nanofibers made from the polyacrylonitrile by a high temperature reaction with water vapor carried in nitrogen gas, a process which is known to increase the surface area per unit mass of carbon black.

Kim et al showed [138] the reinforcing effects of nanofibers in an epoxy matrix and in a rubber matrix using electrospun nanofibers of PBI (poly-benzimidazole). The average diameter of the electrospun fibers was around 300 nm. The nanofibers toughened the brittle epoxy resin. The fracture toughness and the modulus of the nanofiber (15 wt%)-reinforced epoxy composite were both higher than for an epoxy composite made with PBI fibrils (17wt %), which were whisker-like particles.

The process of electrostatic fiber formation, or electrospinning, was used [139] to create biocompatible thin films for use in implantable devices. The morphology of the thin films was found to depend on process parameters including solution concentration, applied electric field strength, deposition distance, and deposition time. A shish kebab model for the filament morphology was proposed. The electrospinning process was shown to be a means of creating porous thin films with structural gradients and controlled morphology that could enhance biocompatibility.

In addition to round nanofibers, electrospinning a polymer solution could produce thin fibers with a variety of cross-sectional shapes. Branched fibers, flat ribbons, ribbons with other shapes, and fibers that were split longitudinally form larger fibers

were observed [140]. The transverse dimensions of these asymmetric fibers were typically 1000 to 2000 nm, measured in the widest direction. The observation of fibers with these cross-sectional shapes from a number of different kinds of polymers and solvents indicated that fluid mechanical effects, electrical charge carried with the jet, and evaporation of the solvent all contributed to the formation of the fibers.

Huang et al [141] produced elastin-mimetic protein fibers and fiber networks by elecrospinning an aqueous solution of a genetically engineered 81 KD peptide polymer. Fibers were generated at ambient temperature and pressure with optimal fiber formation observed with use of an 18 kV electric field and a 15 cm distance between the spinnerette and plated collector. Image analysis of non-woven fabrics produced from a solution concentration of 15 wt% revealed the isotropic orientation of individual fibers with an average fiber diameter of 450 nm. The ultimate tensile strength of these non-woven fabrics was 35 MPa and the material modulus 1.8 GPa.

For conductive CN/Polymer composite fibers to be obtained [142], CNs were incorporated into poly(vinylidene fluoride) (PVDF) in dimethylformamide (DMF) solutions and electrospun to form CN/PVDF fiber mats. The thinnest fiber was 70 nm in diameter. Zeng et al [143] examined the influences of surfactants and medical drugs on the diameter size and uniformity of electrospun poly(L-lactic acid)PLLA fibers by adding various surfactants (cationic, anionic, and nonionic) and typical drugs into the PLLA solution. Significant diameter reduction and uniformity improvement were observed. It was shown that the drugs were capsulated inside of the fibers and the drug release in the presence of proteins K followed nearly zero-order kinetics due to the degradation of the PLLA fibers.

Figure 3. 3 Nanofibers for wound dressing (www.electrosols.com).

Polymer nanofibers can also be used for the treatment of wounds or burns of a human skin, as well as designed for haemostatic devices with some unique characteristics. With the aid of electric field, fine fibers of biodegradable polymers can be directly sprayed/spun onto the injured location of skin to form a fibrous mat dressing ;as shown in Figure 3.3, which can let wounds heal by encouraging the formation of normal skin growth and eliminate the formation of scar tissue which would occur in a traditional treatment [144].

Min et al [145] introduced the silk fibroin SF nanofiber non-woven produced by the electrospinning process for the application of wound dressing. The SF nanofibers were characterized by a wide range of pore size distribution, high porosity, and high surface area-to-volume ratio, which were favorable parameters for cell attachment, growth, and proliferation. Fibers with nanoscale diameters provide benefits due to high

surface area for biomaterial scaffolds. Electrospun silk fibroin-based fibers with the average diameter of 700±50 nm were prepared [146] from aqueous regenerated silkworm silk solutions. Adhesion, spreading and proliferation of human bone marrow stromal cells BMSCs on these silk matrices were studied.

Xu et al [147] succeeded in constructing a unique biodegradable polymer nanofibrous scaffold with aligned architecture by electrospinning. Favorable interactions between the SMCs and the unique scaffold as well as a directional growth of the cells along the fiber orientation were demonstrated by cell morphology, adhesion and proliferation studies. These results strongly suggest a huge potential of this "ideal" scaffold for blood vessel engineering.

3.2 Electrospinning of conductive polymers.

Previous work has been done to produce conductive nanofibers. Electrostatic fabrication of ultrafine conducting fibers was introduced by Ko et al [148]. Ultrafine fibers of Polyaniline doped with camphorsulfonic acid (PANi.HCSA) blended with PEO were prepared by the electrospinning technique. The morphology and fiber diameter of electrospun PANi blend fibers revealed that both the PEO and PANi.HCSA/PEO blend fibers had a diameter ranging between 950 nm and 2100 nm, with a generally uniform thickness along the fiber. The rate for the vapor phase de-doping/re-doping of the electrospun fibers was at least one order of magnitude faster than for cast films, stressing the enormous effect an increase in the surface-to-volume ratio, accomplished by electrospinning the material into fibers, could have on the selected chemical properties of PANi blends. Long nanofibers of conducting electronic polymers and their blends and

also conventional polymers were conveniently fabricated [149] in air by electrospinning. All fibers in a given preparation of certain polymers had diameters<100nm. Fibers of 100% doped PANi as well as its blends in polymers such as PS and PEO had been prepared. Current/voltage in addition to conductivity/temperature relationships of single fibers as small as 419 nm had been obtained. PAN and PS fibers could be easily and uniformly coated from aqueos solution with conducting polypyrrole or with gold by electroless deposition. Figure 3. (4-6) show the electrospun fibers of different conductive polymers [148,149]

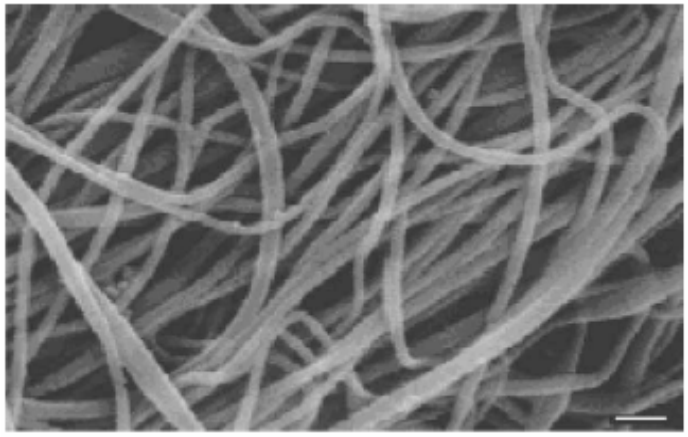

Figure 3. 4 Conducting polypyrrole-coated polyacrylonitrile nanofiber.(1000 nm sacle bar).

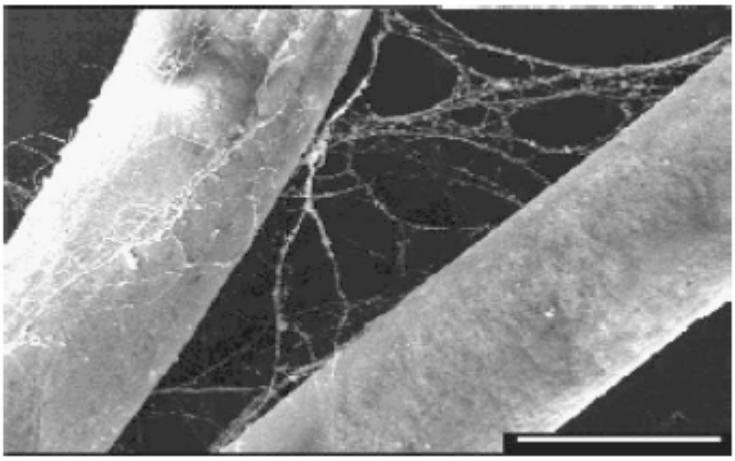

Figure 3. 5 Polystyrene fibers collected on a bent copper wire and subsequently coated with a thin layer of polypyrrole by in situ deposition from aqueous solution.

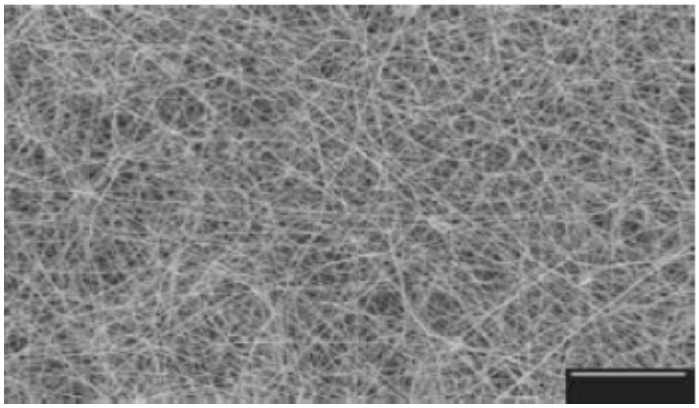

Figure 3. 6 Nanofibers mat of 2wt.% PAni.HCSA & 2wt.% PEO from chloroform solution at 25 kV.(100,000nm scale bar).

Micron size diameter fibers of 2-acrylamido-2-methyl-1-propanesulfonic acid doped polyaniline were prepared [150] via electrospinning. The conductivity of individual fibers was found to be lower than that of a cast film of the same polymer. Using the electroless deposition technique, the fibers were coated with thin films of nickel.

In order to further enhance the electrical conductivity of the electrospun conductive fibers and the mechanical properties, carbon nanotubes were co-electrospun with the conductive polymer. The following chapter will discuss the carbon nanotubes, their properties characterizations and applications.

Chapter 4: Carbon Nanotubes.

Since the discovery of carbon nanotubes (CNTs) by Iijima [151], they have been the focus of intense investigations due to their new and unique properties. These offer the potential for exciting applications such as ultrastrong wires, nanoelectronic devices, field electron emitters, nanoprobes, nanocomposite materials, and more [152]. However, realization of their excellent properties in many cases is hampered by processing difficulties. Carbon nanotubes (Figure 4. 1-b) are tiny strips of graphene sheet (the pure, brittle form of carbon in your pencil lead) rolled into tubes a few nanometers in diameter and up to hundreds of micrometers in length. The graphene (Figure 4. 1-a) has a network of hexagonal rings, leaving it with many unpaired electrons. There are two main types of carbon nanotubes that can have high structural perfection. Single-walled nanotubes (SWNTs) consist of a single graphene sheet seamlessly wrapped into a cylindrical tube (Figure 4. 1-b). Multi-walled nanotubes (MWNTs) comprise an array of such nanotubes that are concentrically nested like rings of a tree trunk (Figure 4. 1-c).

Carbon nanotubes conduct electricity and heat amazingly well, so they are being considered for use as wires for nanosized electronic devices in future computers, charge-storage devices in batteries, and electron guns for semiconductor chip etching and flat-screen televisions and computer monitors. They also could store hydrogen gas to power fuel cells. Furthermore, carbon nanotubes are the world's strongest material in terms of tensile strength and they are light weight and flexible. Consequently, they could be useful as ultralight structural materials for wings of advanced aircraft and space probes

to make them stronger and more energy efficient. Thus, there is an intense interest in finding a way to produce nanotubes in large quantities. In the following section we will discuss the synthesis, characterizations, properties and applications of CNTs.

Despite being structurally similar to a single grapheme sheet , which is a semiconductor with a zero band gap, SWNTs may be either metallic or semiconducting, depending on the sheet direction about which the graphene sheet is rolled to form a nanotube cylinder [153]. This direction in the graphene sheet plane and the nanotube diameter are obtainable from a pair of integers (*n.m*) that denote the nanotube type [154]. Depending on the appearance of a belt of carbon bonds around the nanotube diameter, the nanotube is either of the armchair ($n = m$), zigzag ($n = 0$ or $m = 0$), or chiral (any other n and m) variety. All armchair SWNTs are metals; those with $n - m = 3k$, where k is a nonzero integer, are semiconductors with a tiny band gap; and all others are semiconductors with a band gap tat inversely depends on the nanotube diameter.

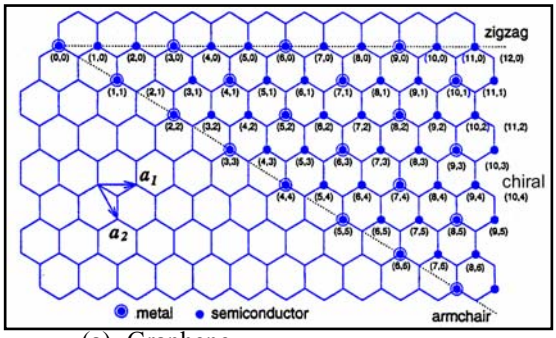

(a)- Graphene

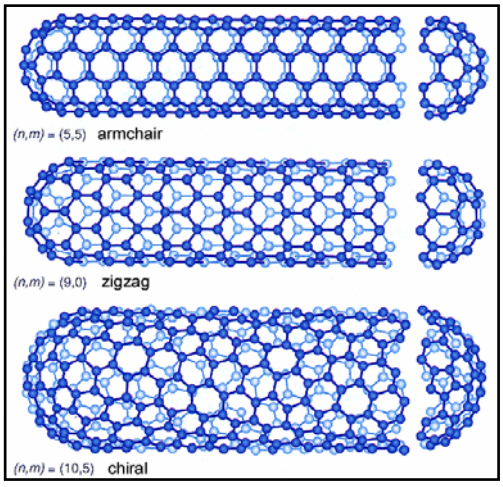

(b)- Single-Walled Nanotubes (SWNT)

(c)- Multi-Walled Nanotubes (MWNT)

Figure 4. 1 Different types of carbon nanotubes.

4.1 Synthesis, Characterizations, and Properties of Carbon Nanotubes.

SWNTs and MWNTs are usually made by carbon-arc discharge, laser ablation of carbon, or chemical vapor deposition (typically on catalytic particles) [155]. Nanotube diameters range form ~0.4 to >3 nm for SWNTs and from ~1.4 to at least 100 nm for MWNTs. Nanotube properties can thus be tuned by changing the diameter. Unfortunately, SWNTs are presently produced only on a small scale and are extremely

expensive: High-purity samples cost about $750/g, and samples containing substantial amounts of impurities cost about $60/g [156]. Many researchers have depended on production facilities started by Rick Smalley of Rice University for purified SWNTs, on laser ablation-produced nanotubes, and now on the high-pressure carbon monoxide (HiPco) nanotubes of Carbon Nanotechnology, Inc. (CNI). CNI "hopes to make around 9 kilograms a day by 2004" [157]; it is hoped that this will bring the price down. All currently known synthesis methods for SWNTs result in major concentrations of impurities. Carbon-coated metal catalyst contaminates the nanotubes of the HiPco route, and both carbon-coated metal catalyst and, typically, ~60% forms of carbon other than nanotubes are formed in the carbon-arc route [94]. These impurities are typically removed by acid treatment, which introduces other impurities, can degrade nanotube length and perfection, and adds to nanotube cost. Another problem, especially for electronic devices, is that the usual synthetic routed result in mixtures of various semiconducting and metallic nanotubes. Metallic SWNTs can be selectively destroyed by electrical heating, so that only the semiconducting nanotubes needed for nantube field-effect transistors (NT-FETs) survive [158]. However no route to substantial quantities of SWNTs of one type is known.

Single wall nanotube reinforced polyimide nanocomposites were synthesized by in situ polymerization of monomers of interest in the presence of sonication [159]. This process enabled uniform dispersion of (SWNT) bundles in the polymer matrix. The pre-dispersed SWNT dispersion remained stable throughout the reaction under sonication, producing reasonably transparent, electrically conductive SWNT-CP2 nanocomposites at very low SWNT fraction. Volume conductivity of the SWNT-SP2 nanocomposite

films was measured, and is shown in Figure 4. 2. The conductivity of the pristine CP2 polyimide was 6.3 x 10-18 S/cm. The resultant SWNT-polymer nanocomposite exhibited significant conductivity enhancement (10 orders of magnitude) at a very low fraction (0.1 vol%) without significantly sacrificing optical transmission.

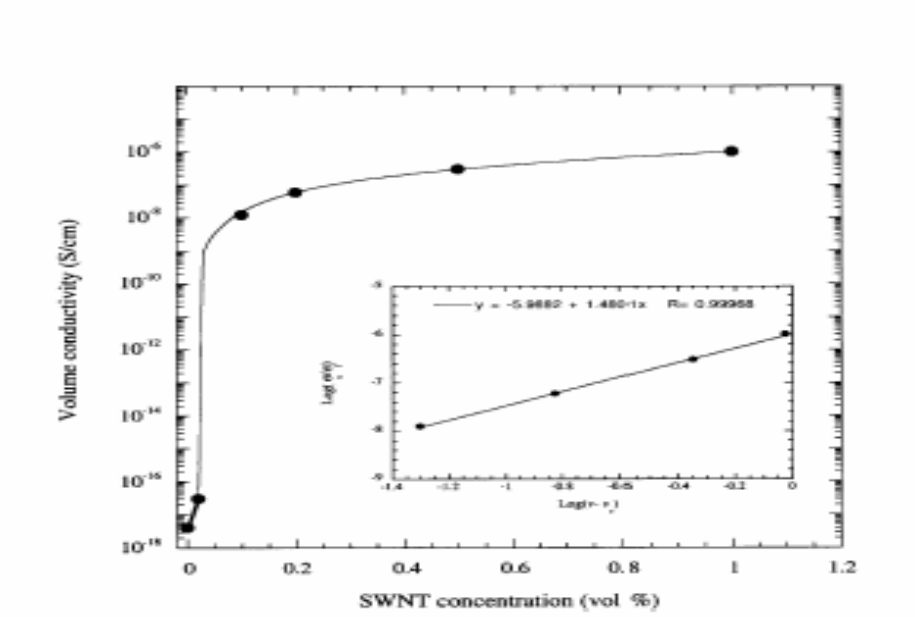

Figure 4. 2 Volume conductivity of SWNT-CP2 nanocomposites. The inset is a power law plot of the conductivity of the nanocomposite with ($\nu - \nu_c$) on logarithmic scale.

Ata et al [160] reported a scalable method for purification and alignment of single-walled carbon nanotubes in and aqueous solution. Arc-synthesis soot containing SWNTs was first treated with a concentrated nitric acid. After removal of most of the impurities and water, macroscopic and well-aligned SWNT bundles up to several centimeters long were formed in a rotary evaporator. Alignment of the SWNT bundles was ascribed to the liquid flow induced by rotary evaporation and van der Waals

interactions among the bundles. The aligned SWNT bundles were further purified by ultrasonic Soxhlet extraction and annealing.

Schattka et al described the transformation of cellulose acetate filters into porous carbon structures by a facile, direct process [161]. Filters from cigarettes were used as the source for cellulose acetate filters. Carbon was obtained by high-temperature treatment under inert conditions without extensive preparative methods. The resulting carbon materials showed structural features on different length scales ranging from the micrometer to the nanometer scale. Single-walled carbon nanotubes had been solubilized in water by non-covalently associating then with linear polymers, most successfully with polyvinyl pyrrolidone and polystyrene sulfonate [162]. That association was characterized by a tight, uniform association of the polymers with the sides of the nanotubes. A general thermodynamic drive for this wrapping was discussed, wherein the polymer disrupts both the hydrophobic interface with water and the smooth tube-tube interactions in aggregates. The nanotubes could be unwrapped by changing the solvent system. This solubilization provides a route to more precise manipulation, purification, fractionation, and functionalization than was possible before, as well as allowing SWNTs to be introduced to biologically relevant systems.

Niyogi et al stated that the dispersion of SWNTs in o-dichlorobenzene (ODCB) leads to the formation of a sonopolymer [163], which adheres to the nanotube surface. If that polymer was prevented from forming, nanotubes wouldn’t form stable dispersions in ODCB. The chemical interaction of the sonopolymer with the SWNTs was found to be irreversible, and, under conditions that might be expected to remove covalent functionalities, degradation of the SWNTs was observed.

Regev et al [164] presented a simple method for unbundling as-produced (unmodified, long) carbon nanotubes in an aqueous solutions of Gum Arabic. The resulting stable dispersion may be dried into an "instant" ready-for-use powder of individual carbon nanotubes. The unbundling and stabilization of the single tubes in solution was demonstrated unequivocally by a combination of X-ray scattering and cryo-TEM imaging. While the former indicated the loss of intertube ordering, i.e., the disruption of the ropes, the latter provided a direct visualization of the individual SWNT. They stated that, the use of GA for stabilization of SWNT dispersions offers a few advantages.

Iijima et al [165] studied the distribution of pentagons and shapes in carbon nanotubes and nanoparticles. The way pentagons were distributed on a closed surface consisting of hexagons and pentagons determines the surface topology. The presented high-resolutions electron microscopy images of carbon nanotubes and nanoparticles, and showed the symmetric and asymmetric distribution of pentagons at their end surfaces.

Islam et al demonstrated a simple scheme to solubilize high weight fraction single-wall carbon nanotubes in water [166]. Suspension concentrations were improved by a factor of 10-100 with respect to commonly used surfactants, and the new sonication technique also dramatically reduced tube fragmentation. Preliminary transport measurements on these tubes suggested that their treatment did not alter the SWNT electronic properties.

Ebbesen et al observed exceptionally high Young's moduli for individual carbon nanotubes [167]. Carbon nanotubes were predicted to have interesting mechanical properties—in particular, high stiffness and axial strength—as a result of their seamless

cylindrical graphitic structure. Their mechanical properties have so far eluded direct measurement, however, because of; the very small dimensions. Atomic force microscopy (AFM) was used to [168] determine the mechanical properties of individual, structurally isolated silicon carbide SiC nanorods (NRs) and multiwall carbon nanotubes (MWNTs) that were pinned at one end to molybdenum disulfide surfaces. The bending force was measured versus displacement along the unpinned lengths. The MWNTs were about two times as stiff as the SiC NRs. Continued bending of the SiC NRs ultimately led to fracture, whereas the MWNTs exhibited an interesting elastic buckling process.

De Heer et al [169] studied the electrostatic deflections and electromechanical resonances of carbon nanotubes. Static and dynamic mechanical deflections were electrically induced in cantilevered, multiwalled carbon nanotubes in a transmission electron microscope. The elastic bending modulus as a function of diameter was found to decrease sharply (from about 1 to 0.1 terapascals) with increasing diameter (from 8 to 40 nanometers), which indicated a crossover form a uniform elastic mode to an elastic mode that involves wavelike distortions in the nanotube.

Rao et al [170] measured the Raman spectrum of individual single walled carbon nanotubes in solution and compared it to that obtained form the same starting material where the tubes were present in ordered bundles or ropes. Interestingly, the radial mode frequencies for the tubes in solution were found to be ~10 cm^{-1} higher than those observed for tubes in a rope, in apparent contradiction to lattice dynamics predictions. They suggested that there is no such contradiction, and propose that the up-shift was due rather to a decreased energy spacing of the Van Hove singularities in isolated tubes over the spacing in a rope, thereby allowing the same laser excitation to excite different

diameter tubes in these two samples. A typical Raman spectrum of the EA-derived SWNT bundles obtained using the 1064 nm excitation wavelength exhibits two prominent features at ω_R~ 160 cm^{-1} (radial band) and ω_T ~ 1590 cm^{-1} (tangential band). The position and the line shape of these bands had been used extensively to determine the SWNT diameter distribution. For an isolated SWNT, theoretical calculations had shown that the radial mode frequency ω'_R exhibits a particularly simple dependence on the tube diameter d' as

$$\omega'_R \sim 224\ cm^{-1} \cdot nm / d' \qquad \text{Equation 2. 10}$$

(Henceforth, primed and unprimed notation corresponds, respectively, to isolated and bundled SWNTs). Equation 2.11 had been widely used to determine the tube diameter distribution in samples containing both isolated and bundled nanotubes, since Raman spectroscopy provides a quick and convenient technique for sample characterization. In case of bundled SWNTs, Equation 2.1 was modified as

$$\omega'_R \sim 224\ cm\text{-}1 \cdot nm / d' + \Delta\omega_R, \qquad \text{Equation 2. 11}$$

where $\Delta\omega_R$ is the anticipated up-shift due to tube-tube interactions which is independent of the tube diameter in the restricted range of diameters ($\Delta\omega_R \sim 14$).

Raman spectra were performed [171] on the double-walled carbon nanotubes DWNTs at different E_{laser} of excitation. The interlayer distance of the DWNTs calculated from radial breathing mode RBM varied from 0.335 to 0.42 nm. The D-band of the carbon nanotubes could be expressed as $\omega_D = \omega_0 + 26.5\ E_{laser}$, where ω_0 was about 1260 cm^{-1} for DWNTs, 1270 cm^{-1} for single-walled carbon anotubes SWNTs and 1285 cm^{-1} for multi-walled carbon nanotubes MWNTs.

Electrical conductivities of individual multi-wall carbon nanotubes were measured [172] using a micro manipulator by a two probe method. The nanotubes were 15 ~ 25 nm in diameter and longer than 20 μm in length. The resistance of tubes was several kΩ/μm, which gave the average conductivity as 1,000 ~ 2,000 S/cm. The current-voltage characteristics at high field were also studied until the dielectric breakdown took place.

A study of the possibilities of the scanning force microscope (SFM) for studying transport properties of CNTs was done by de Pablo et al [173]. SWNTs were deposited on SiO_2. Afterwards, using a mask, the surface was covered with gold, so that some of the CNTs in the surface stick out underneath the fold. In those areas, topographies and electrical measurements with metallic cantilevers were carried out. They developed simultaneous force vs. distance and current vs. distance data along the uncovered length of the nanotubes.

Enomoto et al [174] studied low temperature transport in MWNTs by means of a three-terminal measurement in order to discuss on the contact resistance between the electrode and the nanotube. The net resistance of MWNT and the contact resistance between the MWNT and electrode was determined. No evidence for the exponential behavior was found down to 1 K for both resistances, but the power-law temperature dependence was found. They discussed those power-law behaviors so as to try to fit those into Tomonaga-Luttinger model.

Ultra-small single-walled carbon nanotubes (SWNTs) were successfully fabricated [175] in the channels of zeolite $AlPO_4$-5 (AFI) single crystals by pyrolysis of triproplamine molecules in the channels. These nanotubes had been observed directly by

TEM, as well as by diffuse X-ray scattering and micro-Raman measurements of the nanotube breathing mode. The data consistently indicated a nanotube diameter of as small as 0.4 nm, probably at or close to the theoretical limit. These mono-sized small nanotubes perhaps constituted the best example of one-dimensional (1-D) quantum wires. Corio et al [176] presented a Raman study of SWNTs subjected to high laser intensities. They had observed two irreversible changes in the Raman spectra of the carbon nanotubes induced by a local high temperature. The first one was due to the thermal annealing of structural defects in the as-grown sample, which results in the formation of a more ordered structure of carbon nanotubes. The second effect was the burn off of smaller diameter nanotubes, thus increasing the mean diameter of the nanotube sample which remained after the laser irradiation process.

4.2 Applications and Carbon Nanotube Composites.

The first realized major commercial application of MWNTs was their use as electrically conducting components in polymer composites. Depending on the polymer matrix, conductivities of 0.01 to 0.1 S/cm can be obtained for 5% MWNTs; much lower conductivity levels suffice for dissipating electrostatic charge [93].

De Pablo et al developed [177] a simple method for attaching robust, metallic contact pads to both ends of an individual MWNT. While only a few of the samples studied had been described, they found that MWNTs prepared in that way routinely withstand currents up to a few mA. I(V) data at room temperature indicated a rich behavior which could be qualitatively understood by considering the electronic properties of individual “shells” within the MWNT. They had also conducted

preliminary experiments and had established that MWNT samples prepared in that way could withstand cooling to temperatures of 77 K.

The mechanical behavior of MWNTs/epoxy composites was studied in both tension and compression [178]. It was found that the compression modulus was higher than the tensile modulus, indicating that load transfer to the nanotubes in the composite was much higher in compression. Composites of uniaxially oriented multiwalled carbon nanotubes embedded in polymer matrices were fabricated and investigated by TEM [179]. In strained composite films, buckling was ubiquitously observed in bent nanotubes with large curvatures. By analyses of a large number of bent nanotubes, the onset buckling strain and fracture strain were estimated to be ~ 5% and ≥ 18%, respectively.

Zhou et al reported [180] a method to fabricate polymer-based composites with aligned carbon nanotubes, and a procedure to determine the nanotube orientation and the degree of alignment. The composites were fabricated by casting a suspension of carbon nanotubes in a solution of a thermoplastic polymer and chloroform. They were uniaxially stretched at 100 ^{o}C and were found to remain elongated after removal of the load at room temperature.

Winey et al demonstrated [181] the successful fabrication of nanocomposite films and fibers consisting of a PMMA matrix with ≤ 8 wt% SWNTs. Melt mixing promoted nanotube dispersion and should be applicable to most thermoplastic matrix polymers. The high draw ratios (λ = 20-3600) available in melt spinning align the SWNTs along the fiber axis such that the mosaic distribution FWHM was as small as 4^{o}. Due to the alignment of the SWNTs, these PMMA-SWNT nanocomposite fibers showed

improved mechanical properties, and the nanocomposite films showed increased electrical conductivity.

Successful dispersion of high purity single wall carbon nanotubes (laser and HiPco) was achieved [182] in the Nafion polymer at doping levels between 0.1 and 18% w/w. Due to the electrical conductivity of high aspect ration SWNTs and the resulting efficient percolation pathways within the polymer composites, they exhibited superior performance as actuators when compared to metal-doped Nafion films.

R. Smalley et al [183] synthesized Poly(p-phenelyne benzobioxazole) (PBO) in the presence of single wall carbon nanotubes (SWNTs) in poly(phosphoric acid) (PPA) using typical PBO polymerization conditions. PBO and PBO/SWNT lyotropic crystalline solutions in PPA had been spun into fibers using dry –jet wet spinning. They recorded that the tensile strength of the PBO/SWNT fiber containing 10% SWNTs is about 50% higher than that of the control PBO fibers containing no SWNTs by 50% and reduction in shrinkage with high-temperature creep.

A study on the interaction between SWNTs and the soluble polymer poly(3-octylthiophene) (P3OT) was presented [184]. Composites of SWNTs embedded in the polymer matrix were fabricated by drop casting of the nanotube/P3OT mixture dissolved in chloroform and had been studied using absorption spectroscopy, electrical characterization methods and high-resolution electron microscopy. The electrical conductivity was measured as a function of the SWNTs content in the solution. As the nanotube concentration increased form 0 to 20 wt. %, the conductivity of the resulting films increased by five orders of magnitude.

The novel organic light emitting diodes with the structure of [ITO-coated glass/PEDT:PSS/SWNTs-PVK (polyvinylcarbazole) nanocomposites/(4-(dicyanomethylene)-2-methyl-6-(p-dimethylaminostyryl)-4H-pyran (DCM)- doped) Alq_3/Li:Al] were fabricated and characterized [185]. Single-walled carbon nanotubes were synthesized by the laser ablation method and dispersed with the hole conducting polymer PVK in toluene. SWNTs-PVK nanocomposite was spin-coated on the PEDT:PSS/ITO-coated glass and then DCM-doped Alq3 was deposited by the cluster beam deposition methods. Zhou et al [186] showed that composites with improved uniformity and dispersion could be formed using chemically functionalized carbon nanotubes. A significant enhancement of the mechanical properties was obtained at low nanotube fraction. Contrary to previous results form pristine nanotubes, the composites showed efficient load transfer between the fillers and the matrix.

Zheng et al discovered [187] that nucleic acid polymers form hybrid material swith carbon nanotubes. That finding links one of the central molecules in biology to a technologically very important nanomaterial, and opens the door to carbon-nanotube-based applications in biotechnology.

The PVDF/DMF solutions with CNs were electrospun successfully through the control of the solution viscosity and surface tension [188]. The thinnest fiber had a thickness of 70 nm. The percolation threshold for the insulator-to-conductor transition was 0.003 wt % CN for CN/PVDF/DMF solutions, 0.003 wt% CN in solution or 0.015 wt% CN for CN/PVDF spin-coated films, and 0.008 wt% CN in solution or 0.04 wt% for CN/PVDF electrospun fiber mats.

The electrospinning process was used successfully to fabricate PEDT nanofibers in which multiwalled carbon nanotubes were embedded [189]. Initial dispersion of MWNTs in water was achieved using amphiphiles, either as small molecules SDS or as a high molecular weight, highly branched polymer (Gum Arabic). These dispersions provided separation of the SWNTs and their individual incorporation into the PEDO nanofibers by subsequent electrospinning. A theoretical model was presented for the behavior of rodlike particles representing CNTs in electrospinning.

4.3 Characterizations.

4.3.1 Raman Spectroelectochemical Studies.

Raman "in situ" spectroelectochemical studies had been carried out [190] in order to elucidate the electrochemical doping of poly(3,3'-dibutozy-2,2'-bithiophene). Raman spectra registered at different poltentials strongly depend on the position of the excitation line with respect to the electronic spectrum of the polymer. In particular, blue (458nm) and red (676 nm) excitation lines were very insensitive toward the oxidative doping of the polymer and independent of the electrode potential, always give spectra characteristic of the unoxidized segments of the chain. Figure 4. 3 shows the FT-IR spectrum of poly(3,3'-dibutoxy-2,2'-bithiophene). As expected, the spectrum showed the bands characteristic of a three-substituted thiophene ring similar to those in the case of poly(3-alkylthiophene)[191].

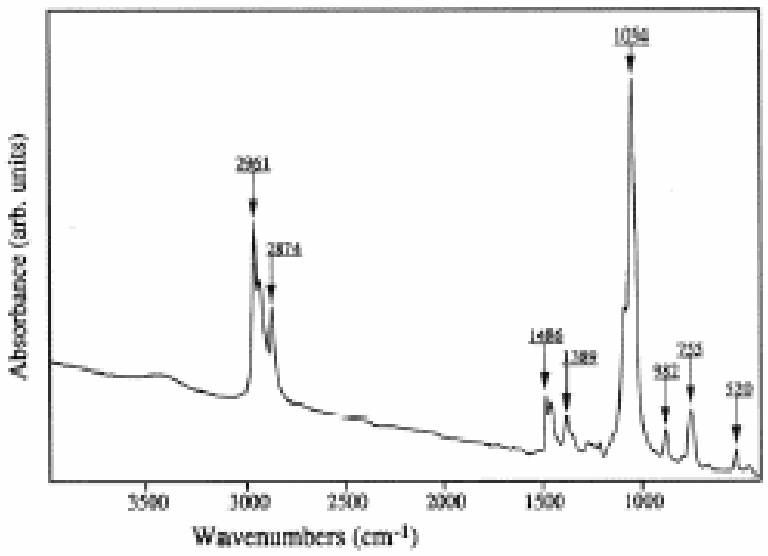

Figure 4. 3 FT-IR spectum of reduced poly(3,3'-dibutoxy-2,2'-bithiophene).

On the contrary, the infrared excitation line (1064 nm) allowed for detailed monitoring of the oxidative doping. The changes in the spectra occurring upon increasing potential of the electrode were consistent with the doping-induced transformation to the quinoid structure. The proposed assignments of the observed Raman bands had been confirmed by the vibrational analysis involving the calculation of the force field and frequencies via Fourier's dynamical matrix.

Froyer et al [192] carried out the study of EDT and its electrochemically synthesized polymer by means of Raman and UV-vis-NIR absorption spectroscopies. Figure 4. 4 shows the Raman spectra of EDT and PEDT at 514 and 1064 nm excitation lines respectively.

They also studied the doping-dedoping process of PEDT with those methods. An assignment of the Raman lines was attempted for both monomer and polymer, and

dynamical calculations had been performed to obtain characteristic valence-force-field of these compounds. Those results could be seen in the shown Table 4.1 for the different bands of EDT and PEDT. That work provided a good basis for calculations of force constants and coordinates of the perturbed structure created by doping. These resulted in a better understanding of the spectra, structure and optical effects in PEDT and similar compounds.

Table 4. 1 Experimental and calculated Raman band wave numbers/ cm^{-1} and vibrational assignments of EDT and PEDT.

Thiophene	EDT		PEDT		description of vibrations
exp.	exp.	calc.	exp.	calc.	
1504	1487	1485	1516	1520	C=C asym. stretching
	1453	1468		1458	CH_2 scissoring
1408	1424	1425	1423	1452	C=C sym. stretching
1358	1366	1364	1369	1356	C_β–C_β stretching
	1271	1249	1270		CH_2 twisting
	1248	1224	1240	1213	CH_2 twisting
			1226	1223	intercycle C_α–C_α stretching
	1185				CH_2 rocking
1078	1137	1131			C_α–H bending
	1100	1103	1100	1085	C–O–C deformation
	1058				CH_2 rocking
	1023	941	991	988	ring deformation
832	834	842			cycle sym. deformation
	766	744	750	758	ring deformation

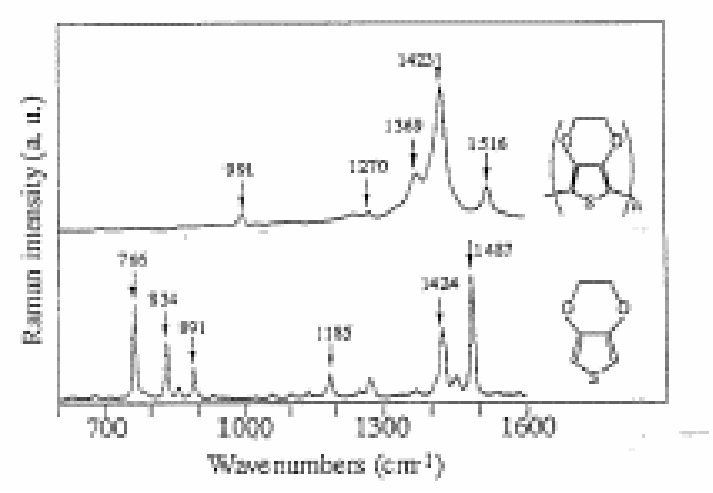

Figure 4. 4 Raman spectra of the monomer EDT and the polymer PEDT in the frequency range 600-1600 cm^{-1}.

4.3.2 Transmission Electron Microscopy for Nanotechnology.

Nanotechnology, as an international initiative for science and technology in this century, is a forced area of current research. Advanced nanomaterials and advanced manufacturing are the foundation of nanotechnology. Tracking the historical background of why nanotechnology and why now, it is believed that the following facts may contribute to this global initiative. First, the road map for microelectronics and Microsystems will be reaching its limit in about 10 years [193]. As the size of interconnects is thinner than 100 nm and one electron can ignite the switching of a device (so called single electron device), quantum mechanical phenomena are becoming appreciable and dominant. Nanoscale technology is not simply a miniaturization in sized, but an in-depth revolution in physical concepts, system design, and materials manufacturing. Philosophically, a change in quantity results in a change in quality.

Secondly, the development of transmission electron microscopy and scanning probe microscopy allows direct imaging of atomic structures in solids and on surfaces, and these powerful tools provide the "eyes" and "hands" for imaging and manipulating the nanoscale world, fulfilling the dream of moving atoms "one-by-one". This provides a unique opportunity for deigning, modifying, and constructing nanoscale structures. Third, the newly discovered nanostructures, such as carbon nanotubes, quantum dots, semiconducting oxide nanobelts, etc. display the diversity and richness of the nano-scale world [194]. The unique, novel, and largely improved properties demonstrated by these structures have illustrated a blue print for the next technological revolution in human civilization. Finally, the powerful modeling techniques and supercomputers can predict possible phenomena that could be realized experimentally, providing guidance in materials design and system analysis.

High-resolution transmission electron microscopy (HRTEM) is one of the most powerful tools used for characterizing nanomaterials, and it is indispensable for nanotechnology [133]. In facts, decades before the national nanotechnology initiative, scientists had started examining "small particles" (nowadays these are called "nanoparticles") by HRTEM. It was not until the early 1990s that inventions of various types of scanning probe microspcopy allowed scientists to manipulate at the nanoscale. Traditionally, HRTEM has been mainly applied for imaging, diffraction, and chemical analysis of solid materials [195]. Carbon nanotubes, for example, were first identified by HRTEM [151]. Analysis of such tubular structures requires extensive development of electron microscopy, which has been covered very comprehensively in the book edited by Wang [196]. Conventional imaging and diffraction are the two most powerful

methods in characterizing the phase structure and phase transformation of inorganic materials. With the assistance of energy dispersive X-ray spectroscopy (EDS) and electron energy-loss spectroscopy (EELS), the transmission electron microscope is a versatile and comprehensive analysis tool for characterizing the chemical and electronic structure at nanoscale [197]. HRTEM has been extensively applied to determine the shape of nanoparticles[198,199,200] and structures of nanotubes[136]. In recent years, a number of new and novel developments have been made in HRTEM for nanotechnology, such as in-situ microscopy for observing dynamic processes at nanoscale, nano-measurement techniques that directly correlate physical properties with structures, holographic imaging of electric and magnetic fields, quantitative chemical mapping at sub-nano-meter resolution, and ultra-high resolution imaging techniques.

In consideration of the large diversity and amount of literature available in electron microscopy, instead of giving a vast review about HRTEM, Wang [132] reviews only the novel developments that had been made in the last few years for solving problems in nanotechnology.

Chapter 5: Optimization of the Electrospinning Process.

5.1 Introduction.

Most of the nanofibers produced by electrospinning were collected into a nonwoven web form. The nonwoven web, containing very fine fibers, generally has poor orientation and likely poor mechanical properties. The challenge facing the researchers now is controlling the orientation of these nanofibers. Our research study started out as an exercise of converting electrospun nanofibers to aligned linear assemblies. Optimization of processing conditions was carried out so that yarns could be produced. These yarns were made through Rotary electrospinning on purposely constructed apparatus. The objectives of this part are; to develop a process for the alignment of linear nanofibrous assembly and to carry out systematic experiments to study the processing parameters affecting the diameter of the fibers.

5.2 Materials and Methods.

5.2.1 Polymer solution preparation.

The polymer used for this part of research was Poly(ethylene oxide); PEO, (M_W 900,000 g/mole) and was purchased from Sigma-Aldrich Co. It was used without any further modification or purification. PEO polymer was dissolved into chloroform; $CHCL_3$ (99.8%), which was obtained from Fisher Science Co. The prepared solution has concentration of 3wt%. The solution was very gently stirred for 10:15 hours at room

temperature using a magnetic stirrer; as shown in Figure 5.1, (Make : Corning, inc., Model: PC-351) in order to obtain a homogeneous solution.

Figure 5. 1 "Corning" Hot plate stirrer, model PC-351.

5.2.2 Rotary Electrospinning Prototype.

A rotating disk was driven through AC Motor (1/15 HP, 1550 RPM, 60 HZ, 115 V& 2.8 A) with a regulator which was used to apply different variable speeds. The disk was covered with aluminum foil, to work as fiber collector. The whole assembly was connected to the ground terminal of an electrical power supply as a grounded electrode.

A holder is placed above the disk holding a frame with multiple holes to enable using different numbers of spinnerets (glass capillary pipettes) as illustrated in Figure 5.2. The pipettes are connected to the positive terminal of the electrical supply through a copper wire inserted inside the polymer solution. The holder can move upward and

downward to change the height of spinning & can rotate around its axis to change the spinning angle. All of these parts are covered with a Plexiglas box to minimize the influence of the outside environment.

The Electrospinning Process was carried out when the electrical field was applied between the spinneret (pipette) and the rotary disk (grounded electrode). A drop formed by gravity at the tip of the pipette was deformed into conical shape, by the electric field [23]. When a threshold value of the voltage is reached, the electrostatic forces acting on the surface of the cone overcome the surface tension of the drop, and a jet was ejected from the cone. This cone is called a Taylor cone, for certain polymer-solvent system a "splaying" of the jet into finer filaments could be observed. Then the jet hit the rotating disk into a coil shape and the speed of the rotating disk works to stretch the coils into aligned rings. When the solvent is evaporated, the dry fibers in ring shape can be collected into linear strand to form a nanofibrous yarn.

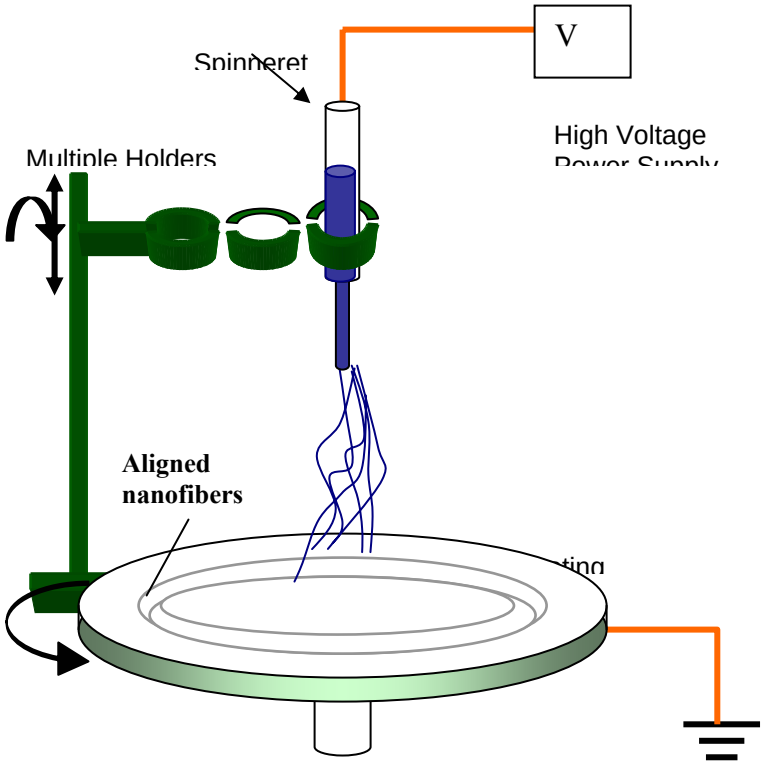

Figure 5. 2 The Rotary Electrospinning apparatus used to align the electrospun nanofibers.

In our study, we fixed the angle of spinning at 90^0 (vertical position) to spin vertically and the speed of rotation to 55% of 1500 R.P.M. and the voltage at 30kV.

We changed other parameters and used them into different combinations to study their influence on the electrospinning process. The studied parameters were as follows:

- The diameter of the pipette, 3 different pipette tip diameters were selected: D = 0.9, 1.3, and 1.7 mm
- The spinning height (distance from the tip of the pipette to the target) was of H = 10, 25, 40 cm which reflects the charge density from 3 to 0.75 KV/cm.

- The radial distance of spinning, the distance from the center of rotating disk to the center of pipette position which was: R = 4, 9, 14 cm.

5.2.3 Diameter and Fiber Alignment Characterization.

Scanning Electon Microscope, SEM

Morphological observation made by using SEM (AMRAY 1830 D4 Tungsten Gun) Figure.5. 3. at 20 kV. The samples were coated by using a gold sputtering machine (DENTON VACUUM DESK II) Figure.5. 4. for 60 sec; according to the sputtering machine catalog the expected coating thickness under the conditions used is = 10-20 nm.

Figure 5. 3 SEM AMRAY 1830 D4.

Figure 5. 4 Denton Vacuum Desk II.

Fibers' Diameter Calculation

Each of the SEM pictures has been divided into four equal regions, an example is shown in Figure.5. 5. Then in each region, the fibers' diameter was measured by using imaging of Scion software. For more accuracy the maximum and equal numbers of fibers were chosen for each region to apply diameter measurements on them.

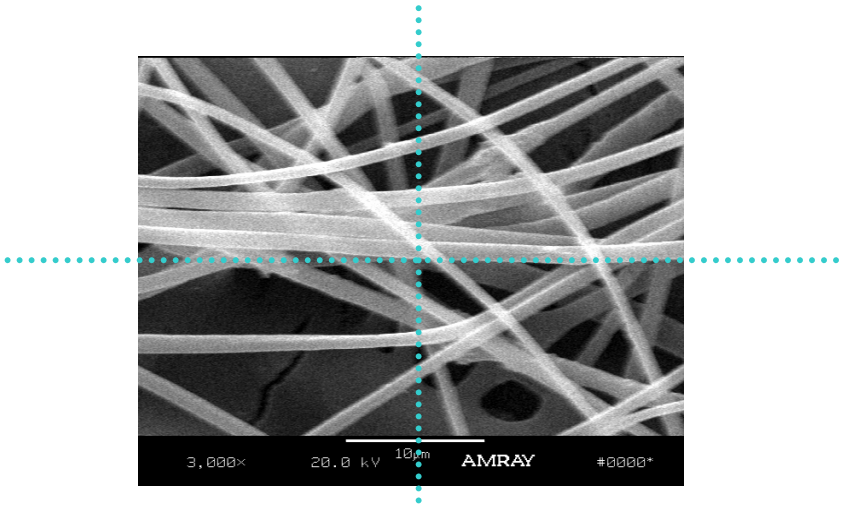

Figure 5. 5 SEM image of the PEO fibers showing the hypothetical lines used to divide the image into four regions to help with measurements.

5.2.4 Response surface analysis.

Our interest here was to study the parameters that help to orient and align these nanofibers. A 3^3 factorial experiment was carried on the Poly(ethylene oxide); PEO, polymer to study the effect of the electrospinning processing parameters on the morphology and orientation of the nanofibrous assemblies. Consequently, a response surface analysis was carried out to determine the optimum processing conditions for the nanofibers and nanofibrous assemblies. The factors affecting the process with the different levels are shown in the following designed matrix.

Table 5. 1 Studied parameters of rotary eletrospinning process.

Factors	**Levels**		
	-1.0	0.0	+1.0
Diameter of pipette(mm) **A**	0.9	1.3	1.7
Height of spinneret (cm) **B**	10	25	40
Radial distance from spinneret (cm) **C**	4	9	14

The designed set of experiments was carried out as shown in Table.5.1. It was found out that 27 experiments were needed to complete the required data of the table. After all the SEM images for each experiment were analyzed, all the fiber diameter results were fed back to Table 5.2. By the help of Response surface software program, it was easily determining the required parameters for the Electrospinning optimization.

Table 5. 2 The F Design of 27 experiments setting required for the Response surface analysis.

Rows	Pattern	Dia-PP	Height	Radial Dis	Dia-Fiber
1	111	0.9	10	4	?
2	112	0.9	10	9	?
3	113	0.9	10	14	?
4	121	0.9	25	4	?
5	122	0.9	25	9	?
6	123	0.9	25	14	?
7	131	0.9	40	4	?
8	132	0.9	40	9	?
9	133	0.9	40	14	?
10	211	1.3	10	4	?
11	212	1.3	10	9	?
12	213	1.3	10	14	?
13	221	1.3	25	4	?
14	222	1.3	25	9	?
15	223	1.3	25	14	?
16	231	1.3	40	4	?
17	232	1.3	40	9	?
18	233	1.3	40	14	?
19	311	1.7	10	4	?
20	312	1.7	10	9	?
21	313	1.7	10	14	?
22	321	1.7	25	4	?
23	322	1.7	25	9	?
24	323	1.7	25	14	?
25	331	1.7	40	4	?
26	332	1.7	40	9	?
27	333	1.7	40	14	?

5.3 Results and Discussions.

The electrospinning process is demonstrated in Figure 5. 6 using the rotating disc to spin the nanofibers. In the figure we can see one pipette used as a capillary while the holder can hold up to 20 pipettes to increase the amount of spun fibers. The figure shows how the nanofibers were electrospun into aligned fibrous assemblies with good orientation. This alignment of the fibers was achieved due to the effect of the sheering force of the rotating speed.

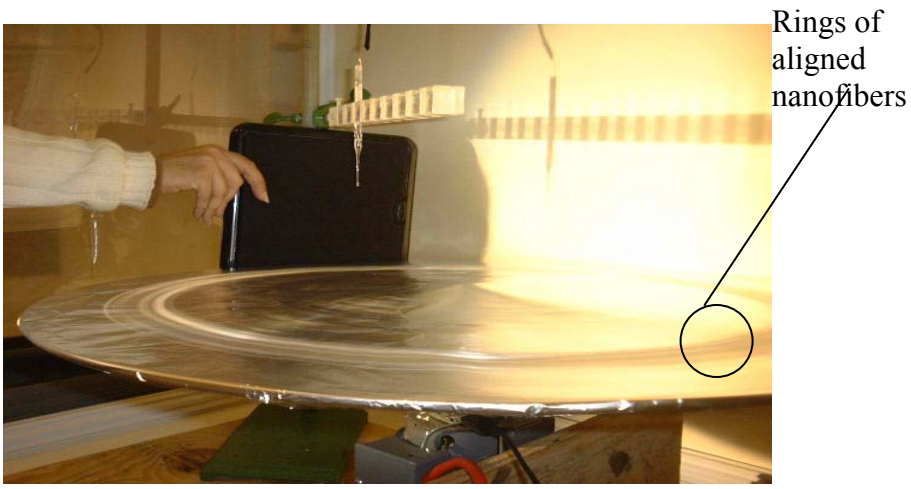

Figure 5. 6 The Rotary Electrospinning prototype.

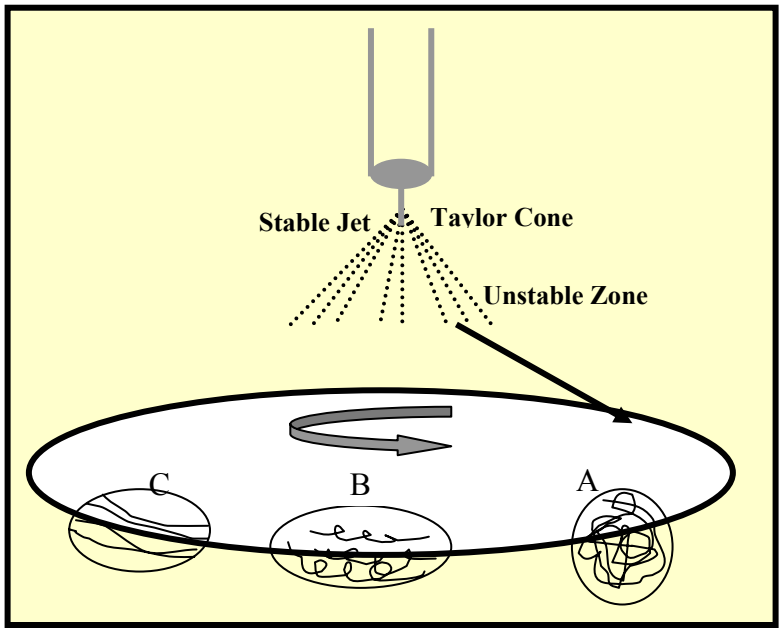

Figure 5. 7 Schematic of the effect of the rotating speed on the forming fibers.

Figure.5. 7. shows a schematic of the electrospinning process showing the Taylor cone and the coiled polymer jet which could be aligned into oriented fibrous yarn by increasing the speed of the Rotary disk. Stage A shows the random fibers formed at very low rotating speed, stage B shows that by increasing the rotating speed a relative alignment will be attained which is improved at stage C. The SEM images; in Figure.5. 8, clarify the polymer jet behavior to make coils instead of straight fibers. By adjusting the controlling parameters; e.g. height, pipette diameter, and the rotating speed a well defined oriented fibers could be collected and twisted into a yarn.

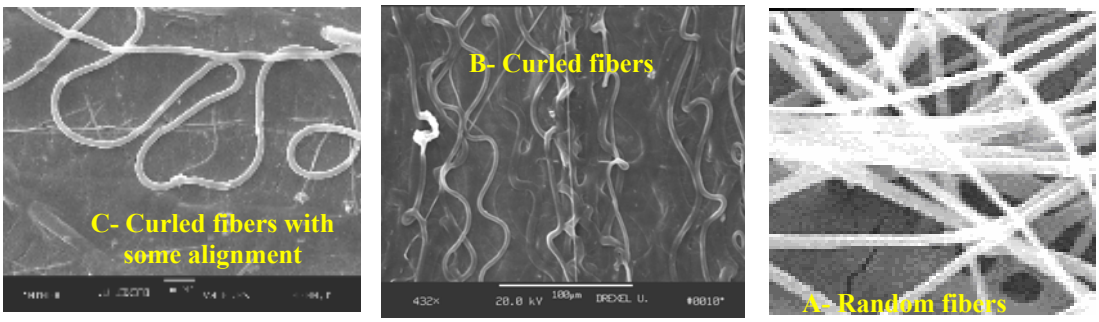

Figure 5. 8 SEM images of 3% PEO/$ChCl_3$ showing the tendency of fibers to be aligned from low speed A to high speed C.

5.3.1 Effect of Rotating Speed on Fibers Alignment.

By controlling the rotating speed of the disc, we found that the fiber alignment differ by changing the rotating speed. The following SEM images will illustrate the effect of increasing the speed on the alignment of fibers which classified into five categories.

First category: steady state

The electrospinning process was carried out while the rotating speed was zero, i.e. not moving and steady. We found out the fibers were random and formed as a web. Figure.5. 9. illustrates how the fibers in random position are and there is no tendency to be aligned.

Second category: Low speed

By increasing the rotating speed of the disc to 10% (of 1500 r.p.m), the fibers were still in random arrangement with slight alignment as shown in Figure.5. 10. It is

clear in figure.5. 10.(c)-(f) that, although the fibers are random there is tendency to be aligned as illustrated with the red arrow.

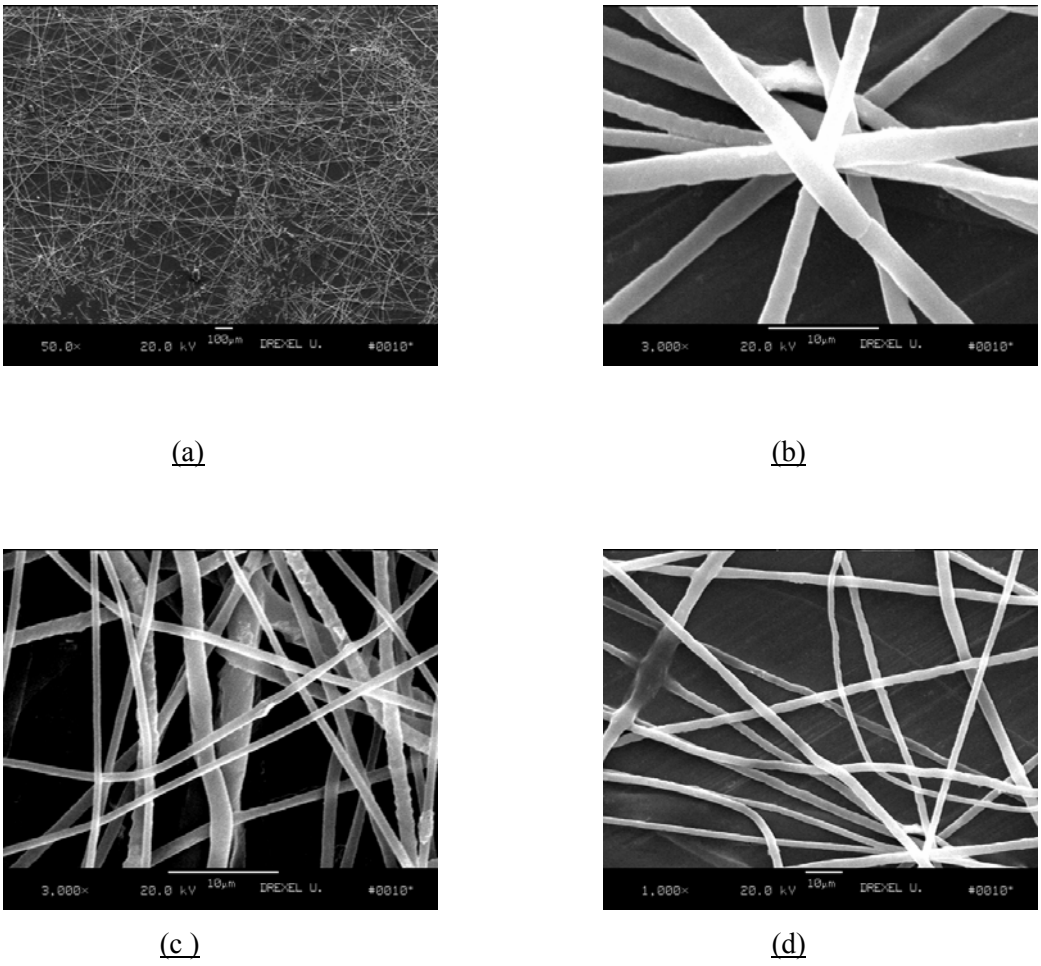

(a) (b)

(c) (d)

Figure 5. 9 SEM images of the steady state category of the rotating disc. (a) the image of fibers at 50X magnification, (b) &(c) the images of the fibers at 3000X magnification and (d) the image of the fibers at 1000X magnification.

Third category: Moderate Speed

We have been encouraged by the tendency of fibers to be aligned, to increase the rotating speed of the disc to 30% (of 1500 rpm). It is evident that the fibers start to be aligned; as obvious in Figure.5. 11, and the red arrow shows the direction of alignment.Figure.5. 11.(a) & (b) demonstrate the more propensity of the fibers to be aligned. Figure.5. 11.(c) –(f) give an idea about the arrangements of the fibers in higher magnifications. It is evident that some of the fibers were aligned straight while others were in the form of coils and curly shapes, hence we will try to go to higher level of speed.

Fourth category: High Speed

By increasing the speed of the rotating disc to 50% (of 15000 rpm), better fiber alignment has been achieved. Figure.5. 12. (a)-(f) illustrate the good alignment of the fibers and the minimum presence of coils along the fiber. In Figure.5. 12.(b), we can see the coil along the fiber tries to be aligned. By reaching the optimum speed (55%) of the rotating disc, we can see in Figure.5. 13. (a)- (f) the good aligned fibers into straight position with the disappearance of coils. At this level we can say that we have electrospun fibers with good alignment.

Fifth Category: Very High Speed

We found out that; when the rotating speed of the disc was increased more than 55% (of 1500 rpm), the fibers start to be again formed into a random arrangement. Also the breakages of fibers start to appear with the higher speed. Figure.5. 14.(a)-(h) illustrate the presence of fiber breakage and the random behavior of the fibers.

After adjusting the required speed to achieve good alignment of fibers, we tried to collect those fibers into twisted yarn. The elecrospinning process' parameters will be analyzed to achieve smaller fiber diameter as shown in the following section.

Yarn formation

After adjusting the required rotating speed, the electrospun fibers were collected and removed from the rotating disc. The electrospun fibers were twisted into yarn and had been tested by the SEM to check the fiber arrangements. Figure.5. 15. shows the twisted yarn and the direction of twist (a) and how the fibers prefer to align along the yarn axis (b, c). We can see better alignment of the fibers in Figure 5. 16 (c) as the rotating speed of the disc were slightly increased, also (a & b) illustrated the added twist to the fibers.

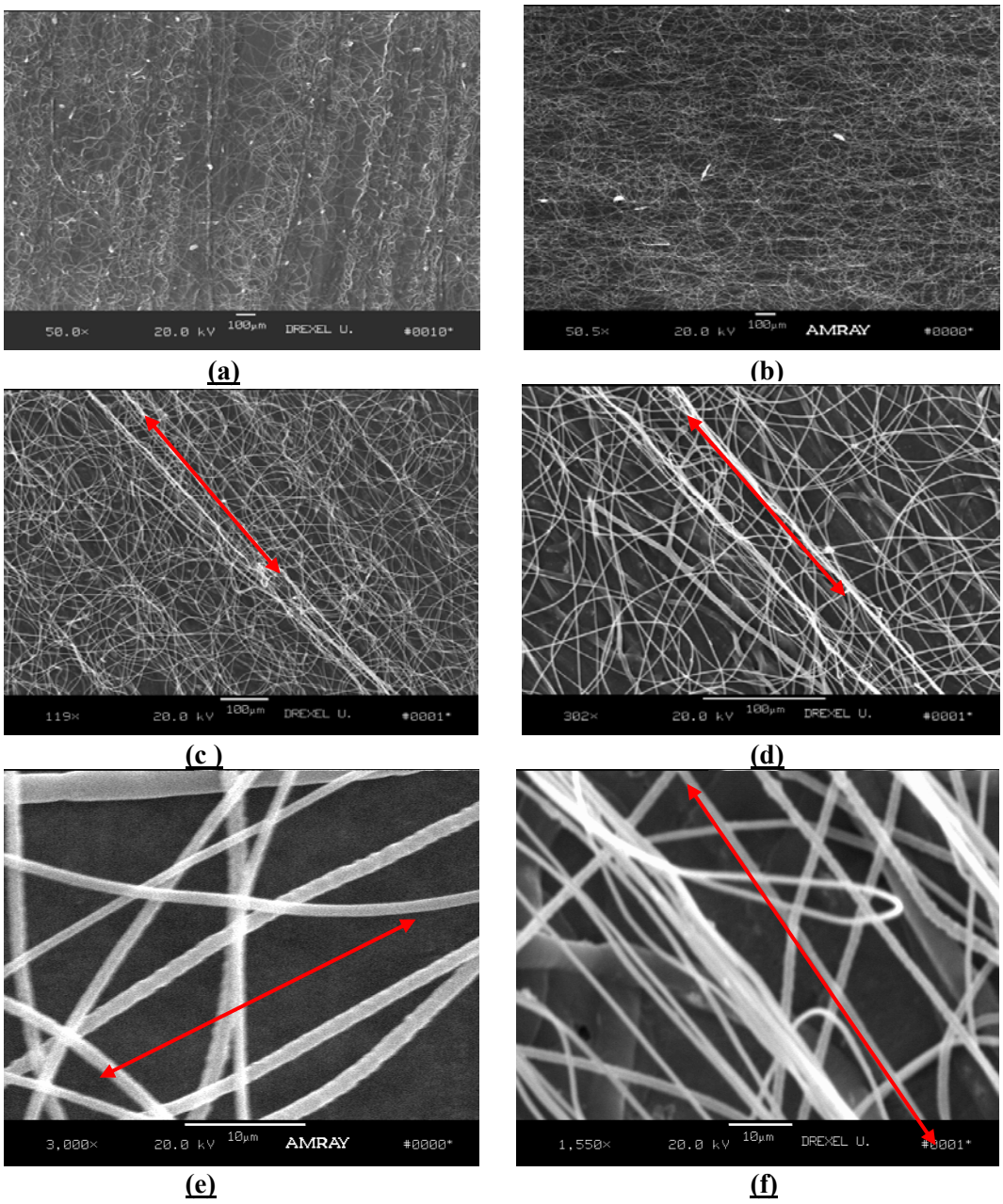

Figure 5. 10 SEM images of the low speed range of the rotating disc (a) & (b) show the random arrangement of fibers with slight alignment at 50X magnification. The red arrow illustrates the tendency of fibers to align at 200-300Xmagnification in (c)&(d) and 1500-3000X in (e) &(f).

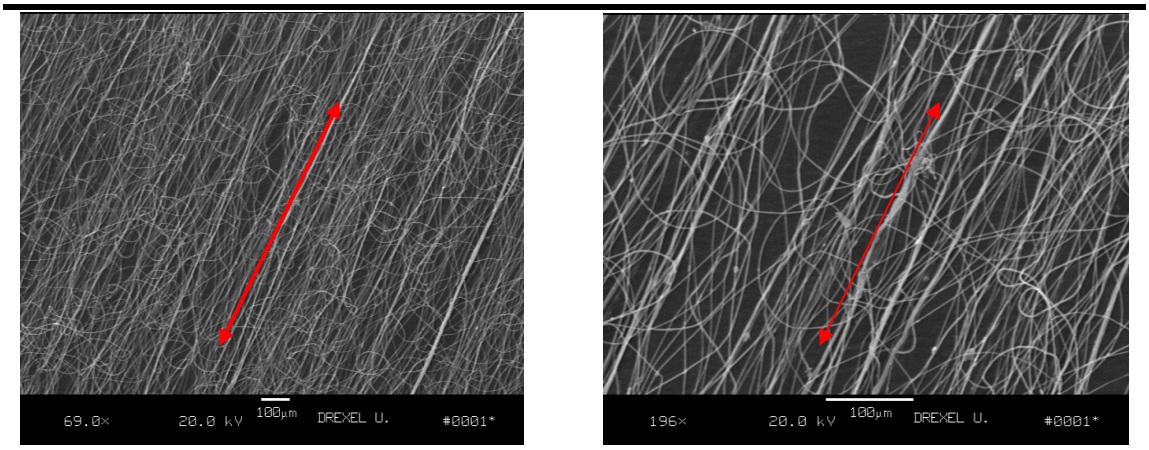

(a) **(b)**

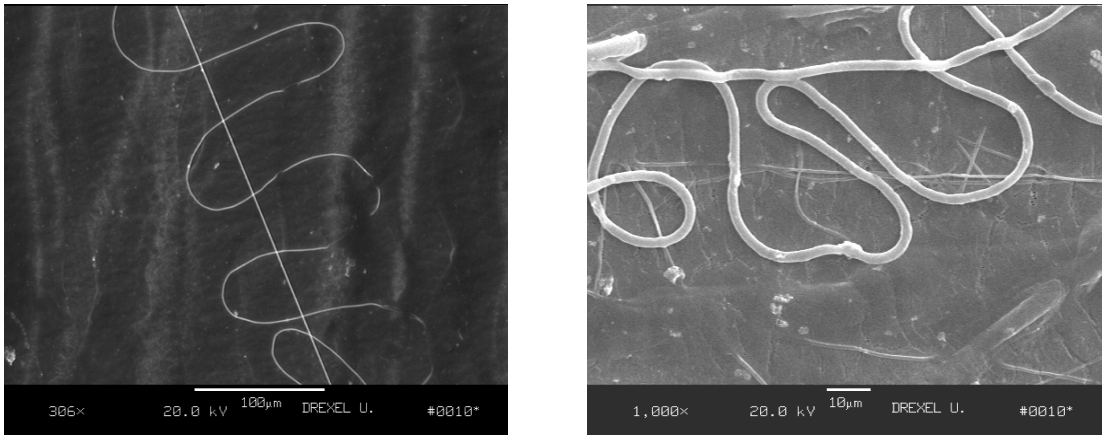

(c) **(d)**

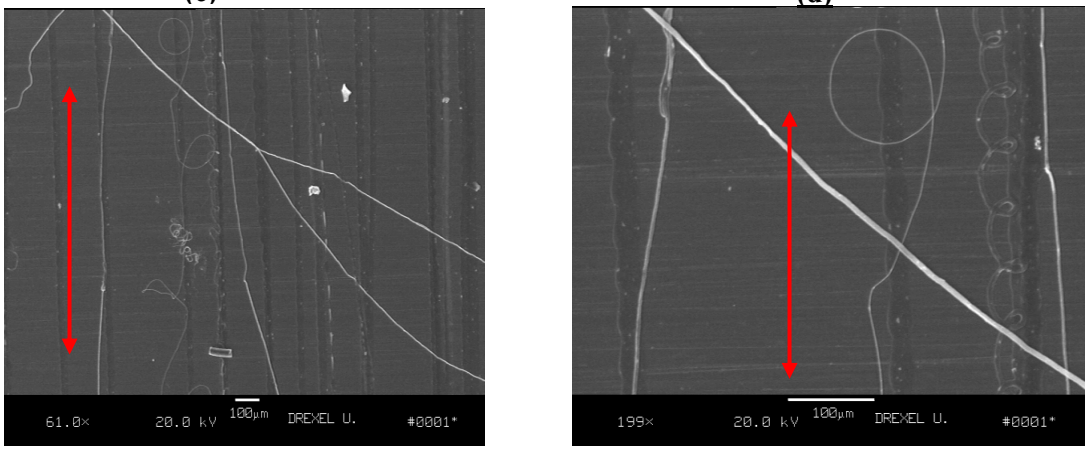

(e) **(f)**

Figure 5. 11 SEM images of the moderate speed range of the rotating disc (a) &(b) illustrate more fibers tend to be aligned (c) –(f) arrangements of straight fibers and coiled one.

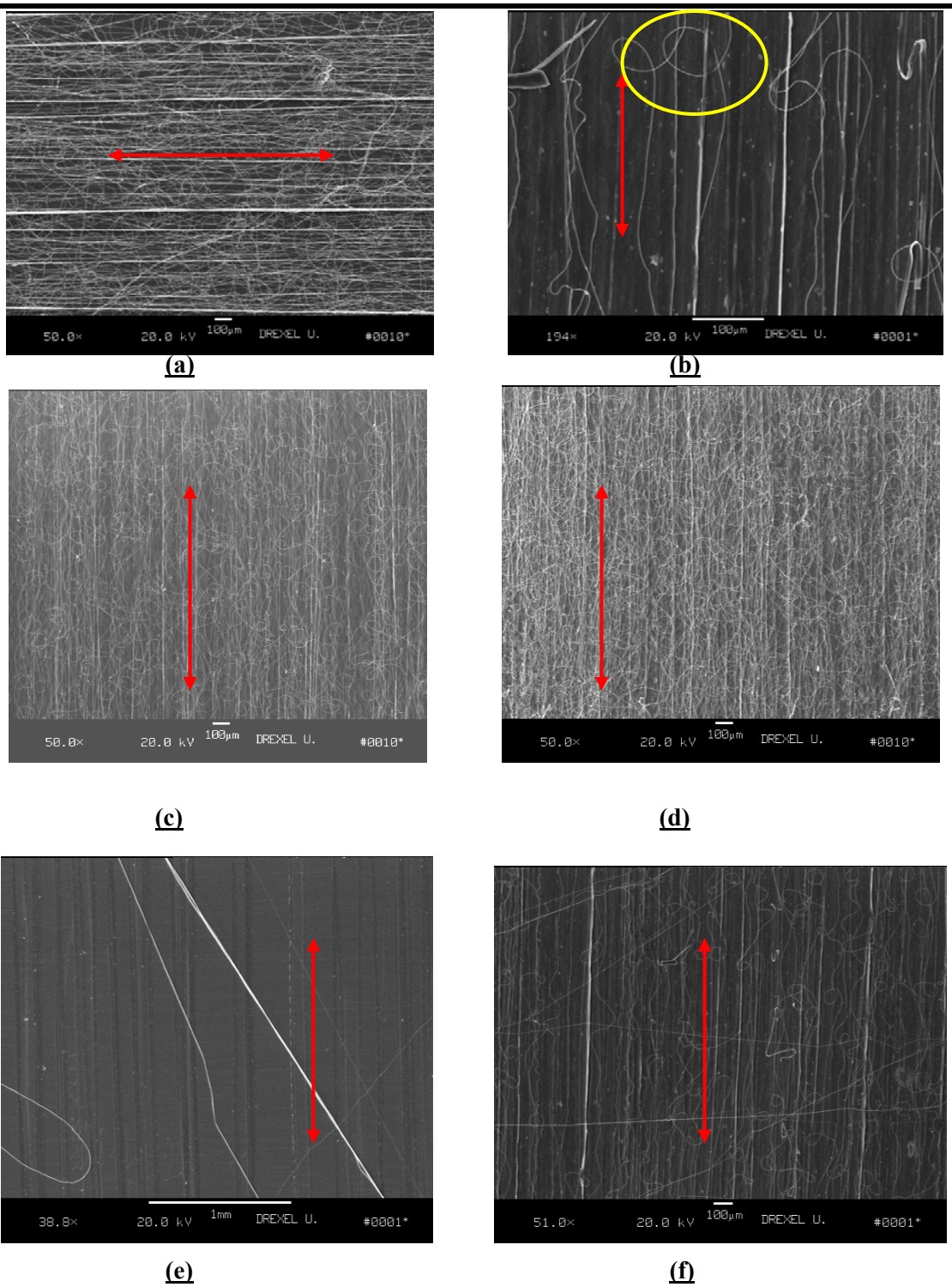

Figure 5. 12 SEM images of the high speed range of the rotating disc. (a)-(f) electrospun fibers with better alignment and minimum coiled ones.

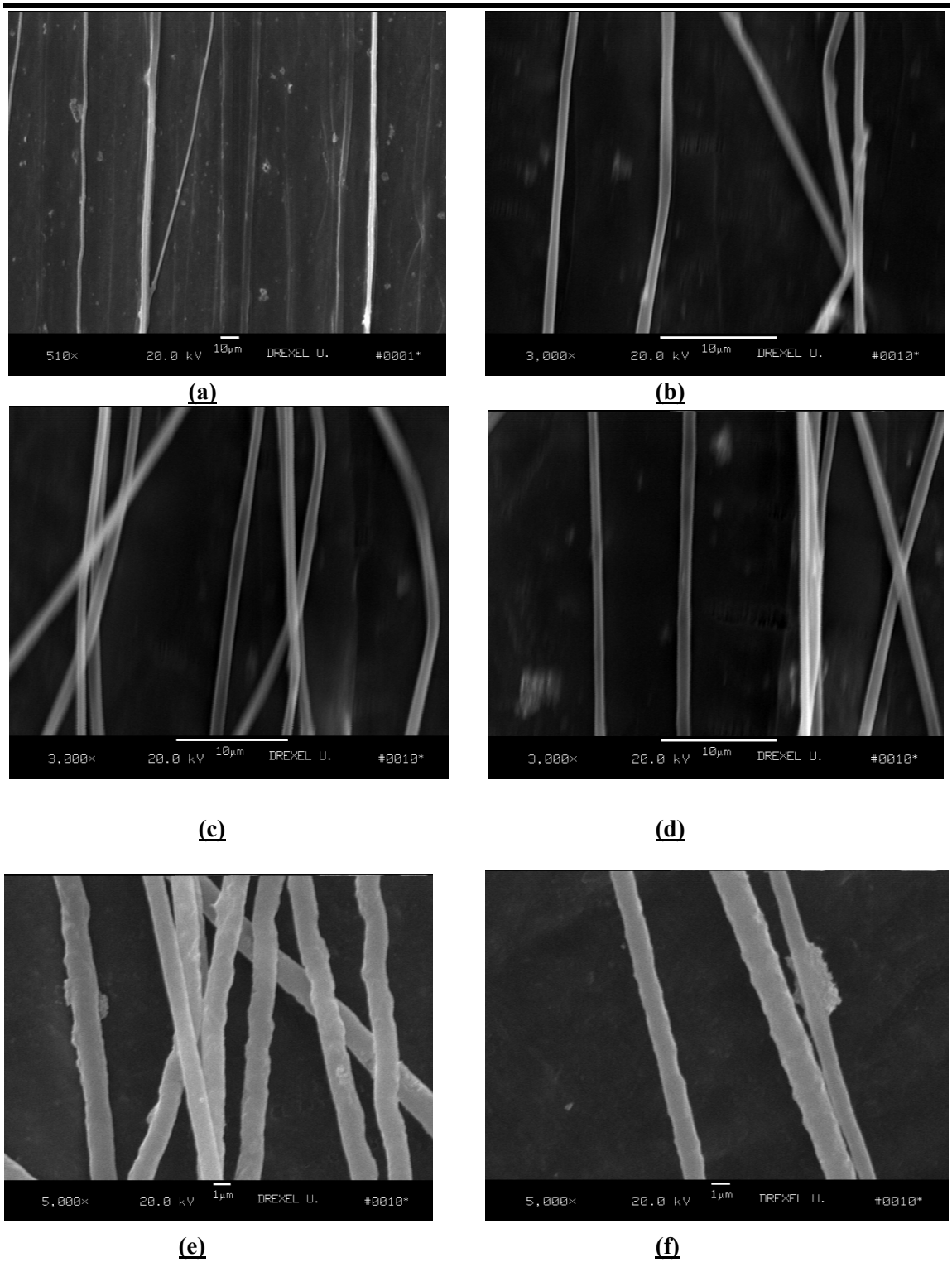

Figure 5. 13 SEM images of the high speed range of the rotating disc (a)-(f) the elecrospun fibers with higher magnifications(3000-5000X) to show the straight fibers with no coils.

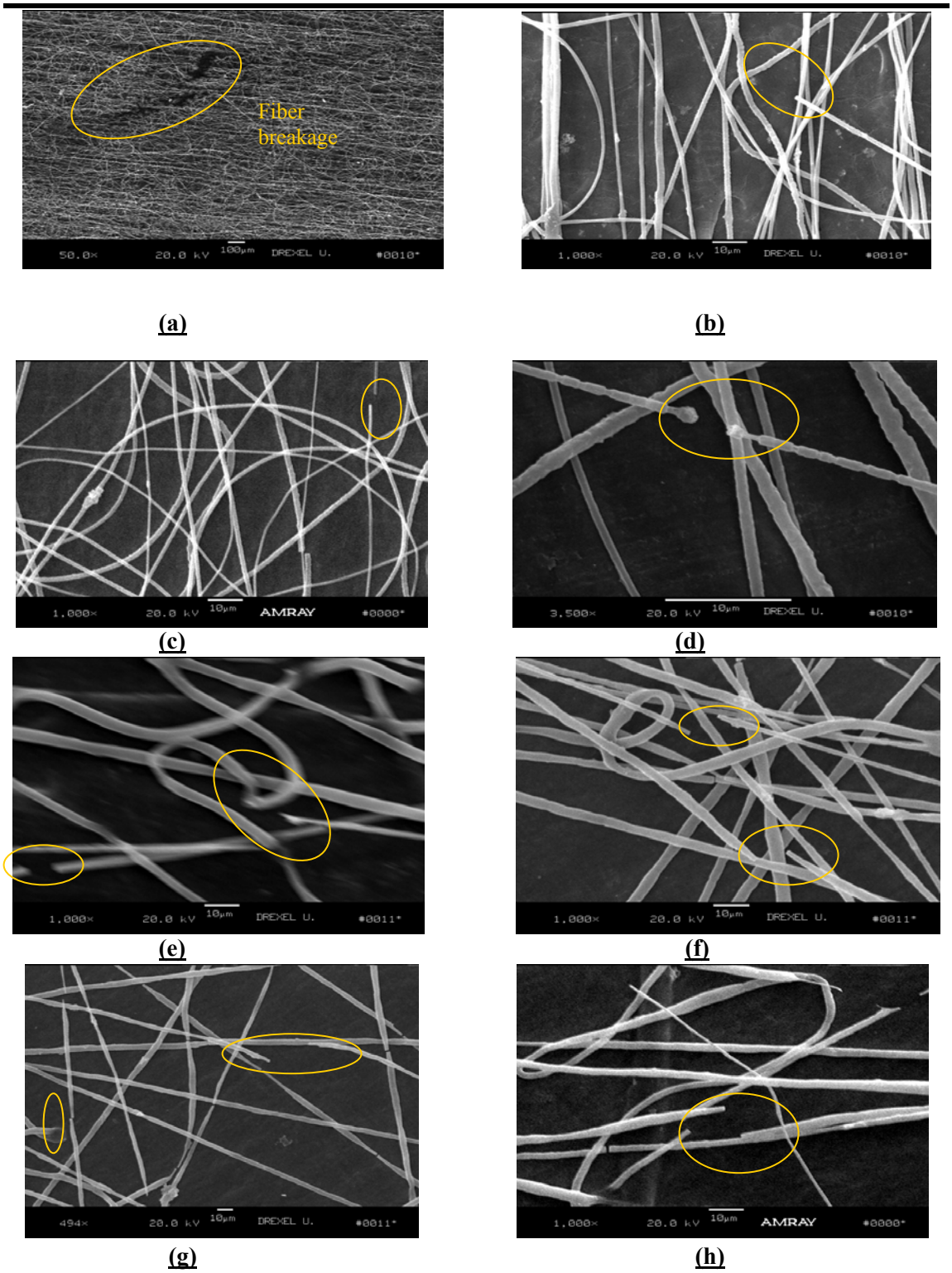

Figure 5. 14 SEM images of the very high speed range of the rotating disc.(a)-(h) the yellow circles show the breakage of fibers and nonalignment of them.

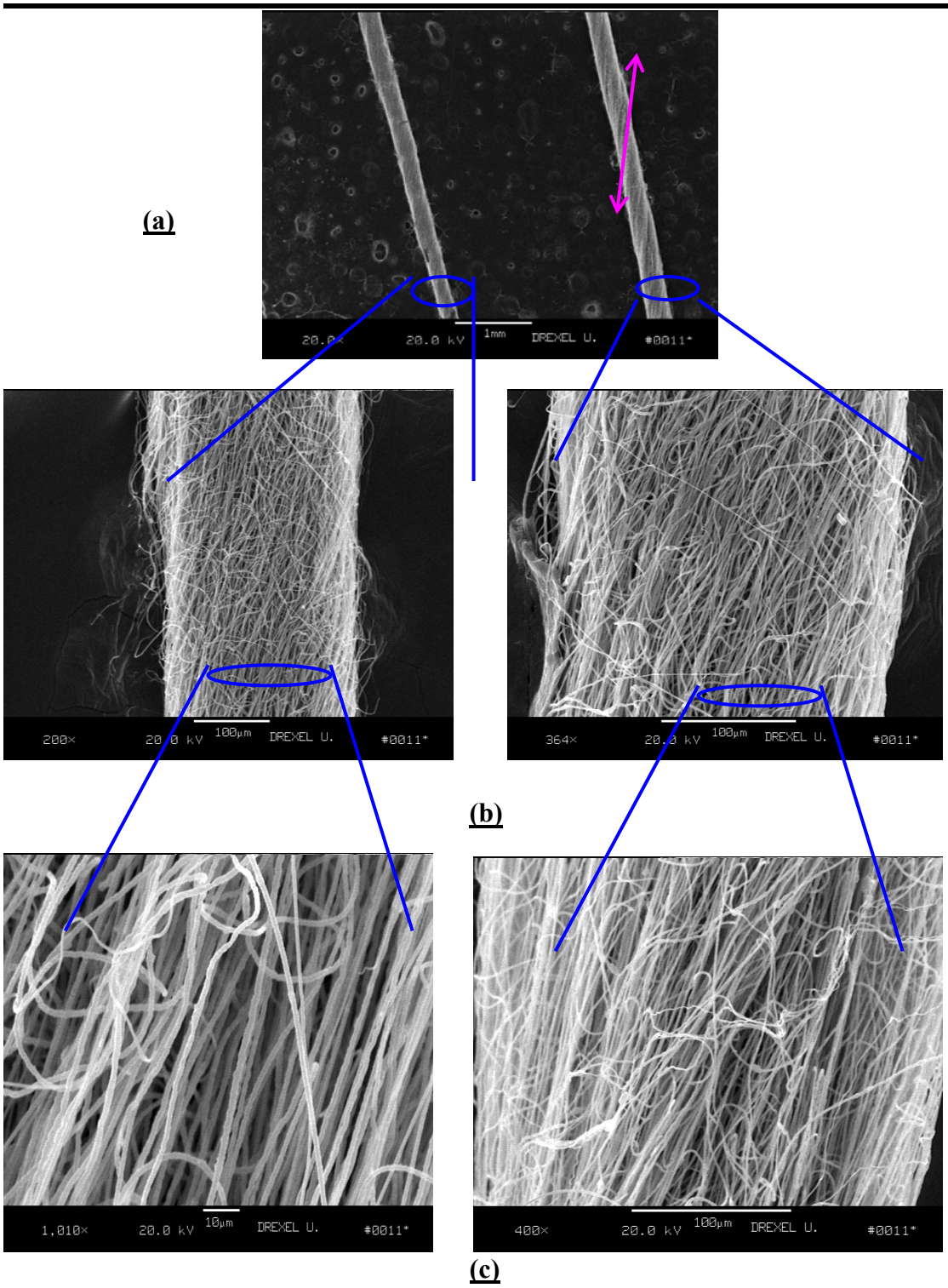

Figure 5. 15 (a) showing the twist direction of two formed yarns (b) & (c) showing the tendency of fibers to be aligned within the yarn.

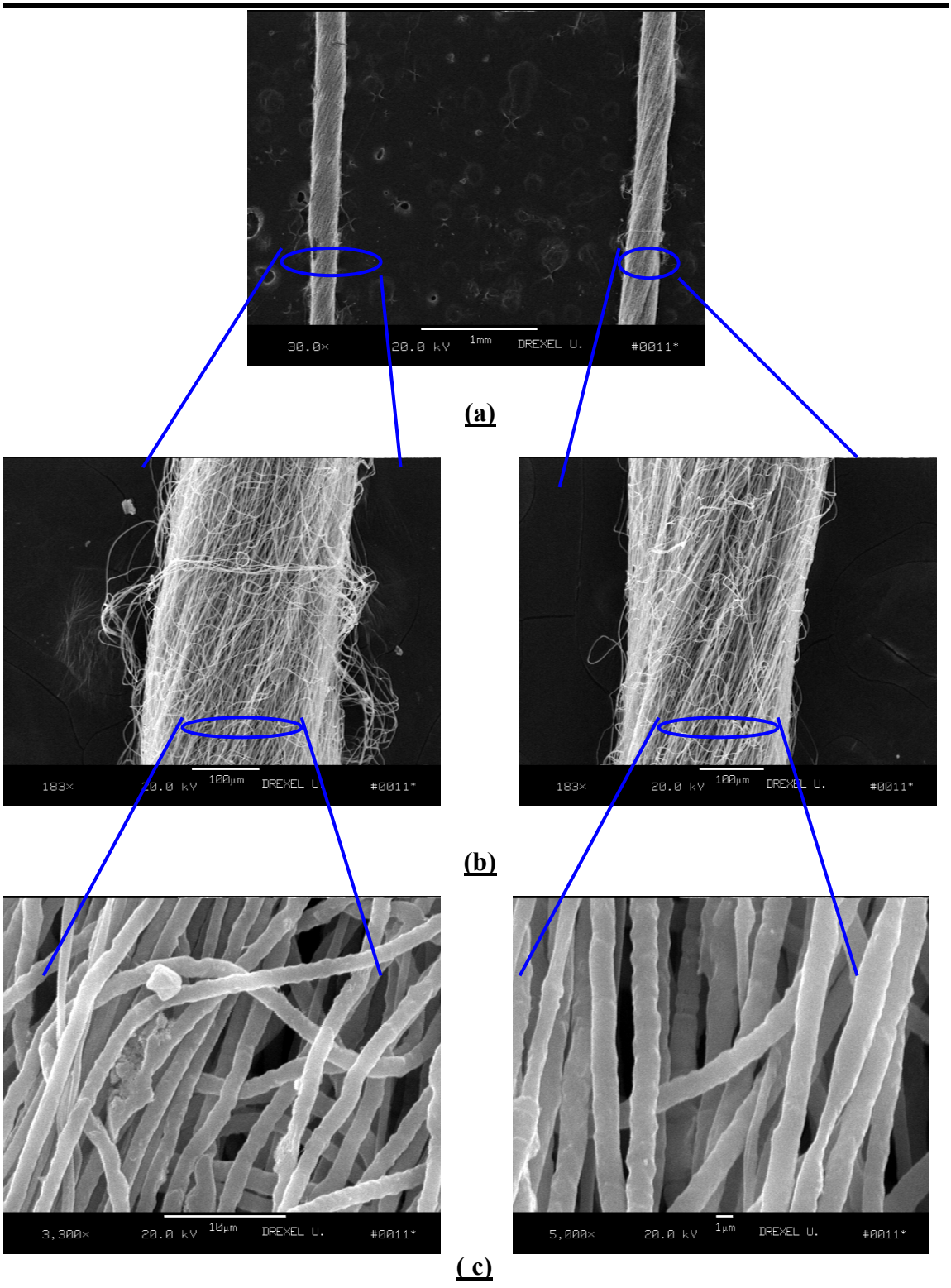

Figure 5. 16 showing better alignment of the fibers (c) within the yarn (b) which was twisted (a) after removed from the rotating desk.

5.3.2 Response Surface Analysis Results.

The detected response parameter was the diameter of the aligned fibers. The fibers diameter was measured by using SEM technique. By measuring the diameters of 20:24 random fibers for each sample, the average fiber diameter was calculated. By feeding the whole data of the experiments to the RS program, the following results were obtained; (see Appendix VII)

1. The best pipette diameter is the middle value; 1.2 mm, with slight increasing to 1.4:1.5 mm as the radial distance increased as shown in Figure.5. 17.(a)&(b)
2. The lower is the height of spinning tip, the finer is the electrospun fibers.
3. By decreasing the radial distance & lowering the height of spinneret, the electrospun fibers become finer as illustrated in Figure.5. 17(c). This effect was enhanced by reaching the middle value of pipette diameter (1.2:1.4) as we can see in Figure.5. 17 (d). If we go further higher pipette diameters, the fibers would become coarser.
4. Figure.5. 17(e)&(f) show that we have a saddle point for the fiber diameter by decreasing the radial distance and optimize the pipette diameter.
5. The following equation gives the relation between the fiber diameter and the optimized parameters of electro-spinning process.

$$D_f = 1.28 d_p + 0.169 H - R_d \qquad \textbf{Equation 4. 1}$$

Where

D_f …….. Fiber diameter

D_p ……. Pipette diameter

H …… Height of spinneret

R_d …….. Spinneret radial distance.

6. The F test shows that the most significant parameter is the pipette diameter, then the height of the spinneret and after that is the radial distance of the spinneret.

Several experiments were carried out and by using the response surface results; we pass through different stages of collecting the fibers. The first stage was collecting the fibers into non-woven web as a random form. The second stage was by using the rotary dry disk; the fibers were electro-spun onto the rotating disk forming concentric rings. Easily the fibers were twisted into fibrous assembly form (yarn). The third stage was applying the optimum conditions to orient and align the nano-fibers into the yarn.

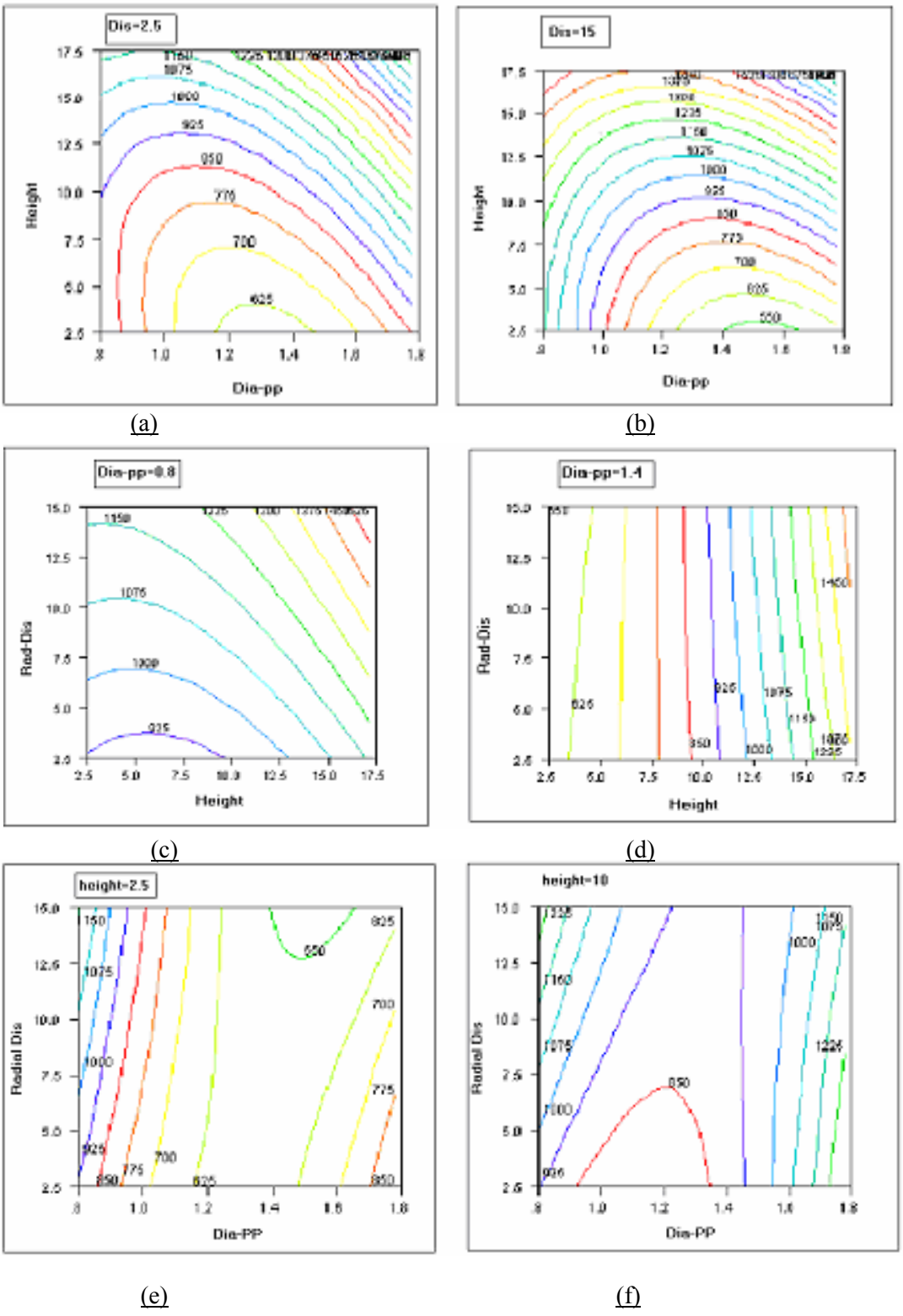

Figure 5. 17 (a,b,c,d&e) Response surface graphs of the Electrospinning parameters.

5.3.3 Diameter distribution of the PEO nanofibers.

Every sample of the 3^3 experiments was tested; by using Scion soft ware, to calculate the fiber's diameter. Each image was divided into 4 parts and from each quarter, five readings were recorded. The whole 20 readings for the 3^3 electrospun nanofibers samples were plotted to demonstrate the diameter distributions. Figure 5. 18 illustrates the fiber diameter versus the number of fibers. The fibers' diameters vary from 100 nanometer to 4.8 microns with an average of 500:700 nanometers.

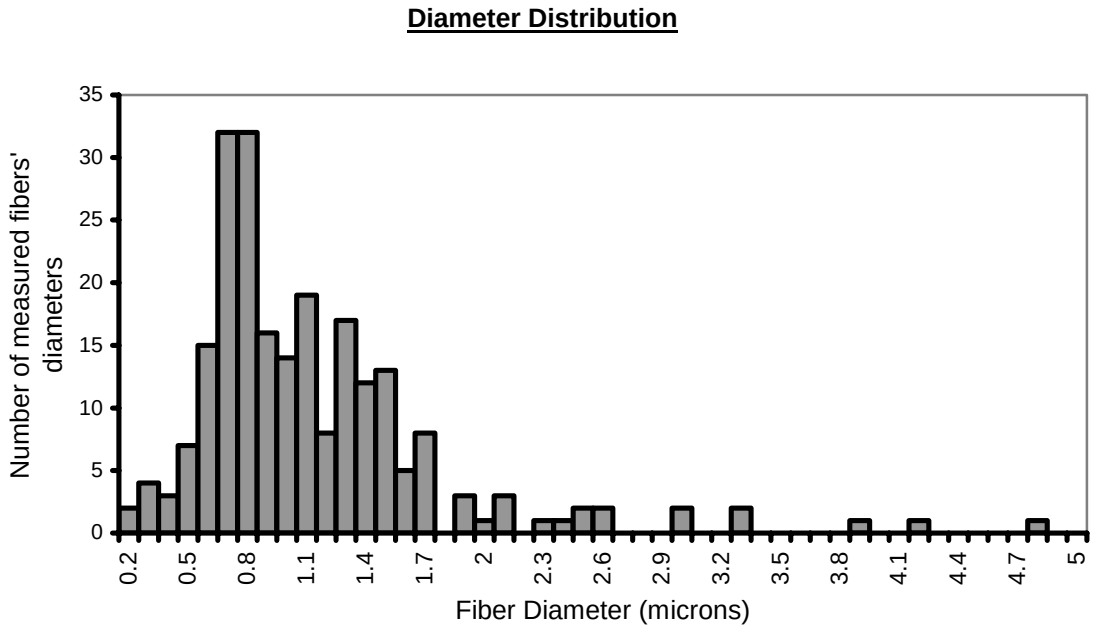

Figure 5. 18 Diameter distribution of 3% PEO nanofibers.

Electrospun PEO polymer gives bigger diameters compare to other polymers. The change in the electrospinning parameters will not lower the fiber diameters of PEO due

to the viscosity of the solution and concentration which should be considered with other polymers to achieve fiber diameter lower than 100 nanometers.

5.3.4 Mechanical Properties.

The mechanical properties of PEO non-woven mat and PEO nanofibrous yarn were characterized by stress-strain measurements. Figure 5. 19 shows typical stress-strain curves of PEO fibrous yarn at 3 wt. % concentrations, and PEO non-woven mat of the same concentration at room temperature and humidity. PEO non-woven mat; of 3 wt. % concentration, shows similar curve with a yield point around 15% strain. The ultimate strength of PEO non-woven mat is in the range of 7 MPa. It is observed that for the same PEO content, the aligned nanofibrous yarn has higher strength than the non-woven mat values. This improvement referred to the alignment of the fibers within the yarn surface, which enables higher number of fibers to share the applied load. The nanofibers are exposed to elongations and draw factor during the process of yarn formation that enables the chain molecules to be oriented within the fibers.

The ultimate strength of PEO nanofibrous yarn is in the range of 15-28 MPa and with yield points around 12-35%, which are comparable higher than the PEO non-woven mats values. It is obvious that PEO yarns are mechanically strong compared to the PEO non-woven mat. It is clear; from Figure 5. 19 that the rotating speed influences the strength of the electrospun yarn. The tensile strength and yield strain of the PEO aligned fibrous yarn at high speed are higher than the strength of PEO yarn at moderate speed by two folds. This is due to the more alignments of the fibers with the high-speed gives higher number of fibers to share with the applied load.

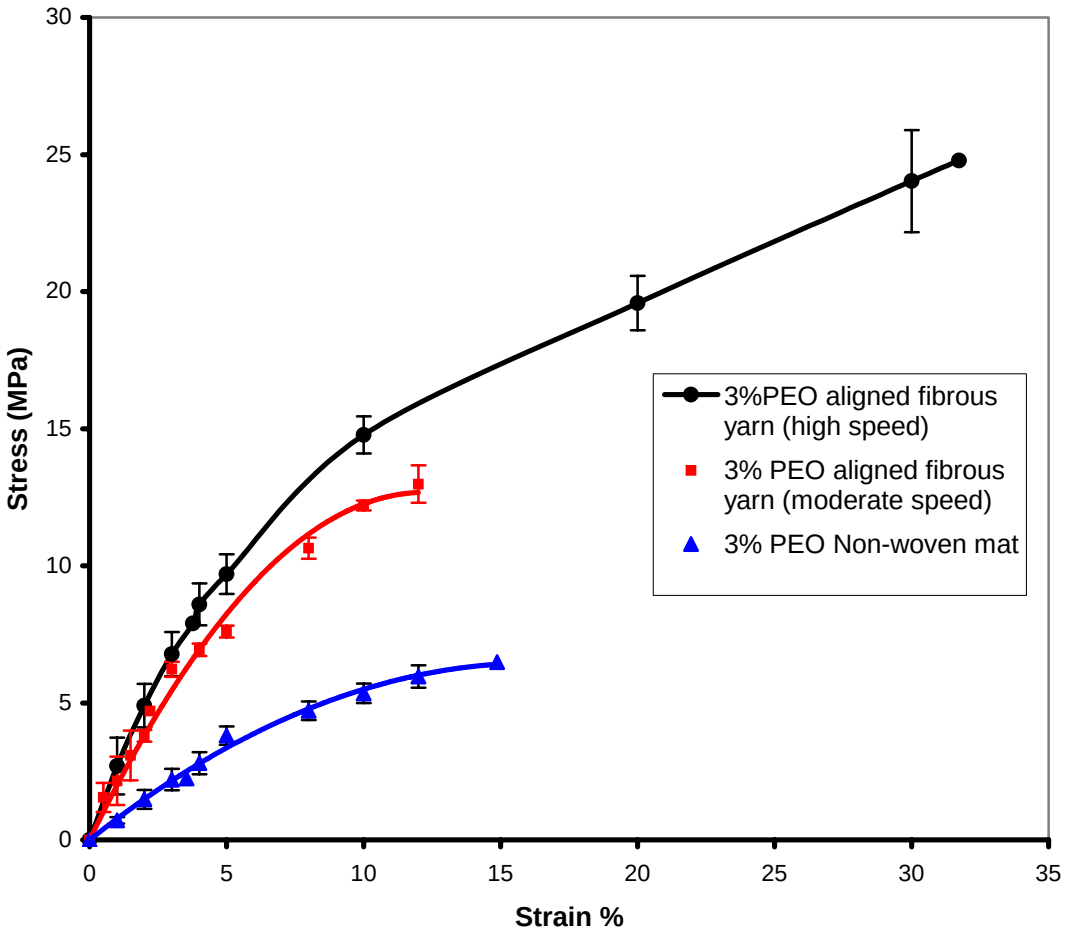

Figure 5. 19 Stress-strain results of 3 wt.% PEO non-woven mat and 3 wt.% PEO nanofibrous Yarn.

Chapter 6: Electrospinning of PEDT Nanofibers Assemblies.

6.1 Introduction.

At this point of research, we tried to look for a useful purpose of producing nanofibers using the electrospinning process. At the same time Prof. MacDiarmid; Nobel Prize Laureate, opened the door for new applications and concepts by using those conductive polymers. We thought it would be beneficial if we could electrospin conductive polymers into flexible fibers. Hence, our goal was to find a new conductive polymer and try to transform it into nanofibers and determine if it will sustain its electrical properties after elecrospinning.

Since Macdiarmid et al, [53] discovered that polyacetylene $(CH)_x$ can reach extremely high electrical conductivities for polymers, the field of conducting polymers, which are often referred to as synthetic metals, has attracted the interest of many scientists[53]. Some efforts were done to transform some of these conducting polymers into nanofibers using the electrospinning process. Ian Norris et al [42] used Poly(aniline) for this purpose. As mentioned in the review of literature, despite of the advantages of the Poly(aniline) as one of the best conductive polymers, numerous industrial and academic groups have limited their research in polyaniline chemistry due to the possible presence of benzidine moieties in the polymer backbone, which might yield toxic (carcinogenic) products upon degradation[60]. After studying all of these facts, we tried to find the suitable polymer for our research work. PEDT/PSS was the chosen polymer because of its conductive properties; it could be a more environmentally friendly system.

From the literature review, PEDT/PSS is a good conductive polymer that has a lot of applications, which is proven by the quick statistical study. Figure 6. 1 verifies the interest in PEDT polymer by showing the great increase in the number of publications over the past decade. This indicates the great awareness of a new material, processes and industrial applications.

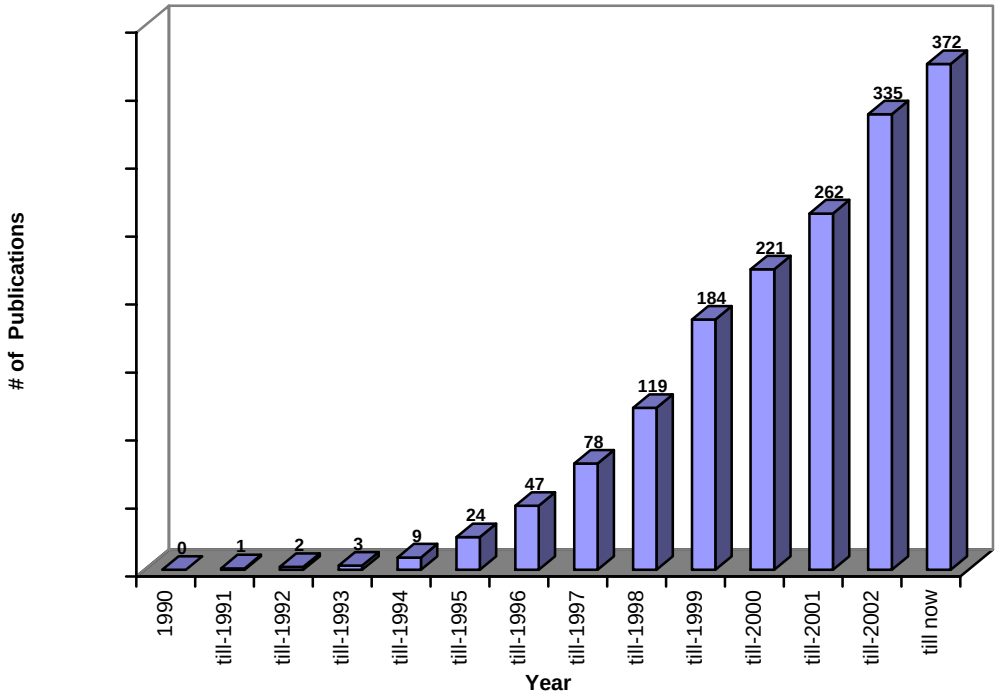

Figure 6. 1 Development of the number of journal publications on PEDT over the past 13 years.

6.2 Materials and Methods

6.2.1 Preparation of Polymer Solution.

Poly(3,4-ethylenedioxythiophene)/poly(styrenesulfonate), (Eleflex-2000) was generously provided by Elecon, Inc.. PEDT was doped with PSS electrolyte to form a conductive dark blue solution, which has the chemical structure shown in Figure.6. 2. Table 6. 1 summarizes the properties and characteristics of the conductive polymer used for this research.

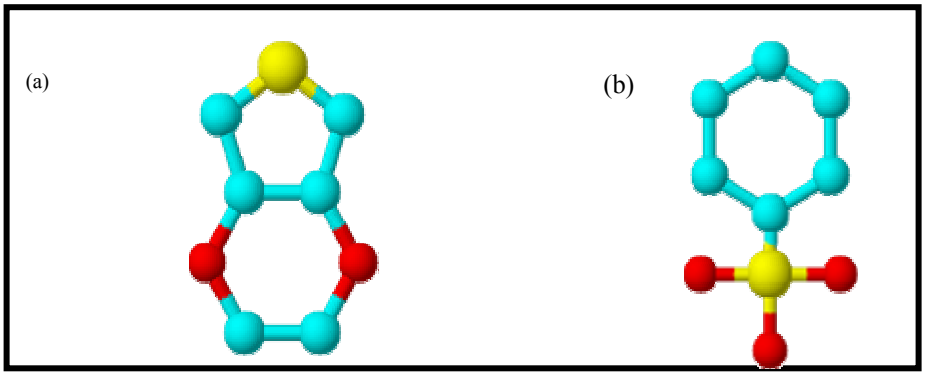

Figure 6. 2 Chemical Structure of (a) Poly(3,4-ethylenedioxythiophene) & (b) poly(styrenesulfonate).

Table 6. 1 The characteristics and properties of the used PEDT conductive polymer.

Characteristic	Value
Chemical Designation	Poly(3,4-ethylenedioxythiophene)poly(styrenesulfonate) [PEDT/PSS] 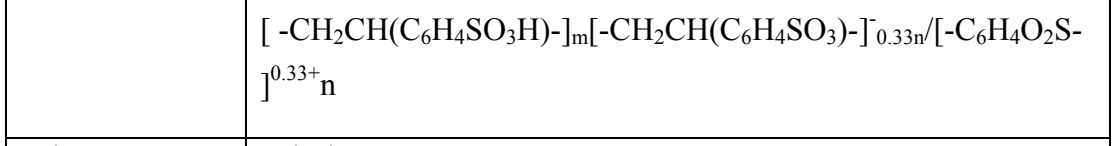
Odor	Odorless
Color	Dark blue
Boiling Point	Approximately 100 ^{o}C
Density	Approximately 1 g/cm3 at 20 ^{o}C
Vapor Pressure	23 mbar at 20 ^{o}C
PH value	1-2 at 20 ^{o}C
PEDT band gap	1.6 eV
Solvent System	80:20 EG:NMP
Viscosity	375 cp, 20 ^{o}C
Coating bulk conductivity	36.6 S/cm
Additional comments	Filtered with 5.0 micron Nylon filter.

Starting from this part of research, we will refer to PEDT/PSS by only PEDT. We couldn't electrospun PEDT as a pure polymer, so we tried to find a spinnable polymer to be the carrier for PEDT. As PEDT is not an easy soluble polymer so the choices of carrier polymers were limited. We found out that water is the best solvent for

PEDT, also PEDT can easily dissolve in DMF, and hence we chose the PAN to be the carrier solvent.

The materials used

Polyacrylonitrile (PAN) was purchased from Scientific Polymer Products, Inc. (Sp^2), in powder form, 150,000 M_w & density of 1.184 g/cc. N,N-Dimethylformamide 99%, (DMF) solvent was purchased from Fisher Scientific, inc.

Preparations of polymer solutions

Measurements were made by weight % by using the digital balance shown in Figure 6. 3.

1. The calculated amount of DMF solvent was weighed and placed into a vial.
2. PEDT polymer weight was measured and mixed with the DMF using the magnetic stirrer for 10 min.
3. Finally, the calculated amount of PAN was mixed with the previous solution and placed onto the magnetic stirrer for 25-30 min applying heat 60 ^{0}C.
4. Step 2 was skipped when pure PAN solution was prepared.

Processing Parameters

The PEDT/PAN solution was electrospun using the electrospinning station shown in Figure 6. 4 using the following parameters:

- Concentrations (wt %) at 8, 10, & 1 2wt% of PAN/DMF and each concentration was mixed with PEDT at 10, 15, 20, 25& 40 wt%.
- Distance from spinneret to target (H in cm) = 15-20 cm
- Electrical Potential (V in volts) = 25 KV.

- Spinning angel, (θ in degrees) = 90^0 (vertical position)& 45^0 (inclined position)
- Environmental conditions = Room Temperature T and Room Humidity (RH %)
- Target was a metal screen covered with aluminum foil.
- Fixed amount (1 ml) of the polymer solution for each run.
- Clean glass pipette of 0.9 mm tip diameter for each run or a (Perfekum Micro-Mate) interchangeable hypodermic syringe of gauge 20 cc with a (precision glide) needle of 18G1 1/2 (with blunt end)

Figure 6. 3 Scientech Digital balance, Model SA-120.

The electrospinning station used for spinning the PEDT-PAN into nanofibers is illustrated in Figure 6. 5. The nanofibrous can be collected into vertical ($\theta = 90^0$) or inclined ($\theta = 45^0$) positions. The form of fibers is self-assembled yarn, which will be discussed, in the following chapter.

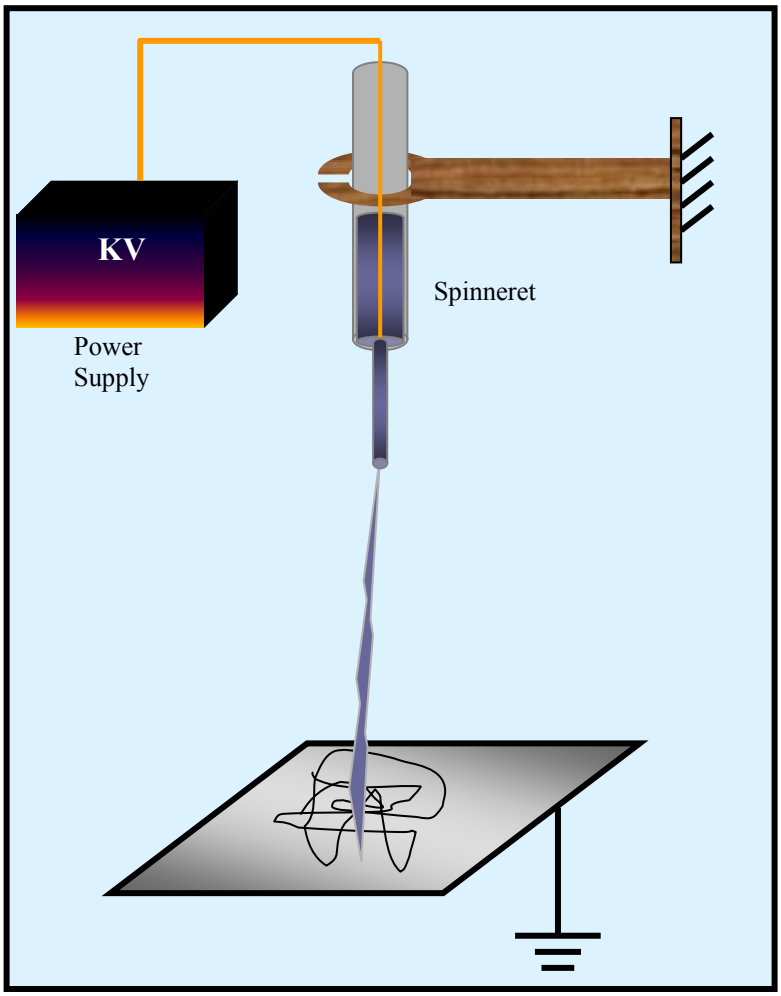

Figure 6. 4 Schematic of the Electrospinning station for foming PEDT-PAN nanofibers.

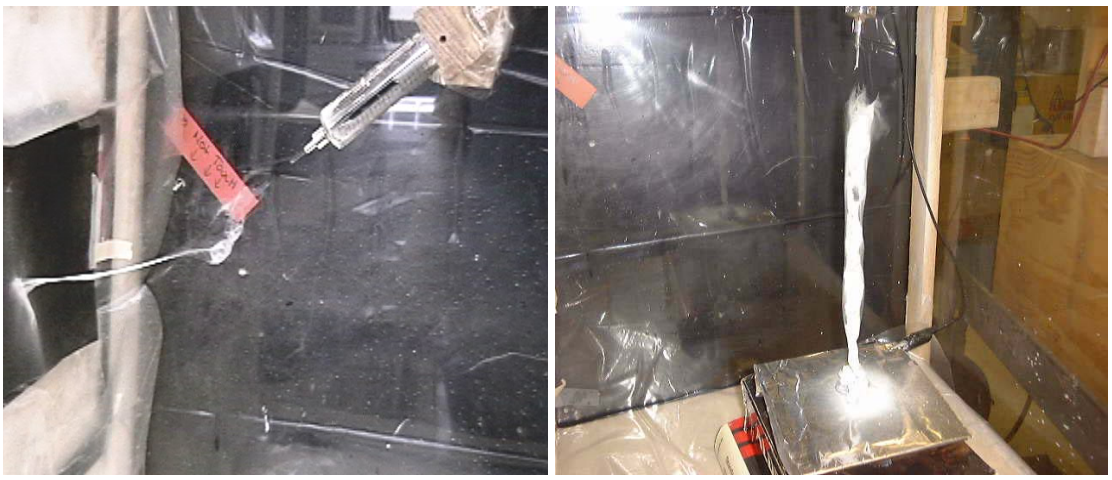

Figure 6. 5 The electrospinning station used for forming PEDT/PAN nanofibrous yarn in inclined and vertical position.

6.2.2 Intrinsic Viscosity Measurements.

Intrinsic Viscosity is the ratio of the specific viscosity of a polymer to the concentration of it at infinite dilution. Also it is defined as the quantity that relates viscosity to the molecular weight and the intrinsic structural differences of the solute molecules (hence, it is obviously important in determining the molecular weight.)

The intrinsic Viscosity of PEDT and PAN were measured to figure out the effect of adding the PEDT to the PAN system. The method used to measure the intrinsic viscosity was carefully explained in **Appendix .I.** The time vs. concentration; for the solvent and each polymer, was measured and has been recorded in the following tables.

Table 6.(2-4).

Table 6. 2 Time vs. Concentration for PAN (M_w 150 000)/DMF.

Concentration (g/dl)%	Polymer wt.	Reading (sec)	Average Time
0	0	10/10/10	10
0.2	0.0144	13-13-13	13
0.4	0.0288	18-18-18	18
0.6	0.0432	24-24-24	24
0.8	0.0576	31-31-31	31
1	0.072	40-40-40	40

Table 6. 3 Time vs. Concentration for PEDT-PAN /DMF.

Concentration(g/dl)%	Reading (sec)	Average Time
0	10/10/10	10
0.2	12/12/12	12
0.4	16-16-16	16
0.6	23-23-23	23
0.8	29-29-29	29
1	38-38-38	38

Table 6. 4 Time vs. Concentration for PEDT/DMF.

Concentration (g/dl)%	Polymer wt.	Reading (sec)	Average Time
0	0	10/10/10	10
0.23800362	0.0167	10/10/10	10
0.409742773	0.0288	10/10/10	10
0.619001647	0.0436	10/10/10	10
0.913015783	0.0645	10/10/10	10
1.249894196	0.0886	10/10/10	10

6.2.3 Differential Scanning Calorimeter: DSC.

All the Differential Scanning Calorimeter (DSC) measurements were carried out using Perkin-Elmer DSC 7 model, which is illustrated in Figure 6. 6. About 20 mg of the tested samples (PAN, PEDT, PEDT/PAN in fiber form) were packed into a stainless steel DSC cell. The samples were tested before by Thermogravimetric Analyzer (Perkin-Elmer TGA 7 model – Figure 6. 7) to determine the range of the temperature used for DSC. To remove any traces of solvent or contaminations, before the DSC measurement, each sample was kept for an hour, in a Dry Oven. The heating/cooling rate used in this study was 10 ^{o}C/min. each sample was heated from 20 to 150 ^{o}C, next cooled to 20 ^{o}C and heated again to 150 ^{o}C.

Figure 6. 6 Differential Scanning Calorimeter (Perkin-Elmer DSC 7).

Figure 6. 7 Thermogravimetric Analyzer (Perkin-Elmer TGA 7)

6.2.4 Morphological analysis and diameter distribution of fibers using Scanning Electron Microscope, SEM.

The Scanning electron microscope used in **Part. I** was used here to examine the morphology of the PEDT-PAN nanofibers and calculate the diameter of the fibers. To set an idea bout the electrical properties of the fibers an image was taken with and without gold sputtering.

6.2.5 Chemical Analysis by FT-IR Spectroscopy.

Fourier transform-infrared (FT-IR) spectroscopy was used to follow the conformation changes that occur in the PEDT/PAN/DMF solution during the dope preparation stage and the electrospinning process that produces solid nanofibers. The "Nicolet Magna- IR 560 Win FT-IR spectrophotometer is shown in Figure 6. 8.

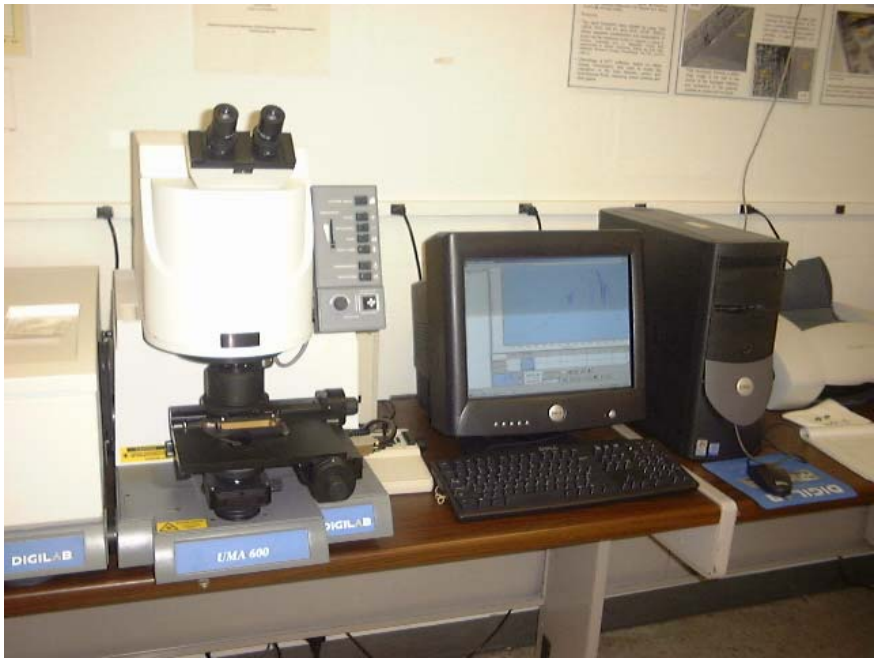

Figure 6. 8 "Nicolet Magna-IR 560" spectrophotometer.

6.2.6 Conductivity Measurements.

A four-point probe device (ALESSI CPS-06 contact probe); as illustrated in Figure.6. 9, was employed to measure the volume conductivity of the electrospun PEDT nanofibers [ASTM (D4496-87) [201]. The measurements were done in two ways; electrospun nanofibers in yarn form and in web form. For the yarn form the resistance was measured directly using the 4-probe device and plotting the readings to obtain the I/V curve analysis as shown in Figure.6. 10. For the non-woven web form, the measurements were done by electrospinning the PEDT-PAN polymer directly to the Si-wafer. The I/V curve of the Si-wafer with and without the fibers was drawn to get the resistance of the wafer and of the wafer with fibers. By considering the Si wafer and the non-woven web as resistors; in parallel connection, the resistance of the non-woven web can be calculated as explained in Appendix III.

By measuring the geometrical parameters; length, weight &area, of the test sample the resistance of the sample can be transformed to conductivity. As shown in the following simple equations (Eq 3. 1-3)

$$V = I * R \qquad \textbf{Equation 3. 12}$$

$$\rho = R * A / L \qquad \textbf{Equation 3. 13}$$

Where

•V …….. The applied volt

•I …… The current in ampere.

•R …….. The resistance of the material in ohms.

•*A* ……. The cross-sectional area that is perpendicular to the direction of the current in cm^2.

•*L* …….. The distance between the two points at which the voltage is measured in cm.

• ρ …….. The resistivity of the material in $ohms/cm^2$.

Hence the conductivity; σ , of the material can be easily calculated, as the conductivity is reciprocal of the resistivity.

Conductivity $\sigma = 1/\rho$ (in $Siemns/cm^2$) **Equation 3. 14**

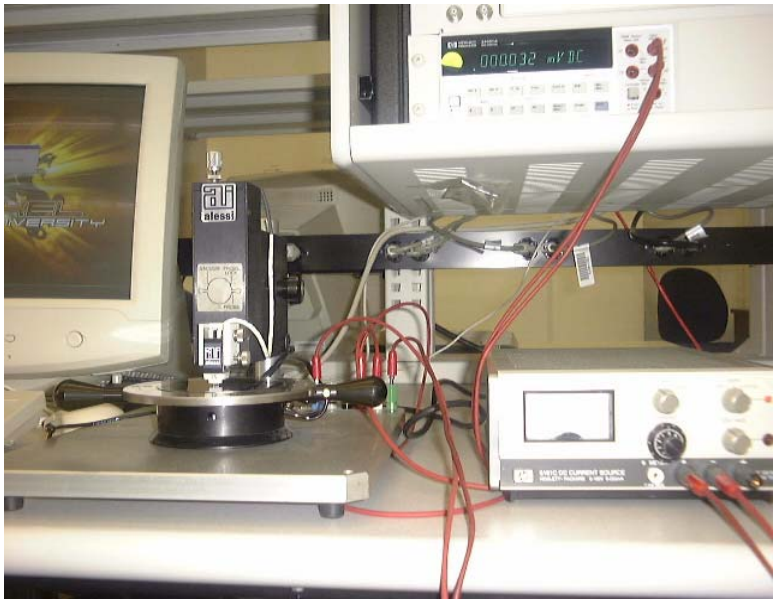

Figure 6. 9 The 4-Prope device used to measure the conductivity of nanofibers materials.

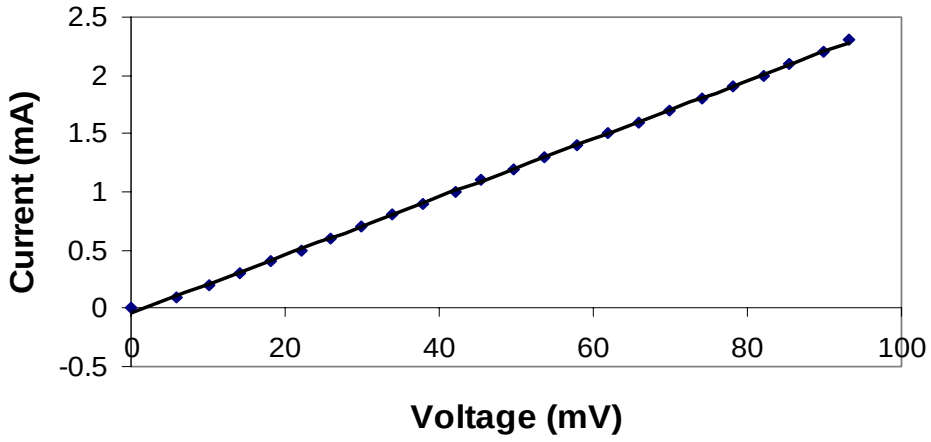

Figure 6. 10 I/V curve obtained from the 4-probe measurement.

6.2.7 Mechanical Properties.

KES G-1 micro tensile tester was used to test the stress- strain behavior of the elecrospun fibers. The used gauge length was 4 cm. Kawabata single fiber tester is shown in figure 6. 11. The tester gives the load-elongation data which is then converted to stress-strain data using the linear density of the tested sample. The details are illustrated in Appendix II.

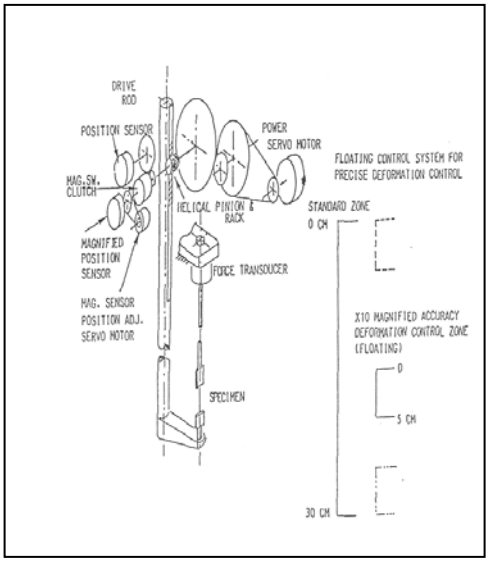

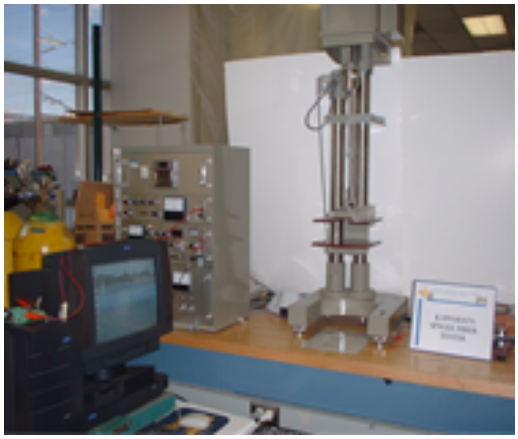

Figure 6. 11 KES G-1 micro tensile tester.

6.3 Results and Discussions.

6.3.1 Intrinsic Viscosity Measurements.

The intrinsic viscosity of PAN and PEDT can be measured as mentioned in previous chapter and illustrated in Appendix I. The following tables and figures summarize these results;

Table 6. 5 Concentration vs. Specific Viscosity/Concentration for PAN (150,000 Mw) /DMF.

Concentration (g/dl)	Specific viscosity/Concentration (dl/g)
0.2	1.5
0.4	2
0.6	2.33333333
0.8	2.625
1.0	3

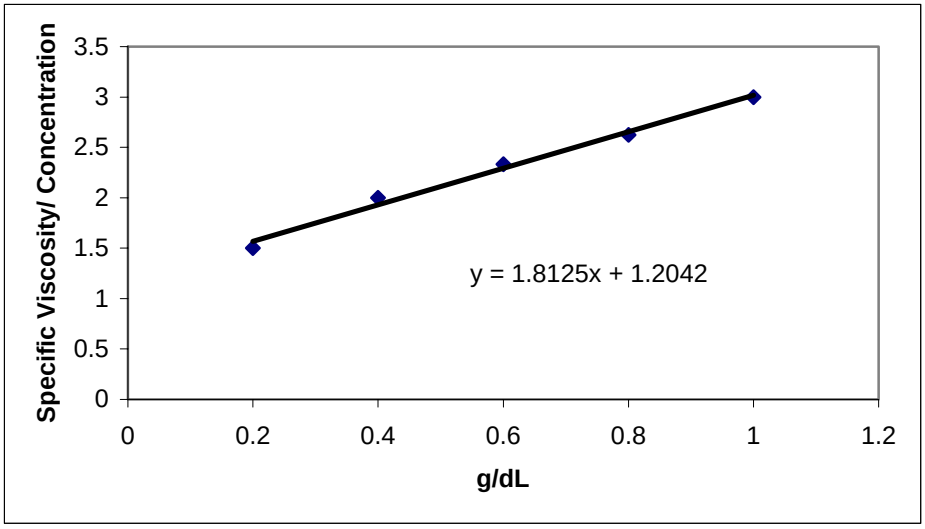

Figure 6. 12 Intrinsic viscosity of PAN & DMF.

Table 6. 6 Concentration vs. Specific Viscosity/Concentration for PEDT /DMF.

Concentration g/dl	Specific Visocity/Concentration
0.409742773	0
0.613357565	0
0.816141465	0
1.018099548	0
1.219236848	0

Table 6. 7 Concentration vs. Specific Viscosity/Concentration for PEDT/PAN /DMF.

Concentration g/dl	Specific Viscosity/Concentration dl/g
0.2	1
0.4	1.5
0.6	2.166666667
0.8	2.375
1.0	2.8

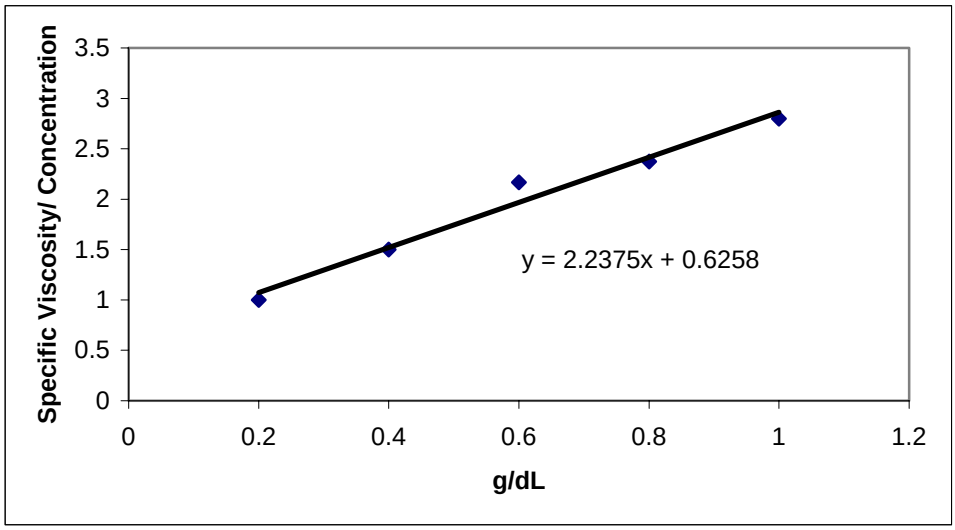

Figure 6. 13 Intrinsic viscosity of PEDT/PAN & DMF.

As shown in the Figures 6. 12 & 6. 13 and Tables 6. 6 & 6. 7, the intrinsic viscosity of PEDT/PAN in DMF is lower than of PAN in DMF 0.6 vs. 1.2 respectively. The reduction in viscosity can be explained due to the liquid form of PEDT, which increase the amount of solvent over the amount of solid content of the whole solution. This is clarified from Table 6. 5; as the PEDT has no influence on the viscosity of DMF solution, which also can be verified by the slight difference in the densities of DMF (0.944 gm/cm^3) and PEDT (1 g/cm^3).

6.3.2 Differential Scanning Calorimeter: DSC.

The TGA thermograms of PEDT powder, PAN, and PEDT/PAN fibers were compared. As observed in Figure 6. 14, the weight loss of PEDT powder was around 400 ^{o}C. The weight loss process corresponded to the degradation of PAN fibers sample was at higher temperature around 500 ^{o}C. The third curve of PEDT/PAN fibers shows the weight loss around 400 ^{o}C as the PEDT is the prominent material and the reason of lowering the temperature of sample degradation.

The DSC thermograms of the fiber samples were presented in Figure 6. 15. The PEDT/PAN fibers sample shows a lower glass transition temperature than the PAN fibers sample while it's higher than the pure PEDT T_g. The PEDT/PAN mixture curve illustrates one peak for the glass transition temperature that means that the PEDT and PAN polymer are miscible in DMF solvent and that was observed experimentally.

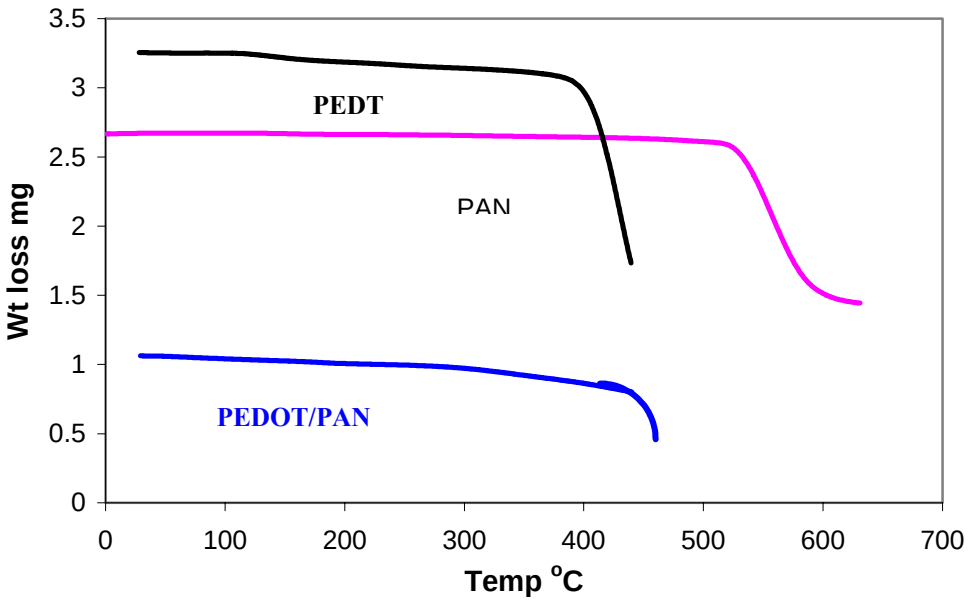

Figure 6. 14 Thermogravimetric curves of PEDT, PAN and PEDT/PAN samples.

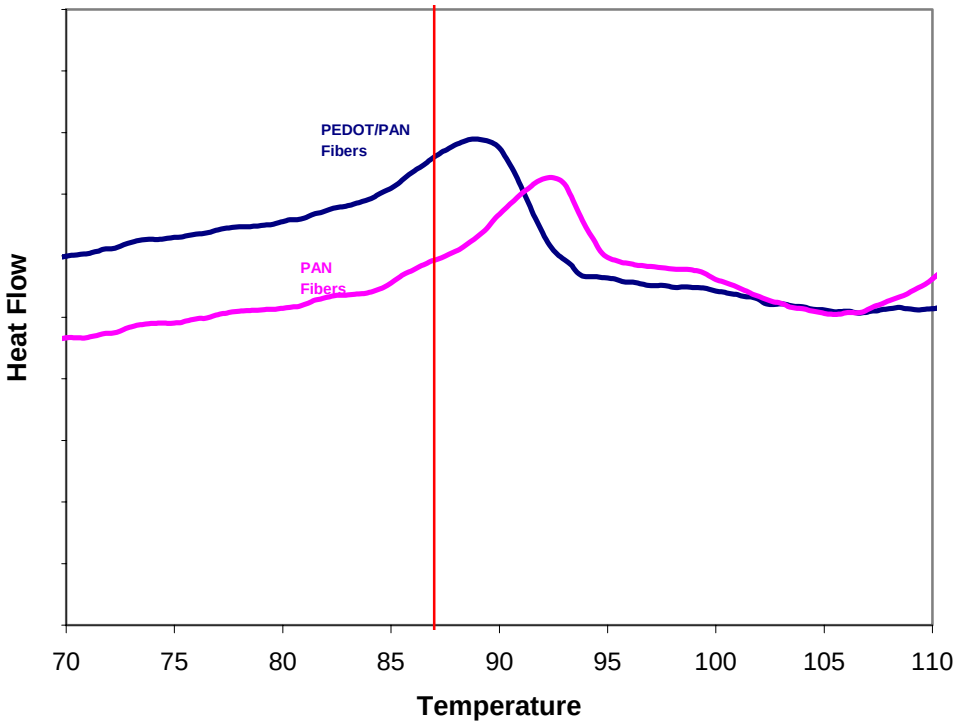

Figure 6. 15 DSC thermogram of PAN fibers and PEDT/PAN fibers.

One of the good observations of DSC results that the glass transition temperature of PAN fiber is higher than the one of PAN polymer (T_g = 87 ^oC). This suggests that the electrospinning probably enhances the polymer crystallization due to the chain orientation within the fiber. This can be understood as the solidification process of stretches chains under high elongational rate during the later stages of electrospinning may align the chain within the fiber and develop secondary bonding forces, which needs higher temperature to be broken. In addition, the overall effect of the electric field is a downward force on the charged jet, which draws it into a continuous fiber with better chain alignments.

6.3.3 Electrospinning of Self-assembled Yarn.

The PEDT/PAN polymer is electrospun into self-assembled yarn. This phenomenon was observed before by Ko et al [202] during electospinning of pure PAN. The PEDT/PAN polymer begins to be spun at certain point of the electrical grounded target and then the nanofibers continue in accumulations above each other forming the nanofibrous yarn. Figure 6. 16 illustrates the effect of PEDT presence in the PAN polymer. Pure PAN and low PEDT wt% concentration form a continuous self-assembled yarn with bigger diameter while increasing the PDEOT content to higher concentration (20-40 wt.%) improves the shape of the yarn producing a finer yarn with smooth surface.

In this process, the self-assembled yarn is initiated by an initial depositing of the nanofibers concentrated in a small area on the target. The fibers are allowed to build up on top of each other until a branched tree-like structure is formed. Once a sufficient

length of yarn is formed, the coming fibers attach themselves to the branches and continue to build up. The steps of the formation of PEDT/PAN nanofibrous yarn via electrospinning are demonstrated in Figure 6. 17. The inclined position was used to illustrate the initiation of the yarn till its complete formation.

A B

C

Figure 6. 16 Electrospinning of 8%PAN polymer with different PEDT content (A) 10 wt.%, (B) 15 wt.% PEDT, (C) 20 wt.% PEDT.

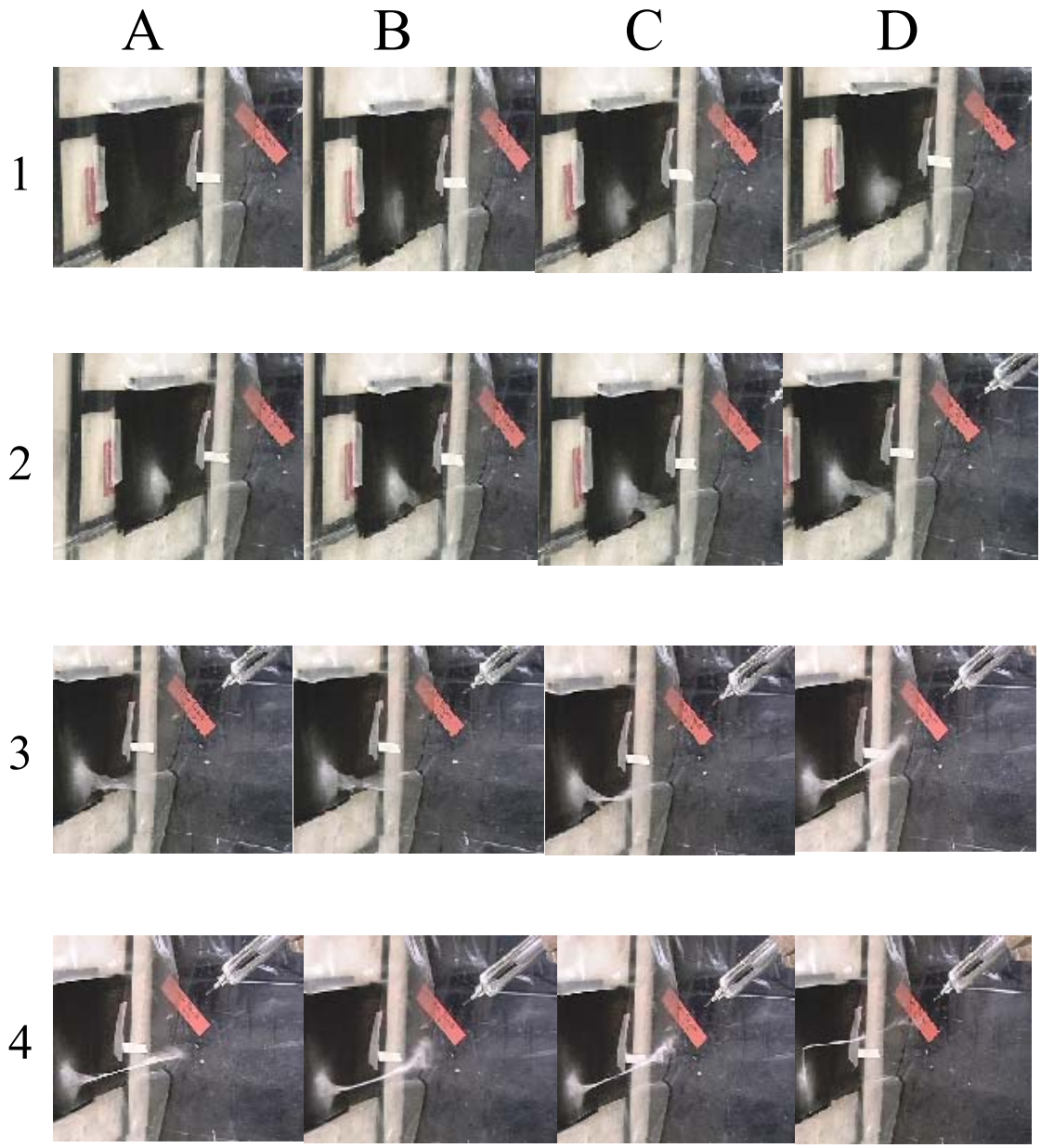

Figure 6. 17 The steps of forming the PEDT/PAN nanofibrous self-assembled yarn via Electrospinning.

Figure 6. 18 (A1-C4) are showing the electrospinning of PEDT/PAN nanofibrous yarn. The PEDT/PAN solution is positively charged; via copper wire which is inserted in

the pipette, at 1.5 kV/cm charge density. The polymer jet is ejected out of the pipette tip forming Taylor cone, the stable zone and then the unstable zone (Figure 5. 7) due to the evaporation of the solvent.

In Figure 6. 17 (A1-A4), the fibers hit the target at 10 cm electrospinning distance and start to initiate (the first whit spot on the black surface) and form the nanofibers. As soon as the PEDT/PAN form a considerable amount of fibers, the nanofibers attract to each other forming the first tip of the yarn that could be now considered as the new target to the coming nanofibers. The nanofibers continue in accumulations forming the self-assembled yarn as shown in Figure 6. 17 (B1-C4).

The electrospinning process could be continuing with the continuity of PEDT/PAN polymer feeding and taking up the formed nanofibrous yarn. Moving the target position downward as illustrated in Figure 4.17-C could be one of the taking up system, or building up a take-up rolling system as will be discussed in the next part.

This phenomenon could be explained by studying the chemical structure of the used polymers. PAN polymer contains a polar Carbon-Nitrogen triple bond; as illustrated in Figure 6.18-a, which carries a negative charge due to the difference in the electronegativity of Carbon and Nitrogen elements, 2.55 & 3.04 respectively. The strong triple C-N bond posses a negative polarity, which is neutralized with the positive polarity of C-C single bond.

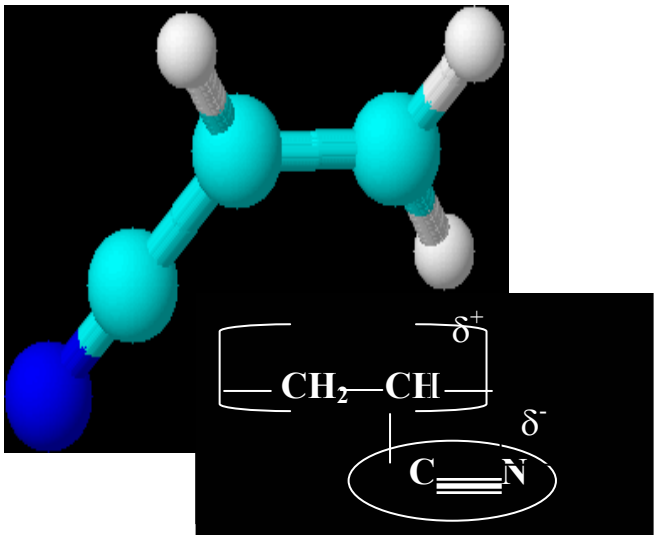

(a)

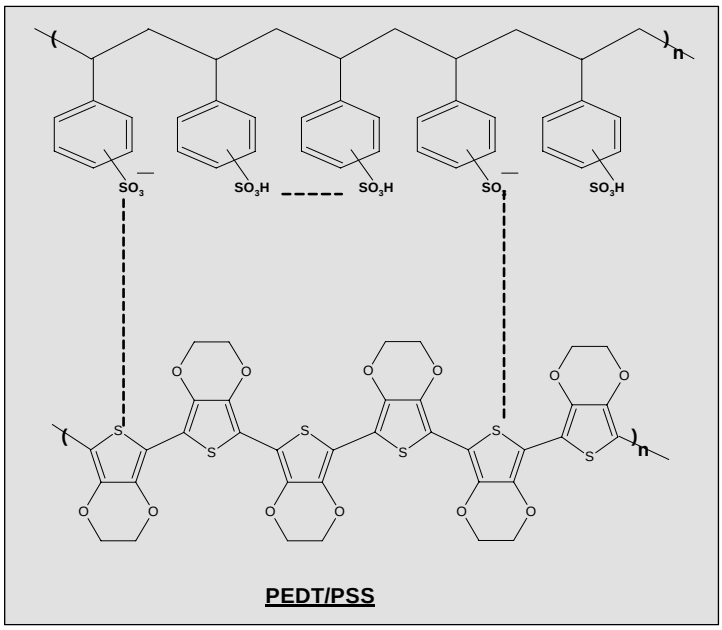

(b)

Figure 6. 18 (a) Chemical Structure of PAN polymer and (b) Chemical Structure of PEDT/PSS$^-$.

If we assume that the polymer is charged with a positive (or negative) charge, this charge starts to leave the polymer as the solvent evaporated leaving very fine fibers with a neutral charge. Now the fibers is exposed to two different types of forces, the first one is the attraction electrical forces (between the fiber and the charged polymer jet) and the second type is the dynamics forces due to the speed and inertia of the jet and the gravity of the fibers. At first the fibers build up under the influence of charge attraction forces and then accumulated to each other resting on the target surface under the influence of the dynamic forces and the help of repulsion forces. The presence of the PEDT/PSS^- negative charge helps with building the fibrous yarn; due to the interaction of the negative charge of PSS, the polymer charge and the polarity characteristic of the PAN molecules, and forms a uniform fine nanofibrous yarn.

To summarize this phenomenon, Figure 6. 19 demonstrates the shape of the formed yarn and the forces that probably control the electrospinning process. The forces could be the dynamic ejecting force of the jet, the weight gravity of the fibers, the electrical attraction forces between the fibers (due to the negativity of PEDT, the positivity of the charged fibers and polarity characteristic of PAN) and the attraction forces between the fibers and the target. In the other direction, we have the repulsion electrical forces of the PEDT and other charged fibers, and the attraction between the polymers charged jet and the fibers. The interaction between those two directions forces form the self-assembled yarn, when they are in balance, the unstable zone is appeared and when the downward forces dominate, the nanofibers start to accumulate and form the continuous yarn.

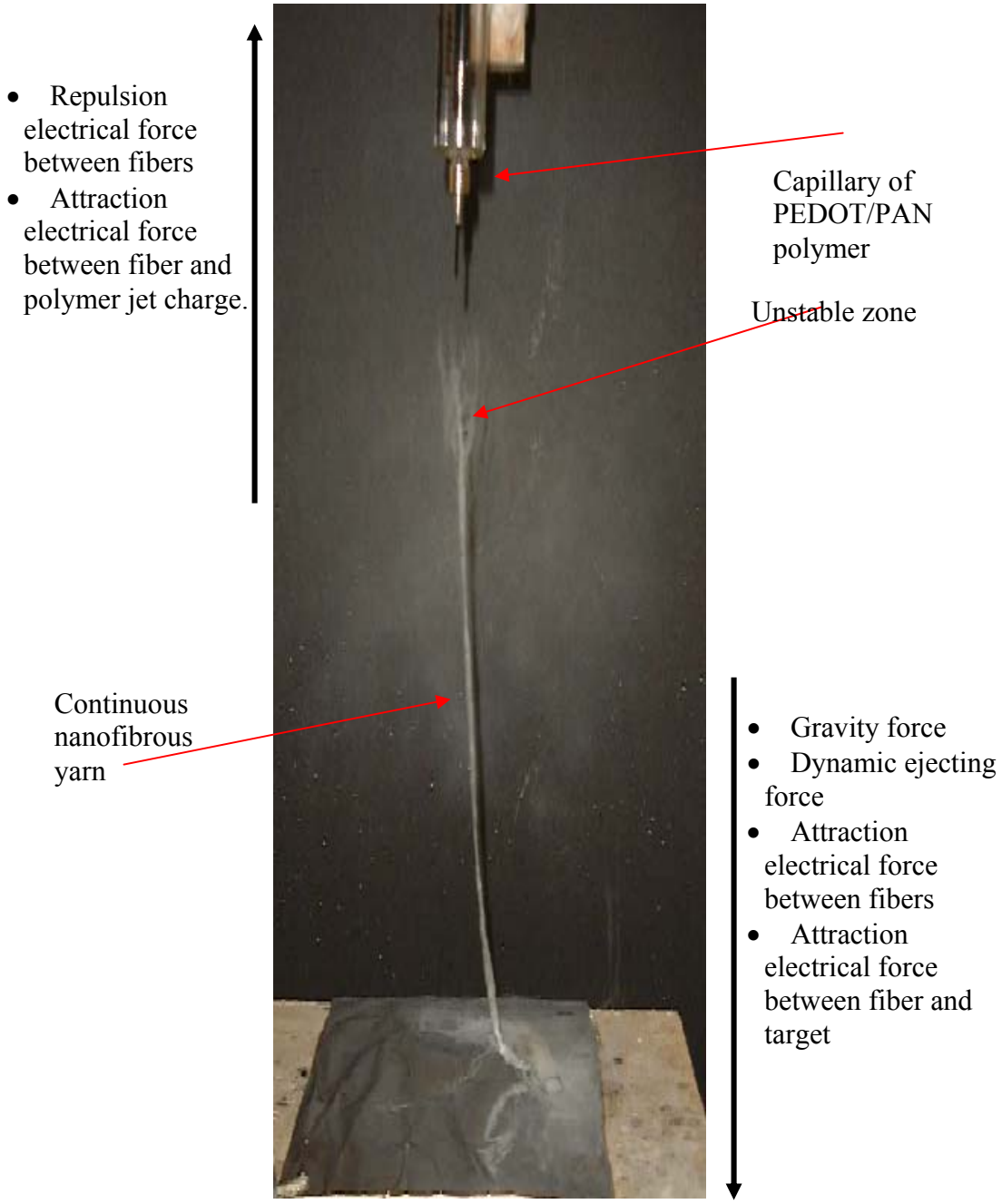

Figure 6. 19 The forces applied to the nanofibers during the formation of electospun yarn.

6.3.4 Morphological analysis and diameter distribution of fibers using Scanning Electron Microscope, SEM.

Pure PEDT polymer was dried into a casting film and examined by the SEM. Figure 6. 20 illustrates the images of the pure PEDT showing the spherulitic structure of the PEDT. This spherulitic structure of PEDT indicates the crystallization region in the polymer which promising better mechanical properties for the electrospun fibers.

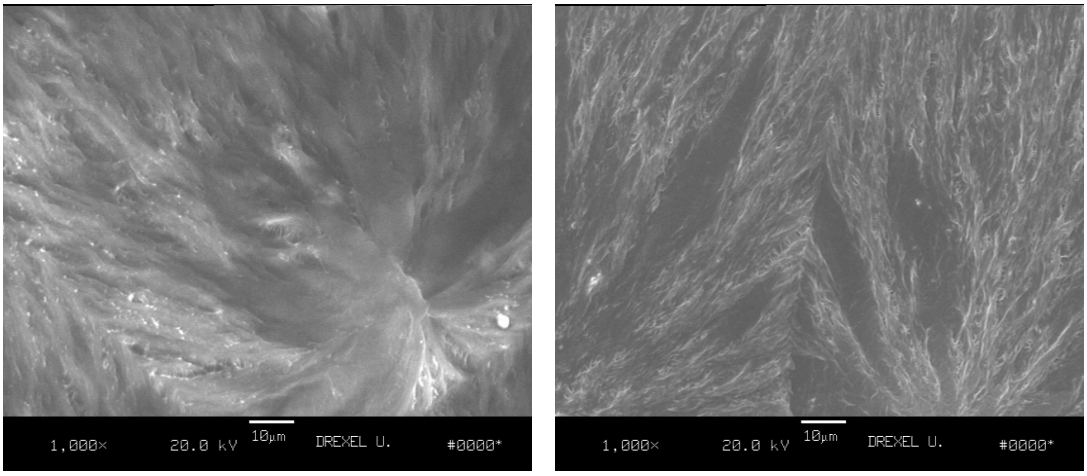

Figure 6. 20 Scanning electron microscopy photographs of pure PEDT (thin cast film) showing its spherulitic structure.

Figure 6. 21 show the diameter distribution of 20%PEDT/8%PAN nanofibers. The fibers diameter range form 150 nm to 450 nm with a minimum fiber diameter of 50 nm. Most of the fibers vary between 200-300 nm. The statically analysis of the recorded data gave an average diameter of 340 nm.

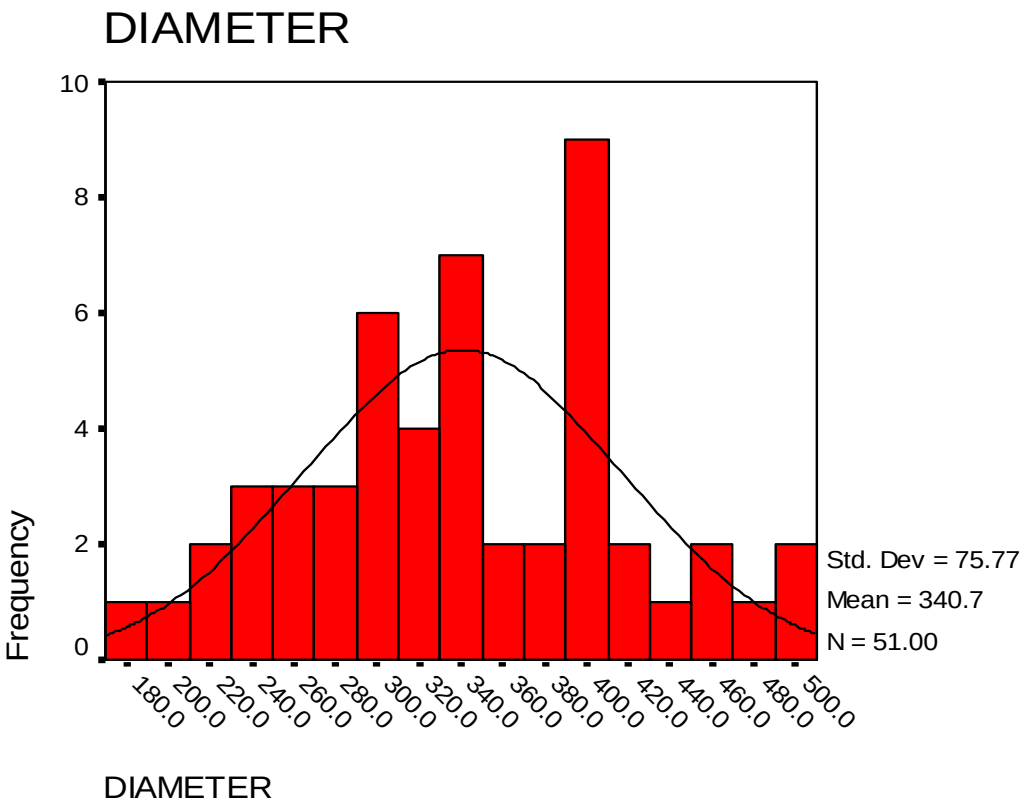

Figure 6. 21 The diameter distribution of 20 wt. % PEDT/8 wt.%PAN nanofibers.

6.3.5 Effect of PEDT on the nanofibers alignment.

Figure 6. 22 demonstrates the influence of PEDT concentration on the alignment of PEDT/PAN nanofibers. At 0 wt. % of PEDT (pure PAN); A1-C1 in the figure, there is tendency of alignment while at 20 & 30 wt. % of PEDT, the SEM images (A2-C3) showing a good alignment of the nanofibers within the yarn.

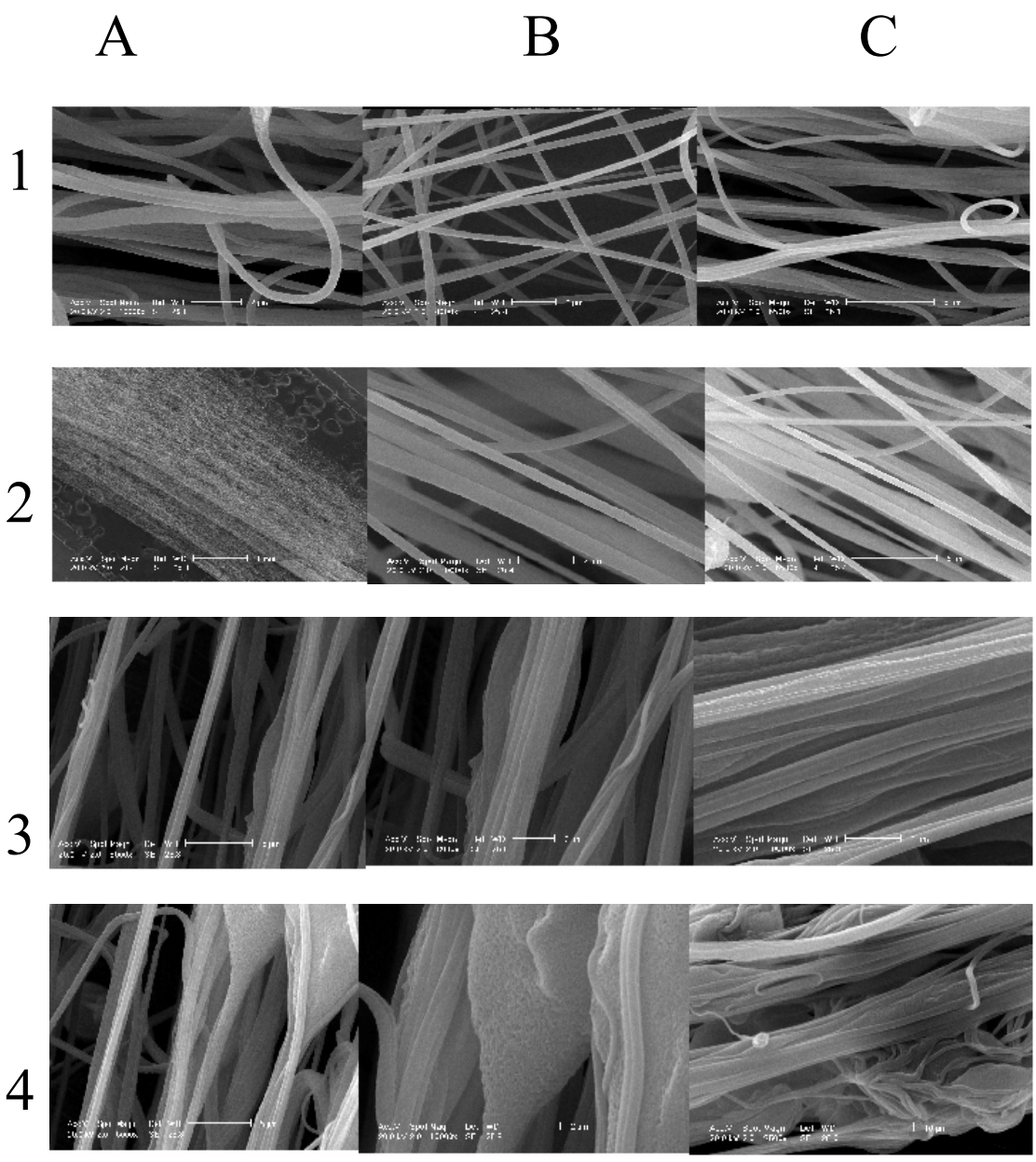

Figure 6. 22 Scanning electron microscope photographs of 8 wt.% PAN with different PEDT content. (A1-C1) 0 wt.% (pure PAN), (A2-C2) 20 wt.%, (A3-C3) 30 wt.%, and (A4-C4) 40 wt.%.

In Figure 6.22 (A4-C4), a partial alignment is observed but a bulk beads are found due to the increase of PEDT content (40 wt. %) which lower the viscosity of the solution and the solvent was not completely evaporated.

8 wt. % PAN with 20 wt. % PEDT blend presents the optimum nanofibers alignment with smooth surface as shown in Figure 6. 23 (a, b& c). The self-assembled yarn has a high degree of fibers alignment which promising better mechanical properties.

6.3.6 Effect of PEDT on the nanofibers diameter.

It was observed that the presence of PEDT in the PAN fiber has a significant effect on the nanofibers diameter. In Figure 6. 24, it is evident that by increasing the PEDT content, the fiber diameter is decreased. Three different PAN concentrations were tested (8, 10, 12%) in the upper histogram, each concentration was blended with three different concentrations of PEDT (15, 20, 25%). For each category of the PAN concentration, the higher is the amount of PEDT content, the lower and finer is the fibers diameter. The lower histogram shows other PAN% categories (7, 8 &9%) with the same three PEDT concentrations. It is clear that the PEDT polymer has a great effect on the diameter of the PEDT/PAN blend. This means that we can reach diameters below 100 nm by increasing the amount of PEDT to higher than 25-30 wt%. To study the morphology of increasing the PEDT content, SEM images need to be done.

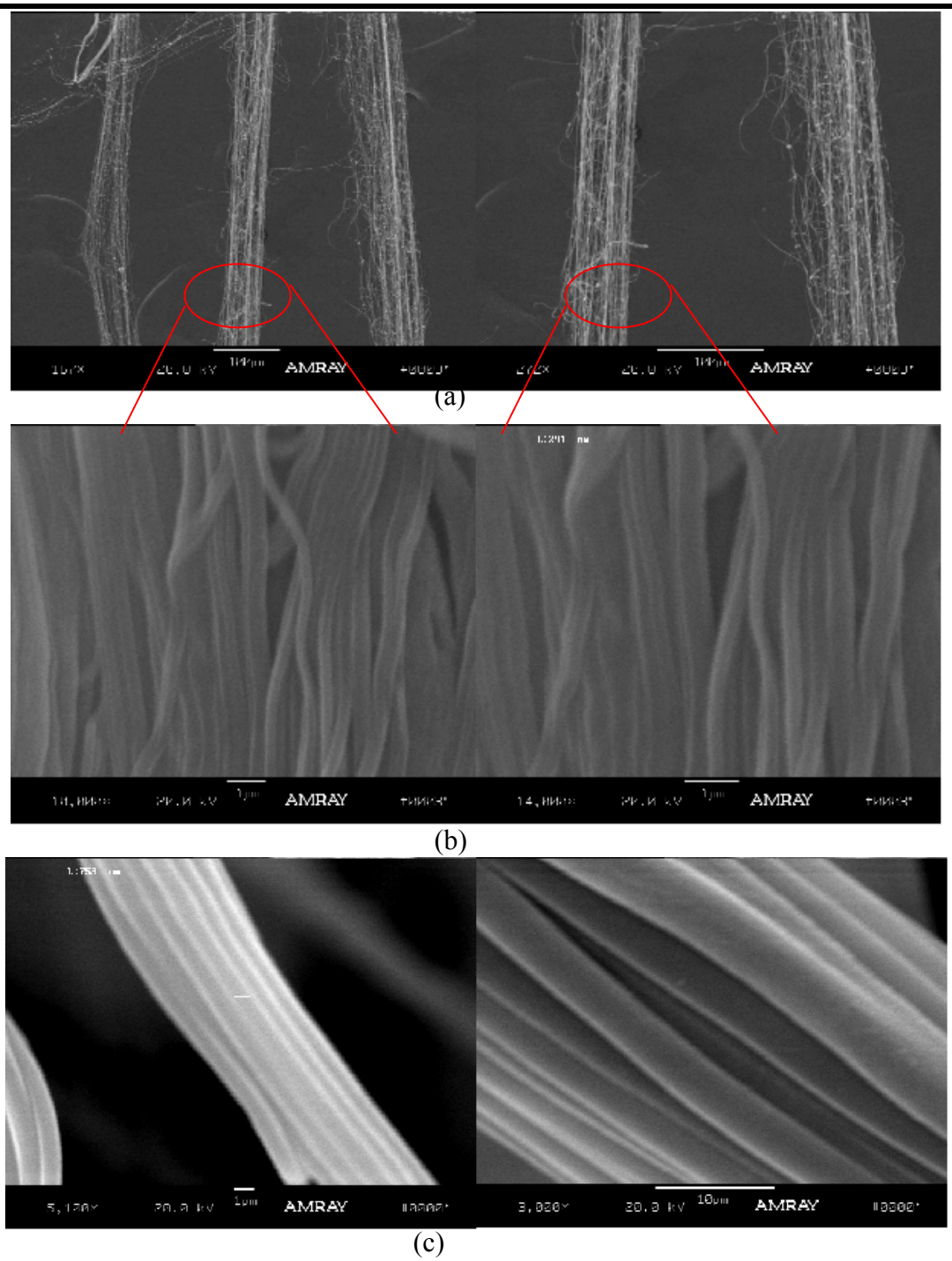

Figure 6. 23 SEM of 8wt.% PAN & 20 wt% PEDT showing the aligned smooth surface nanofibers within the yarn.

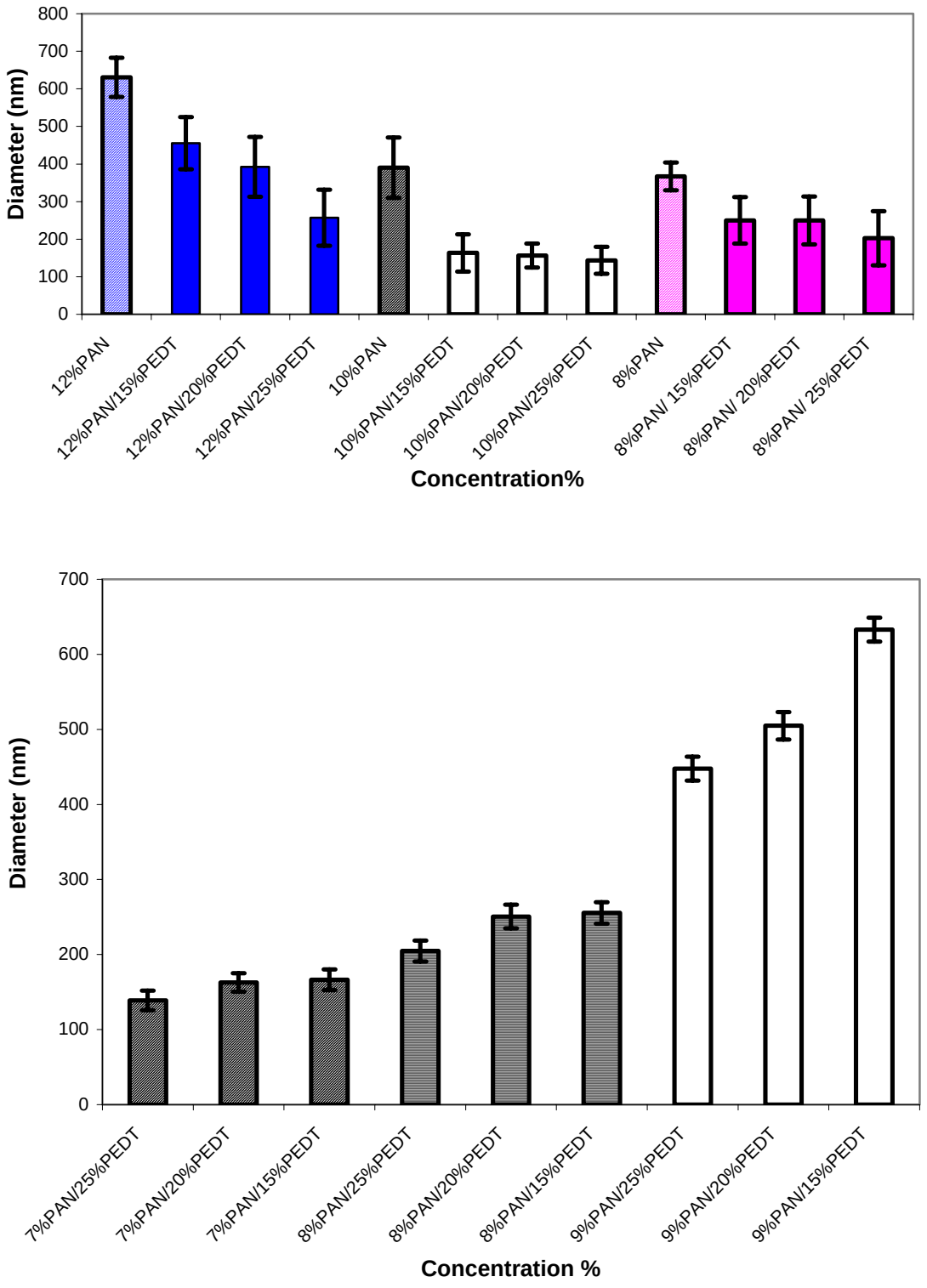

Figure 6. 24 Effect of PEDT content on fibers diameter.

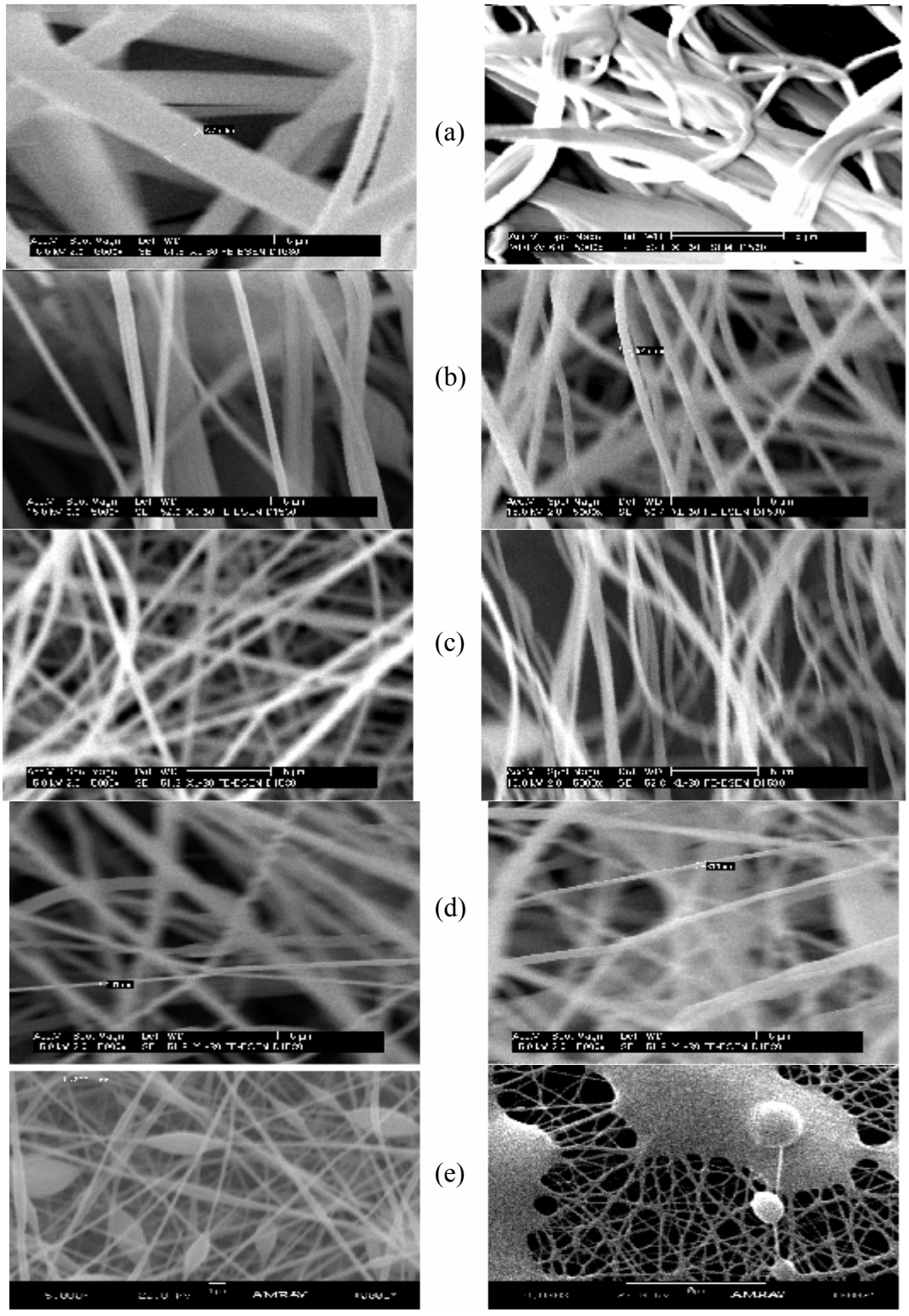

Figure 6. 25 SEM (5000X) of PEDT/PAN fibers at different wt%. (a) 12%PAN/10%PEDT, (b) 12%PAN/25%PEDT, (c) 8%PAN/15%PEDT, (d) 8%PAN/20%PEDT, (e) 8% PAN/40%PEDT.

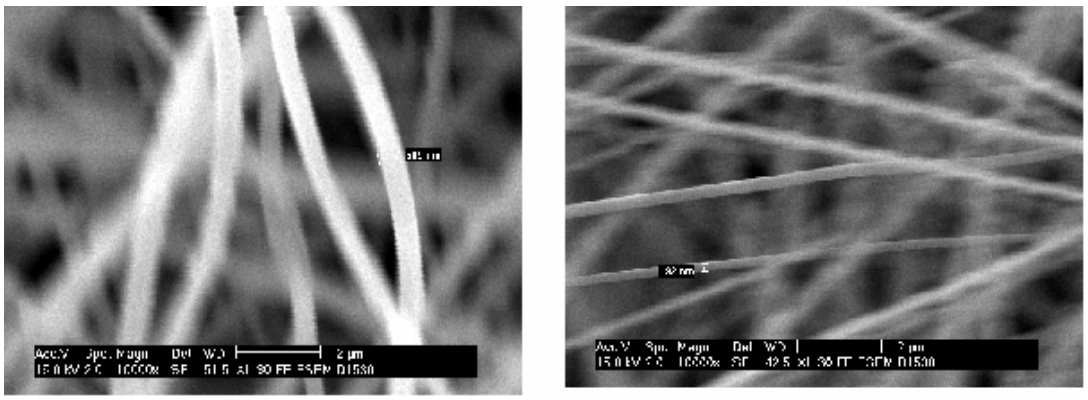

(a) (b)

Figure 6. 26 SEM (10000X) of PEDT/PAN nanofibers (a) 10%PAN/20%PEDT, (b) 10%PAN/40%PEDT.

Scanning electron microscopy photographs of various PAN concentrations with different PEDT content are illustrated in Figure 6. 25. The SEM images emphasis the effect of PEDT on the fibers diameter. In (a&b) for the same 12% PAN concentration with different PEDT content; the fibers diameter has been decreased with increasing the PEDT concentration. Figure 6. 25 (c-d) shows the optimum conditions for nanofibers diameter with 8%PAN and 15-25%PEDT, which give finer fibers with uniform surface. As mentioned above, increasing the PEDT content to higher than 30% would decrease the fiber diameter which is proven in (e) images but the presence of beads and polymer droplets control that trend as increasing the PEDT also decrease the viscosity of polymer and increase the tendency of forming polymer drops with the nanofibers.

Figure 6. 26 shows the great effect of PEDT content on the nanofibers diameter, as the average fiber diameter of 10%PAN/20% PEDT is 400-500 nm while it is 15 nm with 10%PAN/40%PEDT. Therefore, by controlling the concentration of PAN and

PEDT we can reach a considerable low fiber diameter with uniform and smooth nanofibers.

6.3.7 Chemical Analysis by FT-IR Spectroscopy.

Figure 6. 27.30 shows the IR spectra for pure PAN polymer and PAN nanofibers. As illustrated there are no major differences between the two samples in the major peak bands. However, it's also seen that the intensities of some minor peaks either decreases or disappears altogether. This can be attributed to the effect of electrospinning process on the chain alignments within the fibers. The spectra of PAN cast film show clearly the peaks of 2246 cm^{-1}; which assigned to C≡N triple bond and 2931 & 2865 cm^{-1}; which can be assigned to C-H asymmetric and symmetric in CH & CH2 groups.

The inclusion of PEDT polymer is illustrated in Figure 6. 28. There is no major difference between the three spectra of PEDT polymer, PEDT/PAN and PAN fibers. The new peaks may be attributed to the presence of PEDT in the blend, new bands around 1222 cm^{-1} due to the presence of C-O-C linkage and the finger print peaks of PEDT at 900 to 2000 cm^{-1}[187].

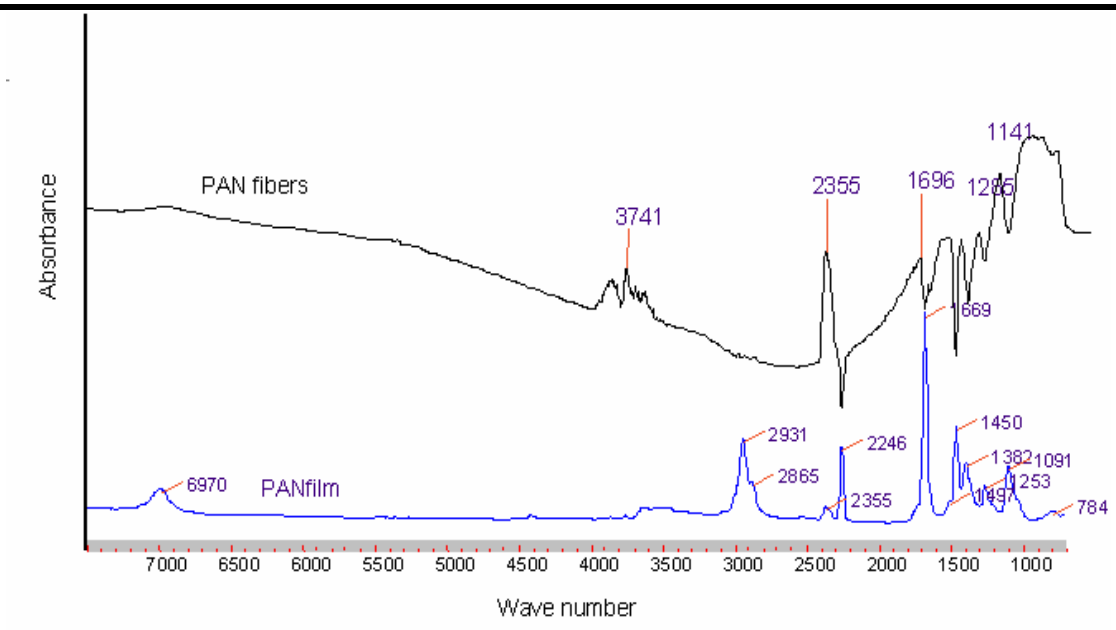

Figure 6. 27 FT-IR spectra of PAN fibers and PAN cast film.

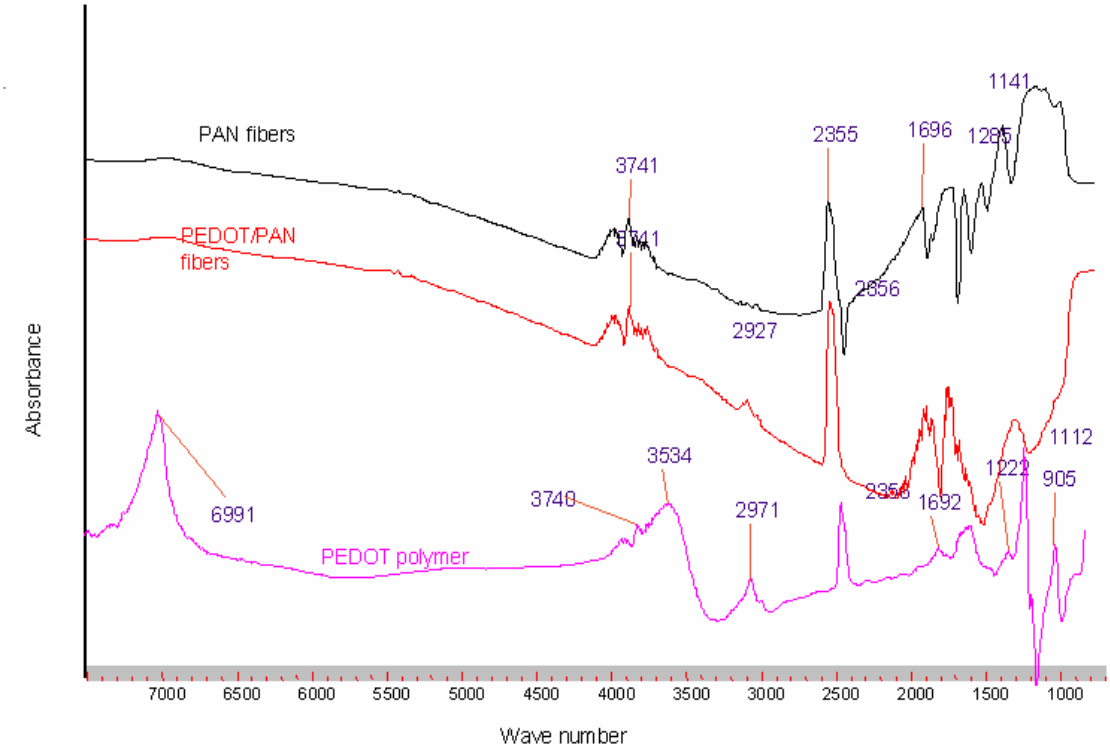

Figure 6. 28 FT-IR spectra of PEDT polymer and PEDT & PAN fibers.

6.3.8 Conductivity Measurements.

Although the process of charge conduction in small diameter polymers is not clearly known, it has been suggested that unusual current conduction properties arise when the size of wires are reduced below certain critical thickness [198]. It has also been argued that a rectifying contact to a wire would perform better if the wire size were reduced to below such a critical thickness. Hence, it is expected that new polymeric wires and contacts may behave more favorably when confined to operate in such reduced dimensional regimes (nanoscale). Also, the fibers in nanoscale give high level of specific surface area that enables high coherence forces between the fibers. Hence, it will result in higher strength, surface energy and higher electrical conductivity.

Figure 6. 29 gives a theoretical example of the effect of fiber diameter and geometry on the conductivity value. By using the simple equation (eq. 3.2) that relates the conductivity of a material with it resistance and geometry, it is easy to show the influence of diameter size on conductivity. It is assumed that we have two wire with different cross-sectional shape; circle (e.g. fibers) and square, having the same length and resistance and the cross-section area varies from centimeters to nanometers. As shown in the Figure 6. 29, the circular cross-sections give higher conductivity values than the square cross-sections and; within each categories, the smaller is the diameter (cross-section area) of the wire the higher is the value of electrical conductivity. This simple derivation proves the hypothesis that reducing the dimensions of the fibers increases the electrical conductivity and also the geometry of the fibers enhances the conductivity.

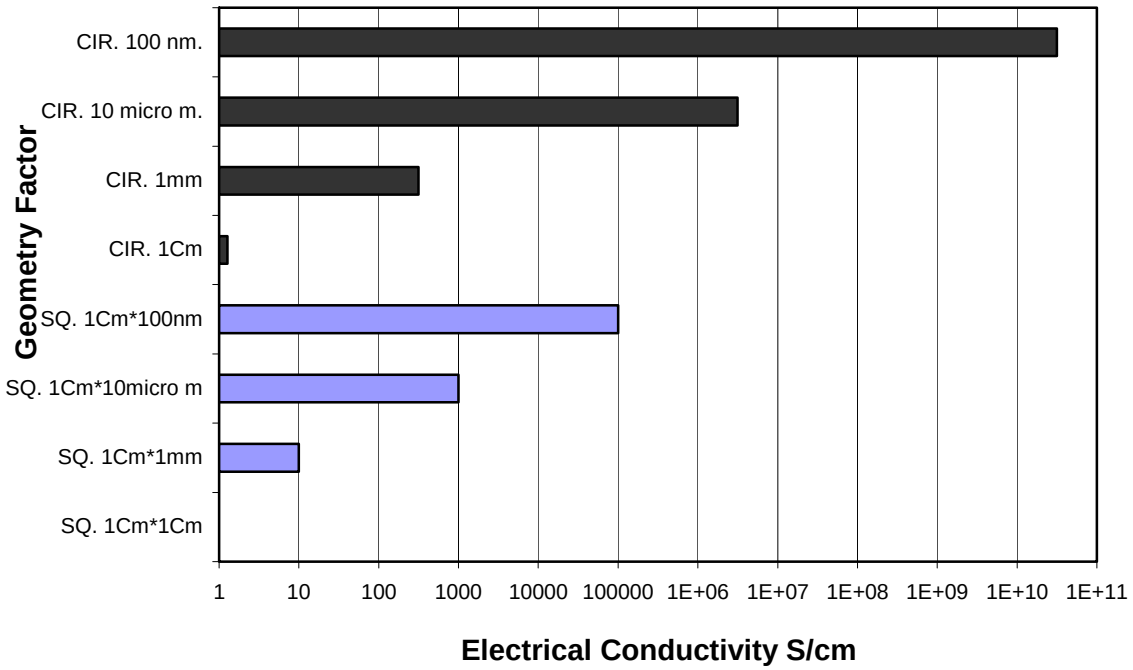

Figure 6. 29 The effect of geometry factor and fibers diameter on the electrical conductivity.

The SEM was used to examine two samples of PEDT/PAN fibers; one sample coated with gold and the other was not exposed to that sputtering process, to give a hint of the electrical properties of PEDT polymer. Figure 6. 30 shows the PEDT/PAN samples with (b) and without (a) gold coating to indicate that PEDT posses electrical properties.

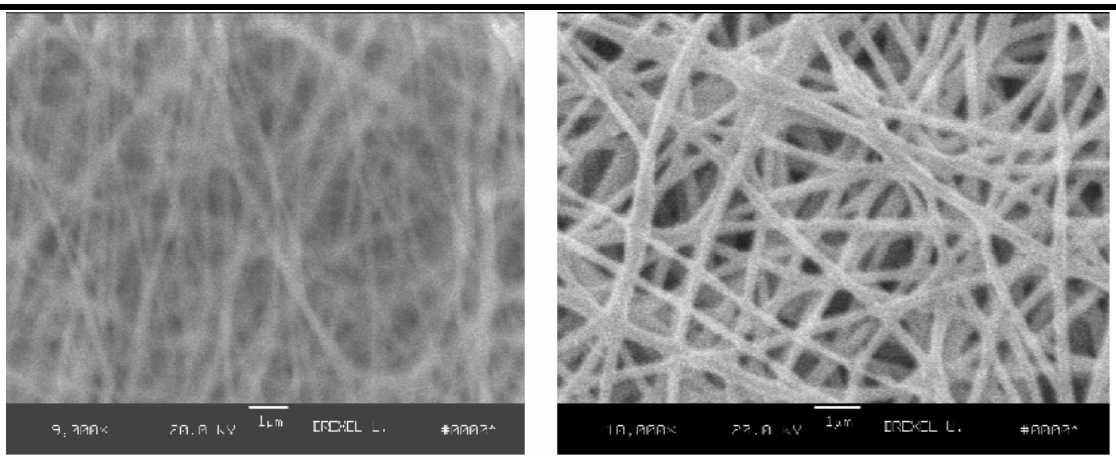

(a) (b)

Figure 6. 30 SEM images of PEDT/PAN nanofibers (a) without gold coating, (b) with gold coating.

6.3.9 The effect of PEDT concentration on the fibers conductivity.

The influence of PEDT concentrations on the electrical conductivity of PEDT/PAN electrospun fibers is shown in Figure 6. 31. Two different PAN (7&6 wt.%) concentrations were blended with three (15, 20, & 25 wt.%) different concentrations of PEDT. It is observed that; within each PAN concentrations, the higher is the PEDT content the higher is the electrical conductivity as PEDT polymer is the predominant factor of conductivity. Also, the lower is the PAN concentration, the higher the conductivity due to the increase of the effect of PEDT polymer in the fiber form. The range of the calculated conductivity was 0.0012 to 0.017 S/cm, which is within the range of conductive materials as indicated in Figure 6. 33.

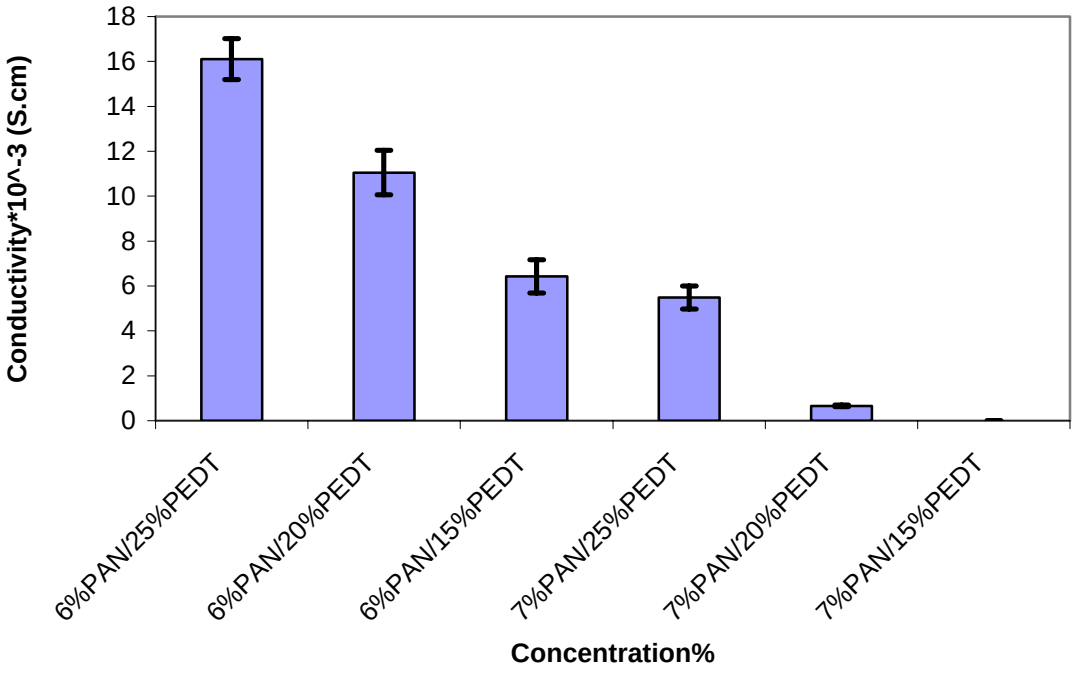

Figure 6. 31 Effect of PEDT/PAN concentration on electrical conductivity.

Figure 6. 32 shows the room-temperature conductivity of the PEDT/PAN electrospun fibers for other PAN concentrations (8 & 10 wt. %). It is evident that the increase of the PEDT content with decreasing the amount of PAN in the blend will significantly increase the electrical conductivity. The range of conductivity (0.001-0.012 S/cm) here is lower than the values in Figure 6. 31 as the PAN concentrations were increased.

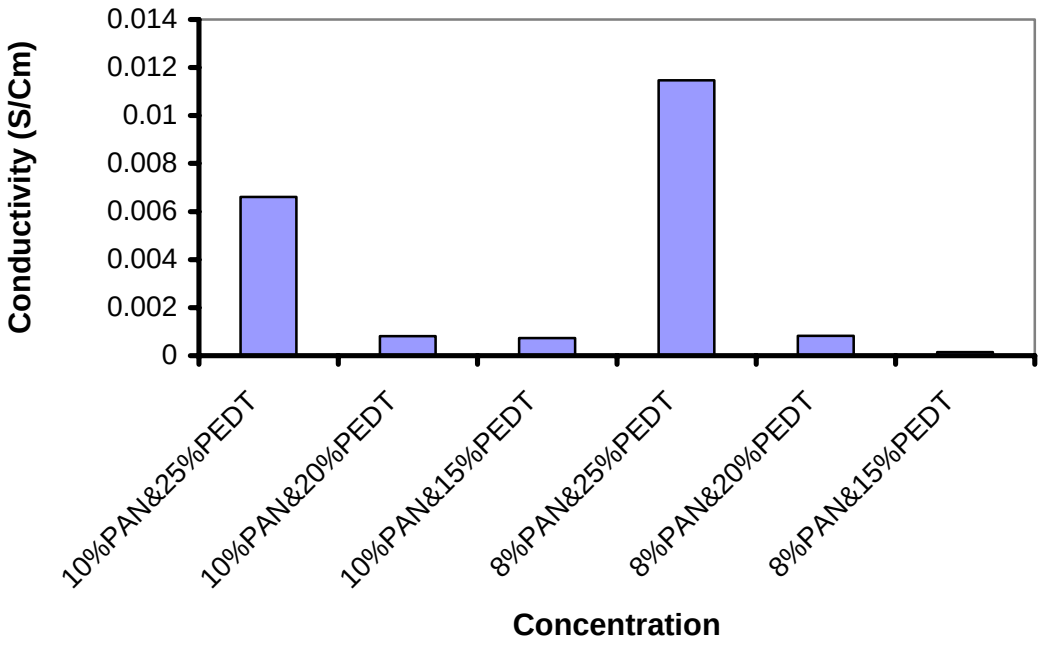

Figure 6. 32 Electrical conductivity of the PEDT/PAN blend electrospun fibers with the increase of PEDT content.

It is obvious that the conductivity of the electrospun fibers in the non-woven mat or self-assembled yarn is significantly lower than that for a cast film of PEDT (~37 S/cm). This is not an unexpected result as the four-point probe method measures the volume resistivity from which the conductivity can then be calculated and not that of an individual fiber. It must be noted that obtaining the conductivity of the non-woven mat or self-assembled yarn was considerably more difficult than measuring the conductivity of a cast film due to the difficulty in obtaining enough thickness to be tested and transferred to linear density. As can be seen form the SEM micrographs of the electrospun PEDT/PAN fibers (Figure 6. 22-23), the fibers are highly porous and therefore the "fill factor" of the PEDT fibers is less than that of a cast film. However, it

is reasonable to expect that the conductivity of an individual electrospun fiber will be higher than that of the non-woven mat or self-assembled yarn and in fact should be approximately equal to the conductivity of the cast film.

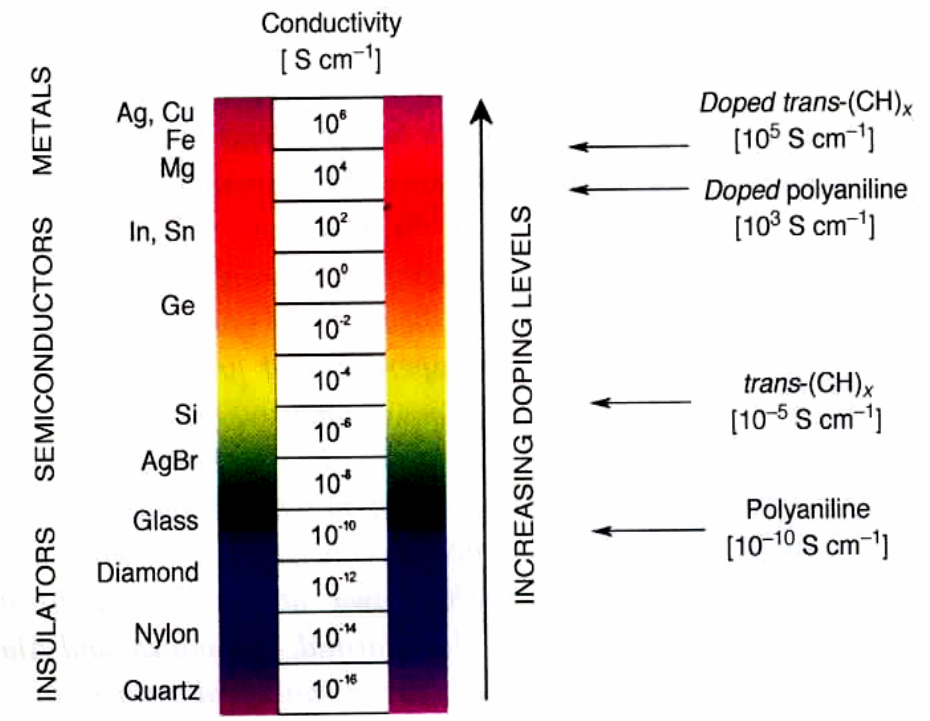

Figure 6. 33 Electrical conductivity of various materials. (a) Insulators: below 10^{-7} S/cm, (b) semiconductors: form 10^{-6} to 10^{2} S/cm, and (c) metals: above 100 S/cm.[95].

6.3.10 The effect of spinneret diameter and fibers' diameter on the conductivity.

Figure 6. 34 llustrates the electrical conductivity of PEDT/PAN fibers at different spinneret gauges. Three different spinneret diameters were used; large, medium, and small (1.2, 0.8 and 0.6 respectively). It is clear that, for each PEDT/PAN blend the lower is the spinneret gauge, the higher is the electrical conductivity, as the spinneret diameter is proportional to the fibers diameters. It is noted that the electrical conductivity is proportional to the amount of PEDT in the fiber form.

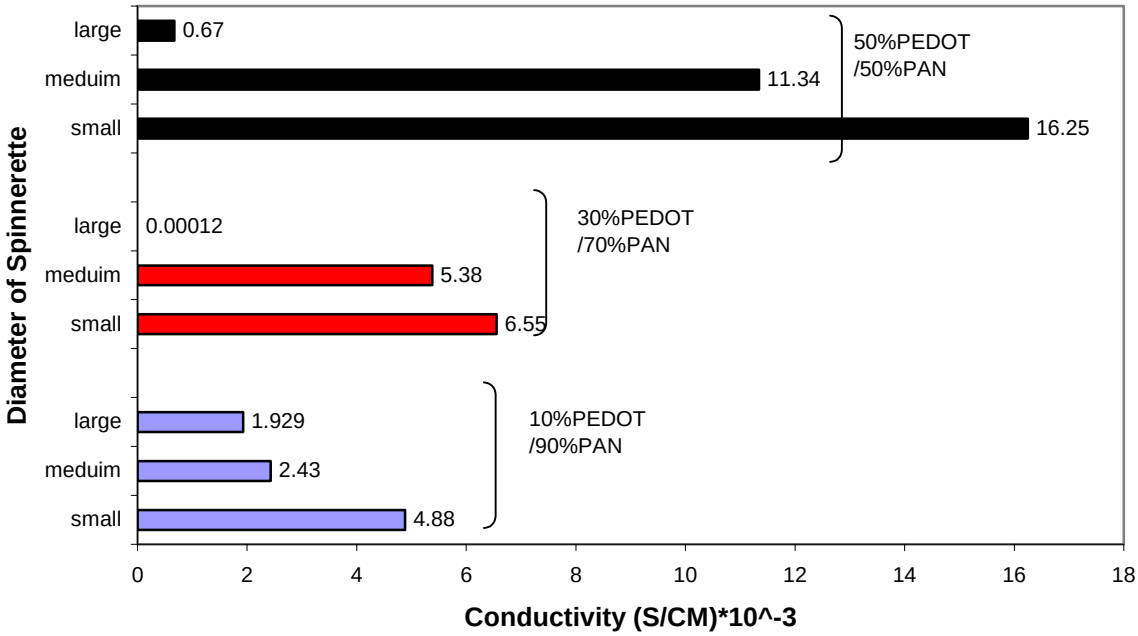

Figure 6. 34 The spinneret diameter VS. The conductivity of nanofibers for different PEDT/PAN blends.

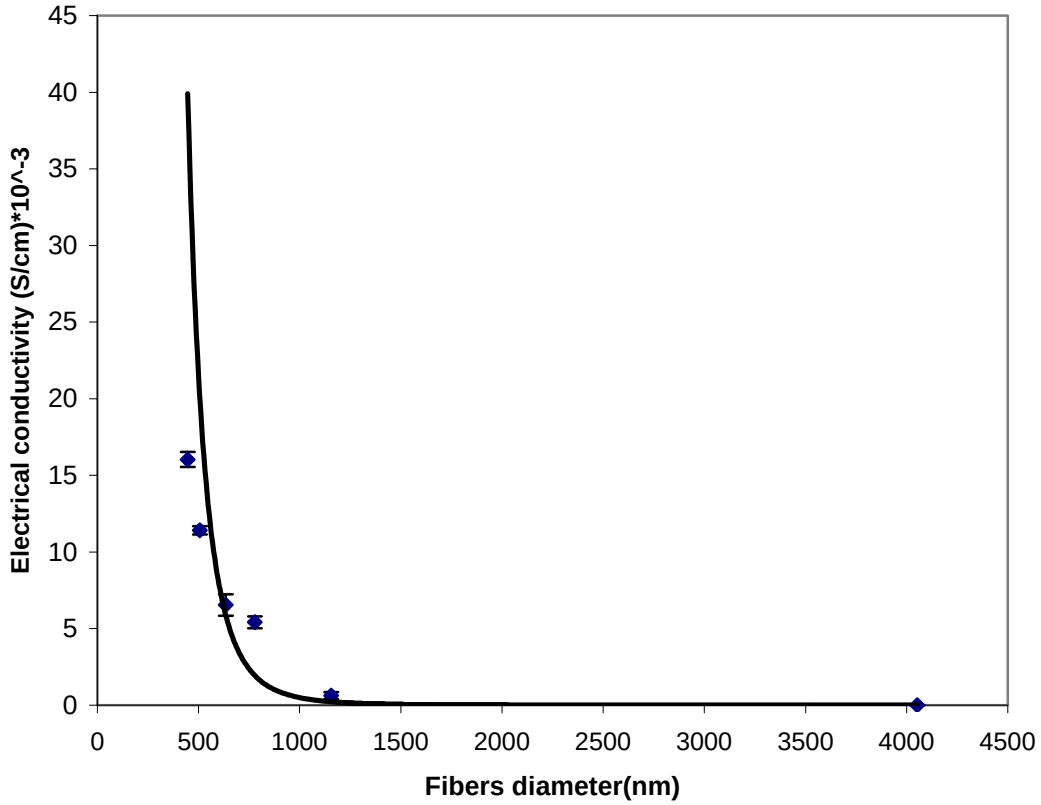

Figure 6. 35 Effect of fiber diameter (greater than 500 nm)on electrical conductivity.

The influence of electrospun fibers diameter on the electrical conductivity is illustrated in Figure 6. 35. The finer is the fibers' diameter, the higher is the value of conductivity. It shows that, interestingly, the smaller the fibers' diameter, the higher the fibers' electrical conductivity, which appears to agree with the hypothesis that elimination of small angle scattering (similar to size confinement), can increase conductivity. Encouraged by those results, PEDT concentrations were increased to reduce the electrospun fibers as mentioned before. Figure 6. 36 shows lower diameters with higher conductivity values, but we should put into considerations that increasing the

concentrations would increase the fibers diameter and at the same time decrease the uniformity of the electrospun fibers due to the beads and polymer droplets. The high surface area provided by the nanoscale fibers help with increasing the volume conductivity of electrospun nanofibrous yarn. The point is by reducing the fiber diameter, the small angle scattering reduces and transport of charge is facilitated that helps electrical conduction.

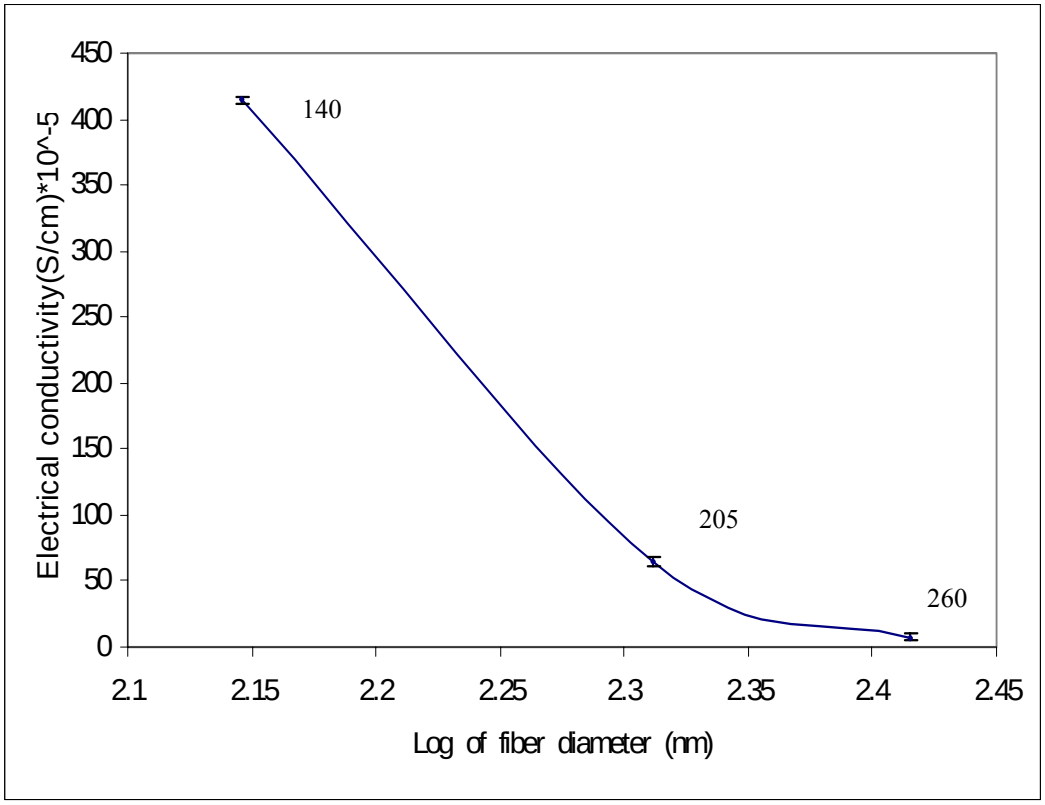

Figure 6. 36 Effect of fiber diameter (less than 500 nm) on electrical conductivity.

6.3.11 Mechanical Properties.

The mechanical properties of PAN fibers and PEDT/PAN fibers were characterized by stress-strain measurements. Figures 6. 37 shows typical stress-strain curves of PEDT/PAN fibrous yarn of different PEDT concentrations, and PAN nanofibrous yarn and mats of different PAN concentrations at room temperature and humidity. PAN non-woven mats; of 6, 7, &8 wt. % concentrations, show similar curves with yield points around 7% strain. The ultimate strength of PAN non-woven mats is in the range of 2.5-5.5 MPa. It is observed that for the same PAN content, the self-assembled yarn has higher strength and yield strain than the non-woven mat values. This improvement referred to the alignment of the fibers within the yarn surface, which enables higher number of fibers to share the applied load. The nanofibers are exposed to elongations and draw factor during the process of yarn formation that enables the chain molecules to be oriented within the fibers as indicated by the DSC results.

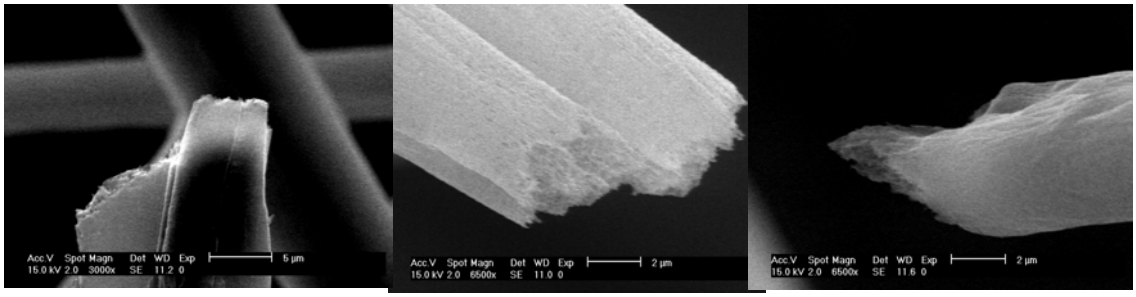

Figure 6. 37 The ductile failure mechanism of the tested PEDT/PAN fibers.

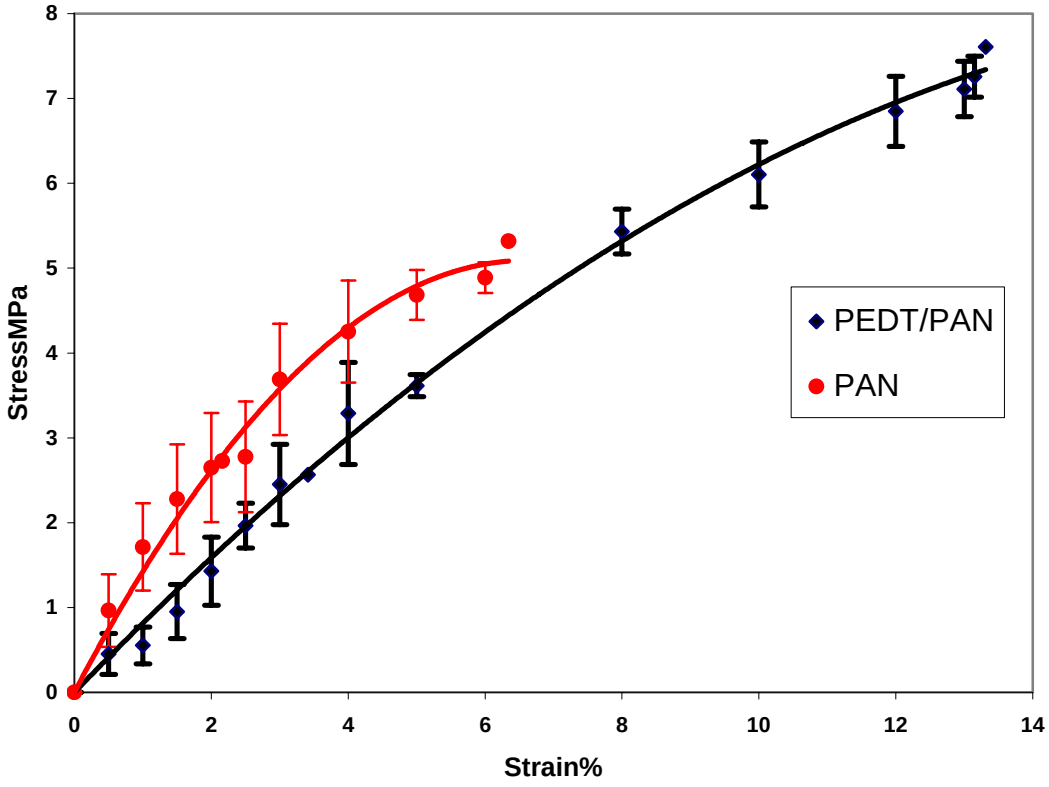

Figure 6. 38 Average stress-strain curves of PAN& PEDT/PAN at different concentrations.

Table 6. 8 Mechanical properties of PEDT/PAN and PAN nanofibrous yarn.

Solution contents	Elongation to break (%)	Ultimate strength (MPa)
PAN non-woven mat	6-7	5.5
PEDT/PAN yarn	12-14	7-8.5

The ultimate strength of PEDT/PAN nanofibrous yarn is in the range of 7-8.5 MPa and with yield points around 12%, which are comparable higher than the PAN values. It is obvious that PEDT/PAN yarns are mechanically strong and tough compared to the pure PAN yarn. This is noted in the ductile failure that illustrated in Figure 6. 38. The crystalline feature of PEDT polymer that reinforces the yarn probably explains the better mechanical properties of PEDT/PAN yarns. It is noted that for higher contents of PEDT, we got lower strength this might be due to the formation of beads with higher concentration, which work as defects and stress concentration in the yarn. The results for PEDT/PAN yarns are summarized in Table 6. 8 with the data for PAN non-woven mats and yarns.

Chapter 7: Co-electrospinning of Carbon nanotubes based PEDT nanocomposites.

7.1 Introduction.

As mentioned previously in the literature review, Carbon nanotubes are remarkable materials, which are presently being studied widely because of their extraordinary electronic and mechanical properties. Recently the interest on using CNTs for various applications has increased, as shown in Figure 7. 1. It summarizes that fact with the increasing in number of publication through the last decade. In recent years the dispersion of nanometer-sized materials in the polymer medium was suggested as an effective method to increase the properties of the system. One promising candidate as the nanocomposite component is the single-walled carbon nanotubes SWNTs. Polymer composites with CNTs are expected to improve the electrical and mechanical properties of the matrix polymer; hence we will introduce the SWNTs to our PEDT/PAN nanofibrous composite and will test the properties before and after the CNTs use.

The single-walled carbon nanotubes (SWNTs) used in this study were generously supplied by Rice University, and were synthesized by the HiPco method. The specifications of the used SWNTs are illustrated in Table 7. 1.

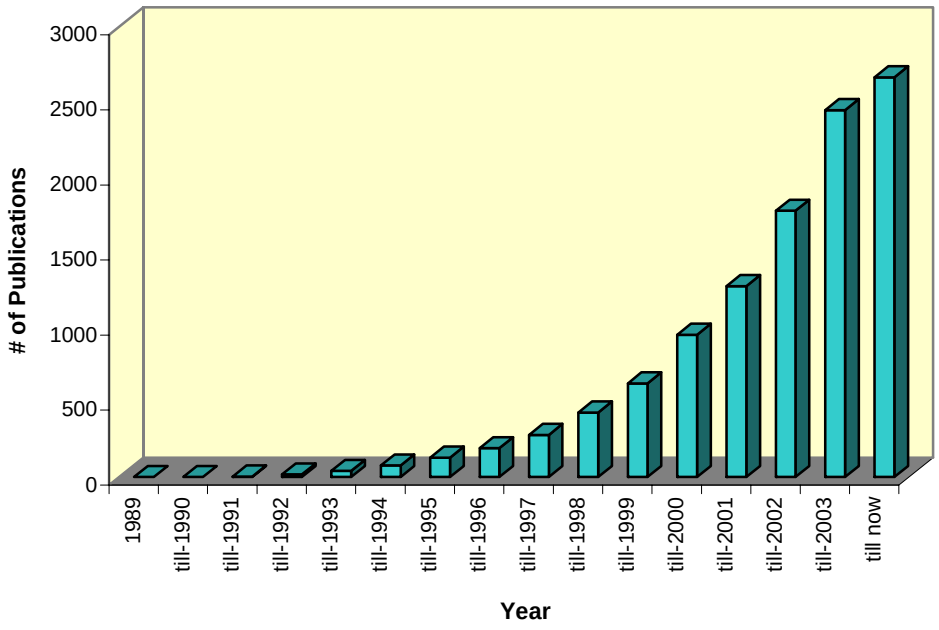

Figure 7. 1 The number of CNTs publications over the last decade.

7.2 Materials and Methods.

7.2.1 Dispersion of SWNT in DMF solvent and polymer solution preparation.

The purification process of the SWNT is explained in Appendix IV. As the SWNTs sample is obtained in the wet state, so drying process is needed before dispersion process. The SWNTs Sample is dried in vacuum oven approximately at 100^{o}C for 2 hours. The reduction in the weight of the sample indicates the purification action and contaminations removal out of the single wall carbon nano-tubes.

Table 7. 1 The specifications of the used SWNTs.

Property	Value
Average diameter	1.2-1.5 nm
Average length	1 - 2 μm
Type	Armchair (10,10)
Density	1.33 g/cm^3
Resistivity	~ 10^{-4} Ω.cm

After the SWNTs are completely dried, they are ground to as a fine powder as possible to facilitate the weighing process. DMF solvent is used as dispersion medium as DMF is the common solvent for both PAN and PEDT polymers.

Doping Preparation Procedures

DMF as a solvent was selected related to achieve good dispersion.

- Weigh the amount of SWNT and place it in the vial and then add the calculated amount of DMF.
- Using the magnetic stirrer, disperse the SWNTs in the DMF for at least 12 hrs (~20 hrs).
- Poly (vinylpyrrolidone); PVP (10,000 Mw purchased from Sigma-Aldrich inc), is used as a surfactant to wrap the nanotubes and prevent them from re-aggregating or agglomerating, 1% of PVP is measured out and added to the SWNTs solution and expose the vial to water bath sonication for 30 min.

- The calculated amount of PEDT is then added to the vial and the whole solution is magnetically stirred for 15 min.
- Finally, the required amount of PAN polymer is measured and added to the previous solution and heat (60 ^{o}C) should be applied during the magnetic stirring for mixing for 25-30 min, till the mixture becomes homogenous.

Processing parameters

- ❖ The SWNTs concentrations used with were: 0.2, 0.5, 0.8 & 1 wt% (CNTs weight in the fiber form) of SWNTs with 20% PEDT-8% PAN, and 3% 5% wt of SWNTs with 10% PEDT-5% PAN. It is evident that the higher is the CNT concentration the higher is the viscosity of the prepared polymer, so for higher CNT concentrations, the solid content of PEDT/PAN should be decreased.
- ❖ Distance from spinneret to target (H in cm) = 15-20 cm.
- ❖ Electrical Potential (V in volts) = 25 KV.
- ❖ Spinning angel, (θ in degrees) = 90^{0} (vertical position).
- ❖ Environmental conditions = Room Temperature T and Room Humidity (RH%).
- ❖ Target was a metal screen covered with aluminum foil.
- ❖ Fixed amount (1 ml) of the polymer solution for each run.
- ❖ Clean glass pipette of 0.9 mm tip diameter for each run or a (Perfekum Micro-Mate) interchangeable hypodermic syringe of gauge 20 cc with a (precision glide) needle of 18G1 1/2 (with blunt end)
- ❖ The same station used with PEDT/PAN polymer is used to electrospun the SWNT/PEDT/PAN solutions.

7.2.2. Morphological Analysis by Environmental Scanning Electron Microscope, ESEM.

The morphological analysis and diameter distribution of nanofibers were examined by utilizing Field Emission Environmental Scanning Electron Microscope (FESEM). The gold-sputtered (for 60 sec) electrospun nanofibers were sized and examined by Phillips XL-30 FESEM (shown in Figure 7. 2) at 20 kV.

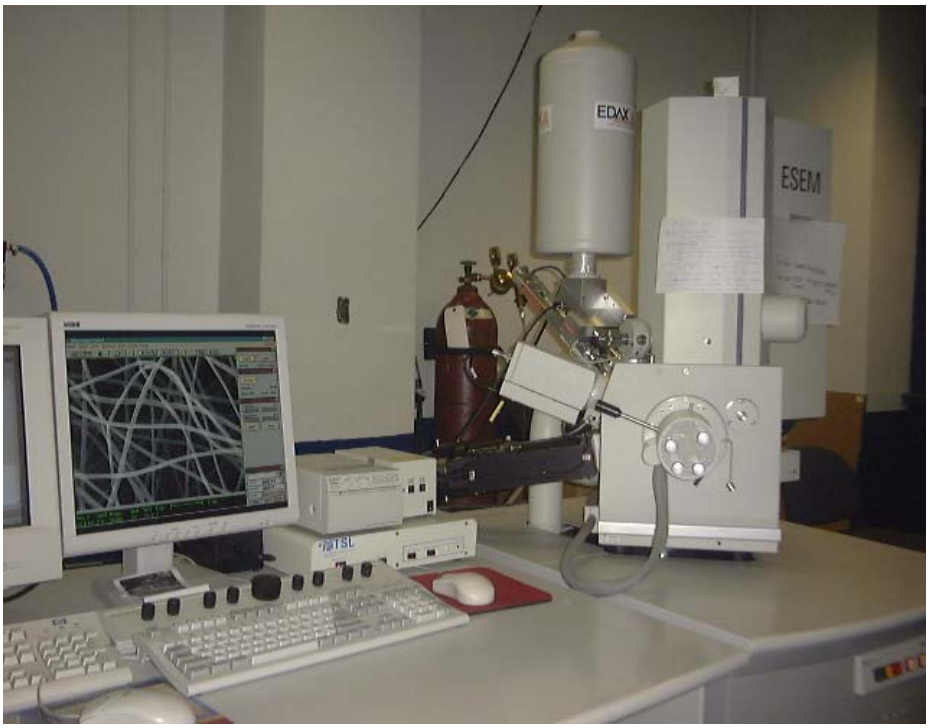

Figure 7. 2 Phillips XL-30 FESEM microscope.

7.2.3 FT-IR.

Fourier transform-infrared (FT-IR) spectroscopy was used to follow the conformation changes that occur in the SWNT/PEDT/PAN solution during the dope preparation stage and the electrospinning process that produces solid nanofibers. The description of FT-IR is illustrated in the previous part.

7.2.4 Chemical Analysis by Raman Micro-Spectrometer.

Renishaw Microspectrometer 1000 with a diode laser (780nm excitation wavelength, 12W/cm^2) as shown in Figure 7. 3 have been used to characterize the chemical properties of the electrospun PEDT and PEDT/CNT nano composite fibrils. There is no specific property for the samples except it should be as flat as possible and its size (area) should be larger than the Laser light diameter. No preparation for the sample is required. (Appendix V)

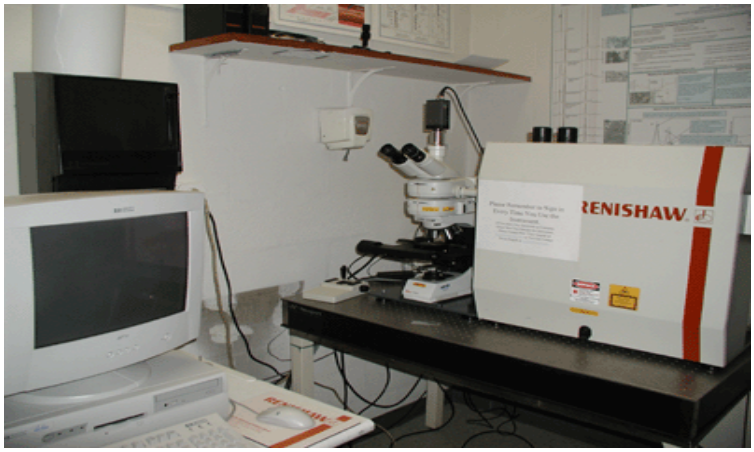

Figure 7. 3 Renishaw Raman Microspectrometer 1000.

Raman spectroscopy is a very useful tool for determining the conformation of SWNTs. It enables us to follow the conformational changes, which occur during the doping stages of solution. It can also reveal information about the presence of CNTs within the nanofibers and estimate the value of the carbon nano-tube diameter.

7.2.5 TEM.

The JEOL 2010F TEM/STEM (Figure 7. 4) with a magnification range from 2000 to 1500000x is a state-of-the-art field emission transmission electron microscope with capabilities ranging from nano-beam and convergent beam diffraction to high-resolution phase contrast, analytical and energy filtered imaging. The 2010F has been optimized for analytical microscopy with a large solid angle for high X-ray throughput, scanning, scanning-transmission, and backscattered electron detectors and a Gatan image filter for energy filtered imaging and electron energy loss spectroscopy. This combination of analytical capabilities makes the 2010F an ideal instrument for the characterization of a wide array of samples, yet the 2010F is also a very capable high-resolution instrument with a point-to-point resolution of 0.23 nm.

An acceleration voltage of 200KV has been used in the TEM to analyze the morphology of our electrospun PEDT-PAN and SWNT-PEDT/PAN, the presence of SWNT within the fibers as well as the alignment of them along the fibers.

TEM instrument was used to characterize the nanofibers and give an evidence of the presence of the CNT within the fibers. (For details see AppendixVI)

Figure 7. 4 TEM JEOL 2010F.

7.2.6 Conductivity Measurements.

The volume conductivity of the SWNT/PEDT/PAN nanofibrous yarn was measured using the four-point probe method mentioned in the previous part and in Appendix III. The resistance of the sample was calculated from the I/V curve and by the help of the sample geometry; linear density, the conductivity could be estimated.

7.2.7 The mechanical properties.

The mechanical properties of the CNTs reinforced PEDT/PAN yarn were tested by using KES G-1 micro tensile tester. Briefly, the electrospun samples were cut into the stripes of length 4 cm and width 0.5 cm. They were then mounted on the sample holders made up of paper having the width of 0.5 cm. This gives a gauge length of 3 cm for the samples. The strain rate used in the experiment was 0.2 mm/sec. The result from the machine was in the form of load (gram force) vs. displacement. The stress/strain results can be calculated as explained in details in Appendix II.

7.3 Results and Discussions.

In this part of research, we introduced the SWNTs as a reinforcement material to the PEDT/PAN yarn. Single-walled carbon nanotubes have the same effect of PEDT on the electrospinning process, as they possess electrical charges. These charges help the flow of the ejected jet and helps with building up a uniform finer surface yarn.

An aluminum mesh was used as a target to collect the fibers of SWNTs/PEDT blend. It was interestingly noted that, the yarn starts to focus in one point of the mesh with the building of the first amount of nanofibers and the yarn keeps on accumulating without the need to a take-up system and sustains the electrospinning distance along the process. The electrospinning continue as long as there is polymer feeding and the yarn stay in one position providing a clean and neat environment without any distorted nanofibrous to other places. The mesh probably works as triode to concentrate and focused the electrical charges into parallel paths which strength the electrical field keep the yarn at one place. It should be noted that the mesh should be cleaned before each use and maintain its holes unclogged with nanofibers unless it will lose its function and turn to be as a regular flat surface.

The amount of accumulated nanofibrous-self assembled yarn and the fine twisted surface yarn are illustrated in Figure 7. 5 with the electrospinning process.

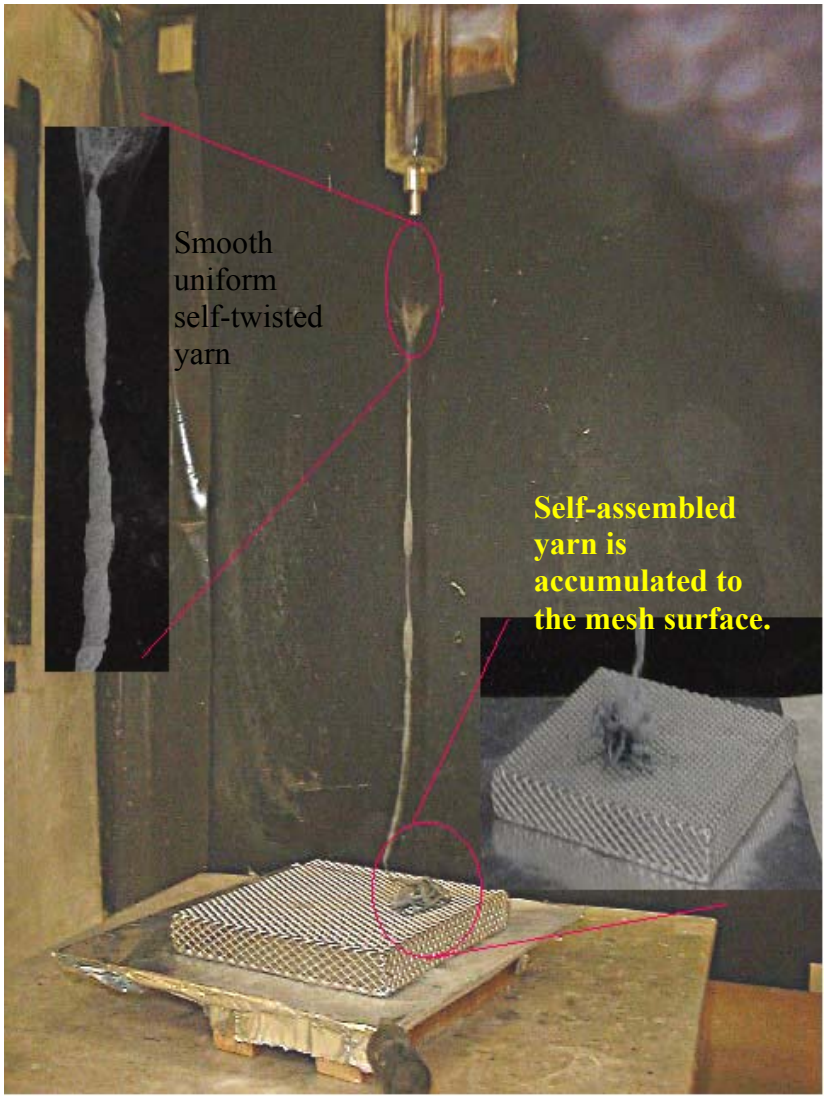

Figure 7. 5 Electrospinning process of SWNT/PEDT nanofibrous self-assembled yarn with using a mesh as a target.

7.3.1 Morphological analysis and diameter distributions of SWNTs/PEDT/PAN electrospun fibers.

The SWNT were successfully co-electrospun with the PEDT/PAN fibers with the following concentrations 0.2, 0.5, 0.8 &1%wt (CNT weight concentration in the fiber form) of SWNT with 20% PEDT-8%PAN and 3% & 5%wt of SWNT with 10%PEDT-5%PAN. It is evident that the higher is the CNT concentration the higher is the viscosity of the prepared polymer, so for higher CNT concentrations, the solid content of PEDT/PAN were decreased. Figure 7. 6 demonstrates the SEM images of 0.2, 0.8, 1, 2, 3, 4 & 5 wt. % SWNTs reinforced with PEDT/PAN blend. For low SWNTs content, the fibers had regular morphology with small variations in diameter (200-300). For the high CNT content PEDT fibers, the fiber morphologies and diameter were different form the low content, and changed with increasing the content of CNTs. Firstly, good fibers alignment, less junctions and bundles of fibers were observed in the sample containing CNTs of (0.2-3 wt %) compared to higher CNTs content. Secondly, the morphologies of fibers became more irregular, and numerous beads appeared, when the CN content increased to 5 wt. % (Figure 7. 6 -a). All these results indicated that the addition of CNTs to PEDT/PAN fibers might influence the solution viscosity, surface tension, and concentration.

Figure 7. 7 (a) & (b) show fiber diameter average of 230 nm and also smooth fine fibers image of the SWNT/PEDT fibers. Also the alignments of fibers within the surface of the yarn still maintained. The presence of SWNTs within the fibers was not clear with the SEM, hence TEM is recommended to examine the CNTs behavior in the fibers.

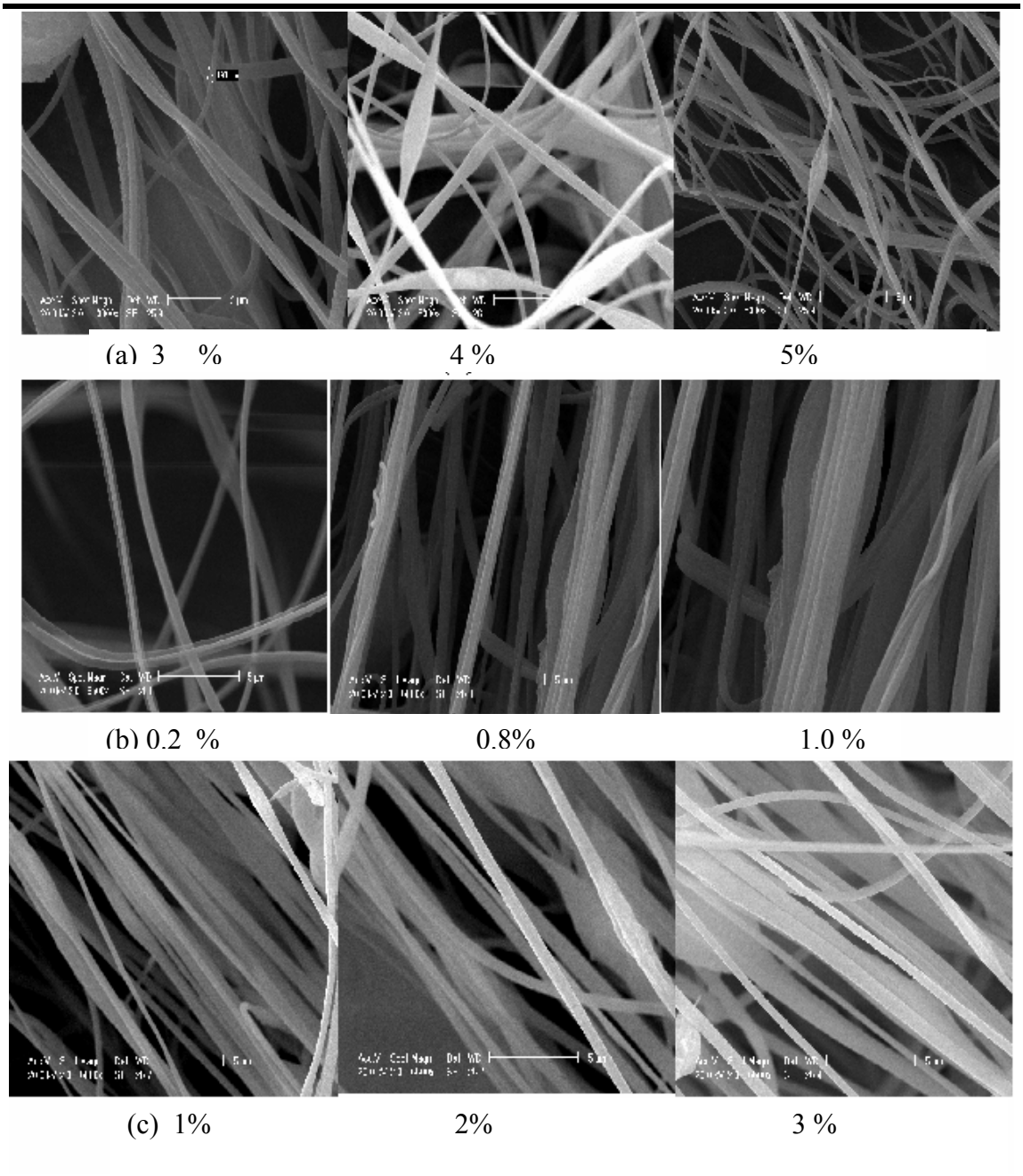

Figure 7. 6 Scanning electron microscopy photographs of various 20%PEDT/8%PAN fibers with SWNTs content. (a) 3, 4, 5wt.%, (b) 0.2, 0.8, 1 wt.%, (c) 1, 2 & 3 wt.%.

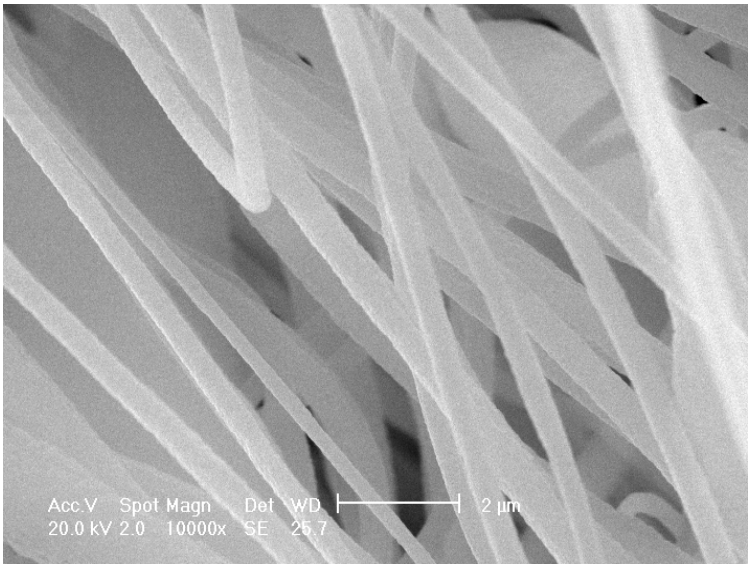

(a)

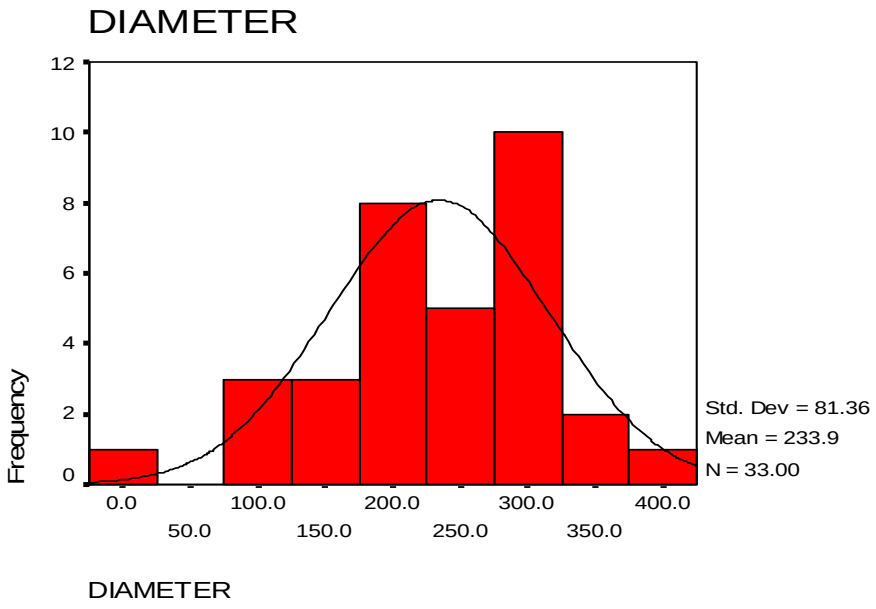

(b)

Figure 7. 7 SEM of the SWNT/PEDT/PAN fibers. (b) Fiber diameter distribution of the electrospun SWNT/PEDT fibers.

7.3.2 Chemical analysis by FT-IR.

Infrared spectroscopy was used to characterize the PEDT/PAN fibers after reinforced with SWNTs. Figure 7. 8 shows that there is no difference after adding the SWNTs and the absorption at 3741& 1500-1600, which are common to most polymers, are characteristics of the various vibration modes of the C-H and C-C bonds. The broader band of 2927 cm -1; at PEDT and SWNTs spectra, was considered to be a measure of the degree of electron dolocalization and thus it is a characteristic peak of PEDT conductivity.

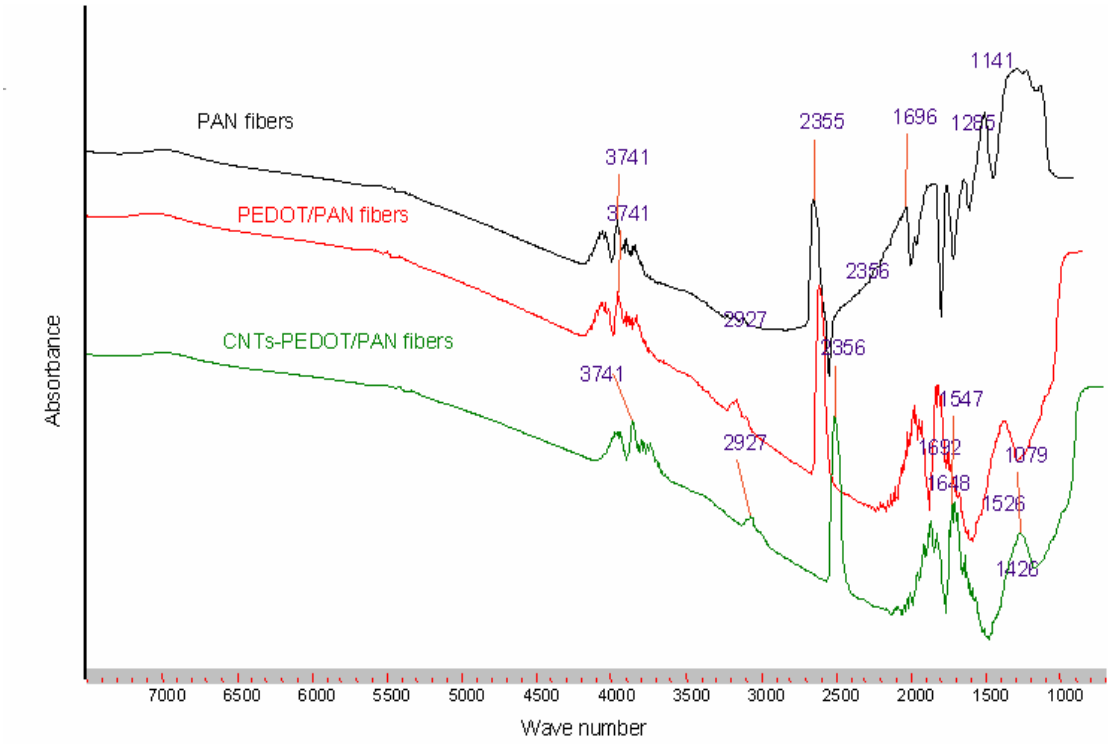

Figure 7. 8 FT-IR spectra of PAN, PEDT/PAN & CNTs/PEDT fibers.

7.3.3 Chemical Analysis by Raman Micro-Spectrometer.

The experimental results of PEDT Raman spectrum were found to agree with the review of literature [116]. The experimental Raman (Figure 7. 9) spectra of PEDT/PAN fibers are mainly characterized by two intense bands. The fact that the C=C bond is the most affected during the doping clearly permits the assignment of the band located near 1420 cm^{-1}. The most intense peak in PEDT is very close in positions 1424 cm^{-1}. It is assigned to the symmetrical $C_\alpha=C_\beta$ stretching vibration, and the band at 1516 is assigned to the asymmetrical $C_\alpha=C_\beta$ stretching vibration.

The normal mode which is assigned to the band observed at 1365 is assigned to the $C_\beta=C_\beta$ stretching vibration. Indeed, this mode is observed at 1370-1380 cm^{-1} in polyalkylthiophenes. In the 600-1000 cm^{-1} range in PEDT we observe especially two bands near 550 and 990 cm^{-1}. They are assigned to the C-S-C bond deformations.

The inclusion of SWNTs in the PEDT/PAN matrix fibril was confirmed using Raman spectroscopy analysis. Figure 7. 10 shows the Raman spectra of pure PAN fibers, pure SWNTs and 1, 2 & 3 wt% SWNTs with PEDT/PAN fibers. The typical peaks of SWNT are the radial breathing mode (RBM) in the 100-275 cm^{-1} range and tangential (stretching) modes in the 1500-1600 cm^{-1} range. They can be seen in the PEDT/PAN-SWNT fibrils and are not observed in the neat PAN fibrils. The peaks of 400-500 and 990 cm^{-1} range are typical of the presence of PEDT within the matrix.

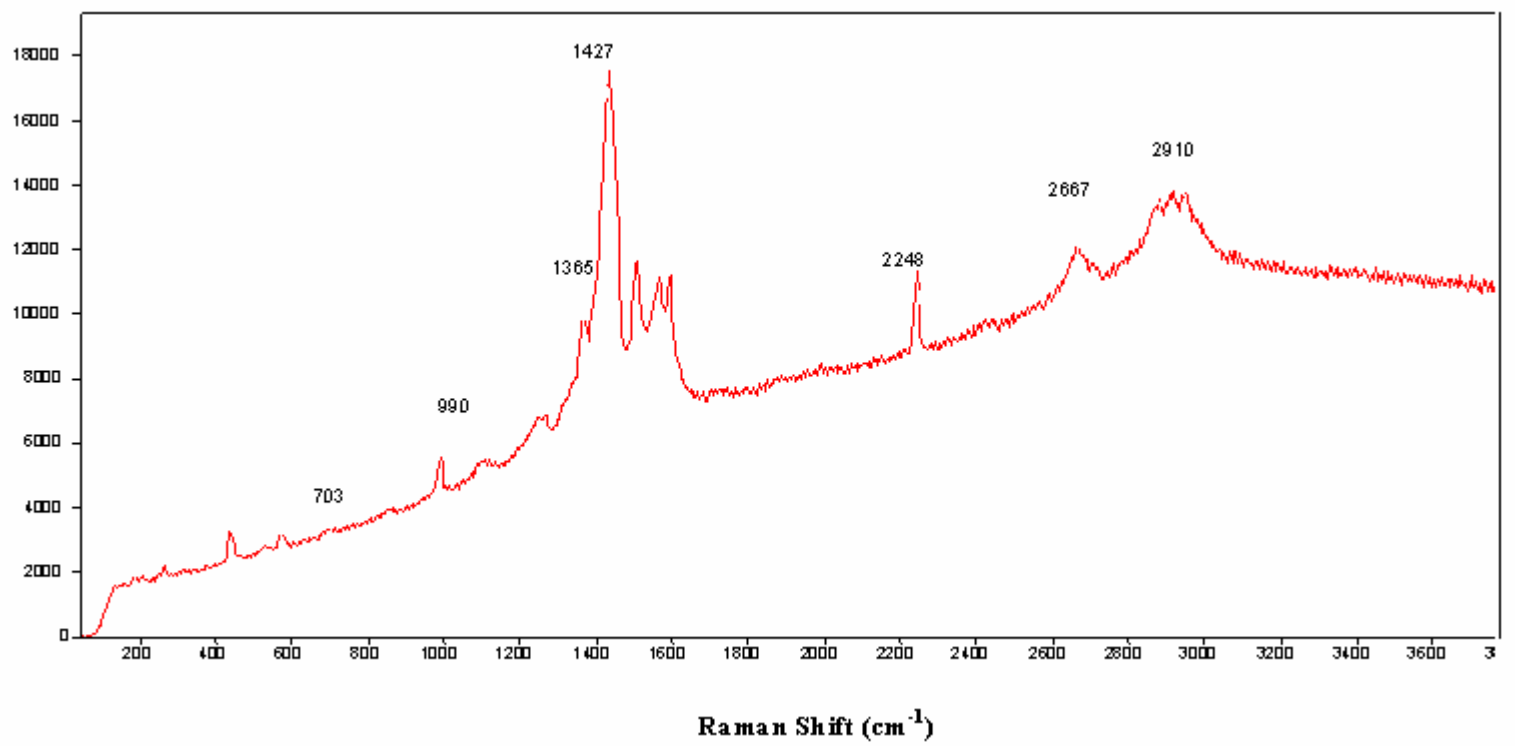

Figure 7. 9 Raman spectra of the CNT/PEDT/PAN fibers.

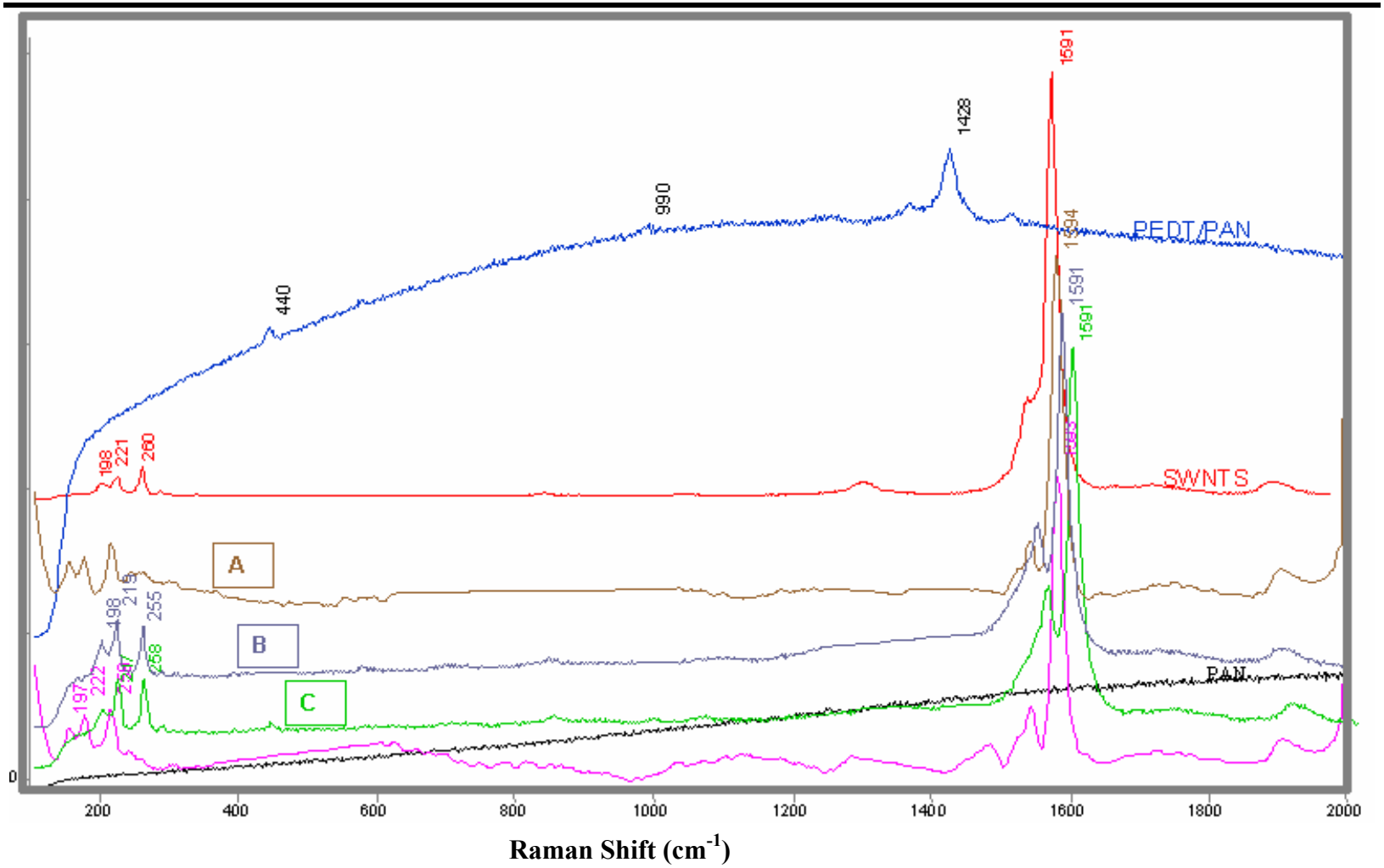

Figure 7.10 Raman spectra of pure PAN, pure SWNTs, and PEDT/PAN fibers with different SWNTs content (A- 3 wt.%, B- 2 wt.% & c- 1 wt.%).

The diameter of the SWNTs can be estimated from the RBM peaks because frequency is inversely proportional to the diameter of a SWNT, following the equation $\omega_R \sim 224\ cm^{-1}/d$, *where* ω_R is the RBM frequency and d is the tube diameter in nanometers. The presence of at least 5 RBM peaks is observed in the range of 153 to 267 cm^{-1}. According to the mentioned equation, this corresponds to a tube diameter range of 0.8-1.5 nm.

7.3.4. TEM.

Transmission electron micrographs were obtained using the TEM to characterize the nanofibers and give an evidence of the presence of the CNT within the fibers. In Figure 7. 11(a), it is showing the crystalline structure of the PEDT and how it is wrapped by the PAN fiber of average diameter of 200 nm. Typical TEM micrographs shown in Figure 7. 11(b) reveal that the electrospun fibers contain SWNTs and illustrate the good arrangements of the CNTs along the fiber and they can be aligned/self-organized into straight lines or bundle-like crystallites.

Figure 7. 12(a) gives a good evidence of the presence of the CNT within the cross-section of the fibers and not only resting on the surface as could be claimed. The actual diameter of the SWNT could be measured to be around 1.2nm. The TEM device characterizes the fiber sample inside a chamber that exposed to a high degree of heat. Sometimes two sticky fibers can be split under the effect of that heat. Figure 7. 12(b) demonstrates the effect of heat on fibers splitting, showing that the two fiber stuck together due to the presence of CNT between them of interact with each other and trying to attract themselves together. Some of these CNT hanging between the two fibers

surfaces and others still work as bridge connecting the two fibers. Typically a high density of protruding carbon nanotubes was observed. Close examination of the fracture surface showed contact and adherence of the polymer to most of the nanotubes. In some cased the entire surface of the nanotube was covered with a layer of polymer.

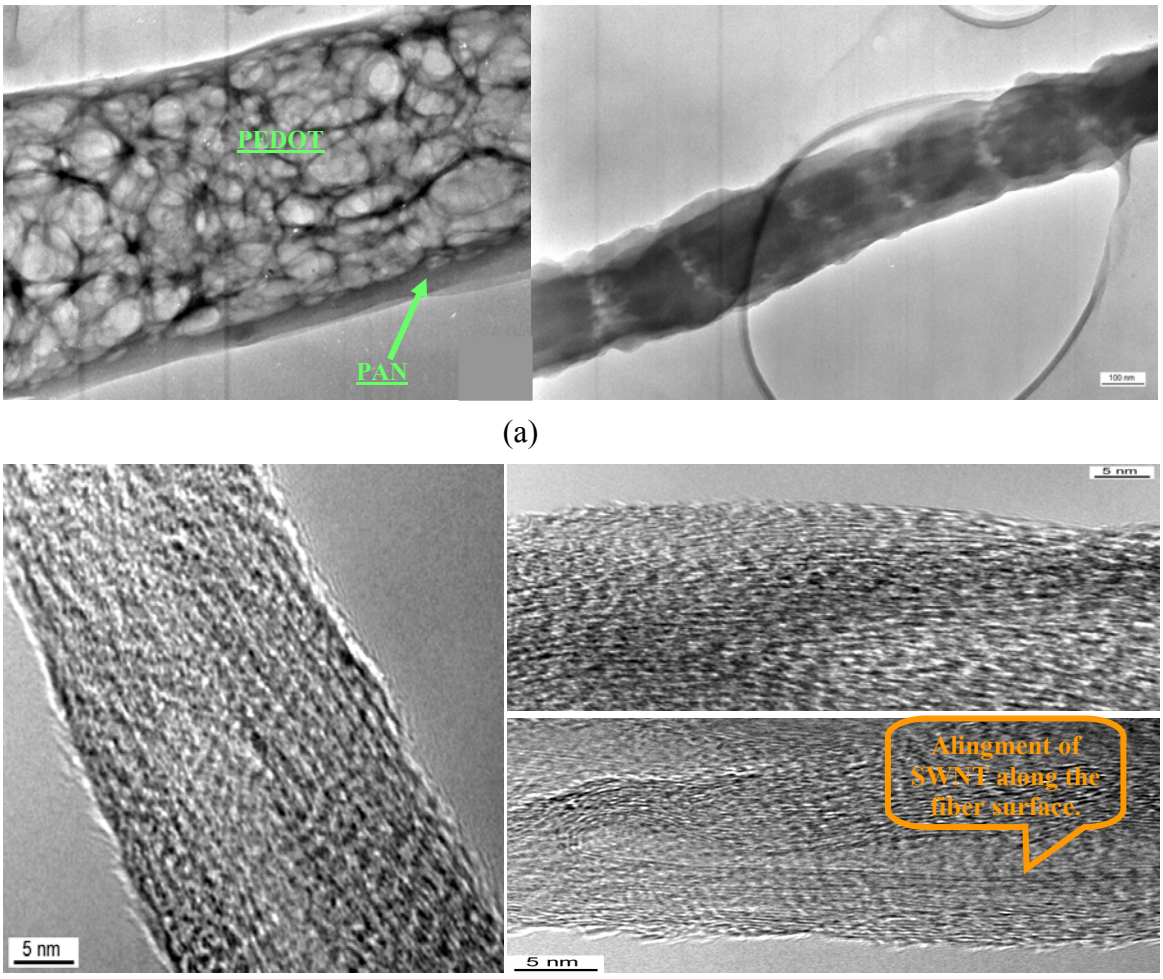

Figure 7. 11 High-resolution electron microscopy (TEM) micrographs showing (a) PEDT/PAN Fiber of 200 nm average diameters. (b) The alignment of 3% SWNT within the PEDT/PAN fiber.

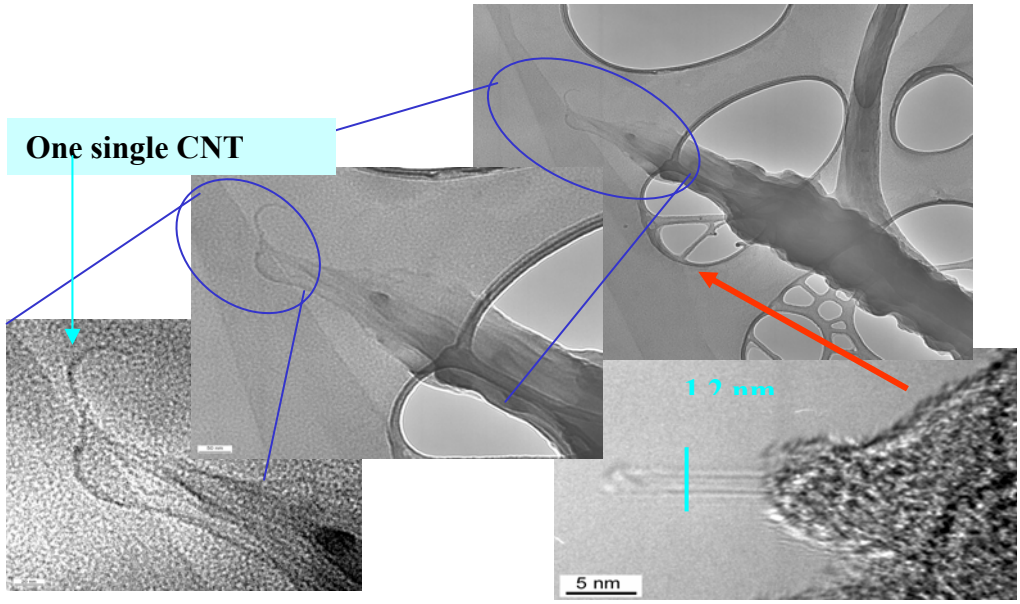

(a)

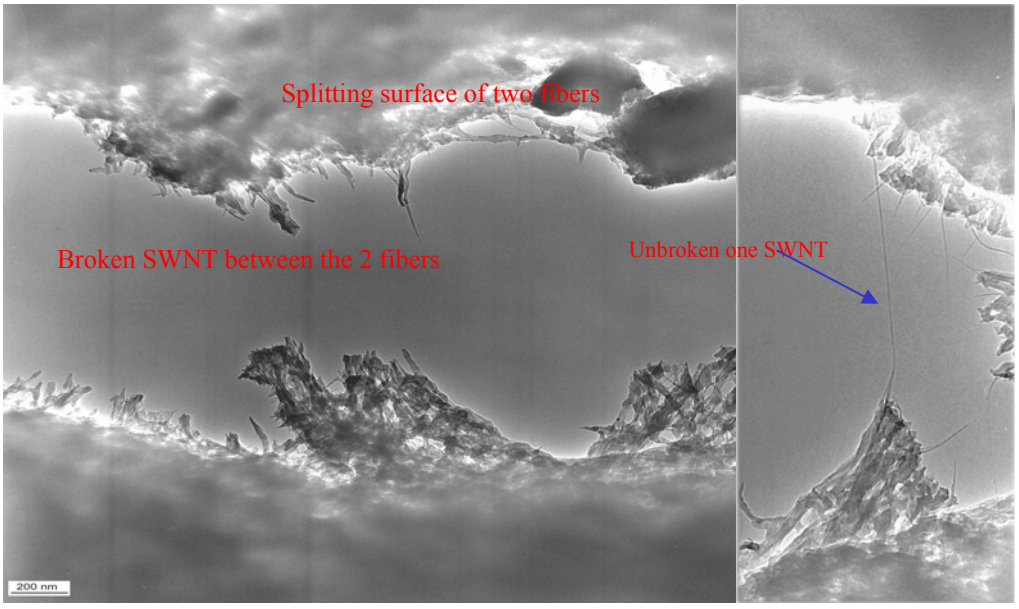

(b)

Figure 7. 12 TEM micrographs of (a) one single CNT protruding from the x-sec of the fiber. (b) Two split fibers show the CNT protruding from the polymer matrix.

7.3.5 Effect of SWNTs on Electrical Conductivity.

The inclusion of SWNTs to the PEDT/PAN fibril matrix affects the value of the electrical conductivity as plotted in Figure 7. 13. The presence of SWNTs results in doubling the conductivity value of the fibers to the range of 0.03 S/cm. The plot shows that increasing the amount of PEDT material will increase the conductivity of the PEDT/PAN blend. The upper curve demonstrates the influence of the CNTs content on the reinforced composite of PEDT/PAN, the higher is the CNTs concentrations, and the higher is the electrical conductivity.

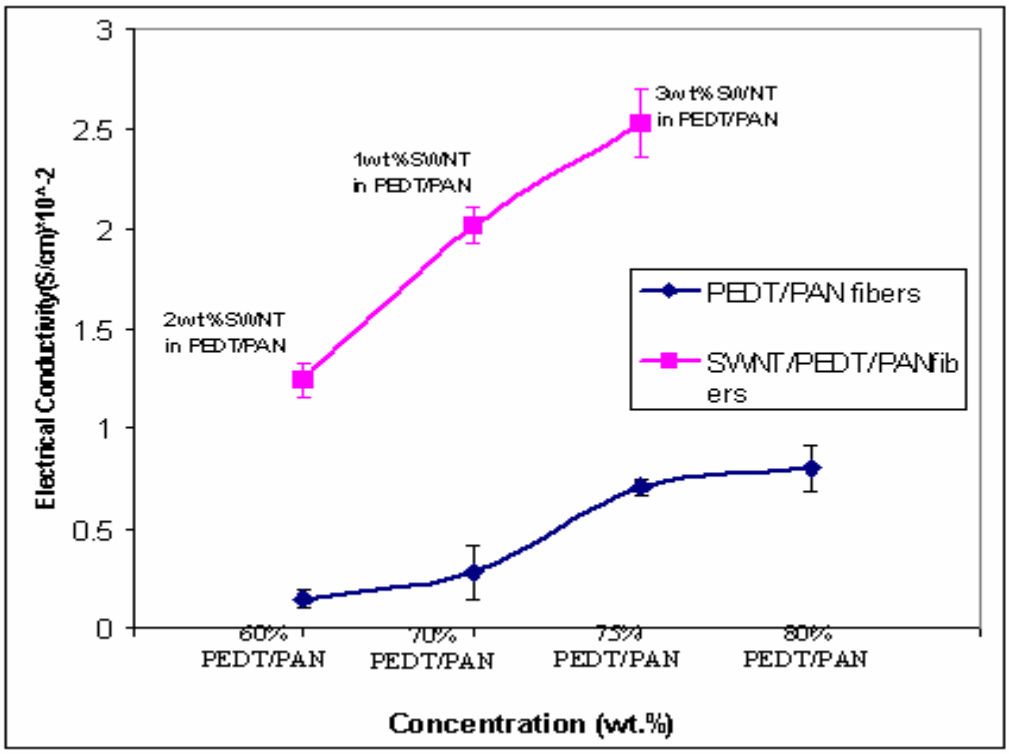

Figure 7. 13 Effect of PEDT/PAN concentration and carbon nanotubes content on electrical conductivity.

The alignment of SWNTs within the fiber helps the increasing in electrical conductivity and even though the presence of carbon nanotubes might be laying discontinuously along the fiber, they would be thought of as conductive islands and the electrons hopping between them to help with increasing the conductivity .

7.3.6 Effect of SWNTs on Mechanical Properties.

Figure 7. 14 illustrates the doubling in tensile strength value when PEDT and SWNTs added to the PAN matrix. It is evident that the crystalline structure of PEDT enhances the tensile properties of the matrix as discussed in the previous part.

The mechanical properties of SWNTs reinforced PEDT/PAN nanocomposites were characterized by stress-strain measurements. Figure 7. 14 shows typical stress-strain curves of PEDT/PAN and SWNTs/PEDT/PAN nanofibrous yarn. The ultimate strength of CNTs reinforced PEDT/PAN yarn is in the range of 10-16 MPa.

The elongation to break of PEDT/PAN; with 3% CNTs content was lower than the PEDT/PAN without CNTs or with low percentage. This predicts lower toughness of higher CNTs content PEDT/PAN yarn with strong mechanical properties.

It was observed that PEDT/PAN nanofibrous yarn with SWNTs content higher than 3 wt. % gives poor mechanical properties, which could be explained due to poor dispersions of the CNT within the fiber, result in forming defects and stress concentrations of the yarn.

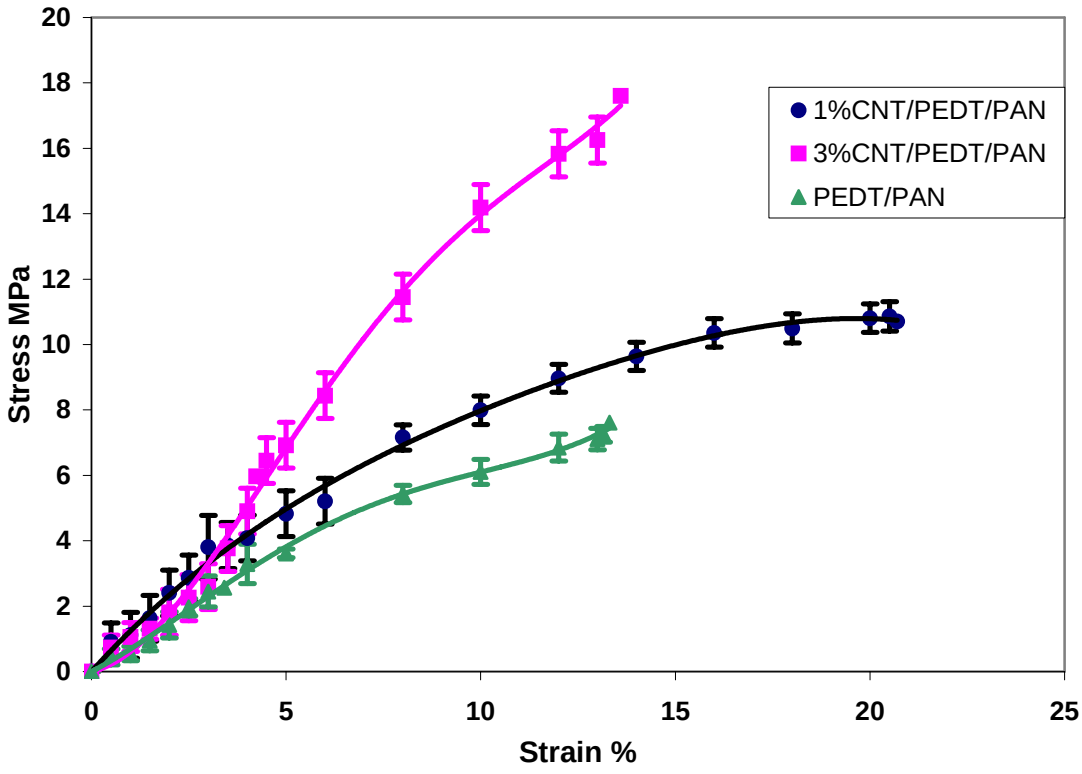

Figure 7. 14 The effect of SWNTs content on the stress-strain behavior of PEDT/PAN fibrils.

Chapter 8: Conclusions and Future Prospects.

8.1 Conclusions

Nanotechnology science attracted the interest of researchers over the last two decades. One of the fields of this nanotechnology is producing fibers with nanoscale size. Electrostatic generation of ultra fine fibers "electrospinning" has been known since the 1930s. This technique has been recently rediscovered for applications such as high performance filters and for scaffolds in tissue engineering that utilize the unique characteristics of the high surface area; 10 m^2/g provided by the fibers. In this thesis, we started by studying the electrospinning parameters and controlling the formed nanofibrous mats into aligned fibers.

Our work focused on the alignment and orientation of nanofibers into linear assemblies. In this research, a new device; to align & orient the nanofibers into linear assemblies, was established. This device was named a "Dry Rotary Electrospinning Disc". We have found that, increasing the rotating speed enhances the alignment of the curly nanofibers. This speed increasing is optimized to a level of 1500 rpm, higher than that might introduce fibers breakages.

The effects of processing parameters on the morphology of individual electro-spun PEO nanofibers have been explored. A systematic study was carried out using Response Surface analysis of a 3^3 factorial experiments to identify the significant processing parameters for producing nanoscale aligned fibrous assembly. Also, we have found that, the orientation and morphology of the electrospun nanofibers were influenced strongly by parameters such as H; height of spinneret (charge density), R_d;

radial distance, and d_p; the pipette diameter. The pipette diameter is the most significant factor to achieve better orientation and finer fibers.

Contour plots showed a saddle point of the fiber diameter by optimize the pipette diameter, lowering the height of spinneret and decreasing the radial distance of spinneret. The diameter size distribution plot behaves as Chi-Square mode with minimum fiber diameter of 100 nm and 500:700 nm average range.

KES G-1 micro tensile tester was used to test the stress- strain behavior of the elecrospun PEO fibers. The measured mechanical properties of aligned fibers yarn showed higher ultimate strength by 50% than the non-woven mat.

Since MacDiarmid discovered that the polymers could reach extremely high electrical conductivities, the field of intrinsically conducting polymers (ICP), which are often referred to as synthetic metals, has attracted the interest of thousands of scientists. ICP in nanofiber form have the potential to play a significant role in wearable electronics. Our research moved a step forward to combine the world of electrospinning with conductive polymers. Poly(3,4-ethylene dioxythiophen)/poly(styrene sulfonate) (PEDT/PSS); abbreviated as PEDT, is one of the conductive polymers that posses high conductivity values (30-300S/cm). PEDT is used as a cast film in numerous industrial applications; e.g LED, as mentioned in literature.

The novelty of this work is we succeeded to electrospin PEDT into nanofibers using poly(acrylonitrile) (PAN) as a carrier. Interestingly, we produced a self-assembled nanofibrous yarn using the blend of PEDT/PAN. Aligned linear assembly of PEDT/PAN polymer has been successfully electrospun by self assembled yarn formation. It was found that PEDT improve the electrospinning of yarn; due to it electrical properties. The

shape of the PEDT/PAN yarn is much smoother and has finer diameter as the negativity of PEDT, the positive charge of the jet and polarity characteristics of PAN help with building up the yarn and also the dynamic effecting force with the fiber inertia move the electrospun yarn downward.

DSC results gave us an interesting proof that the electrospinning process improves the alignments of molecular chains within the fiber resulting in higher fiber transition temperature than the polymer temperature. The PEDT polymer has a significant effect on reducing the nanofibers diameter of PAN by 50~60%; this is evident as the inclusion of PEDT decrease the viscosity of PAN/DMF blend. The electrospun PEDT/PAN fibers showed good alignment tendency with average fiber diameters of 200-300 nm. The increase of PEDT content was controlled by the presence of beads and polymer droplets, 20-30 wt.% of PEDT content gave good fibers appearance while more than 40 wt.% showed irregularity and rough fiber surface. Four-point probe device was demonstrated to be a reasonable method to measure the conductivity of PEDT fibers. It is concluded that the higher is the concentration of the PEDT polymer, the higher is the electrical conductivity. The range of the measured electrical conductivity was 0.001 to 0.017 S/cm, which is within the range of conductive materials. A nonlinear relation between fiber diameter and conductivity was experimentally observed; similar to the confinement theory that size reduction may indeed increase conductivity due to small angle scattering reduced and the transport of charge is facilitated.

It is obvious that the conductivity of the electrospun fibers in the non-woven mat or self-assembled yarn is significantly lower than that for a cast film of PEDT (~37 S/cm).

This is not an unexpected result as the four-point probe method measures the volume resistivity from which the conductivity can then be calculated and not that of an individual fiber. It must be noted that obtaining the conductivity of the non-woven mat or self-assembled yarn was considerably more difficult than measuring the conductivity of a cast film due to the difficulty in obtaining enough thickness to be tested and transferred to linear density. As can be seen form the SEM micrographs of the electrospun PEDT/PAN fibers, the fibers are highly porous and therefore the "fill factor" of the PEDT fibers is less than that of a cast film. However, it is reasonable to expect that the conductivity of an individual electrospun fiber will be higher than that of the non-woven mat or self-assembled yarn and in fact should be approximately equal to the conductivity of the cast film.

The mechanical properties of PAN fibers and PEDT/PAN fibers were characterized by stress-strain measurements. The presence of PEDT in the fibers increased the strength by 30% and the yield point by almost 40%. It is obvious that PEDT/PAN yarns are mechanically strong and tough compared to the pure PAN yarn that was predicted from the spherulitic structure of the PEDT polymer. In order to further improve electrical conductivity and mechanical properties, SWNTs were introduced into the PEDT/PAN polymer by co-electrospinning process.

The first observation of carbon nanotubes was made exactly 13 year ago. As we enter the second decade of nanotube science and technology, the interest and excitement about nanotube-based nanoelectronics is only intensifying. In the last part of our research, we introduced single-walled nanotubes SWNTs and studied its effect on the electrospun yarn characterizations.

It was one of the blessing moments when we used aluminum mesh as electrospinning target. It was amazingly noted that, the yarn focused onto one point and formed a neat shape of electrospun fibrous yarn. The yarn was continuously accumulated up. It is believed that the mesh works as a triode that amplifies and concentrates the electrical charge which helps the nanofiber to be directed to one point without flying into different places. Also, the presence of SWNTs helps the PEDT to improve the fiber diameter and electrospinning process due to its electronic characteristics.

The SEM images of SWNTs reinforced PEDT/PAN nanocomposite yarn, showed alignments of the nanofibers with 0.2-3% SWNTs content, higher than that the fibers started to posses some irregularities and increase the bundles junctions. The average diameter of the nanofibers was in the range of 233 nm. FT-IR results prove that the inclusion of SWNTs wouldn't affect the chemical properties of the PEDT/PAN fibers.

Raman spectroscopy was used to analyze the SWNTs/PEDT yarn. The spectra confirmed the presence of CNTs in the samples with its common typical characteristics of radial breathing mode in the 100-275 cm^{-1} range and tangential modes in the 1500-1600 cm^{-1} range., also Raman spectra showed the typical peaks of PEDT polymer. The calculated carbon nano-tube diameter was 0.8-1.5 nm, which was proved by the TEM micrographs.

TEM micrographs gave wonderful images of the alignment of CNTs within the fiber, the good dispersion of tubes and the evidence of the presence of CNTs with the cross-section of the fibers and not only resting on the surface as could be claimed.

The conductivity measurements of SWNTs/PEDT yarn promising a new level of higher electrical conductivity. The higher is the SWNTs content, the higher is the

measured conductivity. The inclusion of SWNTs to the PEDT/PAN matrix results in doubling the conductivity of the fibers to the range of 0.03 S/cm as the carbon nanotubes worked as conductive islands help with the electrical conductivity. The mechanical strength of SWNTs/PEDT nanocomposites was higher than the PEDT/PAN yarn strength, which illustrated the reinforcement effect of CNTs on the fibers.

A CNTs/PEDT yarn was woven into a fabric to demonstrate the flexibility of the electrospun yarn and its ability to interlace that would open the way to wearable electronics applications as well as the biomedical applications by showing the electrospinning directly onto human hands.

By converting PEDT and its composite into nanofibers assemblies, it enables the formation of several of 2D & 3D fabrics and the fundamental building blocks for wearable electronics.

8.1 Future Prospects.

The future holds nothing but the brightest prospects for nanotechnology and synthetic polymers research. Although the work described in this thesis has provided some answers and new functions, it also raises many more important questions and new discoveries. Here we propose new route to resolution of some of these questions.

Manipulating single nanofiber would be one of the big challenges. More companies and researchers; e.g. Zyvex nanotechnology, dedicate their present and future work to bring new technology to manipulate this nanoscale material, that will give us better ways of characterizing the nano-materials and improve their results. Electrical conductivity of individual nanofiber should be measured.

Scaling up the process from laboratory curiosity to a robust manufacturing process is needed. Making the diameter of nanofibers reproducible and consistently. It is recommended to develop model and simulation technique to guide the process and optimization of properties.

Introducing new levels for nanofibers into yarn, fabric and next step would be braiding will widen the application area. Further development of electronic textiles woven from electrospun SWNTs/PEDT/PAN yarns. To demonstrate the flexibility of the carbon nano-tubes reinforced conductive yarn, a 2*2 inch square fabric was manually woven. This enables the possibility of wearable electronics application. Figure 8.1 illustrate the bending ability of the electrospun CNT/PEDT yarn to interlace and form a woven fabric. It is interestingly observed the good alignment of nanofibers within the electrospun yarn.

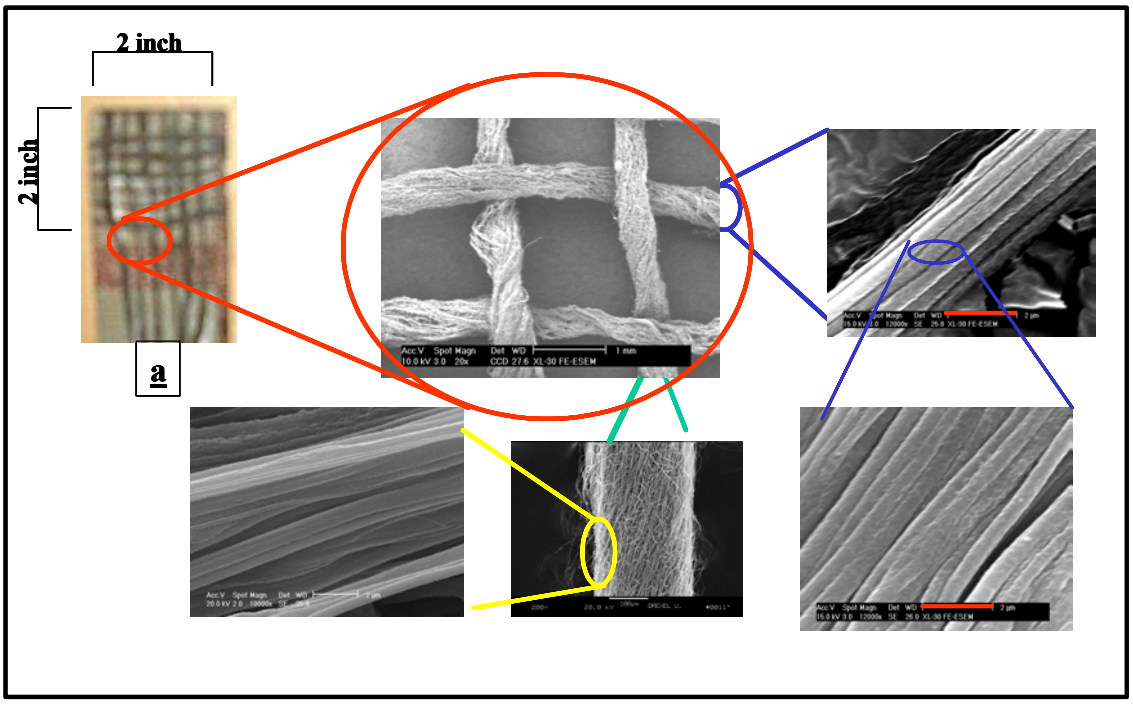

Figure 8. 1 The hierarchical shape of the 1wt. % SWNTs/PEDT nanofibers into a woven fabric.

Other potential applications include tissue engineering, drug delivery, protective mask, biosensors, etc. The use of rubbing alcohol as a solvent affords the opportunity to electrospin disinfected nanofibers directly onto the living tissue, suggesting an interesting approach for wound care. Electrospun fibers are electrically charged and thus mild static dissipation will occur upon grounding, but the very low currents employed in the system render it safe for deposition directly on tissue. We demonstrate this in Figure 8.2, where hands were used as a direct target to the electrospun fibers. Also the conductivity properties of our fibers with the possibility of tailoring the fibers may be useful for e.g. nerve guidance channels application among other applications.

Figure 8. 2 CNTs/PEDT nanofibers electrospun directrly onto human hands.

List of References.

1. F. K. Ko, C. T. Laurencin, M. D. Borden, D. H. Reneker, The Dynamics of cell-fiber architecture interaction, in: Proceedings, Annual Meeting, Biomaterials Research Society, San Diego, April 1998.

2. A. Macdiarmid et al, J. Chem. Soc., Chem Commun. 1977, 578.

3. Handbook of Conducting Polymers, 2nd ed. (Eds: T. A. Skotheim, R. Elsenbaumer, J. Reynolds), Marcel Dekker, New York 1998.

4. Handbook of Organic Conductive Molecules and Polymers, Vols. 1-4 (Ed: H. S. Nalwa), Wiley, Chichester, UK 1997.

5. Handbook of Oligo- and Polythiophenes (Ed: D. Fichou), Wiley-VCH, Weinheim 1999.

6. J. Roncali, Chem. Rev. 1997, 97, 173.

7. D. C. Trivedi, in Handbook of Organic Conductive Molecules and Polymers, Vol. 2 (Ed: H. S. Nalwa), Wiley, Chichester, UK 1997, pp. 505-572.

8. A. Macdiarmid, " Synthetic metals: a novel role for organic polymers", Synthetic Metals, 125 (2002), 11-22

9. F. Lux, Farbe & Lack 1998, 104-32.

10. L. Groenendaal, F. Jonas, D. Freitag, H. Pielartzik, and J. Reynolds. " PEDT and Its Derivatives: Past, Present, and Future", Adv. Mater. 2000, 12, No.7, 481-493.

11. M. Leclerc, et al. , Adv. Mater. 1997, 9, 1087.

12 " Contemporary Polymer Chemistry" by H. Allcock, Lampe.- 2nd ed.

13. A. J. Heeger, et al., Rev. Mod. Phys. 60 (1988) 781

14. R. Friend, et al., Nature 335 (1988) 137

15. R. Friend, et al., Nature 347 (1990) 539.

16. A. Macdiarmid, et al., Science and Applications of Conducting Polymers, Adam Hilger, Bristol, UK, 1990, p. 117.

17. Bayer AG. Eur. Ptentent 339340, 1988.

18. L. Groenendaal, et al. “PEDT and Its Derivatives: Past, Present, and Future”, Adv. Mater. 2000, 12, No.7

19. M. Dietrich, J. Heinze, F. Jonas, J. Electroanal. Chem., 1994, 369, 87.

20. Bayer AG, Eur. Patent 440957, 1991

21. L. Groenendaal, et al. “ PEDT and Its Derivatives: Past, Present, and Future”, Adv. Mater. 2000, 12, No.7

22. FeIII(Ots)3 is commercially available as a n-butanolic solution form Bayer AG (trade name BAYTRON C).

23. E. Havinga, Chem. Mater. 1996, 8, 769.

24. P. Schottland, et al., J. Chim. Phys. 1998, 95, 1258.

25. Philips Electronics N. V.., Eur. Patent Application No. PHN 14385 EPP 1993.

26. O. Inganäs, et al., Synth. Met. 1999, 101, 198.

27. Elecon, inc. company

28. O. Inganäs, et al., Synth. Met. 1999, 101, 561.

29. C. Wang, J. Schindler, C Kannewurf, and M. Kanatzidis., Chem. Mater. 1995, 7, 58-68.

30. O. Inganäs, et al., Synth. Met. 1997, 89, 161.

31. O. Inganäs, et al., Polymer 1994, 35, 1347.

32. W. Wernet, et al., Synth. Met., 1996, 83, 125.

33. Y. Kudoh, K. Akami and Y Matsuya, Synth. Metals.” Chemical polymerization of 3,4-ethylendioxythiophene using aqueous medium containing an anionic surfactant”, 1998, 98, 65.

34. J. Reynolds, et al. Adv. Mater. 1997, 9, 795.

35. T. Yamamoto, Bull. Chem. Soc. Jpn. 1999, 72, 621.

36. T. Yamamoto, et al., Synth. Met. 1999, 100, 237.

37. I. Winter, et al., “The thermal aging of PEDT”, Chemical Physics, Volume 194, Issue 1, 1 May 1995, Pages 207-213.

38. J. Reynolds, B. Sankaran., Macromolecules, 30 (9), 2582-2588, 1997.

39. H. Yamato, K. Kai, M. Ohwa, T. Asakura, T. Koshiba, and W. Wernet , Synthetic Metals, Volume 83, Issue 2, November 1996, Pages 125-130

40. Y. Kudoh, et al., Synthetic Metals, Volume 123, Issue 3, 24 September 2001, Pages 541-544

41. A. Lima, P. Schottland, S. Sadki and C. Chevrot, Synthetic Metals, Volume 93, Issue 1, 28 February 1998, Pages 33-41

42. S. Armes and R. Corradi, Synthetic Metals, Volume 84, Issues 1-3, January 1997, Pages 453-454

43. K. Xing, X. Chen, O. Inganas, W. Salanech and M.Fahlman., Synthetic Metals, Volume 89, Issue 3, September 1997, Pages 161-165

44. J. Reynolds, et al., Synthetic Metals, Volume 85, Issues 1-3, 15 March 1997, Pages 1295-1298

45. X. Chen and O. Inganäs, J. Phys. Chem., 100(37),15202-15206.

46. M. Levin, I. Shlimak, A. N. Aleshin, R. Kiebooms and H. Yu, Synthetic Metals, Volume 94, Issue 2, 30 April 1998, Pages 157-159

47. G. Greczynski, et al., Thin Solid Films, Volume 354, Issues 1-2, 8 October 1999, Pages 129-135

48. A. Heeger, Y. Chang, K. Lee, R. Kiebooms, and A. Aleshin., Synthetic Metals, Volume 105, Issue 3, 15 September 1999, Pages 203-206

49. H. Randriamahazaka, V. noel and C. Chevrot., Journal of Electroanalytical Chemistry, Volume 472, Issue 2, 30 August 1999, Pages 103-111

50. A. Heeger, A. Aleshin, and r. Kiebooms., Synthetic Metals, Volume 101, Issues 1-3, May 1999, Pages 369-370

51. J. Reynolds and M. Morvant, “In situ conductivity studies of PEDOT”,Synthetic Metals, vol. 92, 1998, 57-61.

52. L. Nir, C. Kvarnstrom, K. Froberg, and A. Ivaska, “Electrochemically controlled surface morphology and crystallinity in PEDOT films”, Synthetic Metals, 122 (2001) 425-429.

53. S. Garreau, G. Louarn, S. Lefrant, J. Buisson, and G. Froyer, “Optical study and vibrational analysis of the PEDT”, Synthetic Metal 101, (1999), 312-313.

54. J. Huang, P. Miller, J. de Mello, A. de Mello, and D. Bradley, “ Influence of thermal treatment on the conductivity and morphology of PEDOT/PSS films”, Synthetic Metals, 139, (2003), 569-572.

55. O. Inganas, L. Pettersson, F. Carlsson, and H. Arwin, Anisotropic optical properties of doped poly(3,4-ethylenedioxythiophene), Synthetic Metals, Volume 101, Issues 1-3, May 1999, Pages 198-199

56. D. J. Irvin, C. J. DuBois, J. R. Reynolds, Chem. Commun. 1999, 2121.

57. S. Akoudad, J. Roncali, Synth. Met. 1999, 101, 149.

58. Y. Cao, G. M. Treacy, P. Smith, A. Heeger, J. Appl. Phys. Lett. 1992,60, 2711.

59. S. Ghosh, J. Rasmusson, O. Inganäs, Adv. Mater. 1998, 10, 1097.

60. J. Drummond, S. J. Clarson, J. S. Zetts, F. K. Hopkins, S. J. Caracci, Appl. Phys. Lett. 1999, 74, 368.

61. A. Aleshin, R. Kiebooms, R. Menon, F. Wudl, A. J. Heeger, Phys. Rev. B. 1997, 56, 3659.

62. N. Sakmeche, S. Aeiyach, J.-J. Aaron, M. Jouini, J. C. Lacroix, P.-C. Lacaze, Langmuir 1999, 15, 2566.

63. S. Ghosh, J. Rasmusson, O. Inganäs, Adv. Mater. 1998, 10, 1097.

64. A. Heeger, A. Aleshin and S.Williams, Synthetic Metals, April 2000.

65. Q. Pei, G. Zuccarello, M. Ahlskog, O. Inganäs, Polymer 1994, 35, 1347.

66. S. Garreau, G. Louarn, J. P. Buisson, G. Froyer, S. Lefrant, Macromolecules, 1999, 32, 6807.

67. J. C. Carlberg, O. Inganäs, J. Electrochem. Soc. 1998, 145, 3810.

68. S. Garreau, G. Louarn, S. Lefrant, J. P. Buisson, G. Froyer, Synth. Met. 1999, 101, 312.

69. D. M. Welsh, A. Kumar, E. W. Meijer, J. R. Reynolds, Adv. Mater. 1999, 11, 1379.

70. B. Sankaran, J. R. Reynolds, Macromolecules 1997, 30, 2582.

71. J. C. Gustafsson, B. Liedberg, O. Inganäs, Solid State Ionics 1994,, 69, 145

72. G. A. Sotzing, J. L. Reddinger, J. R. Reynolds, P. J. Steel, Synth. Met. 1997, 84, 199.

73. M. Granström, M. Berggren, O. Inganäs, Science 1995, 267, 1479.

74. T. Yohannes, O. Inganäs, Sol. Energy Mater. Sol. Cells 1998, 51, 193.

75. H. Yamato, M. Ohwa, W. Wernet, J. Electroanal. Chem. 1995, 397, 163.

76. S. Ghosh and O. Inganas, "Self-assembly of a conducting polymer nanostructure by physical crosslinking : applications to conducting blends and modified electrodes", Synthetic Metals, 101 (1999) 413-416.

77. Bayer AG, Eur. Patent 821 025, 1998.

78. Y. Kudoh, K. Akami, Y. Matsuya, Synth. Met. 1999, 102, 973

79. Bayer AG, Eur. Patent 340 512, 1989.

80. F. Larmat, J. R. Reynolds, Y.-J. Qiu, Synth. Met. 1996, 79, 229.

81. Bayer AG, Eur. Patent 340 512, 1989.

82. S. Sapp, G. Sotzing, and J. Reynolds, Chem. Mater., 10 (8), 2101-2108, 1998.

83. M. Granström, M. Berggren and O. InganäsPolymeric light-emitting diodes of submicron size: Structures and developments, Synthetic Metals, Volume 76, Issues 1-3, January 1996, Pages 141-143

84. M. Bouguettaya, N. Vedie, and C. Chevrot, Synthetic Metals, 102 (1999) 1428-1431.

85. J. Pelota, Y. Cao, and P. Smith, Adhesive Age, (May 1995) 18.

86. A. Elschner, F. Bruder, H. Heuer, F. Jonas, A. Karbach, S. Kirchmeyer, S. Thurm, and R. Wehrmann, Synthetic metals 111-112 (2000) 139-143.

87. J. C. Carlberg, O. Inganäs, J. Electrochem. Soc. 1997, 144, L61.

88. Bayer AG, Eur. Patent 553 671, 1993.

89. D.M. deLeeuw, P. A. Kraakman, P. F. G. Bongaerts, C. M. J. Mutsaers, Synth. Met., 1994, 66, 263.

90. J. S. Kim, F. Cacialli, R. H. Friend, R. Daik, W. J. Feast, Synth. Met. 1999, 102, 1065.

91. Bayer AG, Eur. Patent 686662, 1995.

92. D. Setiadi, Z. He, J. Hajto, T. D. Binnie, Infrared Phys. 1999, 40, 267.

93. Philips Company, US Patent 5 742 119, 1998.

94. A. C. Arias, M. Granström, K. Petritsch, R. H. Friend, Synth. Met. 1999, 102, 953.

95. M. J. Burchell, M. J. Cole, S. F. Lascelles, M. A. Khan, C. Barthet, S. A. Wilson, D. B. Cairns, S. P. Armes, J. Phys. D: Appl. Phys. 1999, 32, 1719.

96. L. S. Roman, L. C. Chen, L. A. A. Pettersson, W. Mammo, M. R. Andersson, M. Johansson, O. Inganäs, Synth. Met. 1999, 102, 977.

97. B. Nabet, "When is Small Good? On Unusual Electronic Properties of Nanowires", ECE Department, Philadelphia, PA-19104

98. Z. Yao, et al, " Carbon nanotube intramolecular junctions", Nature, vo. 402, no. 6759, pp. 273-276, Nov. 1999.

99. B. Nabet, et al " Heterodimensional contacts and optical detectors", Int. J. High Speed Electronics and Systems, vol. 10, no 1, pp. 375-386, Aug. 2000

100. H. Dai et al. " Controlled Chemical Routes to Nanotube Architectures, Physics, and Devices", J. Phys. Chem. B 1999, 103, 11246-11255

101. Zeleny, J., Physical Review, X (1), 1 (1917).

102. U.S. Pat, 1,975,504 (Oct. 2, 1934), Formhals A.

103. Vonnegut, B and Neubauer, RL, Journal of Colloid Science, 1952, 7, 616 .

104. Baumgarten, PK, Journal of Colloid and Interface Science, 1971, 36, 71.

105. Larrondo L and Manley J, Journal of Polymer Science, Polymer Physics Edition, 1981, 19, 933 .

106. Doshi J and Reneker DH, Proceedings of IEEE Industry Applications Society Meeting Part 3, 3, 1993.

107. Doshi J, and Reneker D, "Electrospinning process and applications of electrospun fibers", Journal of Elecrostatics , 1995, 35, 151-160.

108. Reneker D, and Chun I, "Nanometer diameter fibers of polymer, produced by electrospinning", Nanotechnology,1996, 7, 216-223.

109. Jaeger R, H Schonherr H, and Vansco G, Macromolecules, 1996, 29, 7634-7636.

110. Jaeger R, Bergshoef M, Batlle C, Schonherr H, and Vancso G, Maccromol. Symp., 1998, 127, 141-150.

111. Gibson , and Rivin D, AIChE Jounal, 1999, 45, no. 1.

112. Fong H, Chun I, and Reneker D, Polymer, 1999, 40, 4585-4592.

113. Kim J, and Reneker D, Polymer Engineering and Science, 1999, vol. 39, No.5.

114. Deitzel J, Kleinmeyer J, Harris D, and Tan N, Polymer, 2001, 42, 261-272.

115. Demir M, Yilgor I, Yilgor E, and Erman B, Polymer, 2002, 43, 3303-3309.

116. Dersch R, Liu T, Schaper A, Greiner A, and Wendorff J, journal of polymer Science, Part A: Polymer Chemistry, 2003, vol. 41, 545-553.

117. Guan H, Shao C, Chen B, Gong J, and Yang X, Inorganic Chemistry Communications, 2003, 6, 1409-1411.

118. Kenawy E, Layman J, Watkins J, Bowlin G, Matthews J, Simpson D, and Wneck G, Biomaterials, 2003, 24, 907-913.

119. Viswanathamurthi P, Bhattarai N, Kim H, Lee D, Kim, S and Morris M, Chemical physics letters, 2003, 374, 79-84.

120. Pedicini A, and Farris R, Polymer, 2003, 44, 6857-6862.

121. Zong X, Ran S, Fang D, Hsio B, and Chu B, Polymer, 2003, 44, 4959-4967.

122. Taylor G, "Electrically driven jets", Proc. Roy. Soc. London, 1969, A. 313, 453-475.

123. C. Hendricks, and D. Horning, J. Appl. Phys., 50, 4, 1979.

124. C. O'Konski, and H. Thacher, J. Phys. Chem., 1953, 57, 955.

125. L. Larrondo and R. Manley, Journal of Polymer Science, polymer physics edition, vol.19, 909-940, 1981.

126. D. Smith " The electrohydrodynamic atomization of liquids". IEEE, IA-22, 3, May/June 1986, 527-535.

127. I. Hayati, Colloids and Surfaces, 65, 1992, 77-84.

128. Fang X and Reneker D H. DNA fibers by electrospinning, J. Polymer, 1996, 1-8.

129. D. Reneker, A. Yarin, H. Fong, and S. Koomhongse, Journal of Applied Physics, vol. 87, No. 9, 2000.

130. M.Shin, M. Hohman, G. Rutledge, and M. Bernner, "Electrospinning and electrically forced jets. I: Stability theory", Physics of Fluids, vol. 13, No. 8, 2001,2201-2220.

131. M.Shin, M. Hohman, G. Rutledge, and M. Bernner, "Electrospinning and electrically forced jets. II: Applications", Physics of Fluids, vol. 13, No. 8, 2001,2221-2236.

132. M.Shin, M. Hohman, G. Rutledge, and M. Bernner, "A whipping fluid jet generates submicron polymer fibers.", Appl. Phys. Lett., 2001, 78, 1149-1151.

133. A. Spivak, Y. Dzenis, and D. Reneker, Mechanics Research Communications, vol.27, No. 1, PP. 37-42, 2000.

134. F. Ko, B. Han, K. Chandriani, and A. MacDiarmid, "The relationship of Berry Number to the, morphology of poly(L-lactic acid) nanofibers by electrospinning", Department of Materials Science& Engineering, Drexel University, Philadelphia, PA-19104 (2001).

135. B. Hager, G. Berry, Journal of Polymer Materials, 1993, p 94-95.

136. J. Deitzel, J. Kleinmeyer, J. Hirvonen, and N. Tan, Polymer, 42, 2001, 8163-8170.

137. I. Chun, D. Reneker, H. Fong, X. Fang, J. Deitzel, N. Tan, and K. Kearns, Journal of Advanced Materials, vol. 31, no. 1, 1999.

138. J. Kim, and D. Reneker, "Mechanical Properties of Composites using Ultrafine Electrospun fibers", Polymer Composites, 1999, vol. 20, no.1.

139. C. Buchko, L. Chen, Y. Shen, and D. Martin, Polymer, 40, 1999, 7397-7407.

140. S. Koombhongse, W. Liu, and D. Reneker, Journal of Polymer Science: Part B: Polymer Physics, Vol. 39, 2598-2606, 2001.

141. L. Huang, K. Nagapudi, A. McMillan, V. Condcello, B. Pourdeyhlml, and E. Chaikof, Polymeric Materials: Science & Engineering, 2001, 84, 1069-1070.

142. C. Seoul, Y. Kim, and C. Baek, Journal of Polymer Science: Part B: Polymer Physics, Vol. 41, 1572-1577, 2003.

143. J. Zeng, X. Xu, X. Chen, Q. Liang, X. Bian, L. Yang, and X. Jing, Journal of Controlled Release, 92, 2003, 227-231.

144. Z. Huang, Y. Zhang, M. Kotaki, and S. Ramakrishna, Composites Science and Technology, 63, 2003, 2223-2253.

145. B. Min, G. Lee, S. Kim, Y. Nam, T. Lee, and W. Park, Biomaterials, 25, 2004, 1289-1297.

146. H. Jin, J. Chen, V. Karageorgiou, G. Altman, and D. Kaplan, Biomaterials, 25, 2004, 1039-1047.

147. C. Xu, R. Inai, M. Kotaki, and S. Ramakrishna, Biomaterials, 25, 2004, 877-886.

148. F. Ko, I. Norris, M. Shaker, and A. MacDiarmid, Synthetic Metals, 114, 2000, 109-114.

149. A. MacDiarmid, W. Jones, I. Norris, J. Gao, A. Johnson, N. Pinto, J. Hone, B. Han, F. Ko, H. Okuzaki, and M. Llaguno, Synthetic Metals, 119, 2001, 27-30.

150. N. Pinto, P. Carrion, and J. Quinones, Materials Science and Engineering, A366, 2004, 1-5.

151. S. Iijima, Nature 1991, 354, 56-58.

152. P. Ajayan, M. Zhou, and o. Top, Appl. Phys. 2001, 80, 391-425.

153. R. Baughman, A. Zakhidov, and W. de Heer, “Carbon Nanotubes-the Route Toward Applications”, Science, vol 297, August 2002.

154. S. Louie, Top. Appl. Phys. 80, 113 (2001).

155. R. Ding, G. Lu, Z. Yan, and M. Wilson, Journal of Nanonscience Nanotechnology, 1. 7 (2001).

156. A listing of commercial suppliers of carbon nanotubes and related materials is available at www.rdg.ac.uk/~scsharip/tubes.htm.

157. P. Ball, Nature 414, 142 (2001).

158. P. Collin, Ph. Avouris, and M. Arnold, Science 292, 706, 2001.

159. C. Park, Z. Ounaies, K. Watson, R. Crooks, J. Smith Jr., S. Lowther, J. Connell, E. Siochi, J. Harrison, and T. St. Clair, " Dispersion of SWNTs by in situ polymerization under sonication", Chemical Physics Letters, 364 (2002) 303-308.

160. H. Huang, H. Kajiura, A. Yamada, and M. Ata, "Purification and alignment of arc-synthesis SWNTs bundles", Chemical Physics Letters, 356 (2002) 567-572.

161. S. Polarz, B. Smarsly, and J. Schattka, " Hierachical Porous Carbon Structures form Cellulose Acetate Fibers", Chem. Mater. 2002, 14, 2940-2945.

162. M. O'Connell, P. Boul, L. Ericson, C. Huffman, Y. Wang, E. Haroz, C. Kuper, J. Tour, K. Ausman, and R. Smalley, " Reversible water-solubilization of SWNTs by polymer wrapping", Chemical Physcs Letters, 342 (2001) 265-271.

163. S. Niyogi, M. Hamon, D. Perea, C. Kang, B. Ahao, S. Pal, A. Wyant, M. Itkis, and R. Haddon, J. Phys. Chem. B 2003, 107, 8799-8804.

164. R. Bandyopadhyaya, E. Nativ-Roth, O. Regev, and R. Yerushalmi-Rozen, "Stabilization of Individual Carbon Nanotubes in Aqueous Solutions", Nano Letters, 2002, vol. 2, No. 1, 25-28.

165. P. Ajayan, T. Ichihashi and S. Iijima, "distribution of pentagons and shapes in carbon nano-tubes and nano-particles", Chemical physics letters, vol. 202, no. 5, 1993.

166. M. Islam, E. Rojas, D. Bergey, A. Johnson, and A. Yodh, "High Weight Fraction Surfactant Solubilization of Single-Wall Carbon Nanotubes in Water", 2003, vol. 3, No. 2, 269-273.

167. M. Treacy, Ebbesen, and J. Gibson, "Exceptionally high Young's modulus observed for individual carbon nanotubes", Natubre, vol. 381, 1996.

168. E. Wong, P. Sheehan, and C. Lieber, "Nanobeam mechanics: Elasticity, Strength, and Toughness of Nanorods and Nanotubes", Science, vol. 277, 1997.

169. Ph. Poncharal, Z. Wang, D. Ugarte, and W. de Heer, "Electrostatic Deflections and Electromechanical Resonances of Carbon Nanotubes", Science, vol. 283, 1999.

170. A. Rao, J. Chen, E. Richter, U. Schlecht, P. Eklund, R. Haddon, U. Venkateswaran, Y. Kwon, and D. Tomanek, " Effect of van der Waals Interactions on the Raman Modes in Single Walled Carbon Nanotubes", Physical Review Letters, vol. 86, No. 17, 2001.

171. J. Wei, B. Jiang, X. Zhang, H. Zhu, and D. Wu, " Raman study on double-walled carbon nanotubes", Chemical Physics Letters, 376 (2003) 753-757.

172. K. kaneto, M. Tsuruta, G. Sakai, W. Cho, and Y. Ando, "Electrical conductivies of multi-wall carbon nanotubes", Synthetic Metals 103, (1999), 2543-2546.

173. P. de Pablo, M. Martinez, J. Colchero, J. Gomez-Herrero, W. Maser, A. de Benito, E. Munoz, and A. Baro, "Electrical characterization of SWNTs with SFM", Materials Science and Engineering C 15, 2001, 149-151.

174. R. Enomoto, K. Horiuchi, K. Miyamoto, Y. Matsunaga, N. Aoki, and Y. Ochiai, " Low temperature conductance in MWNTs", Physica B, 323, 2002, 249-251.

175. Z. Tang, L. Ahang, N. Wang, X. Zhang, J. Wang, G. Li, Z. Li, G. Wen, C. Chan, and P. Sheng, " Ultra-small SWNTs and their superconductivity properties", Synthetic Metals, 9526, 2002, 1-5.

176. P. Corio, P. Santos, M. Pimenta, and M. Dresselhaus, "Evolution of the molecular structure of metallic and semiconducting carbon nanotubes under laser irradiation", Chemical Physics Letters, vol 360, issues 5-6, 2002, 557-764.

177. P. de Pablo, E. Graugnard, B. Walsh, R. Andres, S. Datta, and R. Reifenberger, "A simple, reliable technique for making electrical contact to multiwalled carbon nanotubes", Applied Physics Letters, vol. 74, No. 2, 1999.

178. L. Schadler, S. Giannaris, and P. Ajayan, "Load transfer in carbon nanotube epoxy composites", Applied Physics Letters, vol. 73, No. 26, 1998.

179. C. Bower, R. Rosen, L. Jin, J. Han, and O. Zhou, "Deformation of carbon nanotubes in nanotube-polymer composites", Applied Physics, Letters, Vol. 74, No. 22, 1999.

180. L. Jin, C. Bower, and O. Zhou, "Alignment of carbon nanotubes in a polymer matrix by mechanical stretching", Applied Physics Letters, Vol. 73, N0. 9, 1998.

181. R. Haggenmueller, H. Gommans, A. Rinzler, J. Fischer, and K. Winey, " Aligned SWNTs in composites by melt processing methods", Chemical Physics Letters, 330, 2000, 219-225.

182. B. Landi, R. Raffaelle, M. Heben, J. Alleman, W. VanDerveer, and T. Gennett, "Single Wall Nanotube-Nafion Composite Actuators", Nano Letters, 2002, vol. 2 No. 11, 1329-1332.

183. S. Kumar, T. Dang, F. Arnold, A. Bhattacharyya, B. Min, X. Zhang, R. Vaia, C. Park, W. Adams, R. Hauge, R. Smalley, S. Ramesh, and P. Willis, " Synthesis, Stucture, and Properties of PBO/SWNT Composites", Macromolecules, 2002, 35, 9039-9043.

184. E. Kymakis, I. Alexandou, G. Amaratunga, "SWNT-polymer composites: electrical, optical and structural investigation", Synthetic Metals 127, 2002, 59-62.

185. J. Kim, M. Kim, H. Kim, J. Joo, and J. Choi, "Electrical and optical studies of organic light emitting devices using SWCNTs-polymer nanocomposites", Optical Materials 21, 2002, 147-151.

186. H. Geng, R. Rosen, B. Zheng, H. Shimoda, L. Fleming, J. Liu, and O. Zhou, "Fabrication and properties of composites of PEO and functionalized CNTs", Advanced Materials, 2002, 14, No. 19, 1387-1390.

187. M. Aheng, A. Jagota, E. Semke, B. Diner, R. Mclean, S. Lustig, R. Richardson, and N. Tassi, " DNA-assisted dispersion and separation of carbon nanotubes", Nature materials, Vol. 2, 2003.

188. C. Seoul, Y. Kim, and C. Baek, "Electrospinning of PVDF/DMF solutions with carbon nanotubes", Journal of polymer science: Part B: Polymer Physics, vol. 41, 2003, 1572-1277.

189. Y. Dror, W. Salalha, R. Khalfin, Y. Cohen, A. Yarin, and E. Zussman, "CNs embedded in oriented polymer nanofibers by electrospinning", Langmuir, 2003, 19, 7012-7020.

190. A. Pron, G. Louran, M. Lapkowski, M. Zagorska, J. Glowczyk-Zubek, and S. Lefrant, " In Situ Raman Spectroelectrochemical studies of Poly (3,3'-dibutoxy-2,2'-bithiophene)", Macromolecules, 1995, 28, 4644-4649.

191. G. Louarn, J. Kruszka, S. Lefrant, M. Zagorska, I. Bayer, and A. Pron, Synthetic Metals, 1993, 61, 233.

192. S. Garreau, G. Louarn, S. Lefrant, J. Buisson, and G. Froyer, "Optical study and vibrational analysis of PEDOT", Synthetic Metals, 101, 1999, 312-313.

193. Zhong Lin Wang, "New Developments in TEM for Nanotechnology", Advanced Materials, 2003, 15, No. 18, 1497-1514.

194. Z. Wang, Y. Liu, Z. Zhang, handbook of Nanophase and Nanostructured Materials, Vols. I-IV, co-published by Kluwer Academic Press, New York, and Tsinghua University Press, 2002.

195. P. Buseck, J. Cowley, L. Eyring, "high resolution TEM: Theory and Applications", Oxford University Press, New York 1989.

196. Z. Wang, C. Hui, "Electron Microscopy of Nanotubes", Kluwer Academic Publisher, New York, 2003.

197. Z. Wang, Z. Kang, "Functional and Smart Materials-Structural Evolution and Stucture Analysis", Ch. 6-8, Plenum Press, New York 1998.

198. Z. Wang, J. Phys. Chem. B, 2000, 104, 1153.

199. Z. Wang, Adv. Mater. 1998, 10, 13.

200. Z. Wang, Z. Dai, and S. Sun, Advanced Materials, 2000, 12, 1944.

201. ASTM Designation: D4496-87, 453.

202. F.Ko, Y. Gogotsi, A. Ali, N. Naguib, H. Ye, G. Yang, C. Li, and P. Willis, "Electrospinning of Continuous Carbon Nanotube-Filled Nanofiber Yarns", Adv. Mater. 2003, 15, No. 14, July 17.

Appendix I: Intrinsic Viscosity Measurement

Procedures

I-Apparatus

1- Six clean vials

2- The glass viscometer, CANON Instrument Company Type: 200 653B , be sure it is clean and dry.

3- Digital balance (Scientech SA120 Max. 120 g. with d= 0.0001 g).

4- The used Polymer and solvent

5- Clean glass pipette 1.1 mm.

6- Pipette pump-II, Bel-Art Products, up to 25 ml.

7- Clean Spatula

8- Rubber tube with 10 ml plastic syringe.

II-Preparation of Polymer Solution

The amount; that should be used with the prescribed viscometer, is at least 6 ml. So, we adjusted the amount of solution to be; for all concentration, 6 ml.

The recommended concentrations are 0.0,0.2,0.4,0.6,0.8&1.0 in (g/dl).

Where: dl. = 10^{-1} (l) or 100 (cm^3).

Note that the density of the solvent and the required polymer should be known.

Experimental example

Density of polymer ρ_p = 1.2 (g/cm^3)

Density of solvent ρ_s = 1.1 (g/cm^3)

To figure out the weight of the polymer and solvent, the following calculation should be carried out.

As 0.002 (g/ml) = 0.2 (g/dl)

0.2 (g/dl) = (polymer mass (g)/100ρ_p)/((polymer mass (g)/100ρ_p) + (Solvent mass (g)/100ρ_s))

Also; As 6 (ml) polymer solution;

6 ml = $6x10^{-3}$ L = $6x10^{-2}$ dl.

6 ml. = (Polymer mass (g)/ρ_p) + (Solvent mass (g)/ρ_s)

So we can get:

0.002 (g/ml) = (polymer mass (g)/ρ_p)/(6) = polymer mass (g)/6ρ_p

Polymer mass (g) = 0.012 ρ_p = 0.012 x 1.2 = 0.0144 g

Solvent mass (g) = [6-(0.0144/1.2)] x 1.1 = 6.5868 g

Which means by wt.% = ((0.0144/0.0144) + 6.5868) x 100 = 0.218142%

Hence, the following table can be filled:

Table I. 1 Calculation of Polymer and Solvent Weights for Different Concentrations.

Concentration (g/dl)	Polymer (g)	Solvent (g)
0.0	**0.0**	**6.6**
0.2	**0.0144**	**6.5868**
0.4	**0.0288**	**6.5736**
0.6	**0.0432**	**6.5604**
0.8	**0.0576**	**6.5472**
1.0	**0.072**	**6.534**

III- Measuring time vs. Polymer Concentrations

By using the set up of viscometer and the stopwatch you can take three reading for the time per each concentration see Figure I-1.

Steps:

1-Pour the polymer solution into the clean viscometer

2-Suck the polymer solution by using the syringe and the rubber tube till it reach the level over the ball shape in the viscometer

3-Take off the syringe

4-Start the timing when the solution pass by the upper level and stop it when it pass the lower level below the ball shape in the viscometer see Figure I-2

5-Repeat steps from 2-4 two times more

6- Fill in table.I.2. with your results.

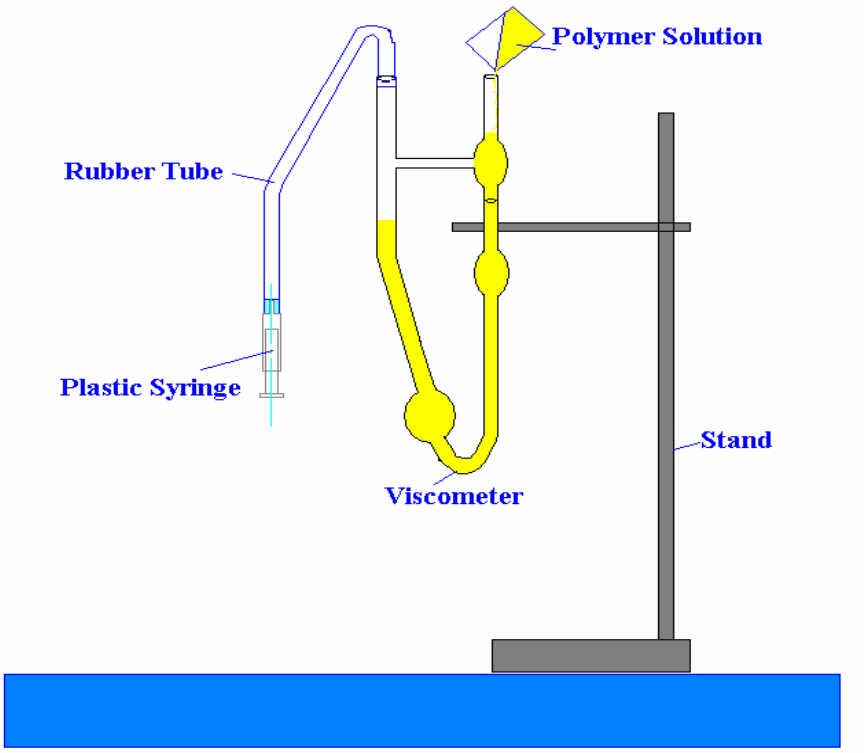

Figure I. 1 Set-up Schematic Diagram.

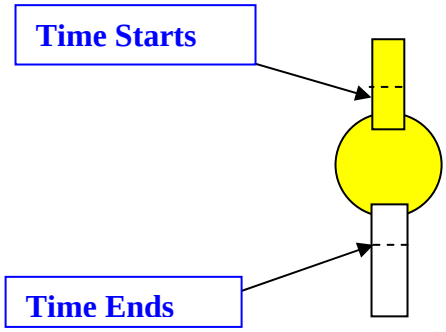

Figure I. 2 Illustration Figure.

Table I. 2 Time vs. Concentration.

Concentration (g/dl)	Three Time Readings (sec)	Time Average (sec)
0.0	21,21,21	21=t0
0.2202	31,31,31	31=t1
0.4404	42,42,42	42=t2
0.6606	57,57,58	57.3=t3
0.8808	76,76,75	75.7=t4
1.101	95,98,100	97.7=t5

IV- Calculation of Specific Viscosity.

Use the following equation to calculate the specific viscosity at each concentration;

Specific viscosity = (ti/t0)-1

Where i = 1 to 5, Then fill the following table

Table I. 3 Concentration vs. Specific Viscosity/Concentration.

Concentration (g/dl)	**Specific viscosity/Concentration (dl/g)**
0.2202	2.162536
0.4404	2.270663
0.6606	2.616669
0.8808	2.957268
1.101	3.317331

Then the relationship between the concentration and Specific viscosity/Concentration can be plotted as in Figure I.3.

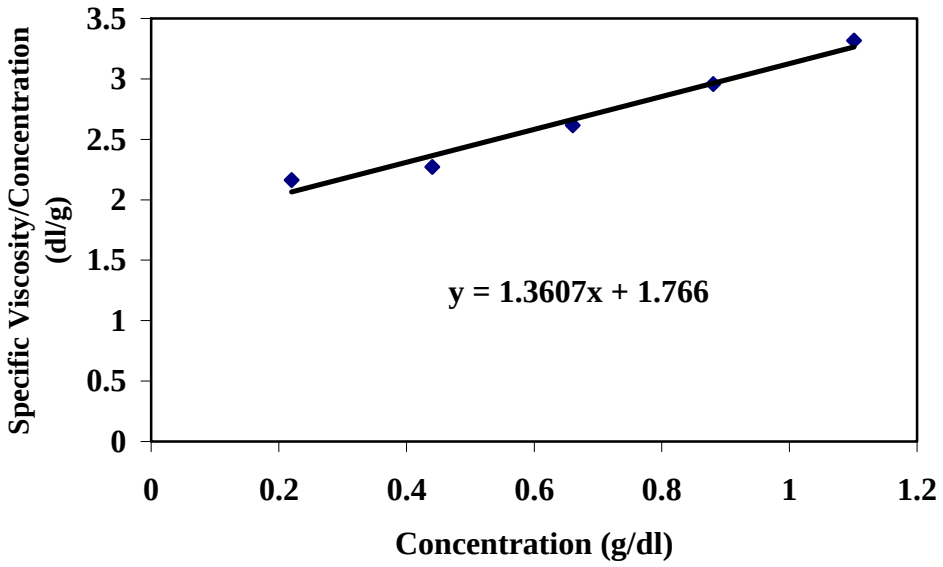

Figure I.3 Intrinsic Viscosity (DMSO and PAN Mw 150000).

The intrinsic viscosity will be the intersection of the fitting line with the y-axis which is equal; in our example, [η] = 1.766.

Table I. 4 Some Polymer/ Solvent Types and Their Densities.

Polymer	**Density (g/cm^3)**	**Solvent**	**Density (g/cm^3)**
Polyacrylonitrile (PAN)	1.184	Dimethylformamide (DMF)	0.994
"	"	Dimethylsulfoxide (DMSO)	1.101
Polyethylene oxide (PEO)	1.13	Desteld Water (H2O)	1.00
"	"	Chloroform (CHCl3)	1.14
Polyvinylidene fluoride/ Tetra fluouro ethanol (PVDF/TeFE)	1.73	Methyl ethyl ketone (MEK)	0.804

Appendix II: Mechanical Properties calculations

Tensile Strength Test for NANO fibers

I. Sample preparation

1- Prepare a cartoon holder for the sample as shown in figure (II. 1). H = guage length (4 cm Recommended.), W = 1 + 4(sample width).

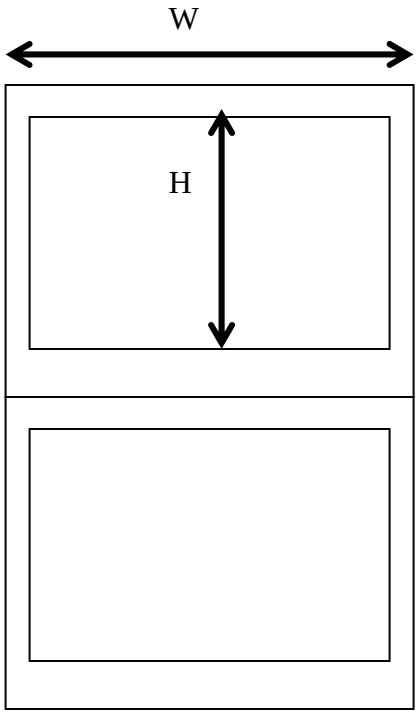

Figure II.1 The sample holder.

2- Apply a epoxy glue to cover the whole flange of the holder. (The horizontal rectangles).

3- Place the center of the sample over the holder as shown in figure (II. 2). (the center of the sample to the center of the half of flange-A-)

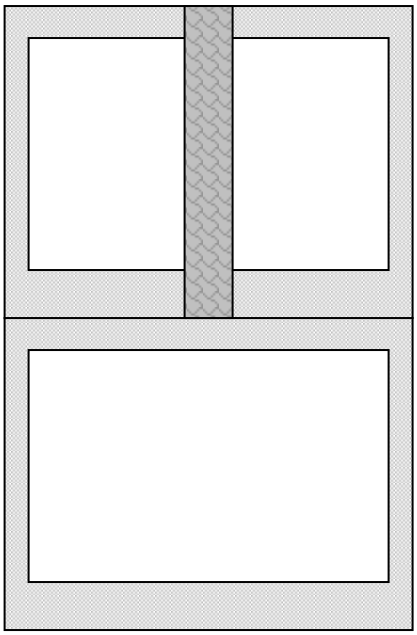

Figure II.2 The sample attached to the holder.

4- Flip the sample with holder as shown in figure (3).

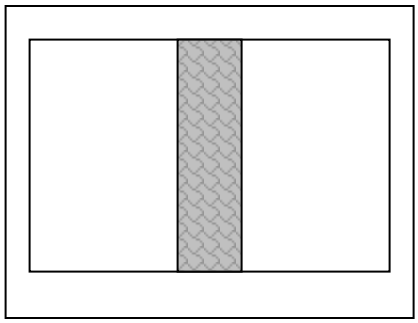

Figure II.3 The final image of the sample and holder.

II. Adjustment of the loading range

1- To adjust the range of load, you have ,Zero adjust button A, transducer button B and SENS buttons C(X1-X10 & 1,2,5) to get different ranges.

2- With button B& C and using the range table, you can get the desired range of load.

SENS / Force transducer	1 X 1	2 X 1	5 X 1	1 X 10	2 X 10	5 X10
A	20	40	100	200	400	1000
B	100	200	500	1000	2000	5000

3- With the aid of button A re-adjust the pointer to zero.

4- Open the Macintosh program; go to tensile tester folder, then to f test icon. Click Windows and then show diagram to change the value in the box to the selected value in the table.

III. Procedure

1- Turn on MAIN power and MOTOR AMP .wait 10 minutes for machine warm-up.

2- Set testing speed by adjusting “FWD” and “SPEED RANGE” dials.

3- Set desired position by adjusting “GAUGE”dial.

4- Adjust “DC BAL” dial to balance the load cell.

5- Adjust the gage height by using the button D

6- Take away the upper clamp & fix the sample tightly.

7- Put the upper clamp back to its position & fix the lower bottom of the sample holder to the lower clamp.

8- Cut the beam holder as shown in figure(II. 4)

Cut here

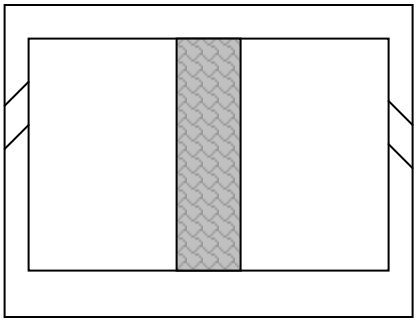

Figure II.4 Illustration of a slit on the both sides of the holder.

9- Start the computer program

10- Start loading by pressing the button REP.

11- Upon the sample reaching the failure condition, the clamp will stop moving down & the program will stop giving the load-deformation data.

12- Press stop button when the specimen breaks, then RSV to return lower clamp to the adjusted position for another test and finally press Stop button again. Take off the broken specimen.

13- Save the data, so you can analyze the data by transferring to excel soft-ware.

Important Buttons

RES **:**Return to preset position at max. Speed.

REP : if under “DISP CONTROL” , cycling test is evoked.

If under “FORCE CONTROL”, the bottom fixture continues

Going down until it hits bottom limit or SROP button is pressed.

SINGLE : single cycle test.

STOP : stops the bottom fixture movement when this button is pressed.

The result from the machine was in the form of load (gram force) vs. displacement. The stress in gm/Tex was calculated using following equation…

$$Stress(gm/Tex) = \frac{Force(gm)}{Areal\ density(gm/m^2)\ X\ width(mm)} \quad (1)$$

The areal density was calculated using following equation…

$$Areal\ density = \frac{Weight(gms)}{Length(m)\ X\ width(m)} \quad (2)$$

The stress in gm/Tex was converted to N/Tex by multiplying it by 0.0098. This was converted into the stress in GPa by dividing it by the density of test material, The strain was calculated by dividing the displacement by gauge length in mm.

Appendix III: 4-Probe Conductivity Measurement Device

INTRODUCTION

Ohm's Law

From Figure.III.1. we can conclude the following relations

$$V = I * R$$

$$\Delta = R * A / L$$

Where

V ……..The applied volt

I ……...The current

R ……..The resistance of the material

A ……..The cross-sectional area perpendicular to the direction of the current.

L ……..The distance between the two points at which the voltage is measured.

Δ ……The resistivity of the material

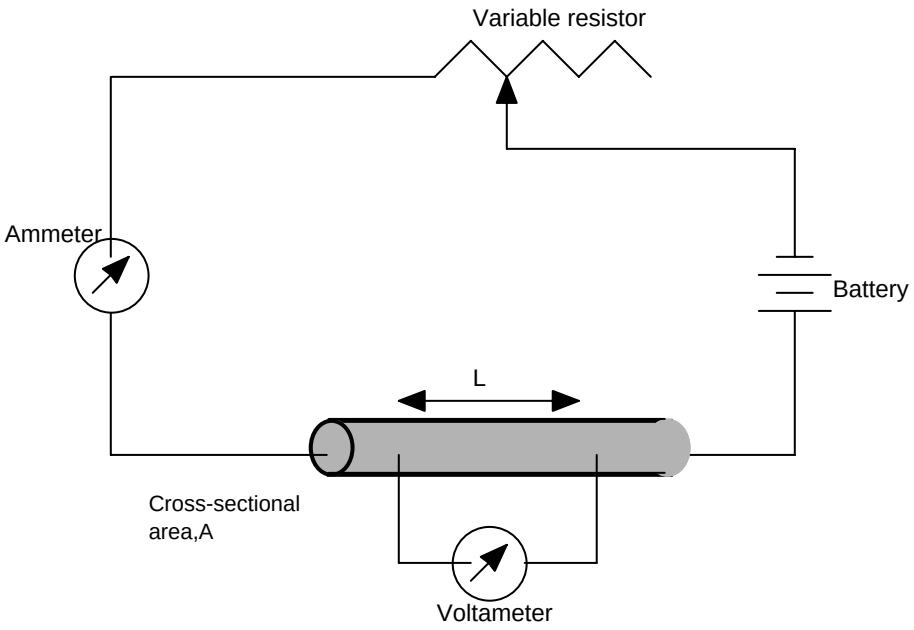

Figure.III.1 Schematic representation of the apparatus used to measure electrical resistivity.

Electrical Conductivity

$\Phi = 1/\Delta$

so

$\Phi = L/(R * A)$

Where

Φ ……. The conductivity

as we are using a semi-conductive material so we will use the four probe test

to measure the conductivity.

Four probe device

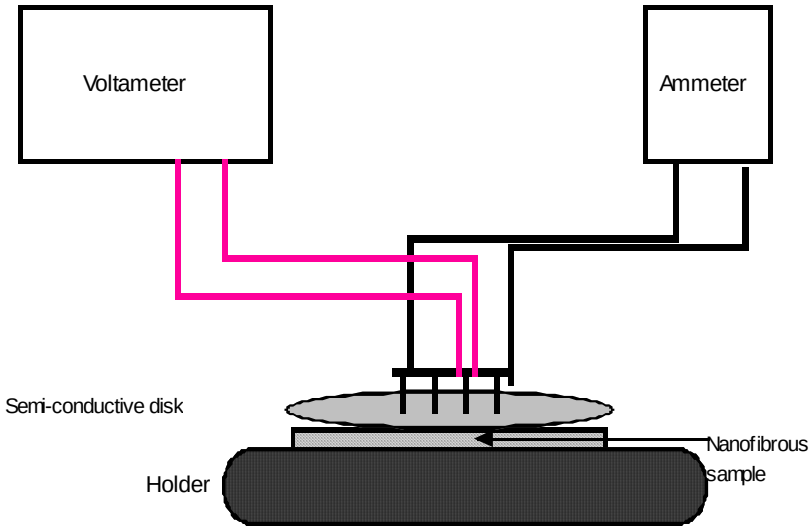

Figure III.2 Schematic of the four-probe device.

This apparatus consists of four Pt wire electrodes - two external electrodes through which a current is passed, and two inner electrodes where the potential drop is measured. The design of the rig used for measuring the volume resistivity of PEDOT films is shown in Figure III.3.

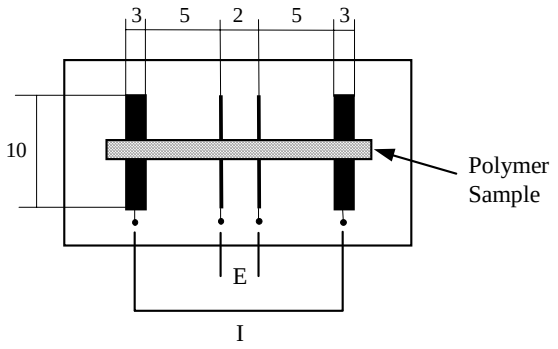

Figure III.3 Four Point Probe Assembly (dimensions in mm).

Procedure

- As shown in figure III.2 the fibrous sample is placed underneath the semi-conductive disk (to increase the sensitivity of the device and have better results)
- After making sure all the connections are in the correct positions start the measuring.
- By increasing the current passing through the sample and Disk (e.g. 0.1-0.2-0.3….), record the corresponding voltage from the voltmeter screen.
- After finishing the experiment (the red light will flash) , plot the current – volt data to get the slope of the curve (which is equal to the resistance of the disk and material together)
- Repeat the previous steps by using only the disk and measure the slope.(the resistance of the Disk)

Calculations

- The sample and the disk are assumed to be connected in series, so the resistance of the fibrous material is the subtraction of the value of the disk resistance and the value of the material-disk resistance.

  Resis.(fibrous material) = Resis.(total Disk and the material) – Resis. (Disk)

- By measuring the area exposed to the current of the fibrous material (e.g. 2.5 * 3.0 cm), the conductivity is easily measured as mentioned above where L will be equal the distance between the probe needle (e.g. 1.3 mm)

Measuring the conductivity directly of non-woven mats

The four-point probe method (Figure III.2) was employed to measure directly the volume resistivity of PEDOT/PAN mats using the procedure outlined in ASTM (D4496-87), with the conductivity being the inverse of the volume resistivity.

To calculate the volume resistivity, R_v, of the PEDOT mat, the following equation (III.1) was applied:

$$R_v = \frac{A}{L} \times \frac{\Delta E}{I} \quad \Omega \text{ cm} \qquad \text{(III.1)}$$

where:

A = The area of the tested sample (cm^2)

L = distance between the inner electrodes (cm)

I = current applied between the outer electrodes (mA)

ΔE = potential difference between the inner electrodes (mV)

The conductivity of the film can be calculated using equation (2.3).

$$\sigma = \frac{1}{R_v} \quad \text{S/cm} \qquad (2.3)$$

The electrical conductivity of nanofibrous yarn

In this stage the PEDOT and SWNTs/PEDOT yarns were tested directly by measuring the resistance between different lengths by using an Ohmmeter and alligator electrodes to avoid damaging the fibers. By calculating the linear density of the tested yarn the resistance of the yarn can be converted into conductivity.

Calibration of the device

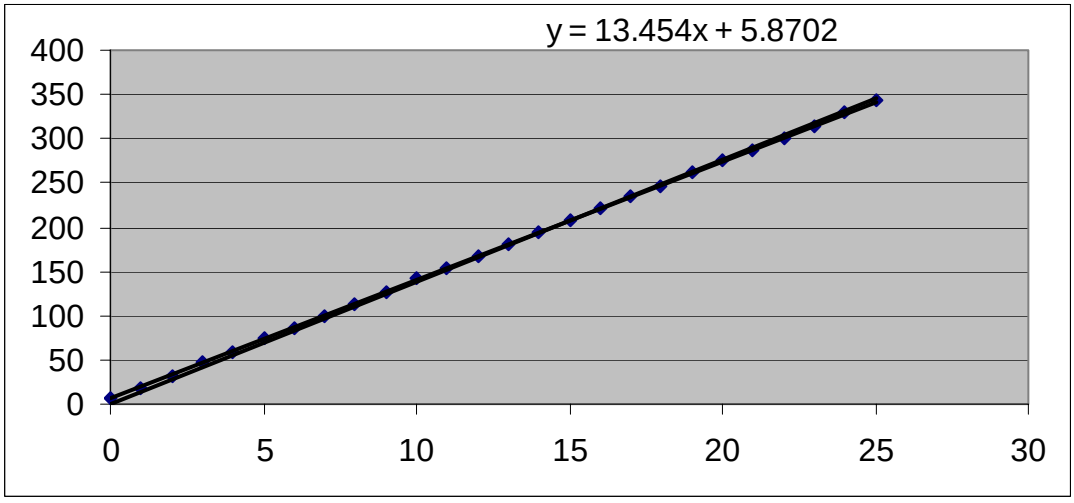

Figure III.4 Resistance of Aluminum wire.

Figure III.3 shows the resistance of aluminum wire measured by the 4-probe device of 13.4 Ohms compared with the actual resistance of the wire which is 13.5 ohms.

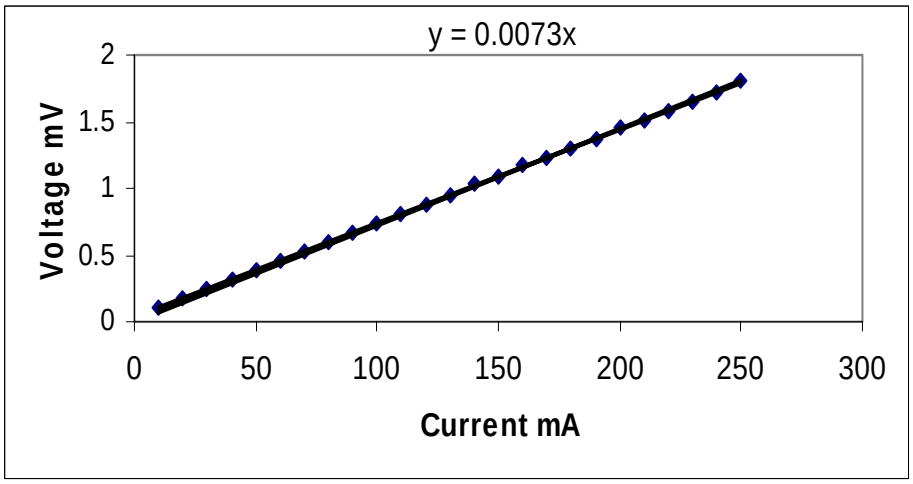

Figure III.5 The resistance of copper wire.

While Figure III.5 demonstrates the measured resistance of a copper wire which agreed with the direct measured value of 0.0069 ohms.

Appendix IV: Purification of Single Wall Carbon Nano-tubes

Purification procedure

Iron entrapped in carbon shells is the predominant impurities of HiPco Single walled carbon nanotube Purification was done in steps to get rid of the Iron catalysts.

Rinsing and Vacuum filtration:

A suitable amount of nanotubes in (gm) were placed on a Teflon filter paper in a Filtration apparatus and was Methanol and de-ionized water (D.I. water) for couple of times and then filtered with vacuum filtration. Methanol was used to activate the Teflon filter papers. The nanotubes were weighed after removing from the filter paper.

Oxidation:

In order to oxidize the iron catalysts the nanotube were placed in a mallet boat inside a tube furnace and heated at 200^{o}C for 15 hours. Continuous oxygen flow was applied over the nanotubes.

Weight gain was observed after the oxidation indicating formation of oxides and hydroxides of the metal impurities.

Notes:

You need to record the following items:

Before oxidation:

1- Weight of empty mallet boat in (gm)

2- Weight of empty mallet boat + moist annotates in (gm)

3- Weight of moist annotates in (gm)

After oxidation:-

1- Weight of empty mallet boat + oxidized annotates in (gm)

2- Weight of empty mallet boat in (gm)

3- Weight of oxidized (dry) annotates in (gm)

4- Rinsing and soliciting with Hydrochloric acid (HCl)

A suitable amount of HCl was added with the oxidized nanotubes and the acid solution instantly turned into yellow color. The yellow coloration indicates Iron chloride formation.

$$FeO + 2HCl \rightarrow FeCl_2 + H_2O$$

The sample was then sonicated for 20 minutes for complete removal of iron from the carbon shells into the solution.

CNT were washed with methanol and D.I. water for couple of times and filtered with vacuum filtration.

Nanotubes were then placed in an Erlenmeyer flask of 250 ml capacity.

Notes:

Before washing with HCl record the following:

Weight of moist nanotubes in (mg)

Weight of empty flask in (gm)

Weight of flask + moist nanotubes in (gm)

Weight of moist nanotubes in (mg)

Realize that weight of moist nanotubes after washing and sonication with HCl will be reduced (Indicates the removal of iron catalyst from the nanotubes).

Appendix V: Raman Spectroscopy Analysis

1- Raman Procedures

1- Turn main power on, both key and button

2- Turn microscope power and its table switch on

3- Turn on computer

4- Open “Grams”

5- Go to collect then experimental set up

6- Make the calibration:

1- Select “static”

2- Time 1 sec

3- Accumulation 1

4- Objective 50

5- Focus 0

6- Power 100%

7- Go to microscope:

8- Focus by 5x then 20x then 50x

9- Use arm with notation “ F” to get hexagon shape and then more focusing then return it back after you finish this step

10- Turn Laser on check it is focusing as one point

11- Turn microscope light off

12- Turn room light off

13- Go to “Grams” menu and click ok

14- Then go to collect “double click on it”

15- Put your sample on glass slid under the microscope and do sub-steps 7 to 12 in step 6.

16- Go to “Grams” and change from static to extended or keep it if you want to focus on a definite Raman shift and put power as low as you know it is suitable for your sample so it can stand for it with out burn it up, then change time or any to your sample information, put name on your sample and take note for the numbers that you used.

17- As sub-step 14 in step 6

18- Save the file as *.sep

19- Do not forget to turn Laser off after each step and as long as Laser off you can turn the room light on

20- Check your peaks (e.g. CNT gives two peaks @ 200 and @ 1600, etc.).

Atypical peaks of SWNT (in the range from 130-275 cm^{-1} and from 1500-1600cm^{-1}) can be found in SWNT/PAN fibers, confirming the successful mixing of SWNT and PAN fibers. The following figures (Figure V 1-3) showing the spectra of PAN, PEDT, SWNTs fibers.

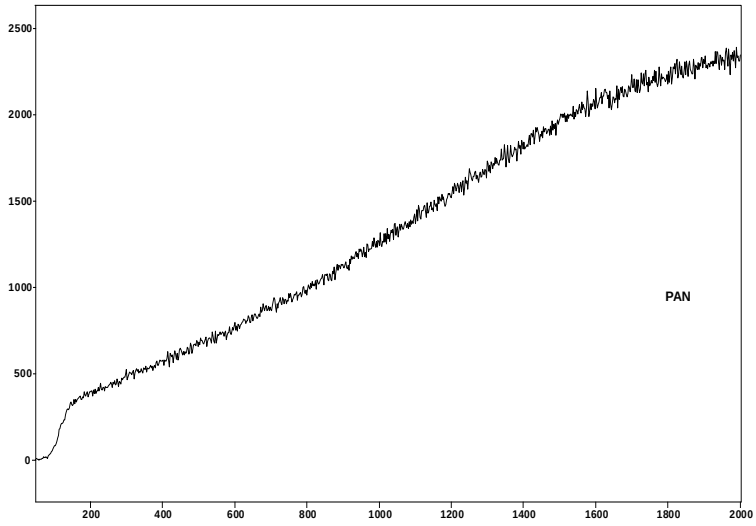

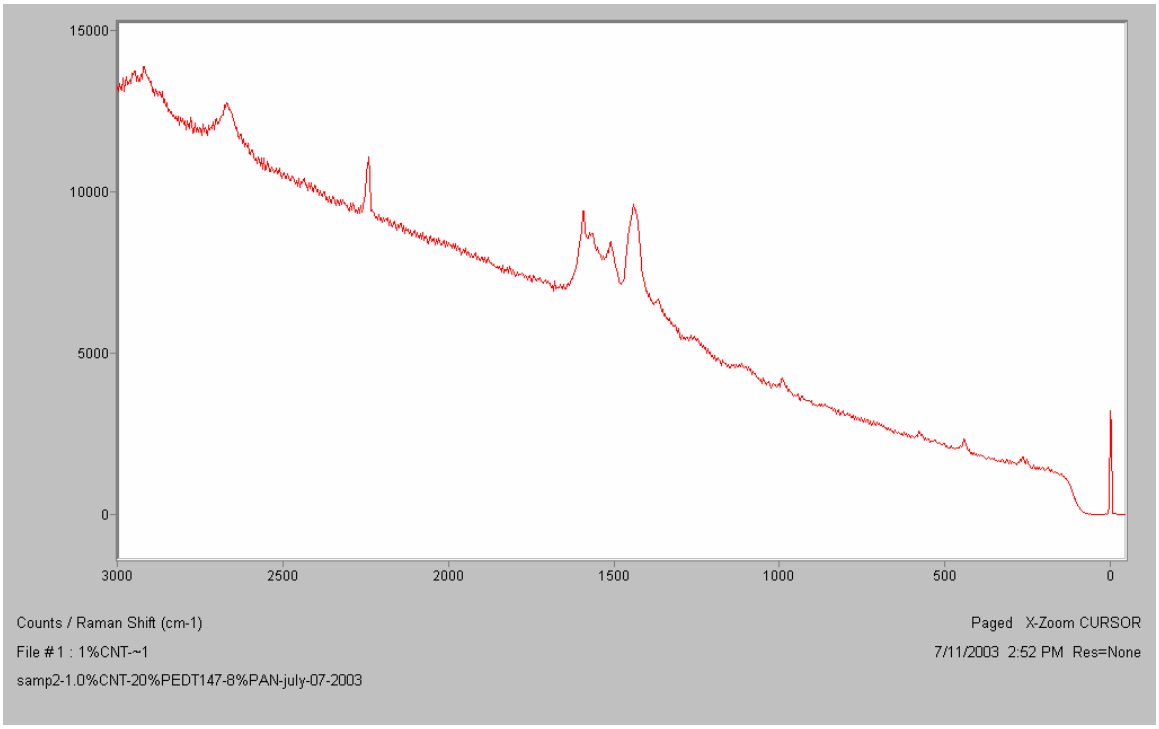

Figure V.1 The Raman spectra of PAN and CNT/PEDOT fibers.

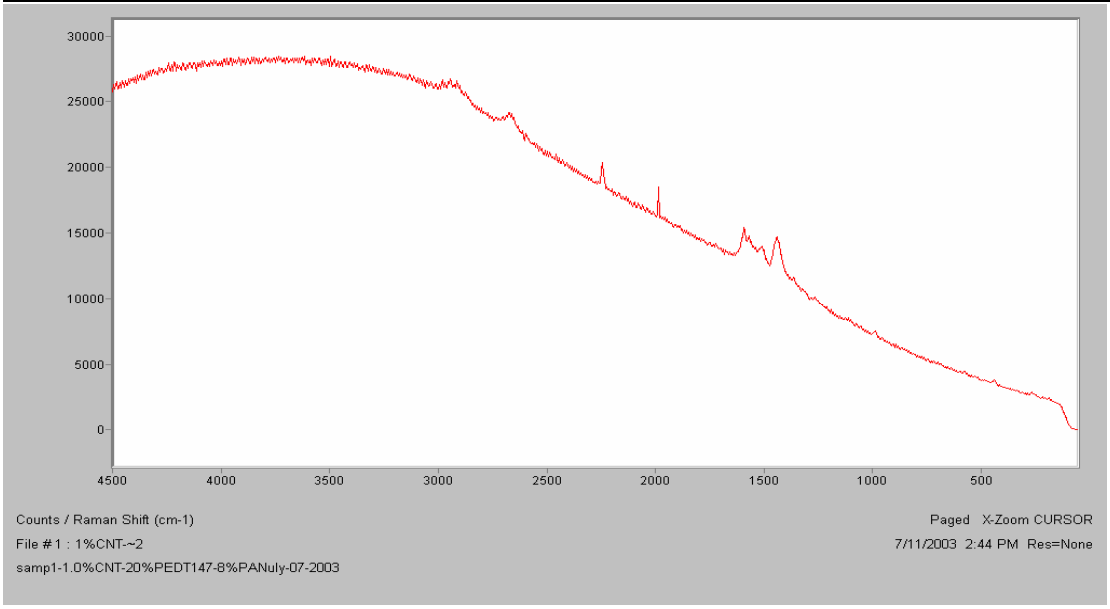

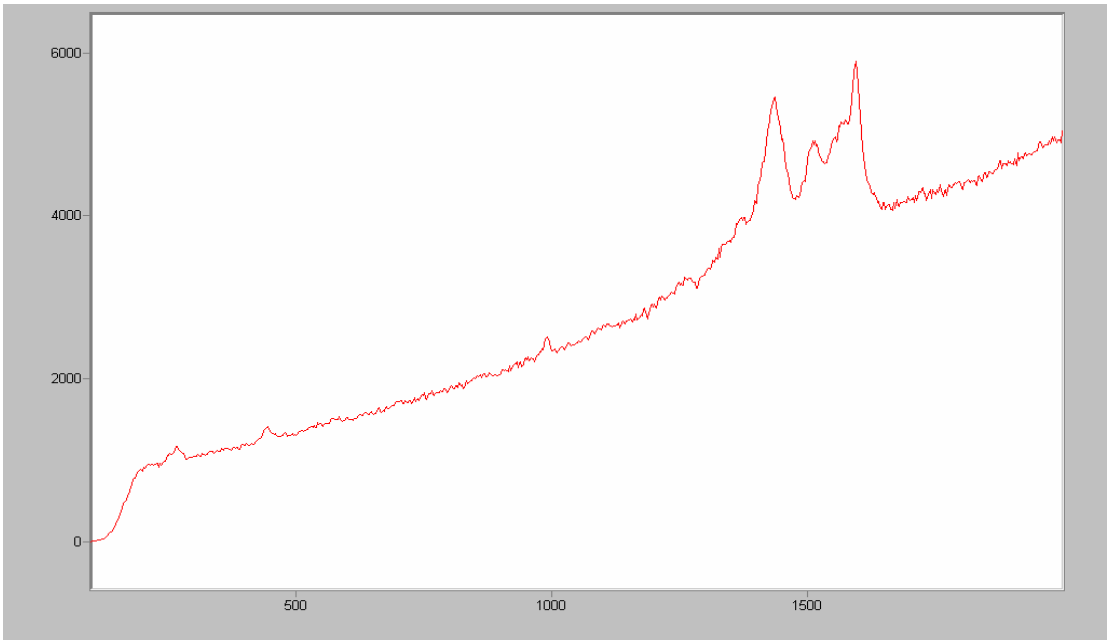

Figure V. 2 The spectra of CNTs/PEDOT fibers.

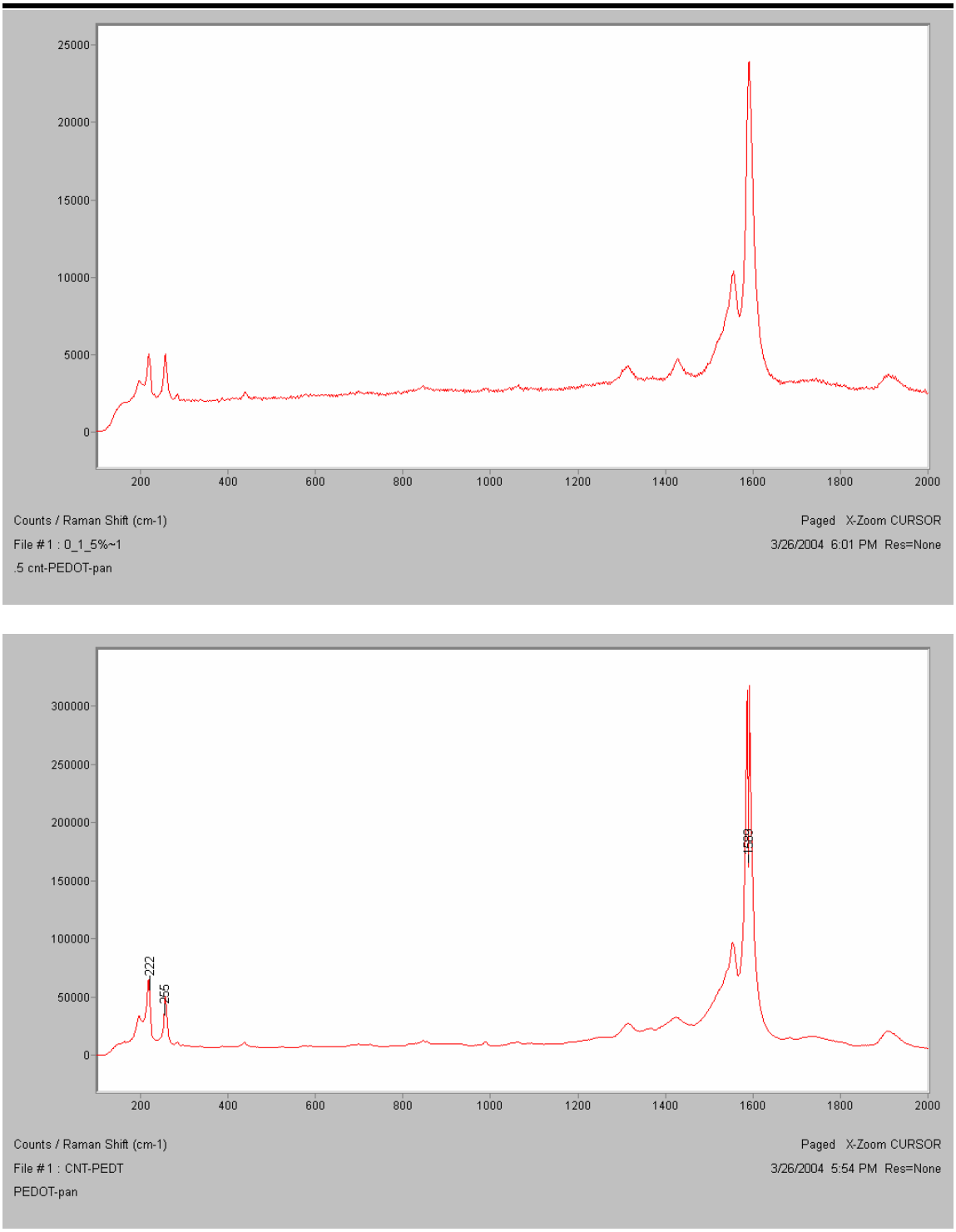

Figure V. 3 The subtracted spectra of SWNTs.

Appendix VI: TEM Procedures

Sample Preparation

The preparation of the TEM samples followed the following procedures:

1- Bring a clean ceramic dish and hammer.

2- Pour a small amount of alcohol in the dish.

3- Use a clean tweezers to catch a small piece of the sample and put it gently in the ceramic dish.

4- Use the ceramic hammer to break up the small sample into smaller pieces inside the alcohol.

5- Bring the TEM carbon grid Figure VI. 1 by using another clean tweezers and fishing the small pieces out of the dish then put it in the TEM carbon grid holder to dry.

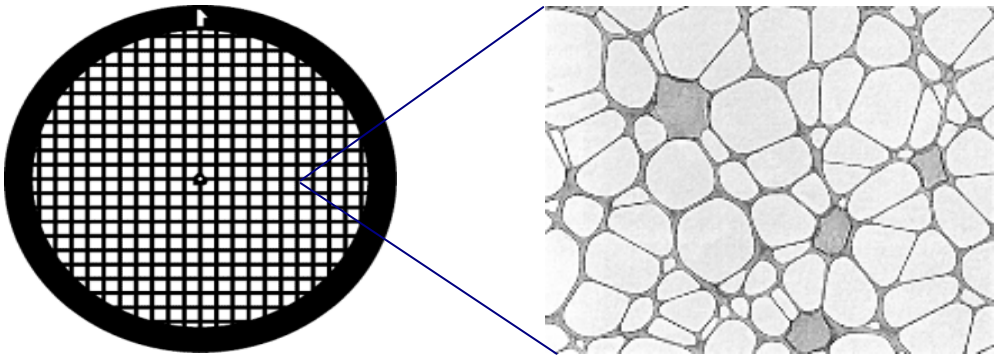

Figure VI. 1 Copper Grid and Carbon Film Coating.

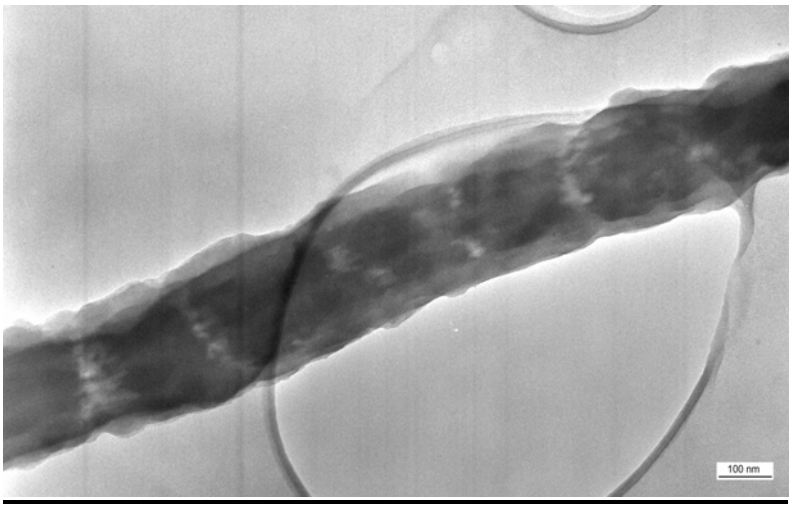

Figure VI. 2 TEM showing the whole image of a nanofiber with Diam.≅ 200nm demonstrates the PAN wrapping the PEDT-SWNT.

Figure VI. 3- 5 showing the different TEM images of carbon nanotubes within the PEDOT/PAN nanofibers.

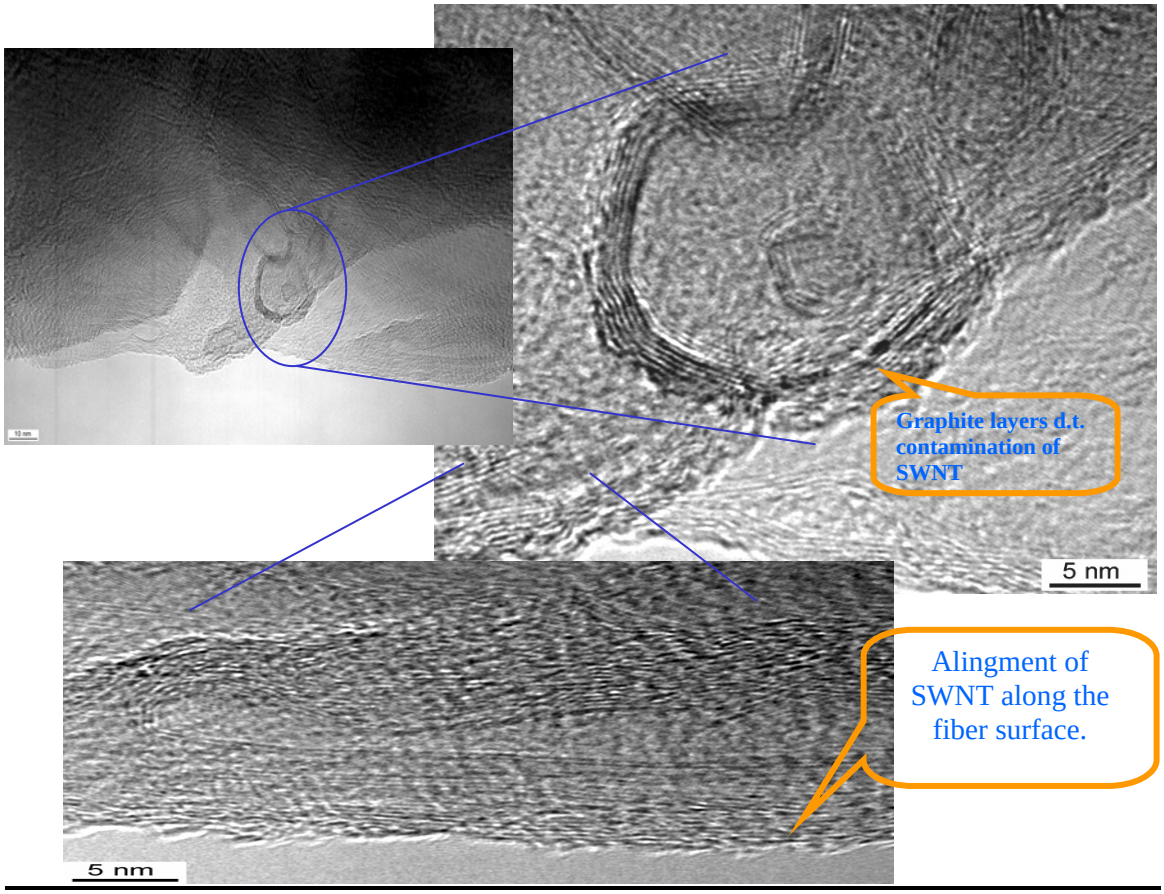

Figure VI. 3 Alignment of SWNTs along the fibers.

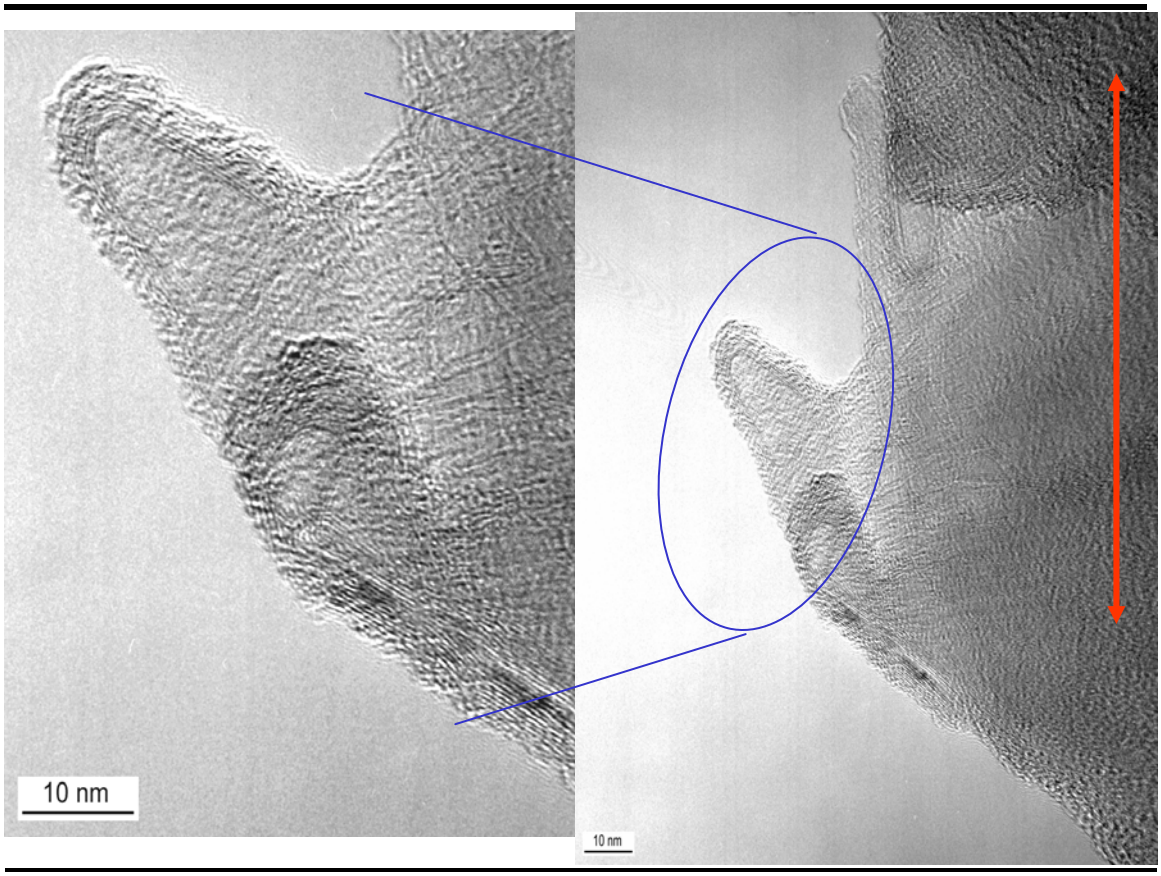

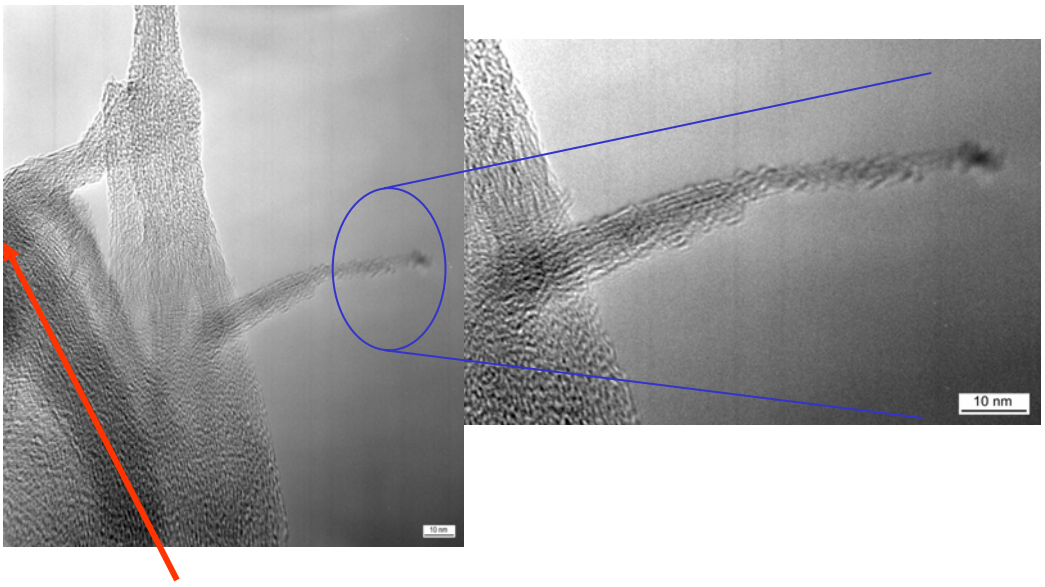

Figure VI. 4 TEM images of CNTs/PEDOT fibers.

Figure

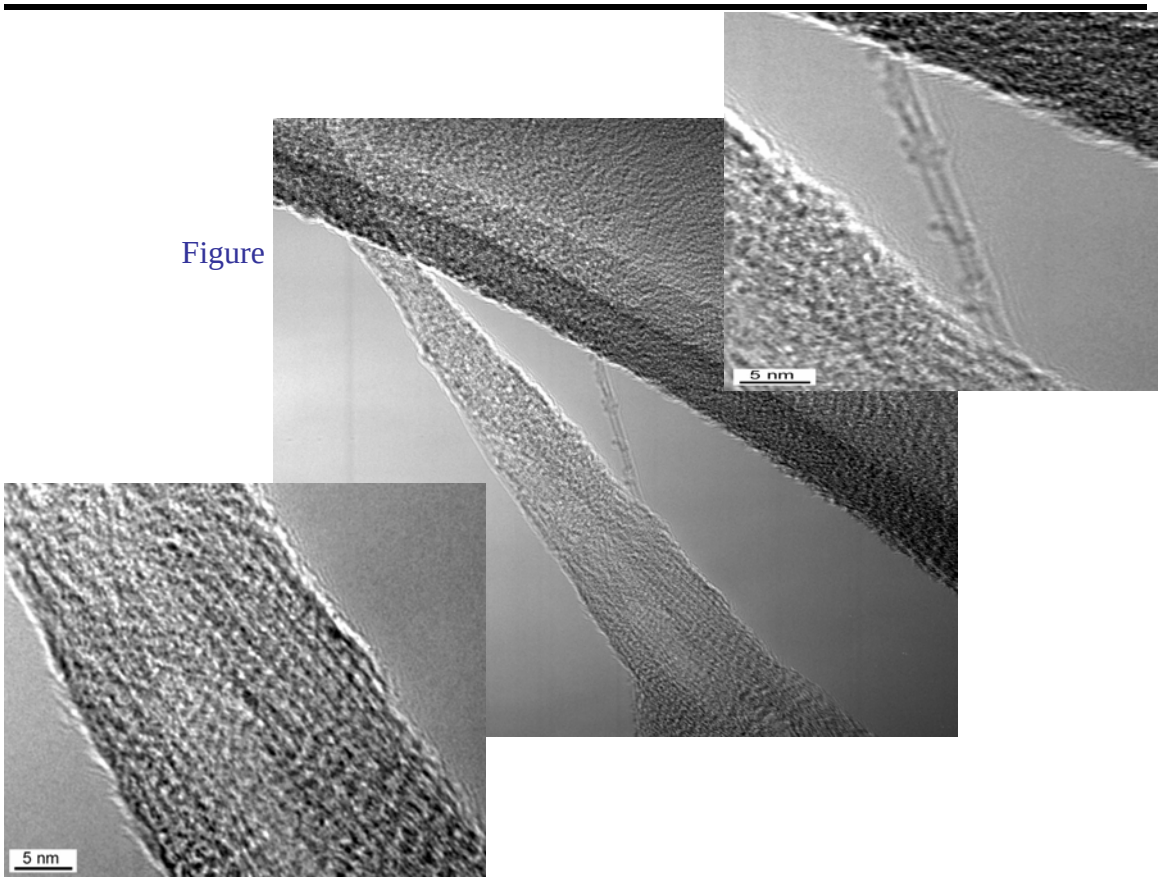

APPENDIX VII: Response Surface Analysis Results

A JMP 5.1 statistics software for data analysis used for these 27 experiments

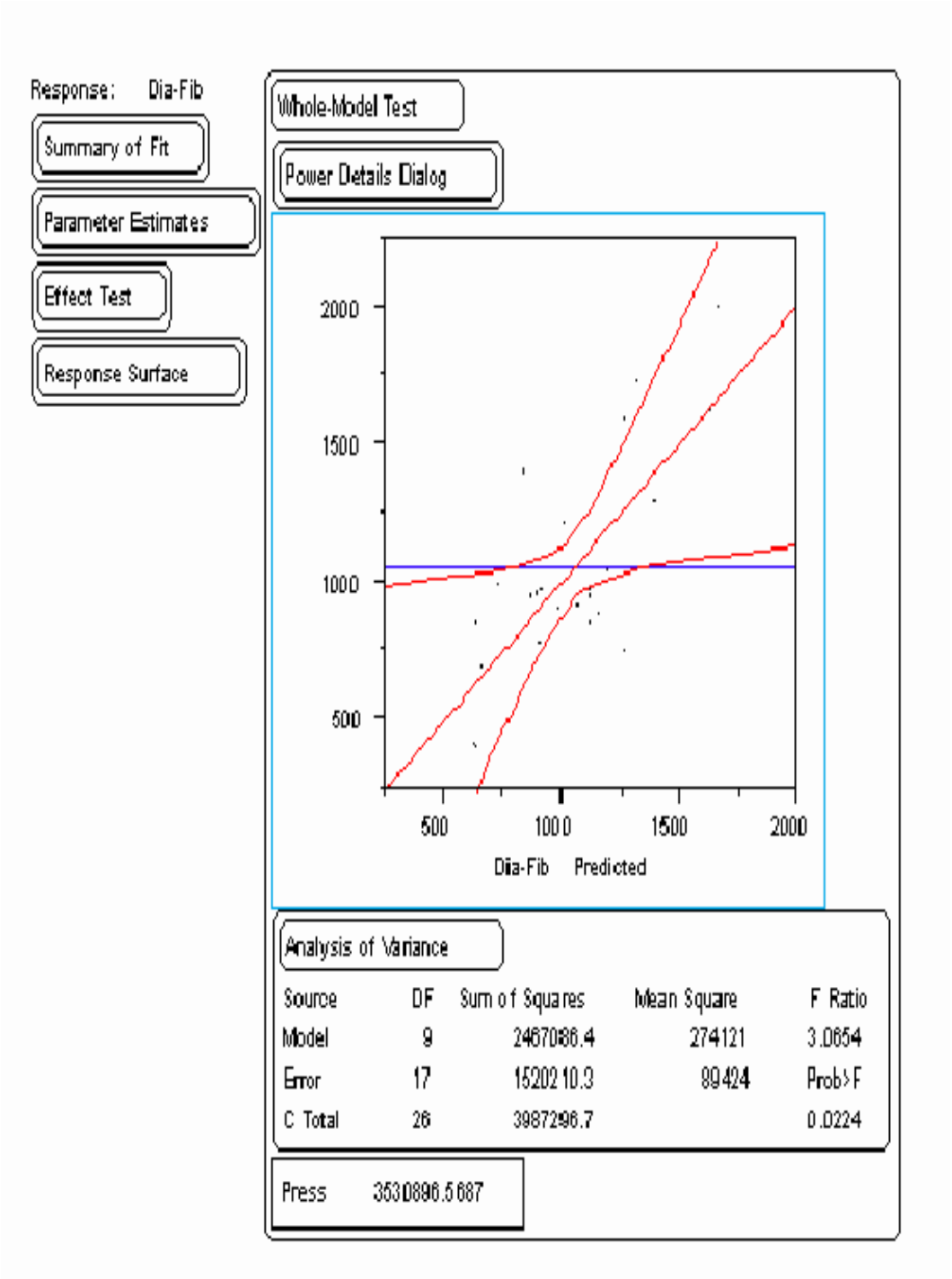

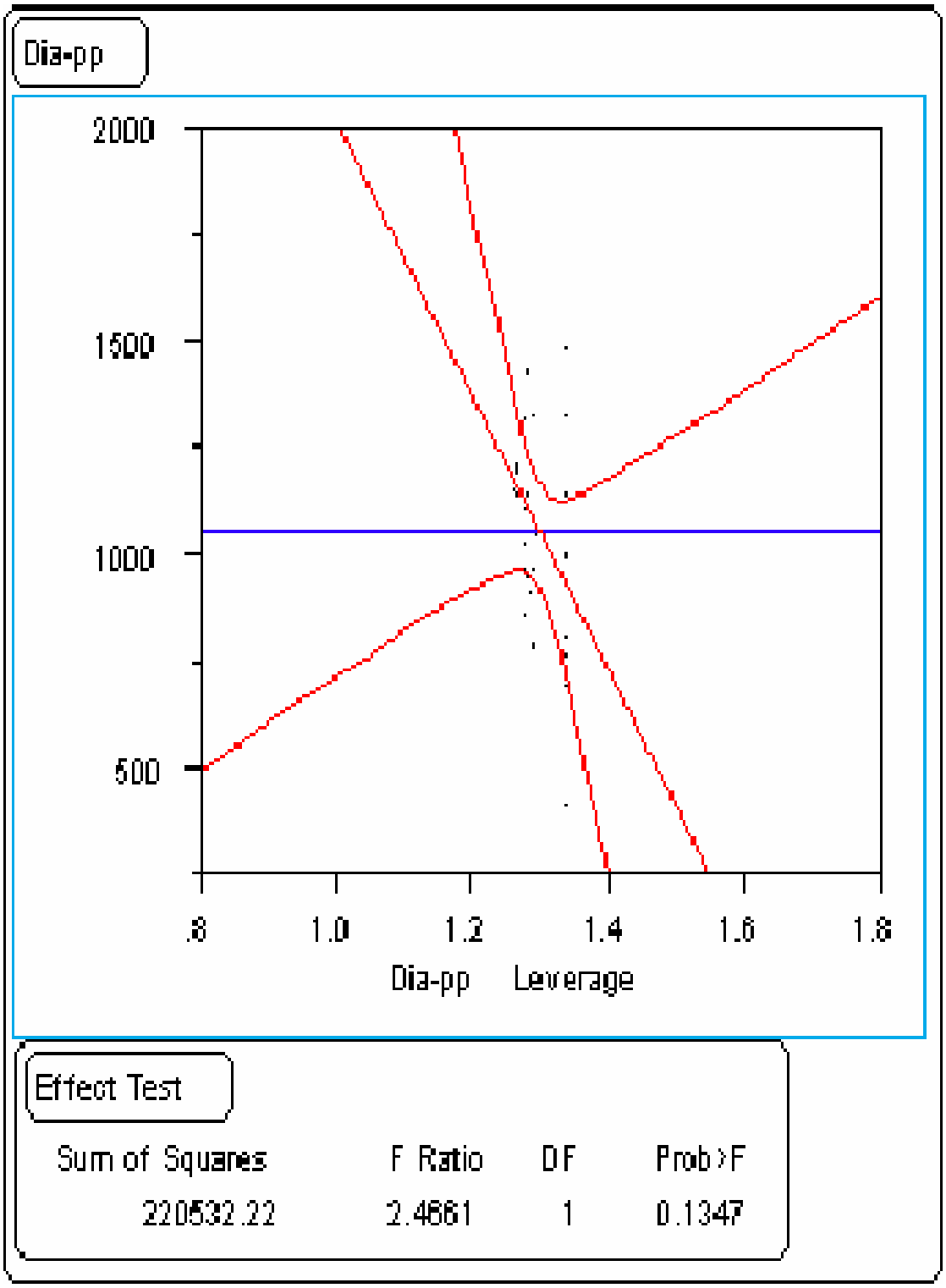

Effect Test

Sum of Squares	F Ratio	DF	Prob>F
220532.22	2.4661	1	0.1347

height

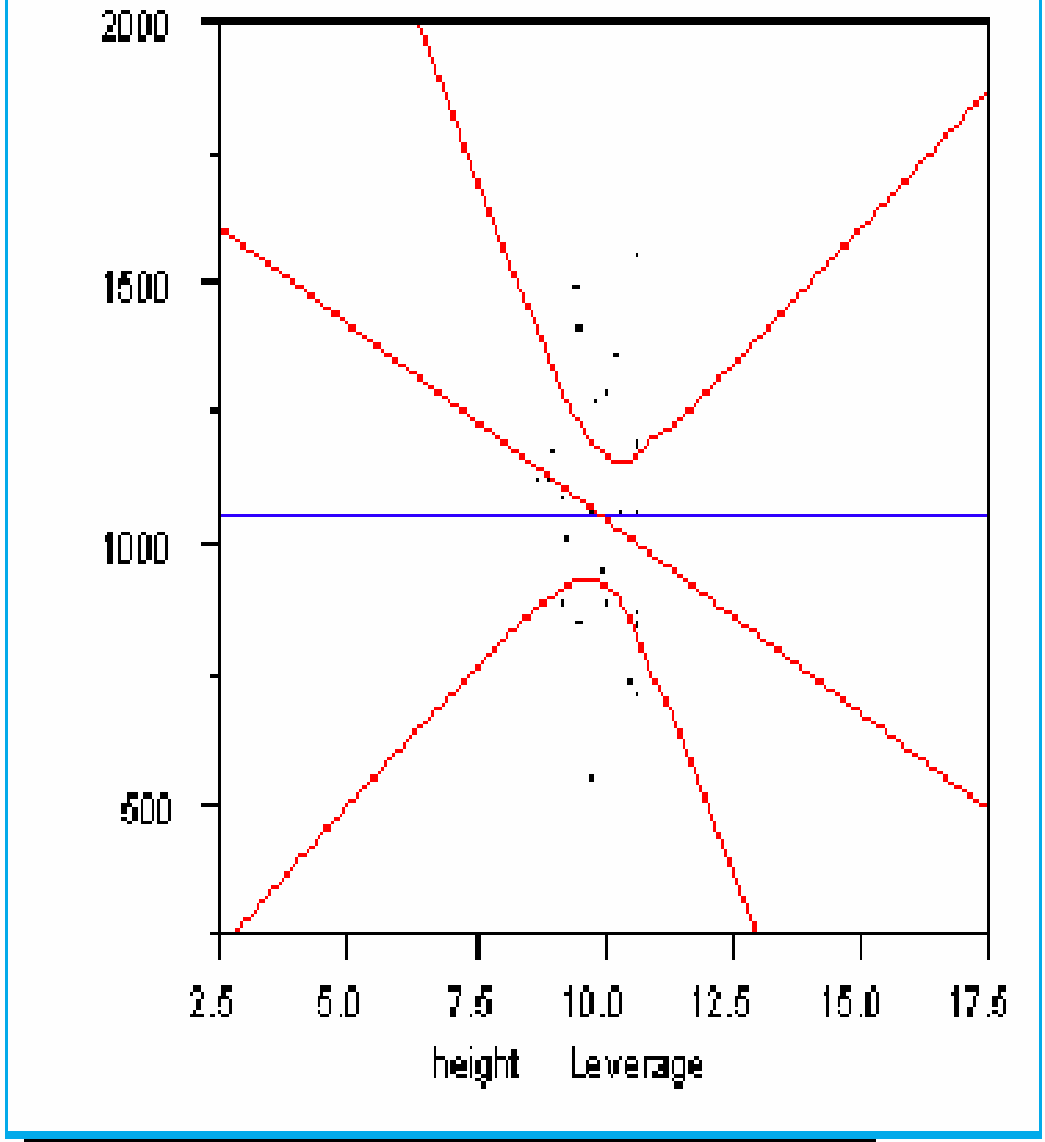

Effect Test

Sum of Squares	F Ratio	DF	Prob>F
65208.781	0.7292	1	0.4050

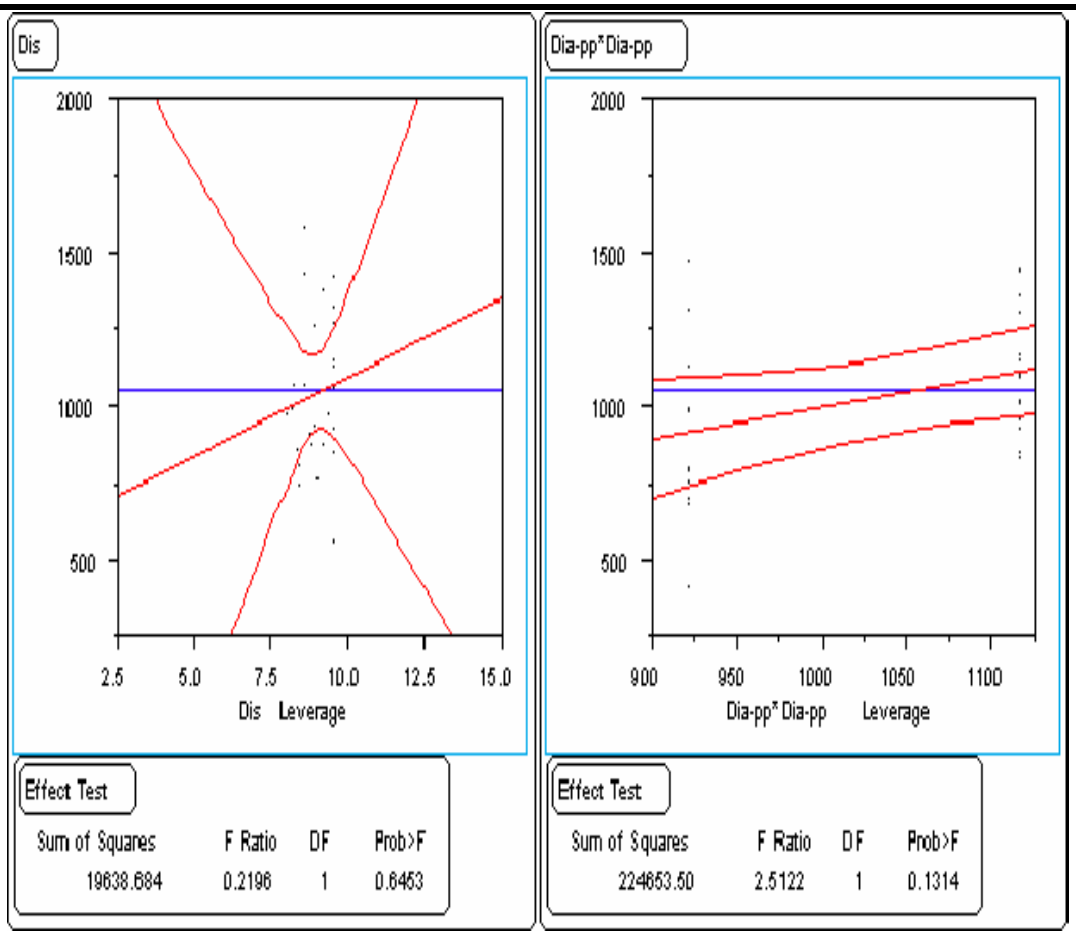
Dis
2000
1500
1000
500
2.5
5.0
7.5
10.0
12.5
15.0
Dis Leverage
Effect Test
Sum of Squares F Ratio DF Prob>F
19638.684 0.2196 1 0.6463
Dia-pp*Dia-pp
2000
1500
1000
500
900
950
1000
1050
1100
Dia-pp*Dia-pp Leverage
Effect Test
Sum of Squares F Ratio DF Prob>F
224653.50 2.5122 1 0.1314

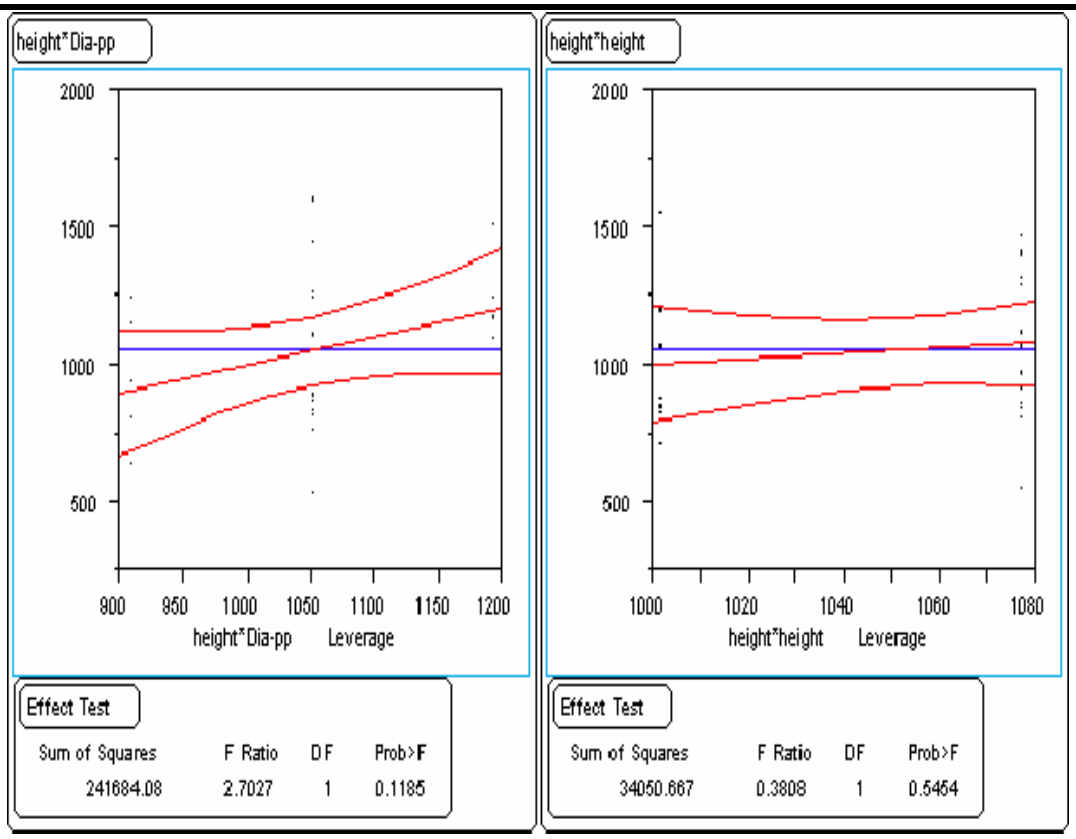
height*Dia-pp
2000
1500
1000
500
800
850
1000
1050
1100
1150
1200
height*Dia-pp Leverage
Effect Test
Sum of Squares F Ratio DF Prob>F
241684.08 2.7027 1 0.1185
height*height
2000
1500
1000
500
1000
1020
1040
1060
1080
height*height Leverage
Effect Test
Sum of Squares F Ratio DF Prob>F
34050.667 0.3808 1 0.5464

Dis*Dia-pp

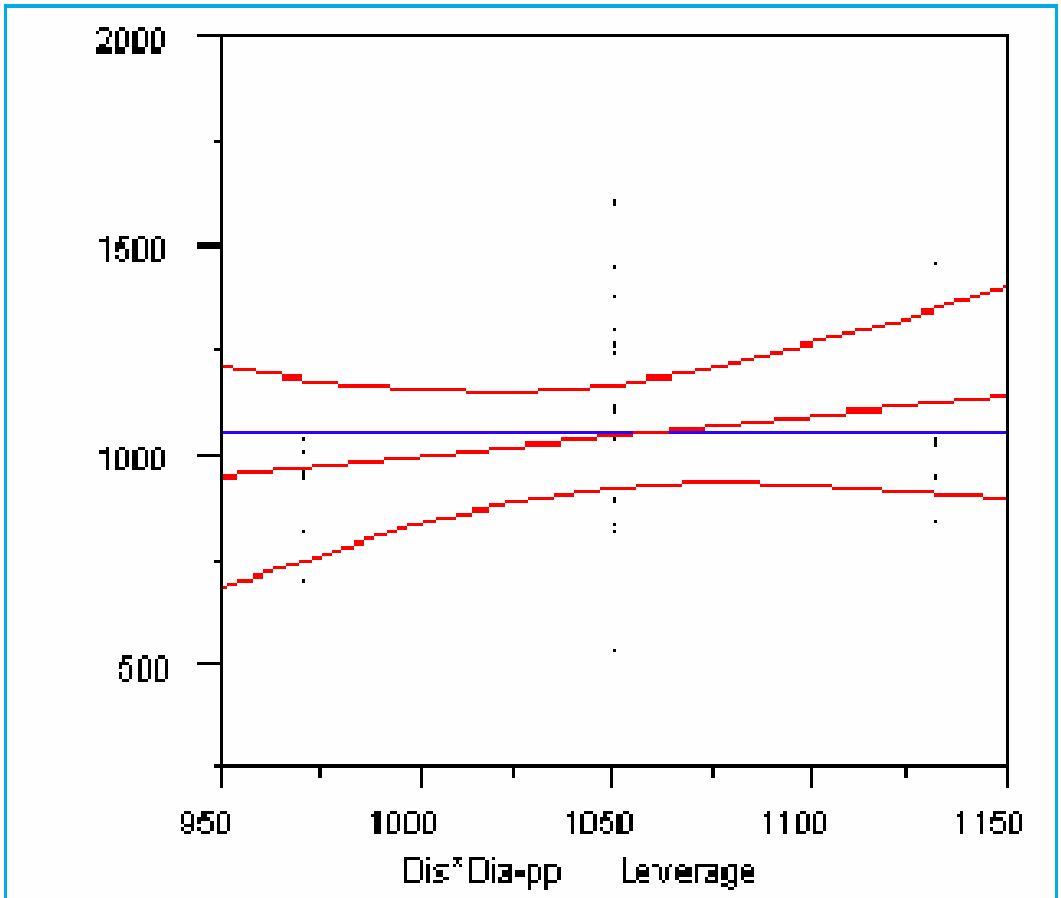

Effect Test

Sum of Squares	F Ratio	DF	Prob>F
77441.333	0.8660	1	0.3651

Dis*height

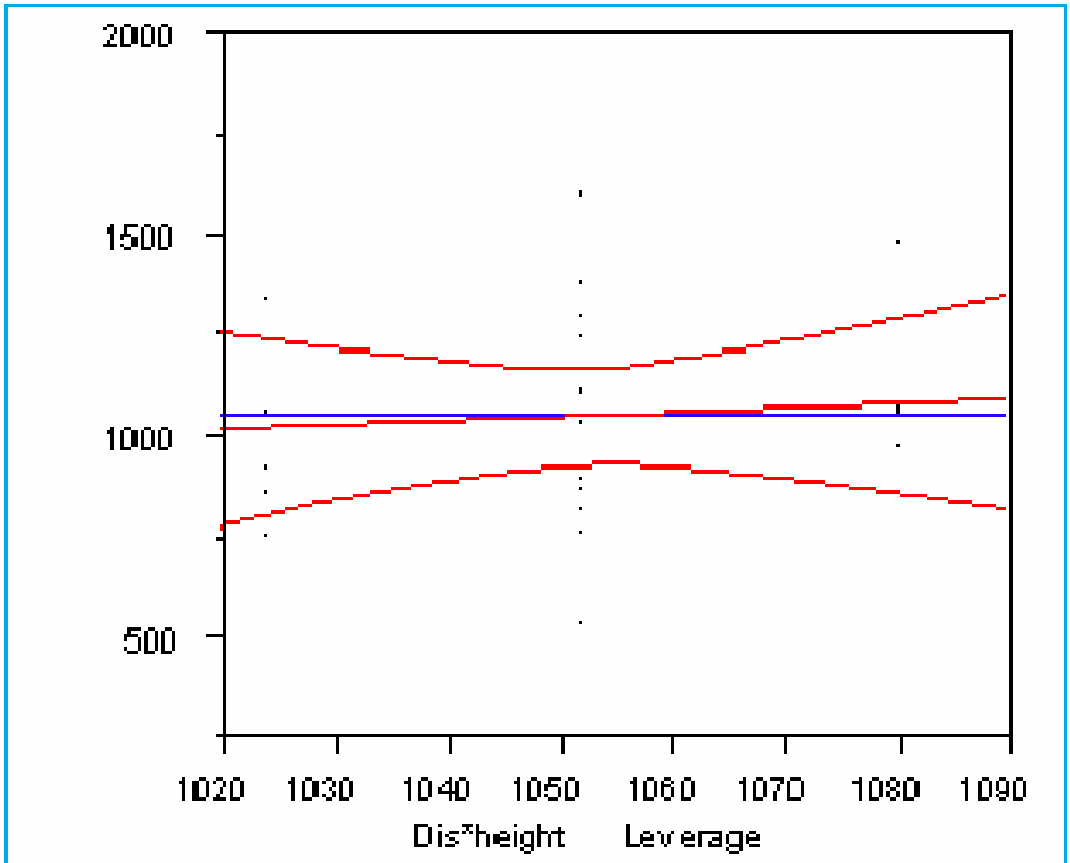

Effect Test

Sum of Squares	F Ratio	DF	Prob>F
9578.7500	0.1071	1	0.7475

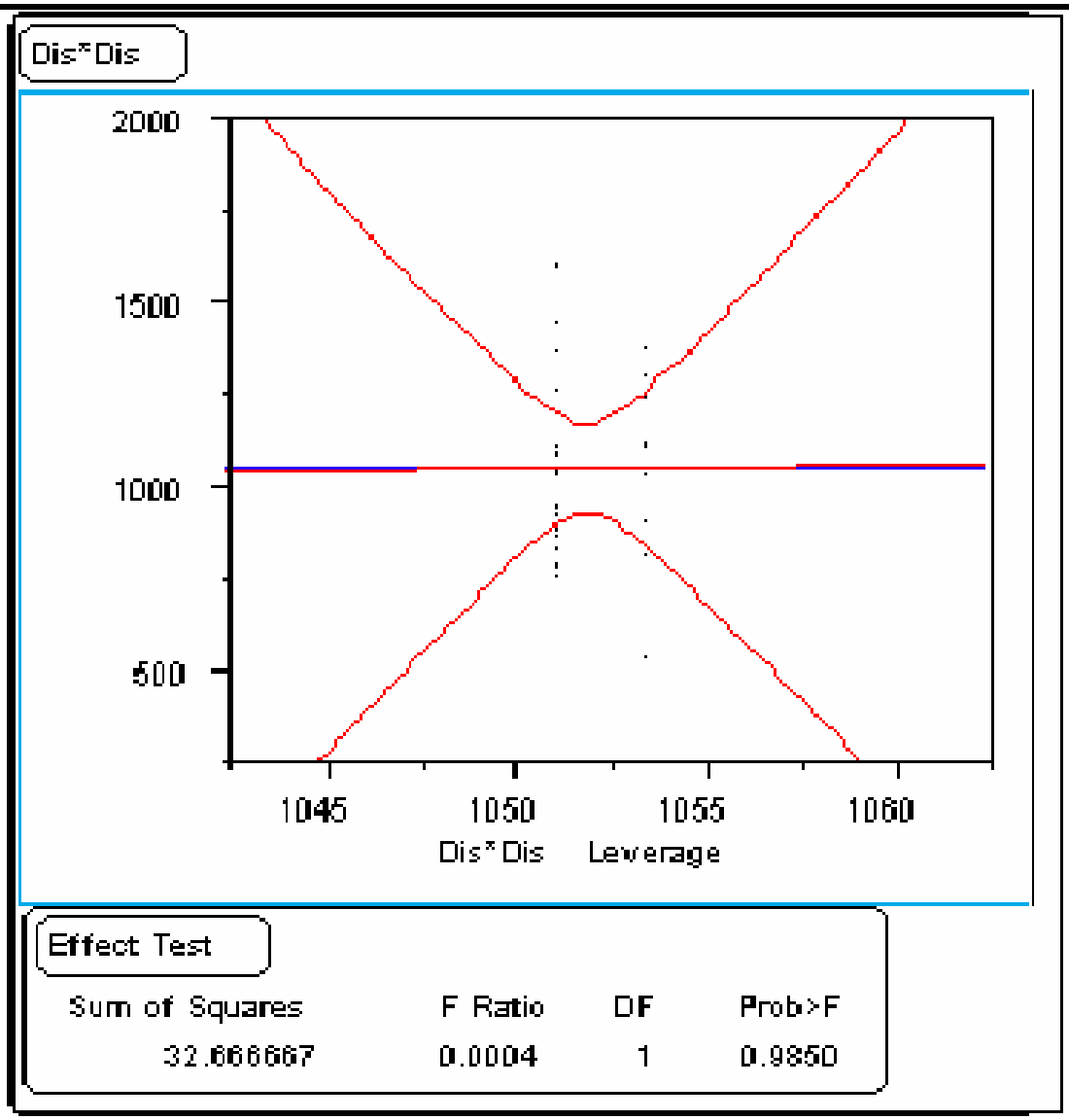

Effect Test

Sum of Squares	F Ratio	DF	Prob>F
32.666667	0.0004	1	0.9850

Response: Dia-Fib

Summary of Fit

RSquare	0.618737
RSquare Adj	0.416891
Root Mean Square Error	299.0387
Mean of Response	1051.889
Observations (or Sum Wgts)	27

Parameter Estimates

Term	Estimate	Std Error	t Ratio	Prob>|t|
Intercept	2736.4111	1500.352	1.82	0.0858
Dia-pp	-3236.278	2060.806	-1.57	0.1347
height	-74.4206	87.15004	-0.85	0.4050
Dis	51.124444	109.0937	0.47	0.6453
Dia-pp*Dia-pp	1209.375	763.0127	1.58	0.1314
height*Dia-pp	59.131944	35.96876	1.64	0.1185
height*height	2.0925926	3.391168	0.62	0.5454
Dis*Dia-pp	-40.16667	43.16252	-0.93	0.3651
Dis*height	0.9416667	2.877501	0.33	0.7475
Dis*Dis	-0.093333	4.883281	-0.02	0.9850

Effect Test

Source	Nparm	DF	Sum of Squares	F Ratio	Prob>F
Dia-pp	1	1	220532.22	2.4661	0.1347
height	1	1	65208.76	0.7292	0.4050
Dis	1	1	19638.68	0.2196	0.6453
Dia-pp*Dia-pp	1	1	224653.50	2.5122	0.1314
height*Dia-pp	1	1	241684.08	2.7027	0.1185
height*height	1	1	34050.67	0.3808	0.5454
Dis*Dia-pp	1	1	77441.33	0.8660	0.3651
Dis*height	1	1	9576.75	0.1071	0.7475
Dis*Dis	1	1	32.67	0.0004	0.9850

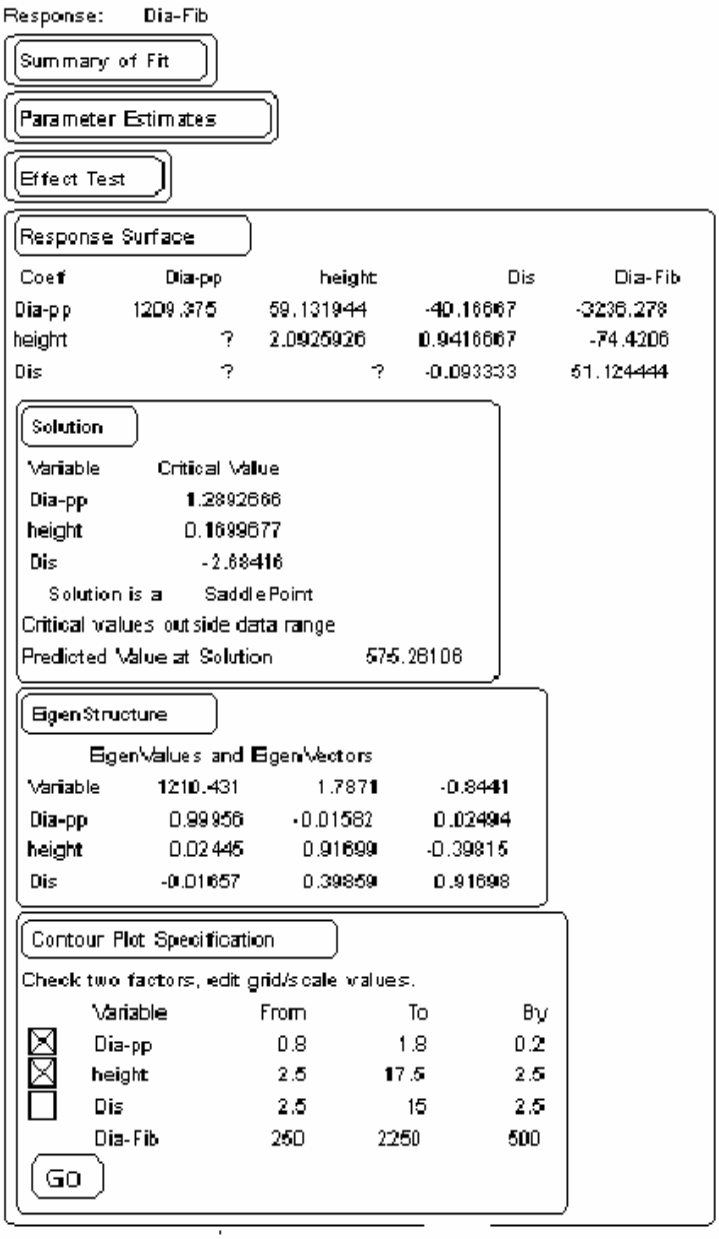

Response: Dia-Fib

Summary of Fit

Parameter Estimates

Effect Test

Response Surface

Coef	Dia-pp	height	Dis	Dia-Fib
Dia-pp	1209.375	59.131944	-40.16667	-3236.278
height	?	2.0925926	0.9416667	-74.4206
Dis	?	?	-0.093333	51.124444

Solution

Variable	Critical Value
Dia-pp	1.2892666
height	0.1699677
Dis	-2.68416

Solution is a Saddle Point

Critical values outside data range

Predicted Value at Solution 575.26108

EigenStructure

EigenValues and EigenVectors

Variable	1210.431	1.7871	-0.8441
Dia-pp	0.99956	-0.01582	0.02494
height	0.02445	0.91699	-0.39815
Dis	-0.01657	0.39859	0.91698

Contour Plot Specification

Check two factors, edit grid/scale values.

	Variable	From	To	By
☒	Dia-pp	0.8	1.8	0.2
☒	height	2.5	17.5	2.5
☐	Dis	2.5	15	2.5
	Dia-Fib	250	2250	500

GO

Contour Plot Specification

Check two factors, edit grid/scale values.

	Variable	From	To	By
☒	Dia-pp	0.8	1.8	0.2
☒	height	2.5	17.5	2.5
☐	Dis	2.5	15	2.5
	Dia-Fib	250	2250	75

GO

Contour Plots

Dis=2.5

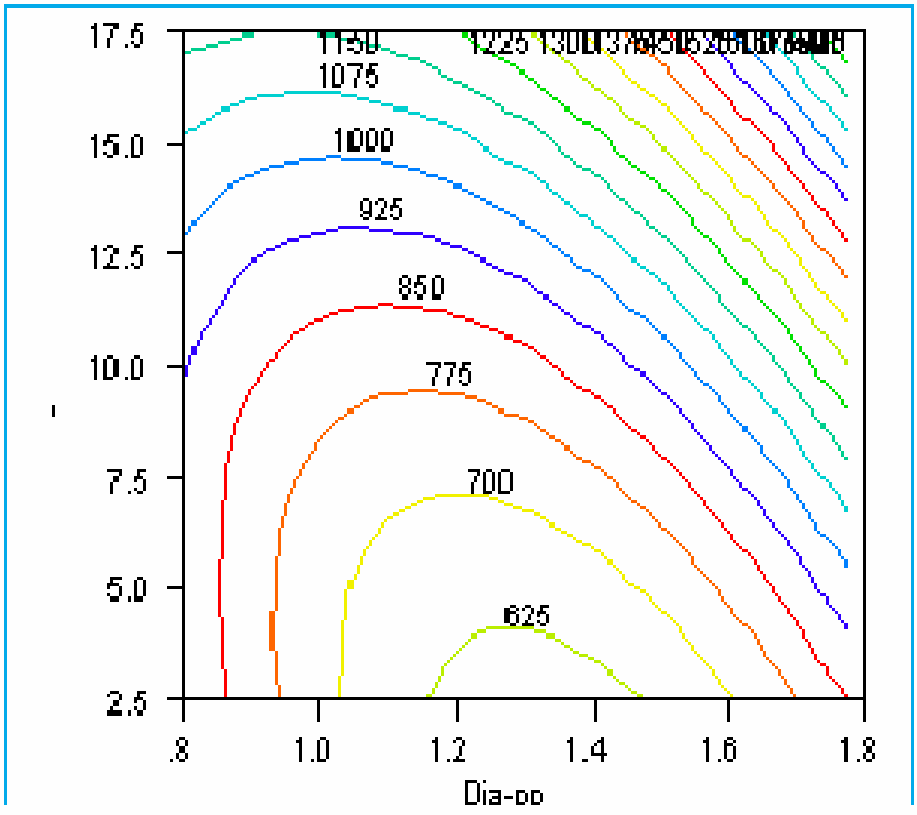

Contour Plot Specification

Check two factors, edit grid/scale values.

	Variable	From	To	By
☒	Dia-pp	0.8	1.8	0.2
☒	height	2.5	17.5	2.5
☐	Dis	2.5	15	2.5
	Dia-Fib	250	2250	75

GO

Contour Plots

Dis=5

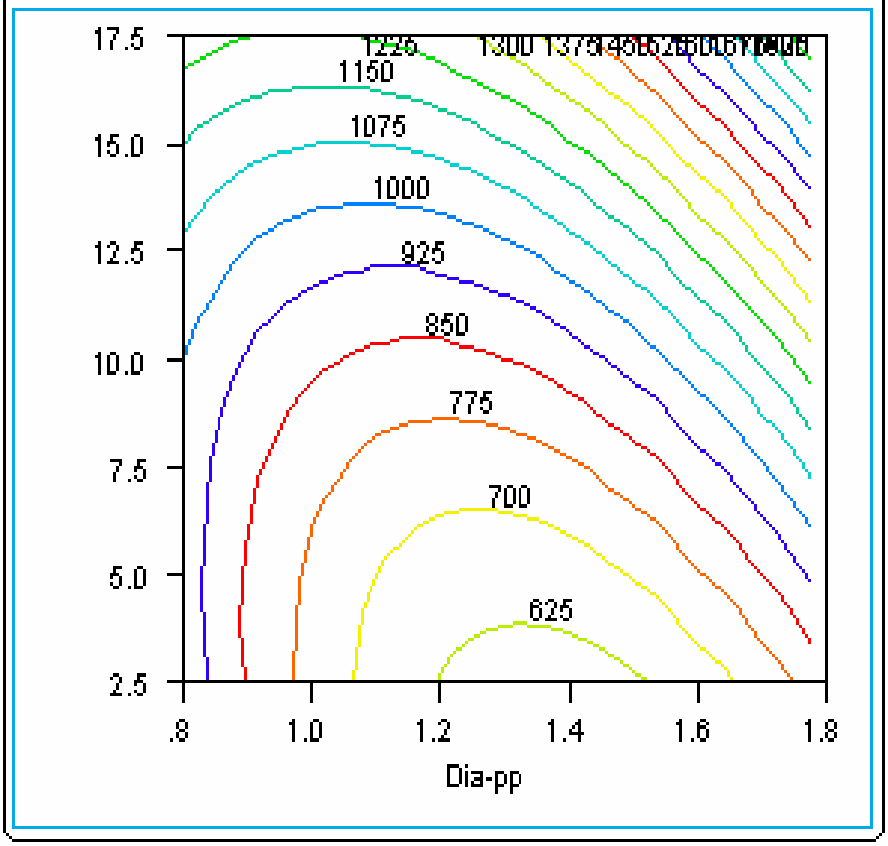

Contour Plot Specification

Check two factors, edit grid/scale values.

	Variable	From	To	By
☒	Dia-pp	0.8	1.8	0.2
☒	height	2.5	17.5	2.5
☐	Dis	2.5	15	2.5
	Dia-Fib	250	2250	75

GO

Contour Plots

Dis=7.5

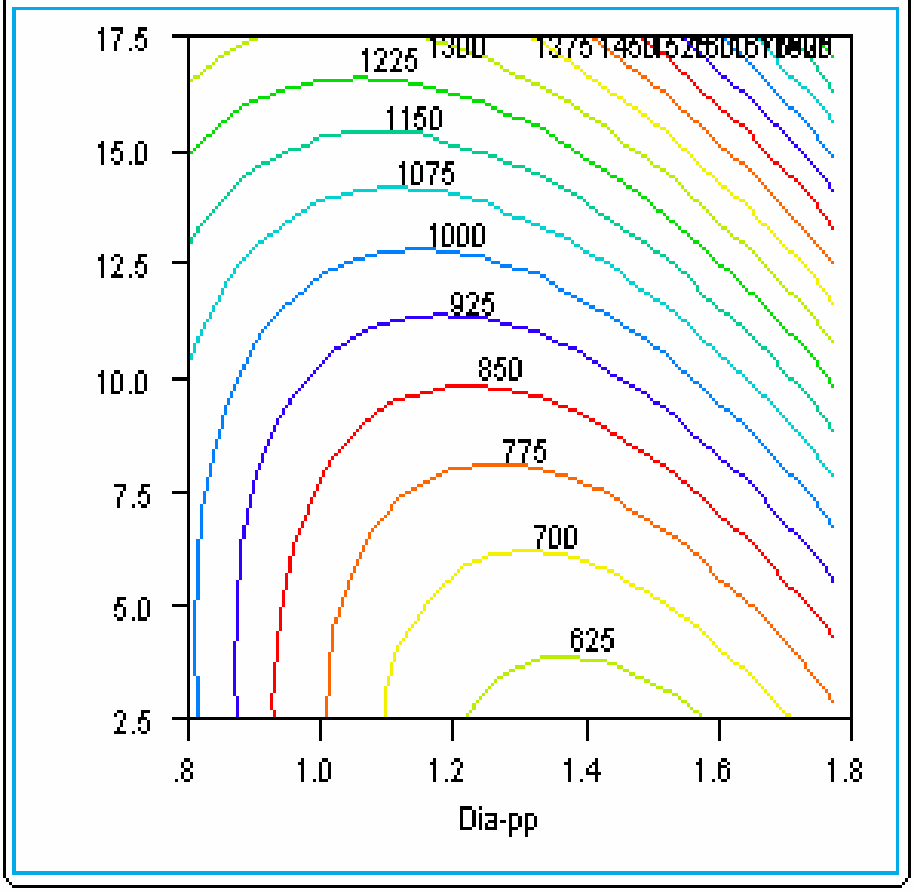

Solution

Eigen Structure

Contour Plot Specification

Check two factors, edit grid/scale values.

	Variable	From	To	By
☒	Dia-pp	0.8	1.8	0.2
☒	height	2.5	17.5	2.5
☐	Dis	2.5	15	2.5
	Dia-Fib	250	2250	75

GO

Contour Plots

Dis=10

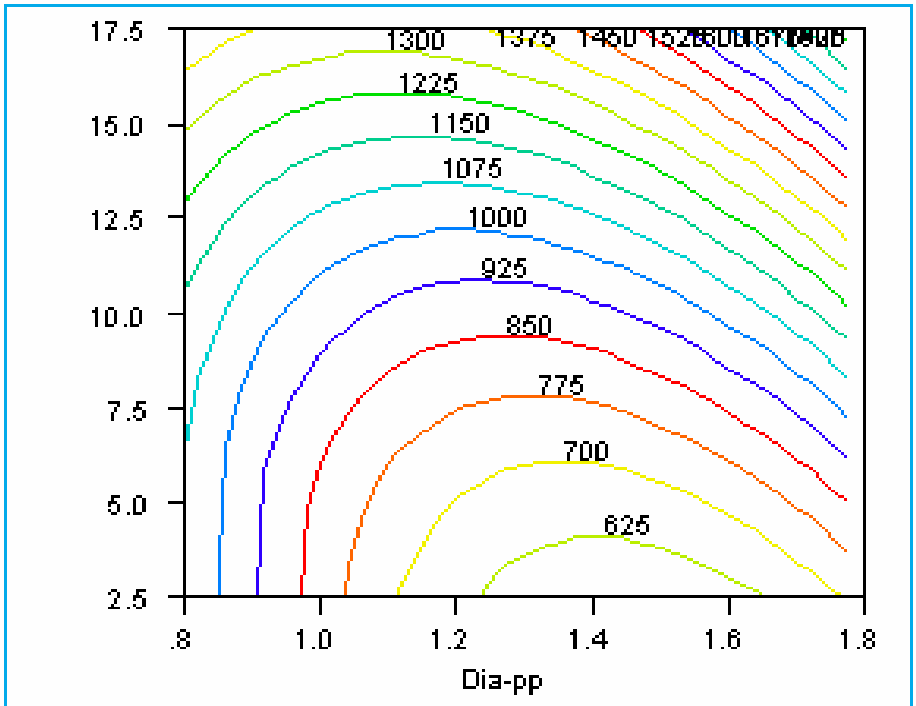

Contour Plot Specification

Check two factors, edit grid/scale values.

	Variable	From	To	By
☒	Dia-pp	0.8	1.8	0.2
☒	height	2.5	17.5	2.5
☐	Dis	2.5	15	2.5
	Dia-Fib	250	2250	75

GO

Contour Plots

Dis=12.5

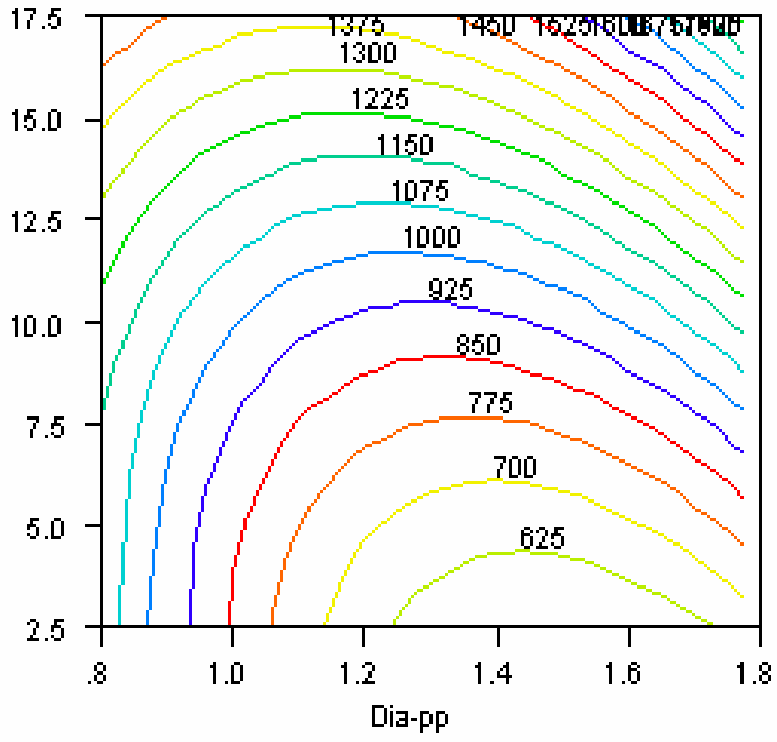

Eigen Structure

Contour Plot Specification

Check two factors, edit grid/scale values.

	Variable	From	To	By
☒	Dia-pp	0.8	1.8	0.2
☒	height	2.5	17.5	2.5
☐	Dis	2.5	15	2.5
	Dia-Fib	250	2250	75

GO

Contour Plots

Dis=15

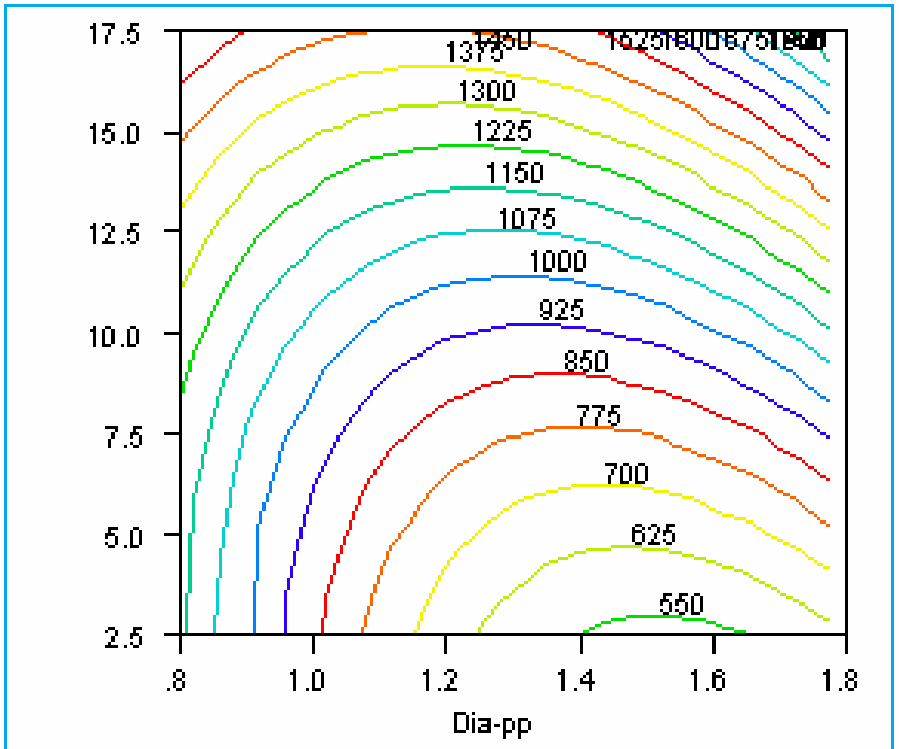

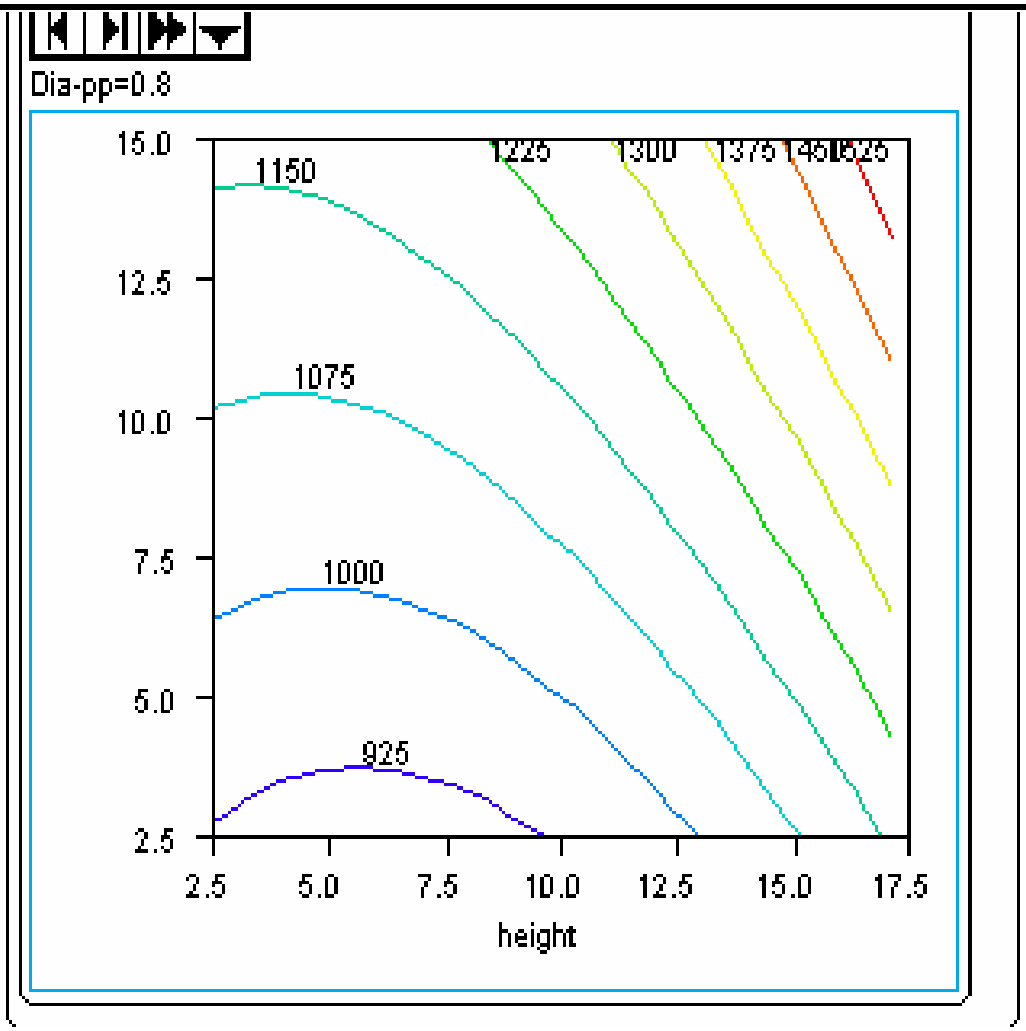
Dia-pp=0.8
15.0
12.5
10.0
7.5
5.0
2.5
1150
1225
1300
1375
1450
1525
1075
1000
925
2.5
5.0
7.5
10.0
12.5
15.0
17.5
height

Response: Dia-Fib

Summary of Fit

Parameter Estimates

Effect Test

Response Surface

Coef	Dia-pp	height	Dis	Dia-Fib
Dia-pp	1209.375	59.131944	-40.16667	-3236.278
height	?	2.0925926	0.9416667	-74.4206
Dis	?	?	-0.093333	51.124444

Solution

Eigen Structure

Contour Plot Specification

Check two factors, edit grid/scale values.

	Variable	From	To	By
☐	Dia-pp	0.8	1.8	0.2
☒	height	2.5	17.5	2.5
☒	Dis	2.5	15	2.5
	Dia-Fib	250	2250	75

GO

Contour Plots

Dis=2.5

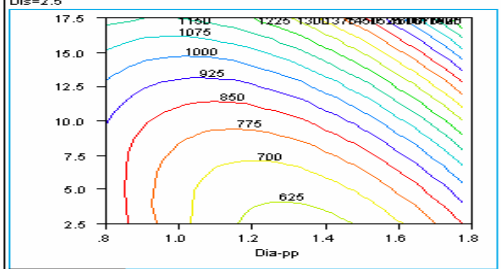

height=5

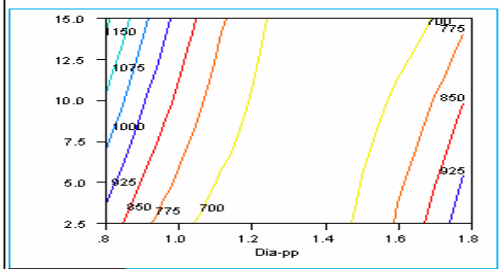

Dia-pp=1

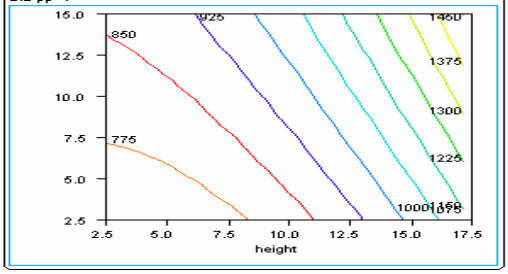

Whole-Model Test | Dia-pp | height | Dis | Dia-pp*Dia-pp | height*Dia-pp | height*height | Dis*Dia-pp | Dis*height | Dis*Dis

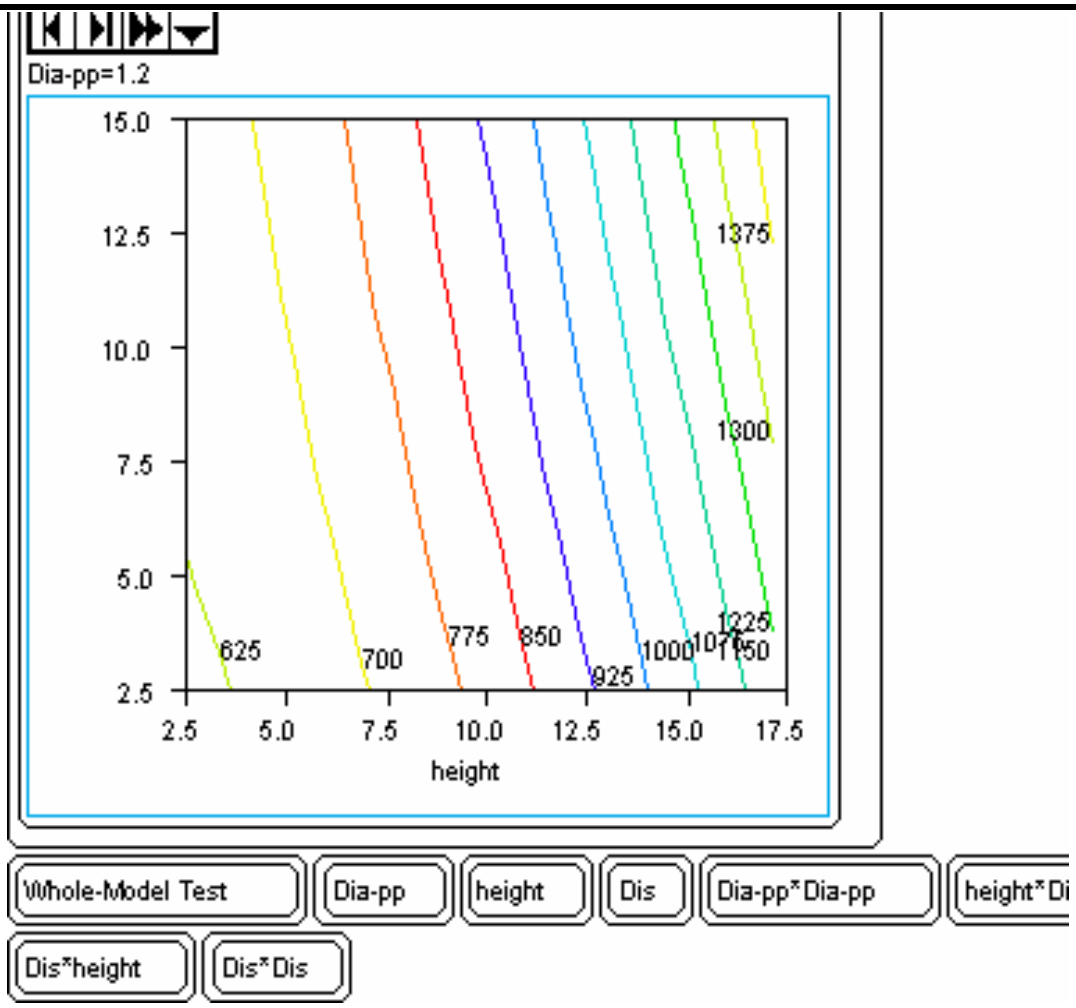
Dia-pp=1.2
15.0
12.5
10.0
7.5
5.0
2.5
625
700
775
850
925
1000
1075
1150
1225
1300
1375
2.5
5.0
7.5
10.0
12.5
15.0
17.5
height
Whole-Model Test
Dia-pp
height
Dis
Dia-pp*Dia-pp
height*Di
Dis*height
Dis*Dis

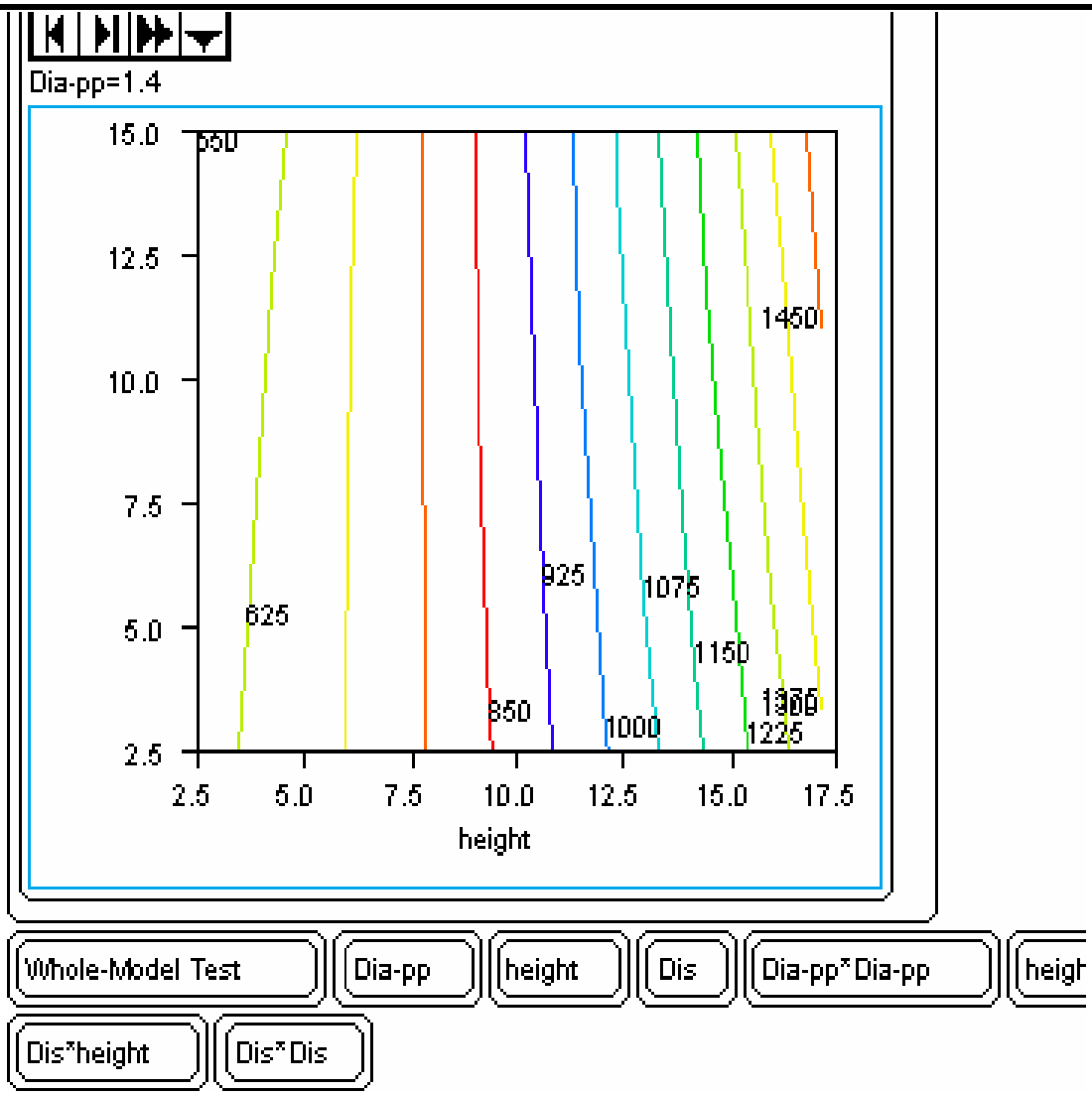
Dia-pp=1.4
15.0
12.5
10.0
7.5
5.0
2.5
550
625
850
925
1000
1075
1150
1225
1300
1450
2.5
5.0
7.5
10.0
12.5
15.0
17.5
height
Whole-Model Test
Dia-pp
height
Dis
Dia-pp*Dia-pp
Dis*height
Dis*Dis

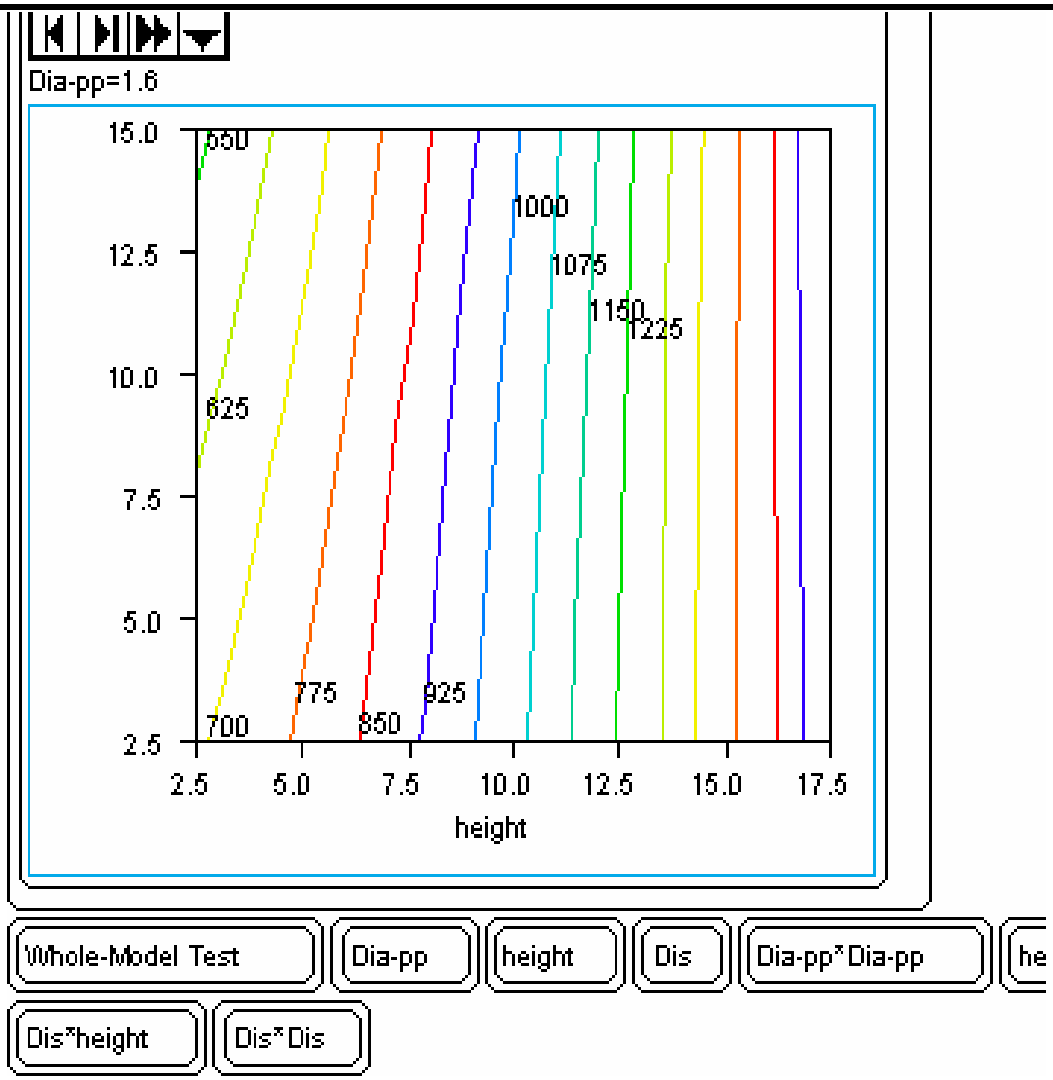
Dia-pp=1.6
15.0
12.5
10.0
7.5
5.0
2.5
550
625
700
775
850
925
1000
1075
1150
1225
2.5
5.0
7.5
10.0
12.5
15.0
17.5
height
Whole-Model Test
Dia-pp
height
Dis
Dia-pp*Dia-pp
he
Dis*height
Dis*Dis

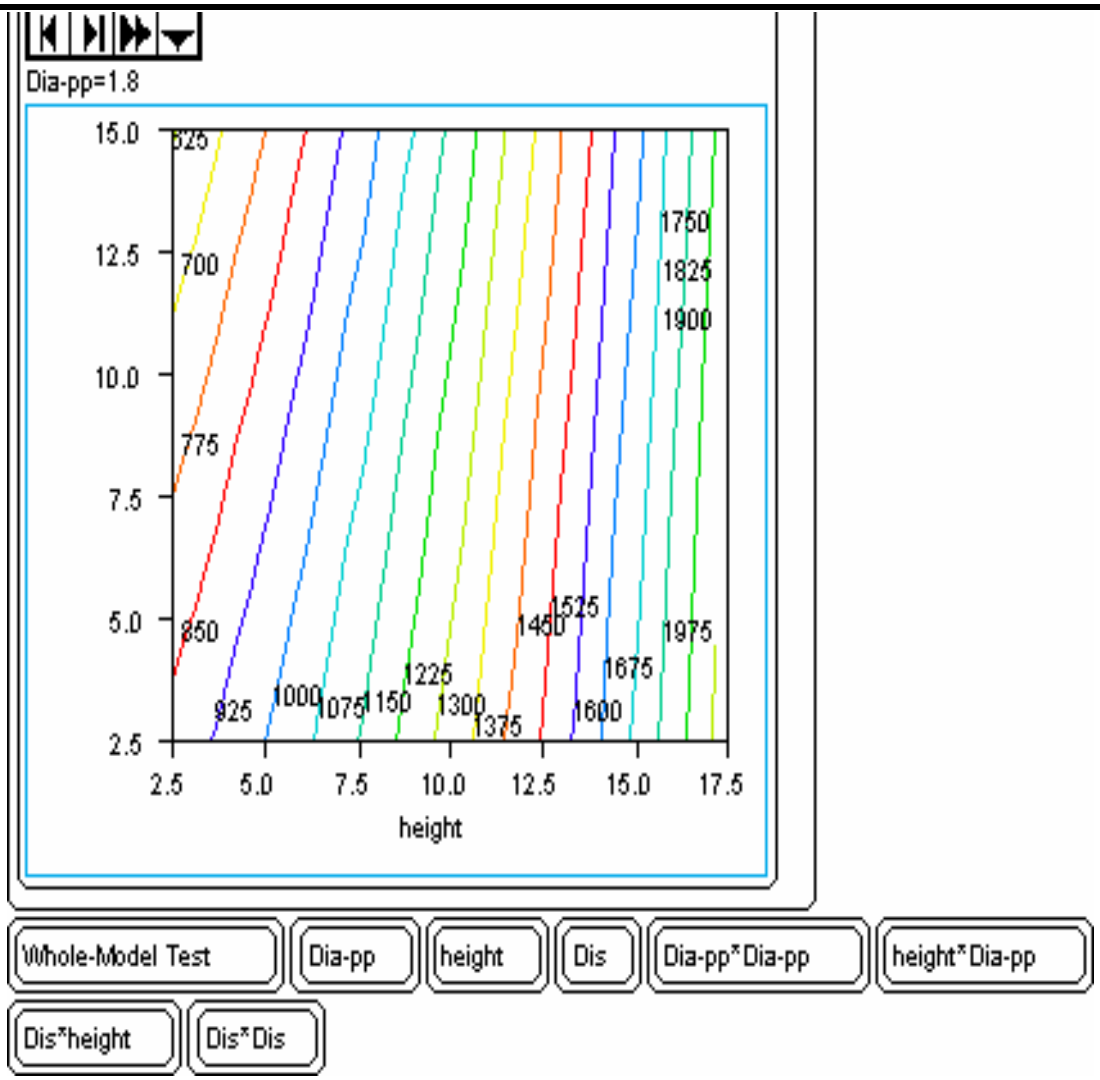
Dia-pp=1.8
15.0
12.5
10.0
7.5
5.0
2.5
625
700
775
850
925
1000
1075
1150
1225
1300
1375
1450
1525
1600
1675
1750
1825
1900
1975
2.5
5.0
7.5
10.0
12.5
15.0
17.5
height
Whole-Model Test
Dia-pp
height
Dis
Dia-pp*Dia-pp
height*Dia-pp
Dis*height
Dis*Dis

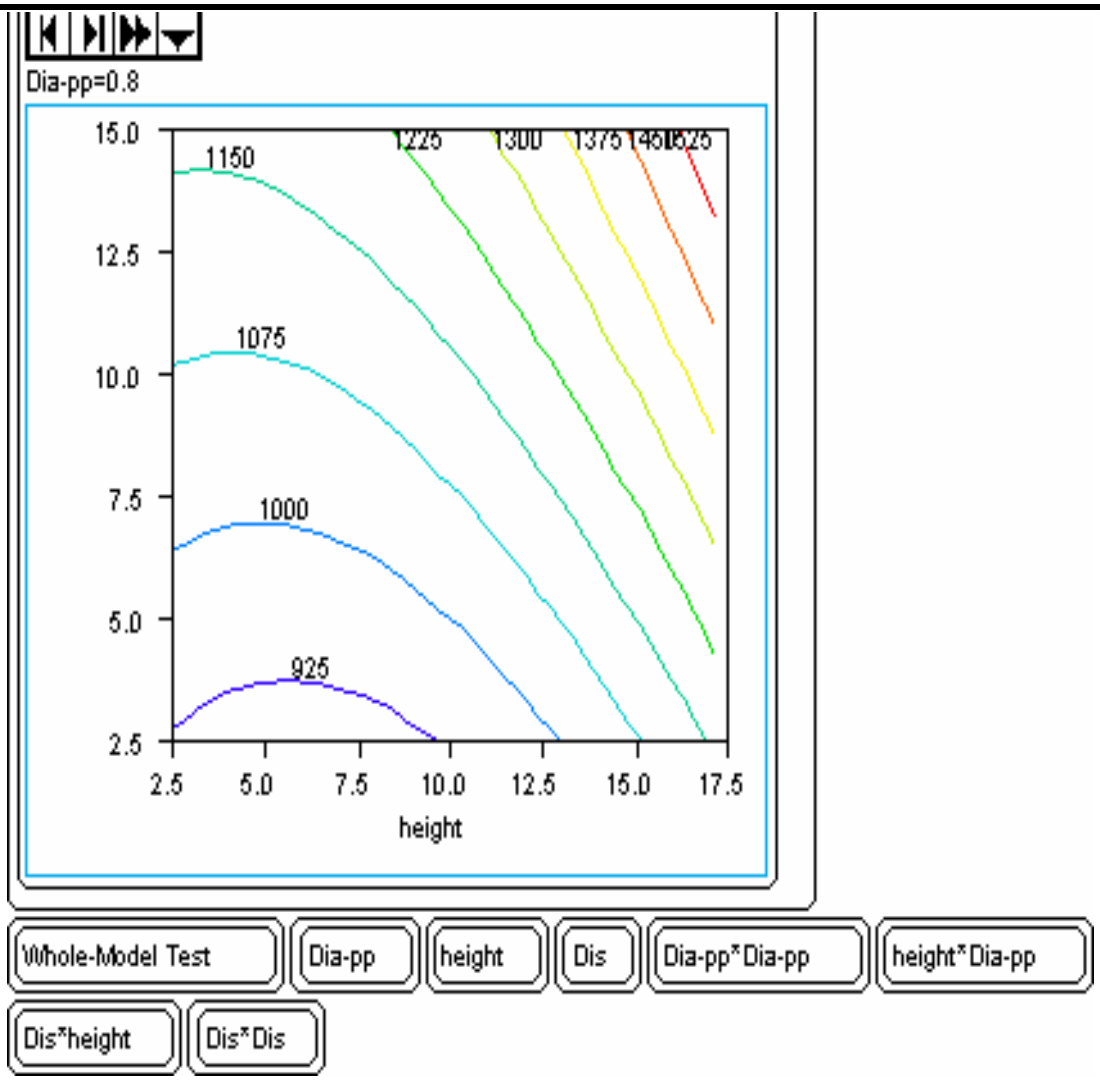
Dia-pp=0.8
15.0
12.5
10.0
7.5
5.0
2.5
1150
1225
1300
1375
1450
1525
1075
1000
925
2.5
5.0
7.5
10.0
12.5
15.0
17.5
height
Whole-Model Test
Dia-pp
height
Dis
Dia-pp*Dia-pp
height*Dia-pp
Dis*height
Dis*Dis

Vita
Afaf Khamis Mohamed El-Aufy

Born May, 1st. 1972, Alexandria, Egypt.

Educations:

PhD Department of Materials Science and Engineering, Drexel University, Philadelphia, March 2004.
Thesis: "Nanofibers and Nanocomposites Poly(3,4-ethylene dioxythiophene)/Poly(styrene sulfonate) by Electrospinning"

M.Sc. Department of Textile Engineering, Alexandria University, Egypt.Decemeber, 1996.

B.Sc. Department of Textile Engineering, Alexandria University, Egypt.June, 1993. Distinction with honor.

Experience:

Teaching :

Teacher assistant in Department of Textile Engineering, Alexandria University, from 1997-1998.
Demonstrator in Department of Textile Engineering, Alexandria University, from 1993-1996.

Research :

Research assistant in Materials Engineering Department, Drexel University, USA, from 1999 to 2004.
Research assistant in Department of Textile Engineering Department, Alexandria University, Egypt from 1993 to 1998.

Awards

- Scholarship for Ph.D. studying in USA sponsored by the Egyptian Government.(1999-present).
- Ideal Student at College of Engineering 1993
- Honors first student in Textile Department 1993.
- Scholarship for practicing Spanish language in Madrid, Spain sponsored by the Cultural Spanish Center in Alexandria. July-August 1991

Publications and Posters.

- Fiber Society Meeting, Aberdeen, MD, Nov., 1999.
- Drexel/MCP Hahnemann Research Day, May, 2000.
- Fiber Society Meeting, NCSU, Raleigh, NC, May 2001.
- Research Day at Drexel University, Philadelphia, PA, May, 2002.
- Research Day at Drexel University, Philadelphia, PA, May, 2003.
- ACS Regional Meeting, Princeton University, NJ, July, 2003.
- The American Chemical Society, ACS International Meeting, New York, NY, Sept., 2003.
- Materials Research Society, Dec., 2003.
- Ko, F.K., El-Aufy, A.K., Lam, H., and MacDiarmid, A. "Electrostatically Generated Nanofibers for wearable electronics", in Wearable Electronics, Editor, Tao, X.M., Woodhead, 2004.